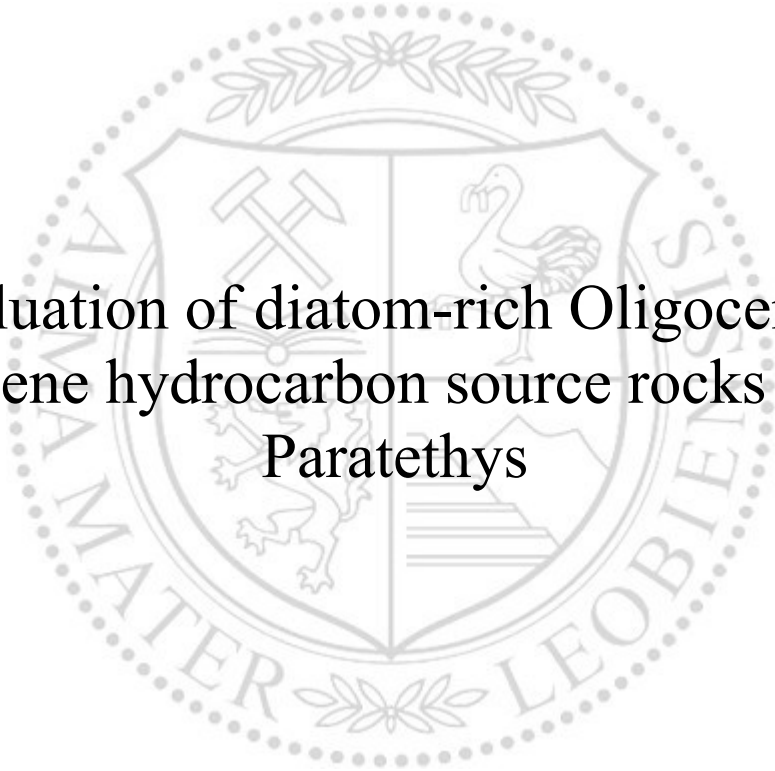




Chair of Petroleum Geology

Doctoral Thesis



Evaluation of diatom-rich Oligocene to  
Miocene hydrocarbon source rocks in the  
Paratethys

Emilia Tulan

July 2020

“Science may set limits to knowledge, but should not set limits to imagination.”

Bertrand Russell



**AFFIDAVIT**

I declare on oath that I wrote this thesis independently, did not use other than the specified sources and aids, and did not otherwise use any unauthorized aids.

I declare that I have read, understood, and complied with the guidelines of the senate of the Montanuniversität Leoben for "Good Scientific Practice".

Furthermore, I declare that the electronic and printed version of the submitted thesis are identical, both, formally and with regard to content.

Date 01.07.2020

---

Signature Author

Emilia, Tulan

## Abstract

Diatom rich sediments are often known for their hydrocarbon potential. A few notorious examples include the Miocene Monterey Formation in California, the Miocene Diatom Suite in Azerbaijan and the Menilite Formation in the Carpathians. In the Paratethys realm the diatomaceous sediments are widespread in the Oligo-Miocene strata, however their hydrocarbon potential still requires attention. For this reason, five locations were selected for this study. The study sites include two Oligocene outcrops in the Western Black Sea Basin and three Miocene outcrops: one in the Eastern Carpathian Bend Zone, one in the Pannonian Basin and another one in the Alpine-Carpathian Foreland Basin. Apart from one outcrop from the Western Black Sea Basin, all the studied sediments were diatom-rich.

However, the results indicate that the diatom-rich sediments can vary significantly in their hydrocarbon potential. For example, the sections studied from Ruslar Formation, Upper Menilites, and the diatom-free İhsaniye Formation proved to have a fair to very good hydrocarbon potential. The Source Potential Index calculations indicate that the above sections can generate on average 0.2 tHC/m<sup>2</sup>. The sections found to have poor hydrocarbon potential are represented by the Limberg Member and the non-calcareous part of the diatomites from the Szurdokpüspöki quarry.

The study sections give a small insight on the Paratethys connections. For example, the brackish water “Solenovian event” [NP 23] has not been observed in the sections on the Black Sea coast. It seems to be hidden in the unexposed lower part of the Ruslar Formation and is probably missing at Karaburun. Moreover, Sibiciu de Sus diatomites indicate that the depositional sequence was deposited during or after the marine connection was closed between the Eastern and Central Paratethys, and before the deposition of the evaporitic sequence (NN3/NN4 zones). The Pannonian Basin System was covered entirely by the Miocene Paratethian Sea which is observed in the Limberg Member and the Szurdokpüspöki diatomites. Furthermore, in the studied sediments the diatoms frustules are found to be abundant and exceptionally well-preserved in the Szurdokpüspöki quarry. In contrast, diatoms in the Limberg Member are highly broken, most probably due to a high energy environment. After all, this thesis provides only a glimpse in the Paratethyan diatom world and advocates for further diatom biostratigraphy studies.

## Zusammenfassung

Diatomeen-reiche Sedimente sind weithin bekannt für ihr Kohlenwasserstoffpotential. Einige Beispiele beinhalten die Monterey-Formation in Kalifornien, die miozäne Diatom Suite in Aserbaidschan und die Menilit-Formation in den Karpaten. Im Parathetys-Raum sind Diatomite im Oligozän und Miozän weit verbreitet, ihr Kohlenwasserstoffpotential ist allerdings ungenügend untersucht. Aus diesem Grund wurden fünf Lokationen für diese Studie ausgewählt. Die Lokationen beinhalten zwei Profile im Oligozän des Westlichen Schwarzmeerbeckens und drei Profile mit miozänen Sedimenten; eines im Grenzbereich der Ost- und Südkarpaten, eines im Pannonischen Becken und ein weiteres im Alpin-Karpatischen Vorlandbecken. Mit Ausnahme eines Profils im Westlichen Schwarzmeerbecken, waren alle untersuchten Sedimente Diatomeen-führend.

Die Ergebnisse zeigen, dass sich das Kohlenwasserstoffpotential der Diatomeen-reichen Sedimente signifikant unterscheidet. Das Limberg-Member und der kalkfreie Teil der Diatomite im Szurdokpüspöki Steinbruch weisen ein geringes Kohlenwasserstoffpotential auf. Die Ruslar-Formation, die Obere Menilit-Formation, und die Diatomeen-freie Ihsaniye Formation zeigen dagegen gutes bis sehr gutes Kohlenwasserstoffpotential. Der Muttergesteinspotential-Index zeigt, dass die untersuchten Profile im Durchschnitt 0.2 t Kohlenwasserstoffe/m<sup>2</sup> generieren können.

Die untersuchten Profile geben einen Einblick in die Meeresverbindungen der Paratethys. Zum Beispiel konnte die Verbrückung des „Solenovian Event“ [NP 23] nicht in den untersuchten Profilen an der Schwarzmeerküste beobachtet werden. Das Event scheint im nicht aufgeschlossenen Teil der Ruslar Formation verortet zu sein und fehlt vermutlich in Karaburun. Des Weiteren zeigt die Ablagerungsfolge der Diatomite von Sibiciu de Sus, dass sie während oder nach der Schließung Meeresverbindung zwischen Ost- und Zentral-Paratethys abgelagert wurde, jedoch noch vor der Evaporitabfolge (NN3/NN4 Zonen). Das Pannonische Beckensystem war insgesamt von der miozänen Paratethys See bedeckt, was im Limberg-Membere und in den Szurdokpüspöki Diatomiten erkennbar ist. In Szurdokpüspöki sind die Silikatskelette der Diatomeen in hoher Menge und aussergewöhnlich gut überliefert. Im Limberg-Member sind die Diatomeen dagegen großteils zerbrochen, wahrscheinlich durch höhere Strömungsenergie. Zusammenfassend eröffnet diese Arbeit einen Einblick in die Diatomeenwelt der Paratethys, verlangt aber nach weiteren biostratigraphischen Studien an Diatomeen.

## Abstract

Rocile bogate în diatomee (diatomitele) sunt adesea cunoscute pentru potențialul lor de a fi roci sursă de hidrocarburi. Câteva exemple includ formațiunea Miocenă Monterey din California, suita Miocenă cu diatomee din Azerbaidjan și formațiunea Menilitelor din Carpați. În regiunea Paratethysului rocile bogate în diatomee sunt răspândite în stratele Oligo-Miocene, cu toate acestea potențialul lor ca roci sursă de hidrocarburi necesită în continuare studii. Din acest motiv cinci locații au fost propuse pentru acest studiu. Locațiile studiate includ două aflorimente de vârstă Oligocenă din bazinul Mării Negre de Vest și trei aflorimente de vârstă Miocen: unul în zona de curbură a Carpaților Orientali, unul în bazinul Panonic și altul în bazinul avanfosei Alpino-Carpatice. Cu excepția unui afloriment din bazinul Mării Negre de Vest, toate rocile din aflorimentele studiate sunt bogate în diatomee.

Cu toate acestea, rezultatele din acest studiu indică faptul că diatomitele variază semnificativ ca potențial de roci sursă de hidrocarburi. De exemplu, secțiunea studiată din formațiunea Ruslar, Menilitele Superioare și formațiunea İhsaniye (fără diatomee) au dovedit că ar putea avea un bun până la foarte bun potențial de roci sursă de hidrocarburi. Calculul indicelui potențial sursă (SPI) indică faptul că secțiunile menționate mai sus pot genera în medie 0,2 tHC/m<sup>2</sup>. Cu toate acestea, valoarea este mică în comparație cu alte roci sursă de hidrocarburi din Paratethys. Secțiunile care au roci cu un potențial slab de hidrocarburi sunt reprezentate de rocile din membrul Limberg și partea necalcaroasă a diatomitelor din cariera Szurdokpüspöki.

Secțiunile studiate oferă indicații despre relația dintre Paratethys și Marea Mediterană. De exemplu „Evenimentul Solenovian” [NP 23] nu a fost observat în secțiunile studiate de pe coasta Mării Negre. Evenimentul pare a fi ascuns în partea inferioară a formațiunii Ruslar (care nu aflorează) și probabil lipsește cu totul în Karaburun. În plus, diatomitele de la Sibiciu de Sus indică faptul că sedimentele s-au depus în timpul sau probabil după ce conexiunea marină a fost închisă dintre Paratethysul de Est și cel Central, dar înainte secvența evaporitică (zonele NN /NN4). În Miocen Bazinul Panonic a fost acoperit în întregime de marea Paratethys, așa cum se observă și în membrul Limberg și diatomitele de la Szurdokpüspöki. Mai mult, în rocile studiate, diatomeele sunt conservate în mod excepțional și deasemenea se găsesc în abundență. Mai puțin în membrul Limberg, unde diatomeele au fost rupte sau fragmentate, cel mai probabil din cauza mediului

energetic de depozitionare. La urma urmei, această teză oferă o perspectivă în lumea diatomeelor din Paratethys și sprijină în continuare studii suplimentare și studii bio-stratigrafice a diatomeelor.

## Contents

<b>Abstract</b>	<b>1</b>
<b>Zusammenfassung</b>	<b>2</b>
<b>Abstract</b>	<b>3</b>
<b>Chapter I</b>	<b>7</b>
1.1 <i>Introduction</i>	7
1.2 <i>Diatoms and their applications in petroleum exploration</i>	9
1.3 <i>Hydrocarbon source rocks – an overview</i>	13
1.4 <i>Oligo-Miocene evolution of the Paratethys and its connection with the Mediterranean Sea</i>	16
1.5 <i>Aims of the study</i>	21
1.6 <i>Selected study areas</i>	21
<b>Chapter II</b>	<b>23</b>
2.1 <i>Geological overview of the studied areas</i>	23
2.2 <i>Western Black Sea Basin</i>	23
2.2.1 <i>Karaburun, Turkey</i>	23
2.2.2 <i>Karadere, Bulgaria</i>	26
2.3 <i>Eastern Carpathian Bend Zone</i>	30
2.3.1 <i>Sibiciu de Sus, Romania</i>	30
2.4 <i>Gyöngyöspata Basin (Pannonian Basin)</i>	35
2.4.1 <i>Szurdokpüspöki, Hungary</i>	35
2.5 <i>Alpine-Carpathian Foredeep Basin</i>	36
2.5.1 <i>Parisdorf and Limberg, Austria</i>	36
<b>Chapter III</b>	<b>38</b>
3.1 <i>Samples and Methods</i>	38
3.1.1 <i>Samples</i>	38
3.1.2 <i>Methodology</i>	38
<b>Chapter IV</b>	<b>45</b>
4.1 <i>Results and interpretation</i>	45
4.1.1 <i>List of published, accepted and submitted articles</i>	45
4.2 <i>Western Black Sea Basin</i>	46
4.2.1 <i>Karaburun, Turkey</i>	46
4.2.2 <i>Discussion and interpretation</i>	59
4.2.3 <i>Karadere, Bulgaria</i>	64
4.2.4 <i>Results</i>	65
4.2.5 <i>Discussion and interpretation</i>	73
4.2.6 <i>Conclusions</i>	77



<i>4.3 Eastern Carpathian Bend Zone</i>	79
4.3.1 Samples and methods	79
4.3.2 Sibiciu de Sus, Romania	79
4.3.4 Results	79
4.3.5 Discussion and interpretation	87
4.3.6 Conclusions	94
<i>4.4 Gyöngyöspata Basin</i>	95
4.4.1 Szurdokpüspöki, Hungary	95
4.4.2 Results	95
<i>4.5 Alpine-Carpathian Foredeep Basin</i>	102
4.5.1 Parisdorf and Limberg, Austria	102
4.5.2 Results	102
4.5.3 Discussion and interpretation	104
4.5.4 Conclusions	110
<b>Summary</b>	<b>111</b>
5.1 Oligocene	111
5.2 Miocene	114
5.3 Hydrocarbon potential of the studied diatomaceous rocks	115
5.4 Diatom preservation	118
<b>Conclusions and outlook</b>	<b>119</b>
<b>References</b>	<b>125</b>
<b>Plates</b>	<b>151</b>
<b>Appendix</b>	<b>172</b>

# Chapter I

## 1.1 Introduction

Diatomites are prolific hydrocarbon source rocks in many basins worldwide. Examples include the Miocene Monterey Formation in California (Isaacs and Rullkötter, 2001), the Oligocene to lower Miocene Menilite Formation in the Carpathians (Kotarba and Koltun, 2006), the middle Miocene Diatom Suite in Azerbaijan (Alizadeh et al., 2017 cum lit.; Sachsenhofer et al., 2018b) and the Middle Miocene Pil'skaya and Kurasiiskaya Formations, which are the best source rocks in Sakhalin (Bazhenova, 2002). For example, the Kaliakra canyon, offshore Bulgaria, is comprised of Oligocene to Middle Miocene sediments including the high petroleum potential Lower Miocene diatom-rich sediments (Mayer et al., 2018a; Sachsenhofer et al., 2018a, 2018b).

Several Miocene diatomaceous deposits are documented in Central Europe (Figure 1.1). In the Pannonian Basin the Middle Miocene diatom-rich rocks are associated with volcanic activity (Dill et al., 2008), while the lower Miocene diatomaceous rocks in the Alpine-Carpathian Foreland Basin has been associated with upwelling conditions (Grunert et al., 2010). To present, the diatoms are understudied in the Paratethys. Moreover, their hydrocarbon potential is often overlooked.

This thesis aims to add a contribution to the still underexplored world of fossil diatoms. Therefore, five locations were selected for further studies. The petroleum potential of these sites is investigated and the fossil diatoms are documented. The locations are described in detail in “Selected areas proposal for study” section.

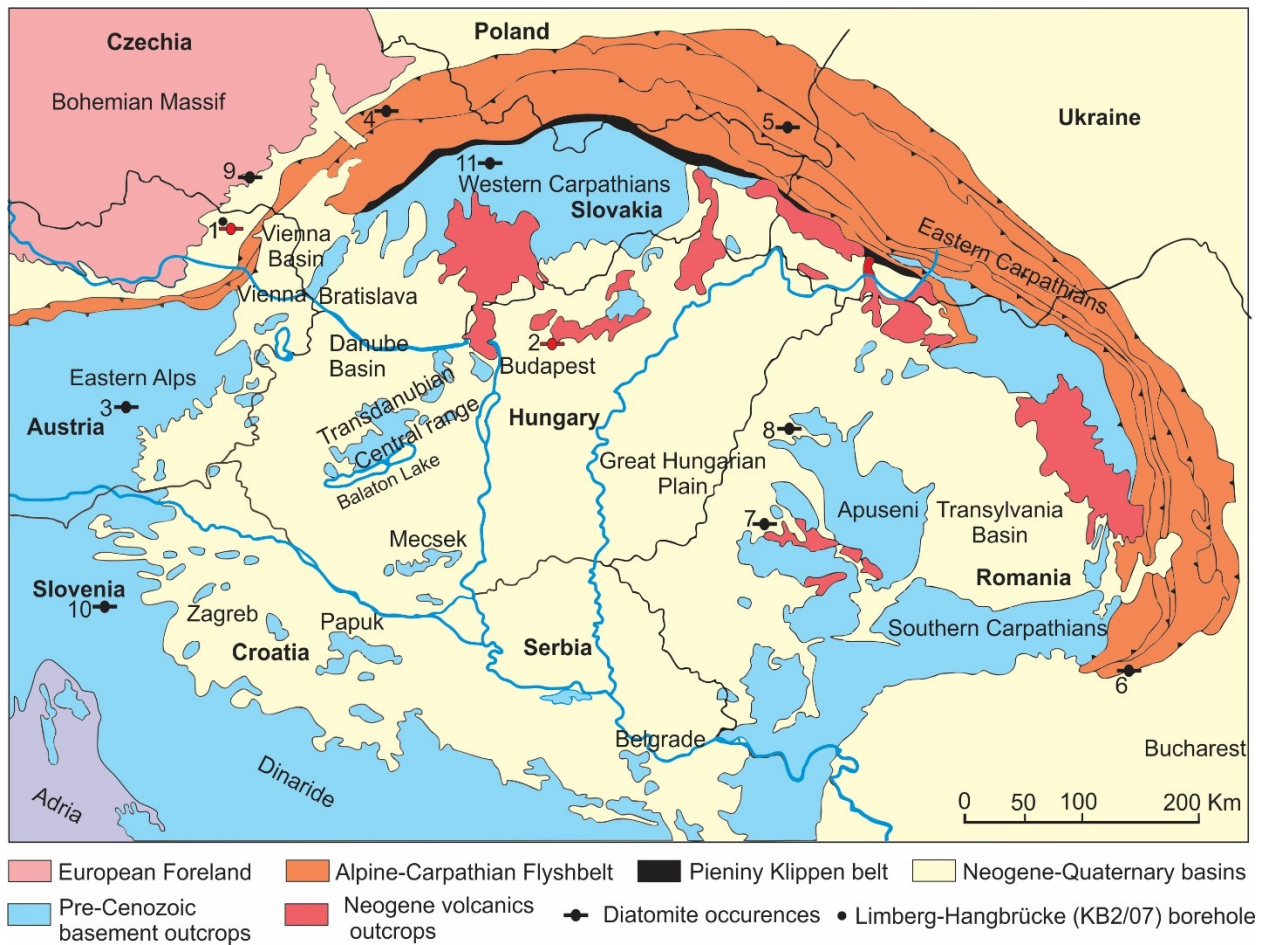


Figure 1.1. Occurrences of significant Oligocene and Miocene diatomaceous rocks in the Central Paratethys (redrawn after Tari and Horváth, 2006). 1 – Parisdorf quarry (this study); 2 – Szurdokpüspöki quarry (this study); 3 – Aflenz Basin (Sachsenhofer et al., 2003); 4 – Loučka section (Jirman et al., 2019); 5 – Jawornik deposit (Figarska-Warchoł et al., 2015); 6 – Sibiciu de Sus quarry (Funzescu and Brănoiu, 2004; this study); 7 – Zarand Basin; 8 – Vad-Borod Basin (Codrea et al., 2018); 9 – Brno-Královo Pole (Basistová, 2007); 10 – Krško Basin (Horvat, 2004) and 11 – Turiec Basin (Ognjanova-Rumenova and Radovan, 2015).

## 1.2 Diatoms and their applications in petroleum exploration

Diatoms (Bacillariophyta) are unicellular, eukaryotic microorganisms which are easily identified by their siliceous cell walls. The cell walls are composed of two valves (Figure 1.2 a), which together with the gridle bands forms a frustule (e.g., Round et al., 1990). The diatoms can have many shapes and sizes (Figure 1.2 b) and usually, the size, shape, and the form of diatom cell walls are taxonomically diagnostic. Moreover, due to their siliceous composition, the diatoms can be found well-preserved in ancient sediments (Smol and Stoermer, 2010). For further understanding morphology and biology of the diatom cell, a comprehensive study is offered by Round et al. (1990).

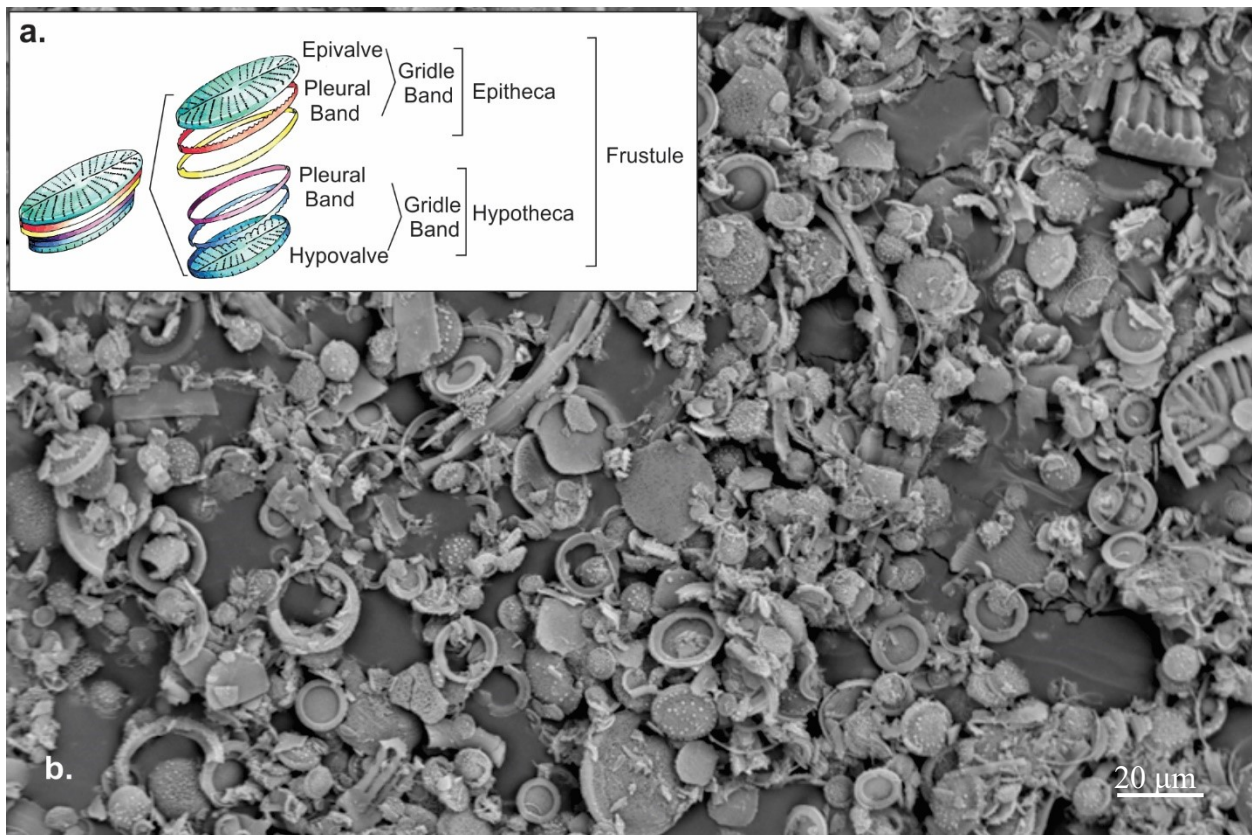


Figure 1.2. a. Sketch of the diatom cell walls and its siliceous components (Ian Nettleton in Zurzolo and Bowler, 2001); b. SEM image of fossil diatoms valves and remains which were extracted from diatomite rocks (scale 20 μm).

The effective study of diatoms started approximately 150 years ago, which is quite late compared with other microfossils. Because of their small size and the necessity of higher magnification microscope, the diatoms gained the reputation of being a difficult group to study

(Smol and Stoermer, 2010). Even today, studies on diatoms are avoided mostly due to requirement of access to expensive optical equipment (i.e., scanning electron microscope). After all, diatoms are powerful indicators, and they can be used: to detect changes in the Earth's biogeochemistry (e.g., pollution), in forensic science (i.e. if and where a deceased person was drowned; Peaboy and Cameron, 2010), to interpret environments and many other. Their multitude utilisation points towards a further consideration for detailed studies.

In ancient sediments diatoms remains are commonly found in sedimentary rocks known as diatomite. Other names are used such as diatomaceous earth, kieselgur, tripoli or infusorial earth. The diatomite is a porous rock, light-weight, siliceous, being a result of accumulation and compactions of diatom remains. Besides the diatom remains, the diatomite may contain clay and silt. The diatoms accumulate in areas where the rate of deposition of diatoms frustule is higher than the deposition of other sediments (e.g., Berger, 1970; Barron 1987).

Mainly, the diatomite is highly used in current industry for filtration, absorption, building materials, insulation, coatings, food additives, and many more. A diatomite deposit purity decreases when silt, clay and organic matter are present, which limits the industrial utility (Harwood, 2010). The diatomite application is not limited only to the current industry. For example, in petroleum exploration, the diatom-bearing sediments can be used as an indication of the depositional setting. The diatoms can live in every aqueous environment, which makes them a great tool for indicating the paleoenvironment.

Furthermore, during burial the temperature is increasing (depends on the thermal gradient) and the diatom frustules composed of amorphous silica ( $\text{SiO}_2 \cdot n\text{H}_2\text{O}$ ; known as opal-A) is gradually transformed to anhydrous silica ( $\text{SiO}_2$ ; known as opal-CT) and further to quartz as chert ( $\text{SiO}_2$ ). During this transformation, the porosity of the diatomite is decreasing, and the density and hardness increases (e.g., Bramlette, 1946; Issacs, 1981; Issacs and Rullkotter, 2001).

In order to have an appropriate paleoenvironment assessment, the fossil diatoms can be used in age dating and strata correlating, especially where the calcareous microfossils have a poor recovery, or they are completely missing. This can be easily the case in sediments which are deposited below the carbonate compensation depth or in lacustrine and brackish-water setting (Krebs et al., 2010). Correlation and age dating of the strata are important in hydrocarbon

exploration since the geological history of the prospected basin is critical in understanding the formation of the source rocks, reservoir, structures, seals and timing.

For instance, in Japan, in California, in the Bearing Sea of Alaska and Sakhalin Island in Russia, the marine fossil diatoms are extremely useful for petroleum exploration. In the above-mentioned areas, the marine diatoms are commonly found in Neogene diatomaceous rocks which have little calcareous microfossils or with long geological range. Therefore, the diatoms can be used for biostratigraphy instead (Krebs et al., 2010). Also, the diagenesis of the diatoms can be observed on their valves under the microscope, besides the diatomaceous rock property changes during diagenesis and can be recognised in seismic reflection (e.g., Murata and Larson, 1975; Iijima and Tada, 1981; Isaacs, 1981, 1983; Pisciotto, 1983; Tada and Iijima, 1983). Further, the diagenesis of the diatom-bearing sediments may create fractured siliceous reservoir (Krebs et al., 2010).

The diatomaceous sediments can be an important source for petroleum. For example, in Sakhalin, the Oligocene Pilengskaya Formation and the Middle Miocene Pil'skaya and Kurasiiskaya formations are highly siliceous, and they are the best hydrocarbon source rock (Bazhenova, 2002). Other examples include the Hondo Field, offshore of California represented by a fractured reservoir which is derived from the diagenesis of diatom-bearing sediments of the Monterey Formation. The coeval Belridge Diatomite is an oil shale (Schwartz, 1987). In Japan, the Middle Miocene Onnagawa Formation of the Akita Basin containing various siliceous rocks is the most productive horizon of hydrocarbons (e.g., Aoyagi and Iijima, 1987; Iijima, 1988; Aoyagi and Omokawa, 1992).

To determine the source from which the hydrocarbon accumulation originated, biomarker analysis can be applied. Also, the same analysis can help to identify the presence and abundance of the algal groups (e.g., Volkman, 1986). Sterols are found in all the eukaryotic organisms, and a big source of sterols in the marine setting is represented by the C<sub>27</sub>-C<sub>29</sub> sterols, where C<sub>28</sub> sterol are dominant (Rampen et al., 2010). The sterols can be used for indicating the presence of algae in ancient sediments. The sterols associated with marine diatoms are characterised by 24-methylcholesta-5,22E-dien-3 $\beta$ -ol and 24-methylcholesta-5,24(28)-dien-3 $\beta$ -ol (e.g., Rubinstein and Goad, 1974; Volkman, 1986). Other diatom-related biomarkers are represented by highly branched isoprenoids (HBI) and 24-norcholestane. The HBI alkenes are produced only by the

diatoms and can be useful indicators for petroleum deposits (Sinninghe Damsté et al., 2004). The algal originated biomarker 24-norcholestane is commonly used for determining the age of the petroleum source rock (Holba et al., 1998a, b).

To sum up, the diatom-bearing deposits can have the following applications in petroleum exploration:

- assist in identifying the environment setting at the time of the deposition
- being a potential hydrocarbon source rock for the generation of petroleum, as well as a hydrocarbon reservoir (e.g., chert fractured reservoir)
- being an effective tool for biostratigraphy and age determination where other fossils are scarce or missing.

### 1.3 Hydrocarbon source rocks – an overview

Sedimentary rocks largely contain minerals and organic matter, and the porous space is occupied by either water or hydrocarbons. Commonly, a hydrocarbon source rock is defined as a rock that is (or was) able to generate hydrocarbons. A prerequisite for a rock to generate hydrocarbons is to be rich in organic matter, to reach a thermal maturity and to be able to generate moveable hydrocarbons. However, not every hydrocarbon source rock can meet all the requirements. In order to quantify the quality and quantity of the organic matter total organic carbon content (TOC wt.%) is measured. To be considered a source rock, a minimum of 0.5 wt.% TOC is required, however, a good source rock is considered to have the TOC contents exceeding 2 wt.% (Magoon, 1994). Furthermore, in order to understand the process of hydrocarbon generation, a short description of the process is given below. A graphic representation is given in Figure 1.3.

The organic matter is affected by *diagenesis* during and after the deposition of the sediments, but before reaching burial temperatures higher than 60° C. Nonetheless, the organic matter quality and quantity preserved during this process define the petroleum potential of the rock (Horsfield and Rullkötter, 1994). An increase in the burial depth and temperature causes *catagenetic* process. The catagenesis is divided into *oil window* and *wet gas zone*. Here the liquid oil is expelled and light hydrocarbons are generated, respectively (Tissot and Welte, 1984). Further increase in temperature and burial depth results in *metagenesis* where dry gas is generated in the *dry gas zone*.

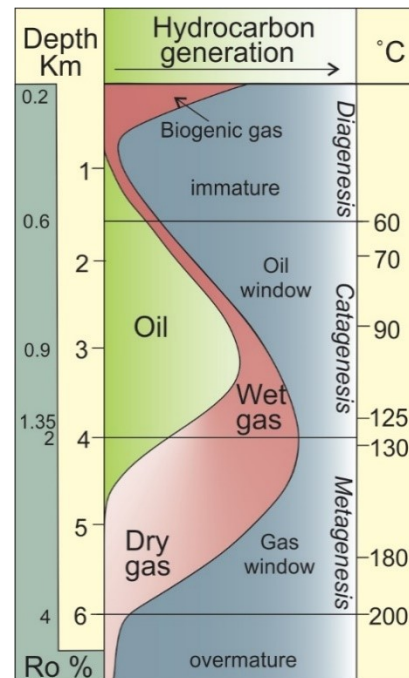


Figure 1.3. Simplified sketch of the process of oil and gas transformation in relationship with depth, temperature and vitrinite reflectance (redrawn after Peters and Cassa, 1994; McCarthy et al., 2011).



To be noted that dry gas is represented as well by biogenic gas that was generated during diagenesis due to microbial activity (Rice and Claypool, 1981).

*Dry gas* is composed of primarily methane (> 90%) with some intermediates and *wet gas* is defined as a containing less methane (< 85%) and more ethane and other more complex hydrocarbons (e.g., Tarek, 2000).

*Thermal maturity* represents the temperature-time reaction which converts the organic matter (source rock) to hydrocarbons (oil, wet gas, dry gas, pyrobitumen) (Peters and Cassa, 1994).

However, the maturity of the source rock can be influenced by many factors such as temperature, burial depth, overburden thickness, basin type (heat flow) and additional heat sources (e.g., Tissot and Welte 1984, Wehner and Kuckelkorn, 1995). The maturity of the source rock can be measured using vitrinite reflectance (Ro) and the Rock-Eval parameter Tmax. The above analysis can be applied in order to classify the source rock type, such as:

- *potential source rock* which refers to the rock which has enough organic matter to expel hydrocarbons but is still immature (0.2-0.6 Ro [%]; <435 Tmax [°C])
- *active source rock* represented by a rock which is generating and expelling hydrocarbons, typically in the oil window (0.6-1.35 Ro [%]; 435-470 Tmax [°C])
- *inactive source rock* characterised by a source rock which has stopped generating hydrocarbons but still shows potential (i.e. the sediments are uplifted, and the temperature decreased, therefore the rock cannot generate further hydrocarbons)
- *spent oil source rock* indicate that the rock has achieved the last stage of maturity and is incapable of further oil generation. However, it might generate wet and dry gas (>1.35 Ro [%]; >470 Tmax [°C]) (Peters and Cassa, 1994).

Moreover, the kerogen is characterized as organic matter insoluble in common organic solvents (Peters et al., 2005) and is divided into three (Tissot et al., 1974) or four kerogen types (Demaison et al., 1983; Larter, 1984). Plotting the bulk H/C and O/C atomic ratios in a “van Krevelen diagram” gives indication of type of kerogen (Tissot and Welte, 1984 as shown in Figure 1.4).

Due to increasing burial depth and temperature, the kerogen is transformed into non-hydrocarbon gases and hydrocarbons (oil, wet gas and dry gas). While this process is happening,

the kerogen loses primary oxygen, which is given to CO<sub>2</sub> and H<sub>2</sub>O and later the kerogen is losing more hydrogen which evolves into hydrocarbons (Figure 1.4.) (McCarthy et al., 2011).

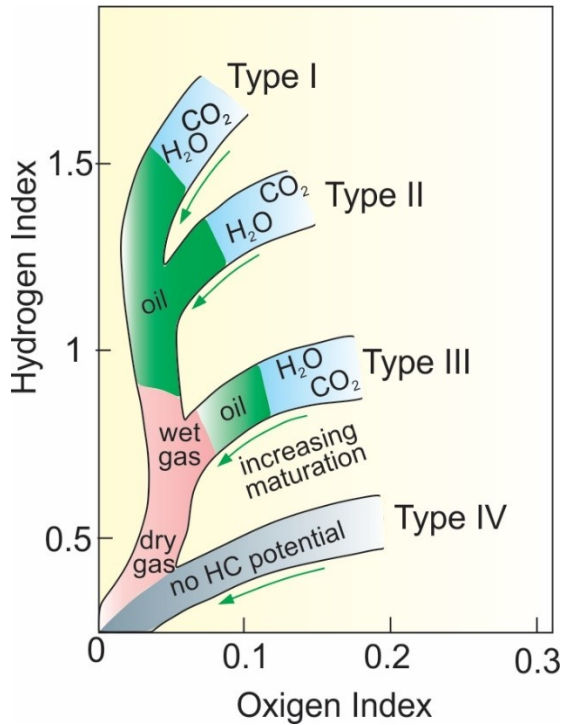


Figure 1.4. Kerogen types plotted on a modified van Krevelen diagram indicating the changes to kerogen due to increasing heat during burial (redrawn after McCarthy et al., 2011).

To characterize the origin of organic matter hydrogen index (HI) parameter is used. The HI is calculated from Rock-Eval data using the formula  $HI = S_2/TOC * 100$  [mgHC/gTOC].  $S_2$  represents the amount of hydrocarbons generated of non-volatile organic matter thermal cracking. Oxygen Index (OI) represents a parameter which correlates with the Oxygen (O<sub>2</sub>) to Carbon (C) ratio calculated using formula  $OI = S_3/TOC * 100$  [mgCO<sub>2</sub>/gTOC], where  $S_3$  represents the amount of CO<sub>2</sub> produced during pyrolysis of kerogen (e.g., Tissot and Welte, 1984; Espitalie et al., 1998).

Based on the hydrogen index (HI) and the oxygen index (OI) the kerogen type is defined as:

**Type I** has high H/C (>1.5) and low O/C (<0.1) ratios and is mainly derived from algal or bacterial remains which are often deposited in marine or lacustrine environments. It has high HI values (>600 mgHC/gTOC) and high petroleum potential, especially oil.

**Type II** has relative high H/C and low O/C ratios and is derived mainly from planktonic and bacterial remains deposited in marine environments. Also, a common contribution is given by detrital land plants. HI values (250-600 mgHC/gTOC) are intermediate, and the kerogen has a good oil potential.

**Type III** has low H/C (<1.0) and high O/C (>0.2) ratios. It is generally formed by remnants of vascular plants. It has low HI values (50-250 mgHC/gTOC) and in comparison, to kerogen type I and II, has a poor oil potential and is mainly the source of gas.

**Type IV**-has very low HI values (<50 mgHC/gTOC) and no hydrocarbon potential.

Nonetheless, it is important to note that the petroleum potential can differ vertical or lateral within a source rock (Peters and Cassa, 1994).

#### **1.4 Oligo-Miocene evolution of the Paratethys and its connection with the Mediterranean Sea**

In Cenozoic time, the Tethyan Realm was rearranged due to the African/Apulian/Arabian – Eurasian continent to continent collision. The collision broke up the Tethyan Realm into southern Mediterranean and the northern Paratethyan domain. Starting with Oligocene, the Paratethyan domain became subject to recurrent isolation from the Mediterranean and the world ocean (Figure 1.5) (Popov et al., 2004b). The Paratethys domain is divided into the Central European (Alpine-Carpathian) Central Paratethys and the Euxinian-Caspian basin, known as Eastern Paratethys.

Around the Eocene/Oligocene boundary a sea-level fall in combination with the effects of the Alpine orogeny lead to the disconnection of the Paratethys from the Mediterranean (Rögl, 1999; Allen and Armstrong, 2008). The strong tectonic activity let the Paratethys domain to increase its water depth, which reached more than 1000 m in the depocenters. Deep troughs were spreading from the Western Alps to the Transcaspiian Basin (Rögl, 1999; Popov et al., 2004a, b). Three paleogeographical sketches of the Paratethys Sea for Early and Late Oligocene and Early Miocene times published by Sachsenhofer et al. (2018a) are provided in Figure 1.6.

The early Oligocene isolation of the Paratethys from the Mediterranean Sea caused anoxic conditions and is marked by the deposition of black shales. The isolation reached maximum in the NP23 nanoplankton zone, when carbonate-rich sediments (e.g., Dynow Marlstones) and diatom-rich sediments were deposited in brackish to freshwater environments from the Molasse Basin and

the Carpathians to the Caspian Basin (e.g., Haczewski 1989; Krhovsky et al. 1991; Krhovsky 1995). The marine connection has been resumed starting with the middle part of the Oligocene (nannoplankton zone NP24), providing well-oxygenated bottom water conditions. Due to high tectonic activities in the Mediterranean, in the Late Oligocene (nannoplankton zone NP 25), the Paratethys Sea spread and connected with the Mediterranean Sea in Thrace (Turkey) (Rögl, 1999).

The paleogeographical configuration continued up to lowermost Miocene (nannoplankton zone NN1 to lower NN2), while connections with the Indo-Pacific are documented in early Burdigalian time (upper NN2) (Rögl, 1999). Later, when the earliest Miocene connections towards the Eastern Paratethys and Mediterranean was closing, during Aquitanian and Burdigalian, a marine flooding occurred in the front of the Alps (e.g., Popov et al. 2004; Kováč et al. 2017 a,b). At the Aquitanian/Burdigalian boundary, the gateway opened and the sea flooded the foreland and hinterland of the Carpathian mountain chain (e.g., Kováč et al. 2017b; Kováč et al. 2018). Furthermore, the isolation led to development of hypersaline and hyposaline facies, in the distal part of the Central Paratethys (e.g., Kováč et al. 2017b; Kováč et al. 2018) (Figure 1.5).

In the end of Badenian, the marine connections were strongly restricted, and in Pannonian, the aquatic realm was reduced in Central Paratethys. However, the Pannonian Lake remained in the Carpathian arc, but its salinity conditions were reduced drastically (Rögl, 1999). Freshwater conditions prevailed in Pontian time from the Pannonian Basin to the Black Sea Basin, and southward into the Aegean Basin. In the same time, the Messinian regression and salinity crisis in the Mediterranean Basin is seen (Rögl, 1999).

The isolation of the Paratethys along with cooling and changing to mesophilic humid climate in terminal late Eocene, and deepening of the basin led to thermohaline water stratification, and estuarine water circulation pattern resulted into recurrent episodes of stagnation and accumulation of dysoxic to anoxic sediments (Schulz et al., 2004). This kind of sediments was predominant in the Oligocene and Early Miocene, and they are referred to as “maykopian and menilitic facies” in the Paratethys (Popov et al., 2004 b). In the Paratethys two types of anoxic regimes occurred, one where the oxygen-depleted environment within the uppermost sediment layers resulted in the reduction of benthic organisms and a second one where hydrogen sulphide was present in the water column prohibiting deep-water life (Rögl, 1999; Popov, 2004b).

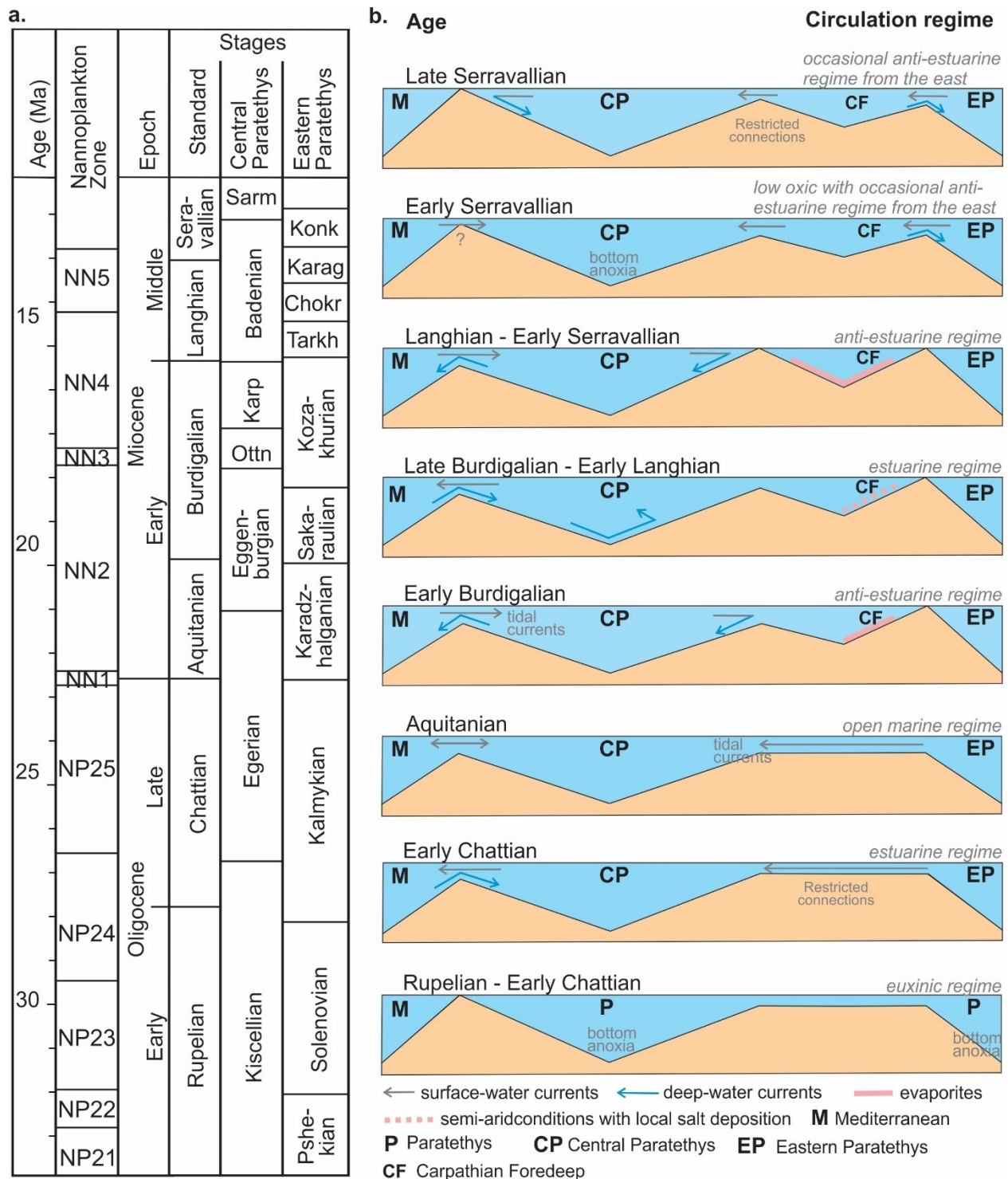


Figure 1.5. a. Standard Oligocene to Miocene chronostratigraphy and biostratigraphy (after Hilgen 2012; Martini, 1971); b. Sketch of the Paratethys circulation regimes during Oligocene and Miocene (redrawn after Kováč et al. 2018).

Besides creating the favourable conditions to develop anoxia and deposit hydrocarbon source rocks, which were later proven (e.g. Maykop and Menilites Suites), endemic benthic fauna has flourished during the Paratethys isolation. The endemic fauna is used for correlation within the Paratethys, and calcareous nanoplankton are used for correlation with the global stratigraphic framework. However, benthic fauna has its limitation since they are absent in the anoxic basin, and the calcareous nannoplankton are usually dissolved, making stratigraphic correlation challenging of the sedimentary successions.

The Oligocene-Miocene typical lithologies in the Paratethys are represented by shales, cherts, diatomaceous shales, marls and coccolith limestones (Sachsenhofer et al., 2018 a, b). Taking into consideration that rich diatom sediments are occurring in the Paratethys realm (e.g., Menilite Formation, Ruslar Formation, Diatom Suite in Azerbaijan), our current understanding of the diatom assemblages still needs attention. However, further work is necessary to obtain a proper understanding of the Paratethys diatom assemblages, and this thesis is providing only a peek into Oligo-Miocene diatoms from Paratethys.

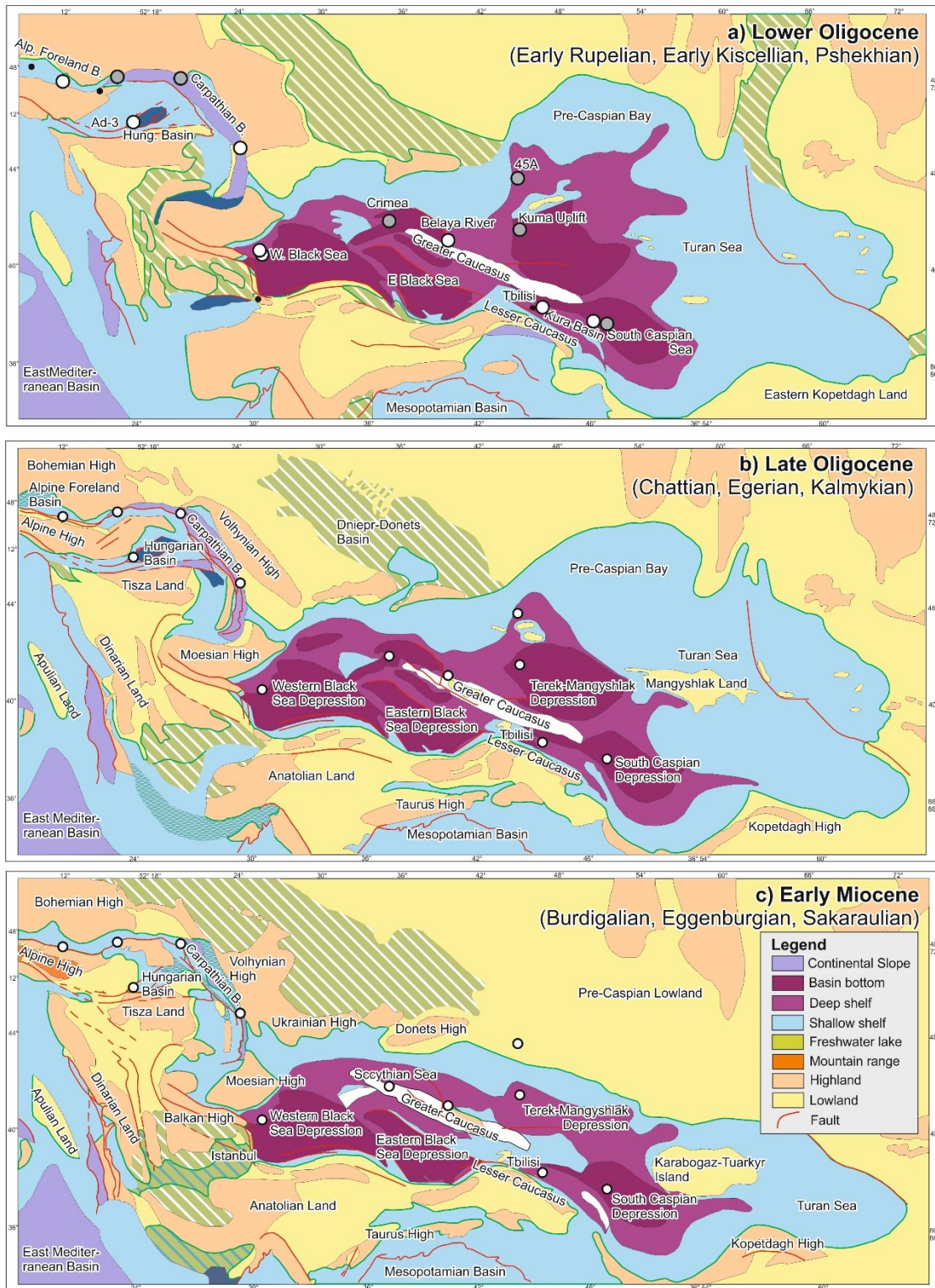


Figure 1.6. Paleogeographic representations of the Paratethys for (a) Lower Oligocene, (b) Upper Oligocene and (c) Early Miocene time after Popov et al. (2004). Deep-water zones with permanent anoxia (dark purple) and zones with temporary anoxia (light purple) are shown for the Eastern Paratethys (Popov and Stolyarov, 1996). Maps from Sachsenhofer et al. (2018a).

## 1.5 Aims of the study

Diatomaceous sediments are often prolific hydrocarbon source rocks. In the Paratethys realm, diatomaceous sediments are widespread in Oligo-Miocene units. Therefore, the main aims of the thesis are to study the source rock potential of diatomaceous rocks from selected locations within Paratethys. The locations are represented by two outcrops in the Western Black Sea Basin and one outcrop in East Carpathian Bend Zone, one in the Pannonian Basin and in two in the Alpine-Carpathian Foreland Basin (see Fig. 1.6). For this purpose, rock samples with high biogenic silica content have been selected. Besides studying the organic matter content of the diatomaceous rocks, in this thesis petrographic analysis (X-ray diffraction, thin section observations) are performed and siliceous microfossils (diatoms and silicoflagellates) and calcareous nannoplankton assemblages are documented. The above data are applied to understand the depositional environment of the studied areas, which is another objective of this thesis.

## 1.6 Selected study areas

For this study, five outcrops have been selected (for locations see Figure 1.6) and the number of the samples collected is described in detail in Chapter III. Due to limited exposure of diatomaceous rocks in the Paratethys two Oligocene outcrops along the Black Sea shore and three Miocene abandoned diatomite quarries were studied.

The outcrops at Karaburun (Turkey) and Karadere (Bulgaria), located at the Black Sea shore, represent equivalents of the lower part of the Maykop Suite, which is a potential hydrocarbon source rock in the Black Sea Basin (eg., Sachsenhofer et al., 2009; Simmons et al., 2020).

- Near Karaburun (Thrace, NW of Istanbul), Lower Oligocene rocks of the İhsaniye Formation are exposed in a rock succession, 70 m thick. They sediments are represented by marls with carbonate-rich siltstone or fine sandstone and minor debris flow horizons.
- The Karadere outcrop provides a 14-m thick section of the Ruslar Formation and gives an excellent opportunity to study its upper part. Here are exposed laminated diatom-rich mudstones with frequent thin sandstone beds and a prominent concretion horizon.



The two outcrops are studied to broaden the regional understanding of source rocks in the southwestern part of the Black Sea which was proved to be bounded (e.g. Simmons et al., 2018; Sachsenhofer et al., 2015, 2018a, b).

An abandoned diatomite quarry near Sibiciu de Sus (Romania) exposes an impressive diatomite sequence in the uppermost part of the Upper Menilites in the Eastern Carpathian Bend Zone. The abandoned quarry is more than 200 m long and 50 m high and offers a great opportunity to study one of the few occurrences of diatom-rich sediments from the Carpathians. However, the diatomite layers are heavily folded and faulted which makes correlations of the layers challenging.



Figure 1.6. Representation of the study sections presented in this thesis.

Another outcrop with Middle Miocene diatomaceous sediments is exposed in the Pannonian Basin in an abandoned quarry located in Szurdokpüspöki (Hungary). Here, two sections of the quarry are studied, exposing diatomaceous sediments, not more than 15 m-thick. In this thesis, diatomite from the Szurdokpüspöki outcrop is compared with diatomaceous sediments of the Lower Miocene Limberg Member at Limberg and Parisdorf (Austria). The Limberg Member forms part of the fill of the Alpine-Carpathian Foredeep and is not more than 7 m thick. However, the quality of the outcrops is poor since they are partly covered by vegetation.

## Chapter II

This chapter describes the geology of the studied areas and all the references are cited accordingly. Moreover, some paragraphs written in this chapter are from articles published in peer-reviewed journals or currently submitted articles (see sub-chapter 4.1.1. for list of publications).

### 2.1 Geological overview of the studied areas

The geology is presented from the East to West of the Paratethys, starting with the Western Black Sea Basin followed by the Eastern Carpathians, the Pannonian Basin concentrated on Gyöngyöspata Basin and the Alpine-Carpathian Foredeep Basin focusing on each location's geology.

### 2.2 Western Black Sea Basin

#### 2.2.1 Karaburun, Turkey

The Karaburun section is located along the southwestern shoreline of the Black Sea, about 60 km northwest of Istanbul (Figure 2.1.). A 15 km wide marine gateway existed between the West Black Sea Basin and the Thrace Basin during Late Eocene and Early Oligocene time (“Çatalca gap”; Okay et al., 2019). The Eocene and Oligocene strata of the Çatalca gap conceal the West Black Sea Fault, a major Cretaceous strike-slip fault, separating the Strandja Massif and the Istanbul Zone (Okay et al., 1994). The Paleogene sequence consists of the Upper Eocene Soğucak Formation, overlain unconformably by the principally Lower Oligocene İhsaniye Formation and the Lower Oligocene Pınarhisar Formation.

The Soğucak Formation overlies the metamorphic rocks of the Strandja Massif in the west (Less et al., 2011), Carboniferous sandstones of the Istanbul Zone in the east and probably Upper Cretaceous volcanic rocks in the north along the Black Sea coast (Okay et al., 2019). The Soğucak Formation is composed of thickly bedded to massive, light grey shallow-marine limestones, 5 to 60 m thick. The limestone contains corals, bivalves, algae, bryozoans and larger benthic foraminifera (Less et al., 2011; Yücel et al., 2020). The top of the Soğucak Formation is formed by a major erosional unconformity.

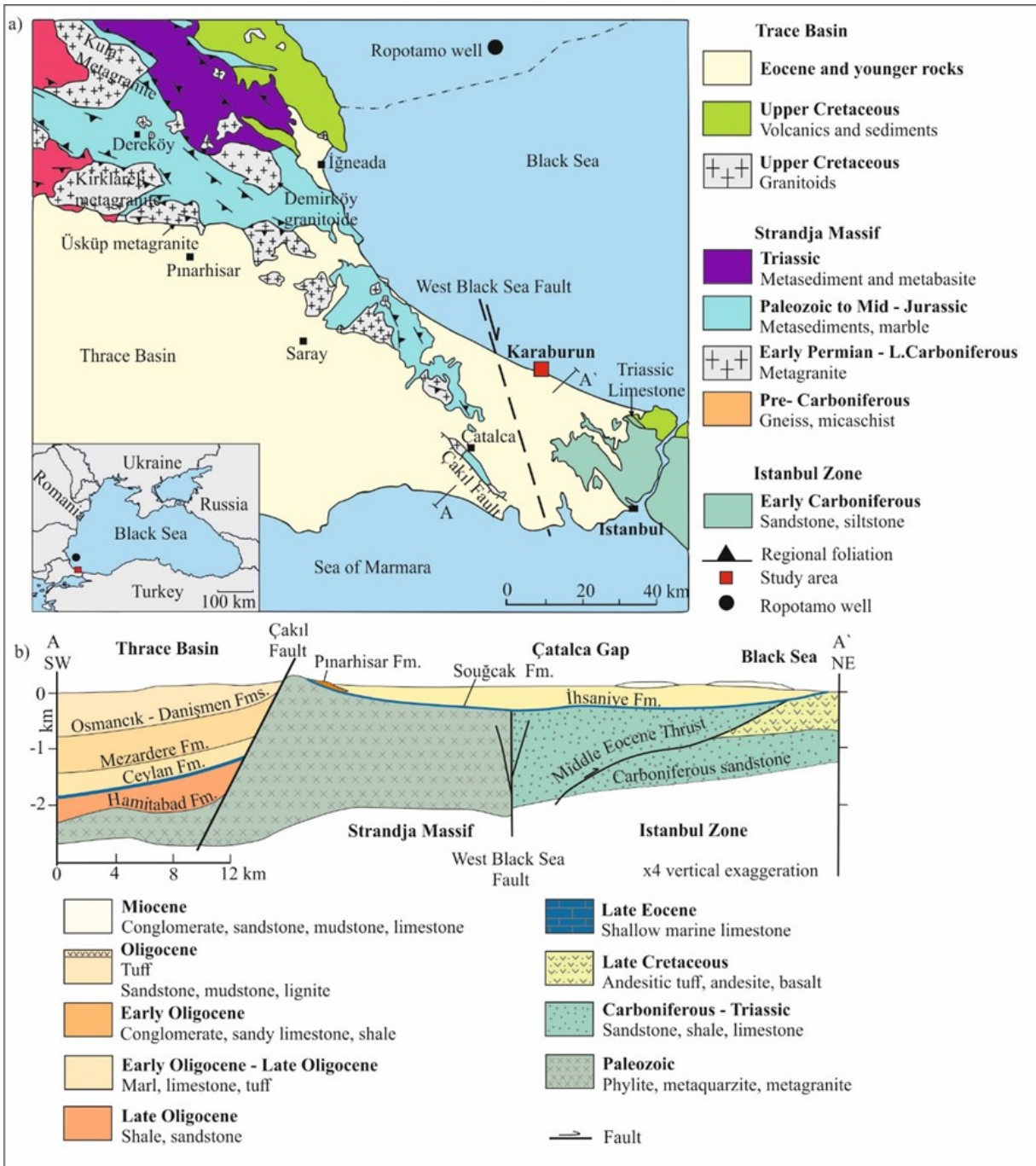


Figure 2.1. a) Geological map of the southern Strandja Massif and the neighbouring regions (after Chatalov 1988; Chestitev and Kancev, 1989; Okay et al., 2001). b) Geological cross-section of the İhsaniye Formation (after Akartuna, 1953; Yurtsever and Çağlayan, 2002; Gedik et al., 2014, Okay et al., 2019).

Deposition of the İhsaniye Formation commenced during the latest Eocene (Late Priabonian) in the center of the Çatalca gap but only expanded to marginal areas including the

Karaburun area in the Early Oligocene (e.g. Okay et al., 2019; Simmons et al., 2020; Figure 2.2). It is composed of open marine marls with a rich microfauna and microflora of foraminifera, calcareous nannofossils and dinoflagellates; calcarenite, acidic tuffs and rare pebbly sandstone beds (Okay et al., 2019; Simmons et al., 2020).

The lower Oligocene Pınarhisar Formation (e.g., Popov et al., 2004b; İslamoğlu et al., 2010), a brackish to lagoonal sequence with sandy limestone and shale, interfingers with the İhsaniye Formation near the Çatalca ridge.

The Karaburun area is one of the few localities in Turkey where Eocene and Oligocene formations are exposed along the Black Sea coast. Several authors have described the stratigraphy of the Karaburun area and attributed a Lower Oligocene age to the İhsaniye Formation (Oktay et al., 1992; Sakınç, 1994; Less et al., 2011; Gedik et al., 2014; Natal'in and Say, 2015; Okay et al., 2019; Sancay and Batı, 2020).

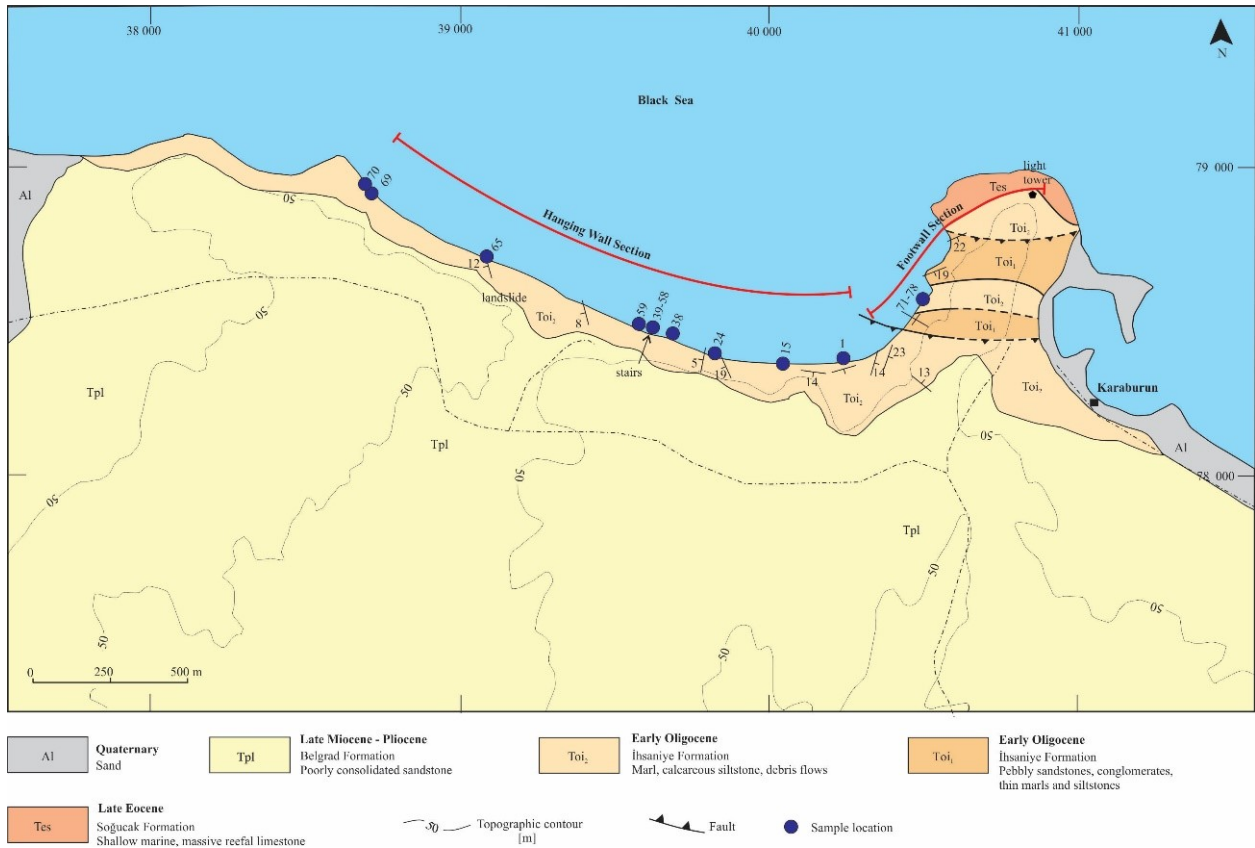


Figure 2.2. Geological map of Karaburun area (after Okay et al., 2019 and Simmons et al., 2020) with the position of the samples collected for this study.

Based on the investigation of calcareous nannoplankton, foraminifera and palynomorphs, Simmons et al. (2020) recognised that the sediments of the İhsaniye Formation are no older than 33.9 Ma (nannoplankton zone upper NP 21) and no younger than 31 Ma (lower NP23). They also presented a revised tectonic interpretation where the deposition of the İhsaniye Formation was controlled by a now inverted normal fault. The following description of the İhsaniye Formation follows these authors. Sediments ranging in age from nannoplankton zone upper NP 21 to lower NP 23 were deposited on the hanging wall side of the fault (“Hanging Wall Section”, Figure 2.2), whereas deposition on the footwall commenced only during NP23 (“Footwall Section”, Figure 2.2).

The Hanging Wall Section is in its lower part (c. 40 m thick) dominated by marls with carbonate-rich siltstone or fine sandstone and minor debris flow horizons. In the upper part of the section, about 30 m thick, debris flow deposits syn-sedimentary faults become increasingly significant. Debris flow deposits contain blocks of Soğucak Formation, more than 1 m in size. Debris flows in the upper part of the Hanging Wall Section contain, in addition, volcanic rocks reworked from the underlying Late Cretaceous succession. Simmons et al. (2020) suggested that deposition of the marl-dominated facies occurred in outer shelf to upper bathyal environments.

The Footwall Section includes two parts. The lower 15 m of the Footwall Section are represented by mixed pebbly calcareous sandstones, siltstones and calcarenites with rare thin marl layers deposited in a fan-delta to shoreface environment. The upper part of the Footwall Section is formed by a 30 m succession of grey marls with thin calcareous siltstone layers, similar to those from the Hanging Wall Section.

### ***2.2.2. Karadere, Bulgaria***

The Kamchia Depression, a foredeep basin, is located to the north of the Balkans thrust front in eastern Bulgaria (Figure 2.3), and continues offshore into the Black Sea (Sinclair et al., 1997; Georgiev, 2011). The sedimentary fill of the basin contains Middle Eocene to Quaternary deposits and is related to the growth of the Balkan mountain belt (Sinclair et al., 1997). Its base is marked by the intra-Middle Eocene Illyrian unconformity (Figure 2.3) (Georgiev, 2011). Another unconformity separates Eocene and Oligocene rocks (e.g., Mayer et al., 2018a).

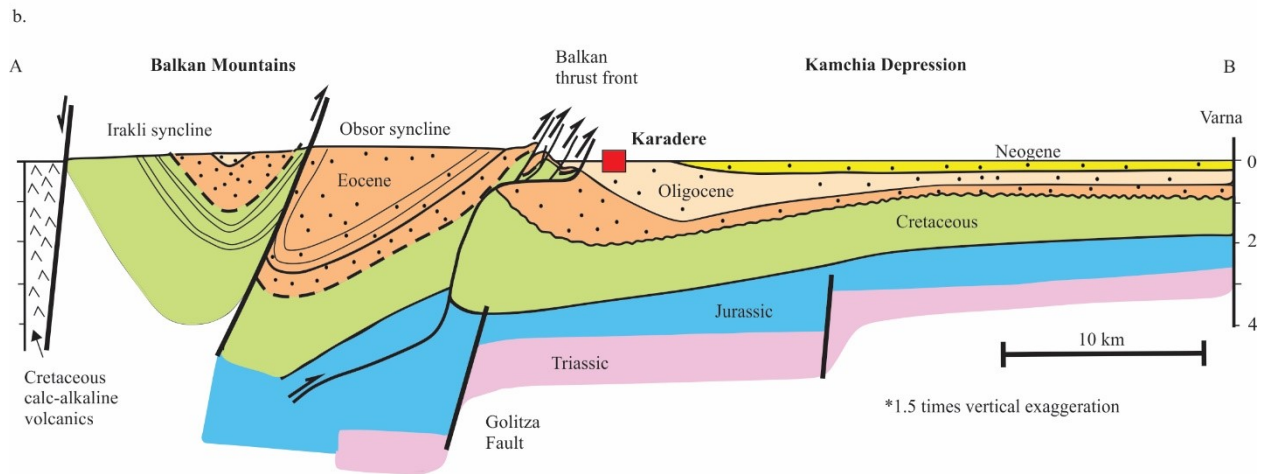
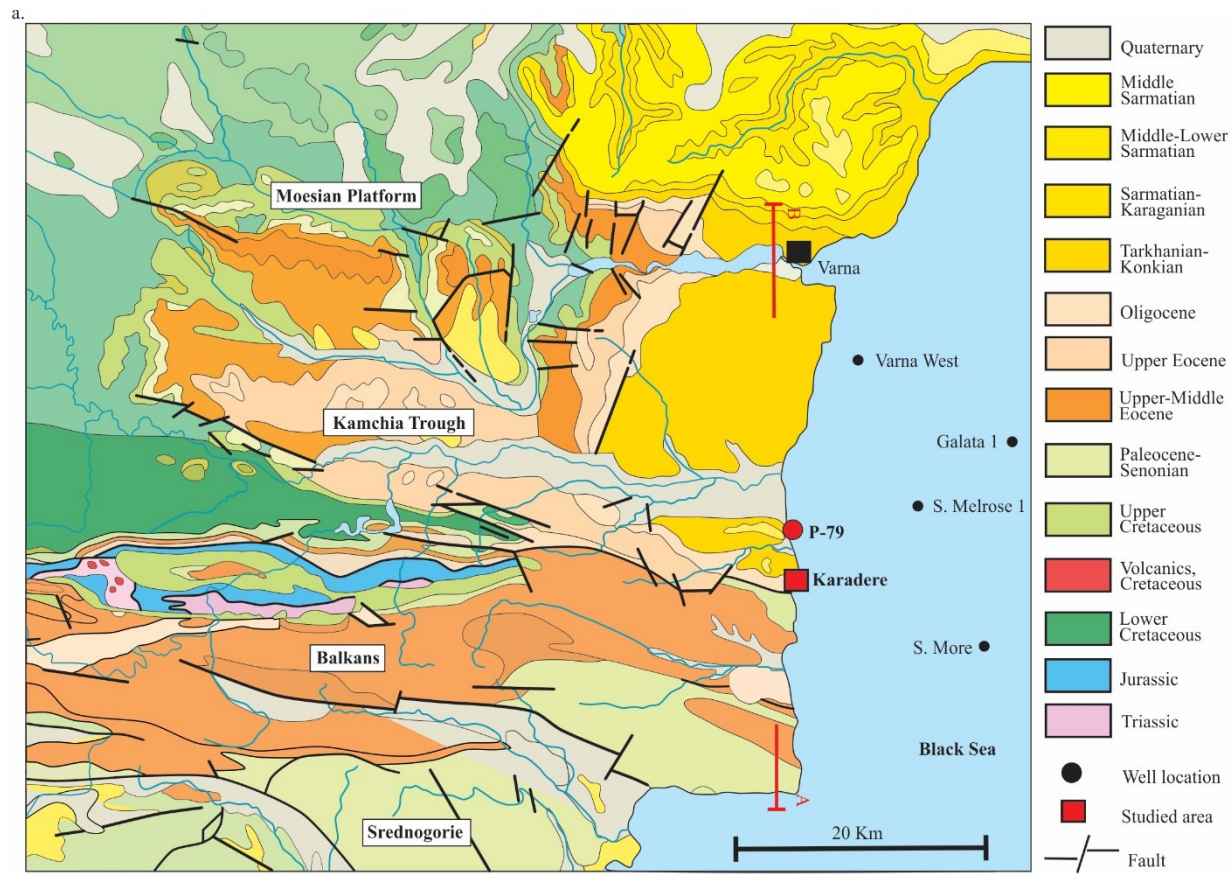


Figure 2.3. a. Geological map of eastern Bulgaria (after Cheshitev and Kancev, 1989) indicating the studied area and the position of the Bulgaria offshore wells; b. S-N cross-section through the Balkan Orogen and the Kamchia Depression along the Black Sea coast (after Sinclair et al., 1997), with the position of the studied area.

The development of the Kamchia Basin began with the stacking of the Eastern Balkan thrust-belt during the Illyrian northward compression in the early Middle Eocene (Georgiev and

Dabovski, 2001) and was controlled by the uplift of the Balkan thrust-fold belt and the opening of the West Black Sea Basin (Georgiev, 2011). This Cenozoic basin is superimposed on the southern margin of the Moesian Platform and the frontal zone of the Balkan thrust-fold belt (Dachev et al., 1988). The Cenozoic sediments are preserved approximately 70 km inland from the coast of the Black Sea (Figure 1); thicker and younger sediments are present offshore (Sinclair et al., 1997).

The Oligocene Ruslar Formation overlies the Middle to Upper Eocene Avren Formation (~ 1.5 km thick; sandy marls with limestone and sandstone intercalations) with a major erosional unconformity and underlies the Middle Miocene Galata Formation (sandstones intercalated with frequent clays and rare limestone beds) (Popov and Kojumdjievam, 1987) (Figure 2.3).

The Ruslar Formation onshore (Valchev et al., 2018) and offshore Bulgaria (Sachsenhofer et al., 2009; Mayer et al., 2018a) typically contains from base to top calcareous shales (assigned to biozone NP21-22), marlstones to limestone (lower part of NP23) and overlying pelitic rocks with low carbonate contents (upper part of NP23 to NP24). Onshore Bulgaria, the base of the Ruslar Formation contains manganese ores and is sandier than offshore. The marlstones and limestones represent the low salinity “Solenovian event”, when Paratethys became isolated from the Tethys ocean during the early part of nannoplankton zone NP23 (Voronina and Popov, 1984; Báldi, 1984; Rögl, 1997; Rusu, 1999 Schulz et al., 2004). Later, the connection with the open ocean was partially restored during upper NP23 (Popov et al., 1993).

The thickness of the Ruslar Formation varies considerably, from some tens of meters north of Varna (Valchev et al., 2018), to ~70 m in the Varna area, to ~400 m in the shelf sector of the Kamchia Basin (e.g., in the Samotino More well, for location see Figure 1; Sachsenhofer et al., 2009; Mayer et al., 2018a), and up to several kilometers in the West Black Sea Basin (e.g. Nikishin et al., 2015). Offshore Bulgaria, the Ruslar Formation is cut by a deep west-east-trending shelf-break canyon (the Kaliakra canyon), which developed during Lower Oligocene (Late Solenovian) time and which became filled with Oligocene to Middle Miocene deposits (Mayer et al., 2018a). Diatom-rich sediments occur in the Lower Miocene part of the canyon fill, which, although partly Oligocene in age, is not considered as part of the Ruslar Formation (Figure 2.4). Near Karadere (known also as Black Cape), a part of the Ruslar Formation is exposed in 20 m-high cliffs on the Bulgarian Black Sea coast (Suttill, 2009).

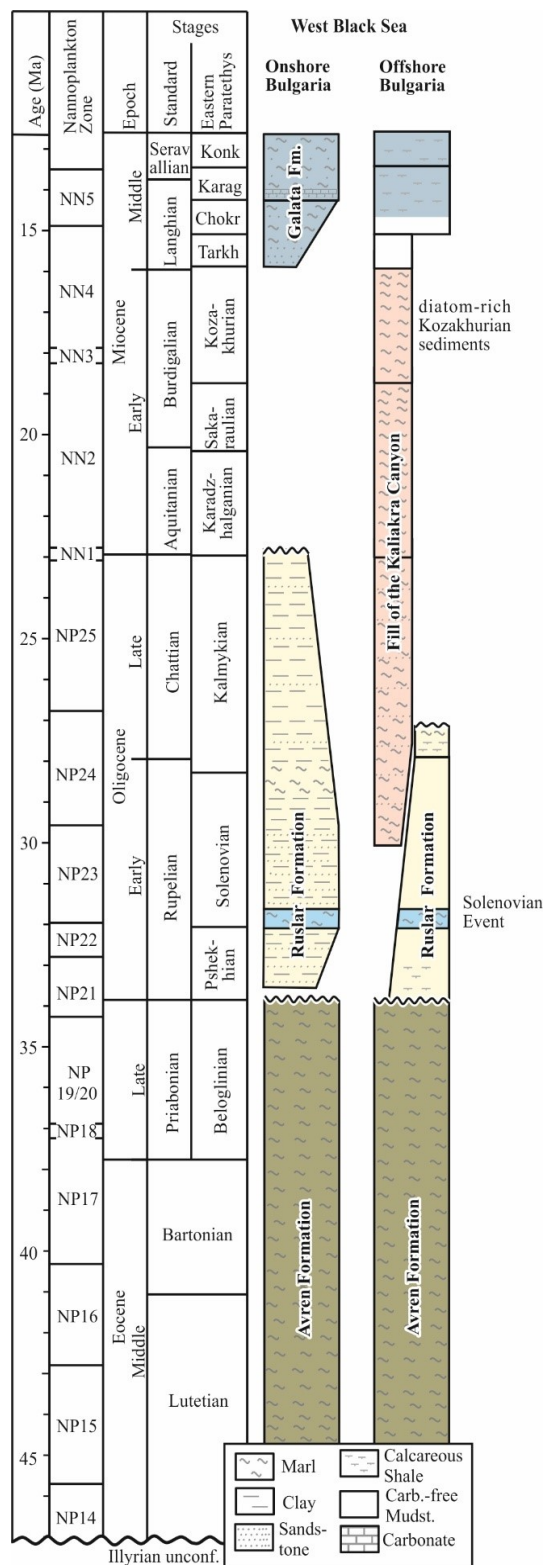


Figure 2.4. Stratigraphy of Middle Eocene to Middle Miocene sediments onshore (mainly after Suttill, 2009 and Valchev et al., 2018) and offshore Bulgaria (after Sachsenhofer et al., 2018b). unconf. – unconformity; Carb.-free Mudst. – carbonate free mudstone.



## 2.3 Eastern Carpathian Bend Zone

### 2.3.1 *Sibiciu de Sus, Romania*

The Eastern Carpathian Bend Zone (ECBZ) is located between the E-W trending Southern and the N-S trending Eastern Carpathians (Figure 2.5). The ECBZ is approximately 80 km long and is represented by the external unit of the Carpathian fold-thrust belt (e.g., Săndulescu, 1984) comprising, from west to east, the Teleajen, Audia, Macla, Tarcău, Marginal Fold and Subcarpathian Nappes. A brief description of the stratigraphy focused on the Tarcău and Marginal Nappes and partly on the Subcarpathian Nappe is presented below.

The stratigraphy commences with Lower Cretaceous deep marine black shales with some sandy turbidites towards the top (Ștefănescu, 1978) followed by Upper Cretaceous variegated shales with radiolarite and calcareous turbidite beds known as Horgazu and Hangu beds (Schleder et al., 2019). The overlying Paleocene and Eocene successions are represented by the Tarcău Formation, a deep marine sandy sequence and the shale-dominated Colți Formation (Schleder et al., 2019).

The Oligocene to Lower Miocene deposits is characterised by two intercalating lithofacies: the Pucioasa-Fusaru and Bituminous Kliwa facies. The distal “Pucioasa-Fusaru lithofacies” (Pătruș, 1955; Grigoraș, 1955) represents deep marine shales interbedded with thin mica-rich sandstone beds derived from uplifted nappes in the west (Săndulescu et al., 1981). The more proximal “Bituminous Kliwa lithofacies” (Patrulius et al., 1968; Săndulescu et al., 1995) is located closer to the foreland and, therefore, it has provenance in East European Platform (e.g., Săndulescu et al., 1995; Grasu et al., 2007).

In the ECBZ, the Bituminous Kliwa lithofacies is divided into several sedimentary units described in detail by Dumitrescu et al. (1970) and their terminology is adopted here. A visual representation of the Bituminous Kliwa lithofacies is provided in Figure 2.6. At the base, the succession commences with the Lower Menilites Formation which is represented by siliceous menilites and bituminous calcareous shales, followed by the Lower Dysodile Formation characterised by dysodile (i.e., shale) with rare sandstone intercalations (Dumitrescu et al., 1970).

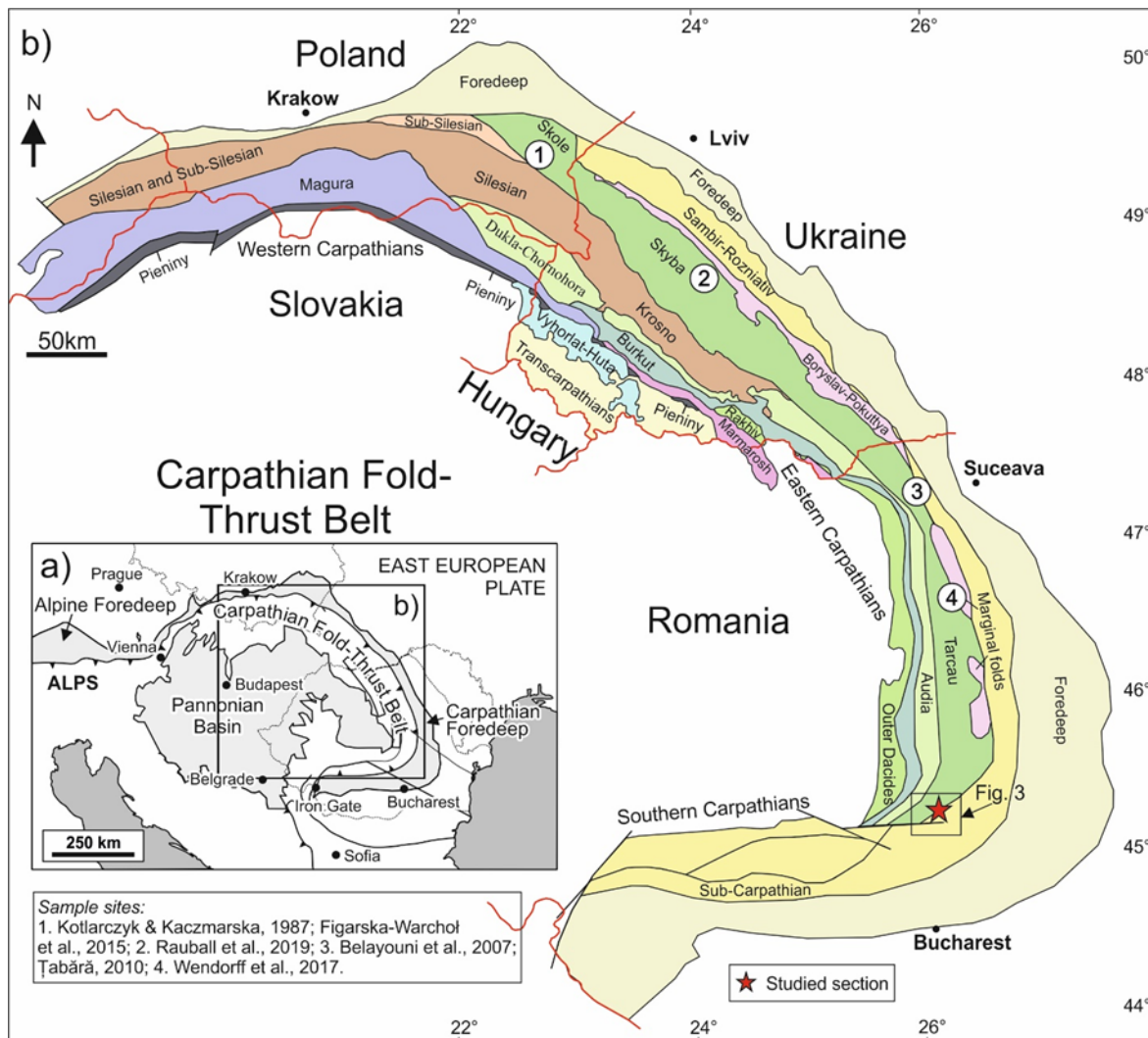


Figure 2.5. a. Outline map of the central-eastern Europe showing the location of the Carpathians; b. Structural map of the Carpathian fold-thrust belt with the position of the studied section and sample locations discussed in the paper; c. rectangle on the main map shows the position of Figure 2.7. Map redrawn after Săndulescu (1984), Glushko and Kruglov (1986), Ślęczka et al. (2006).

The overlying Lower Kliwa Formation is dominated by thick layers of quartz-rich sandstone with rare dysodile intercalations. Locally the Lower Kliwa Formation is covered by the Upper Dysodile Formation, which is composed of dysodiles and rare sandstone intercalations (Dumitrescu et al., 1970). The overlying Podu Morii Formation is defined by calcareous sandstones intercalated with marls.

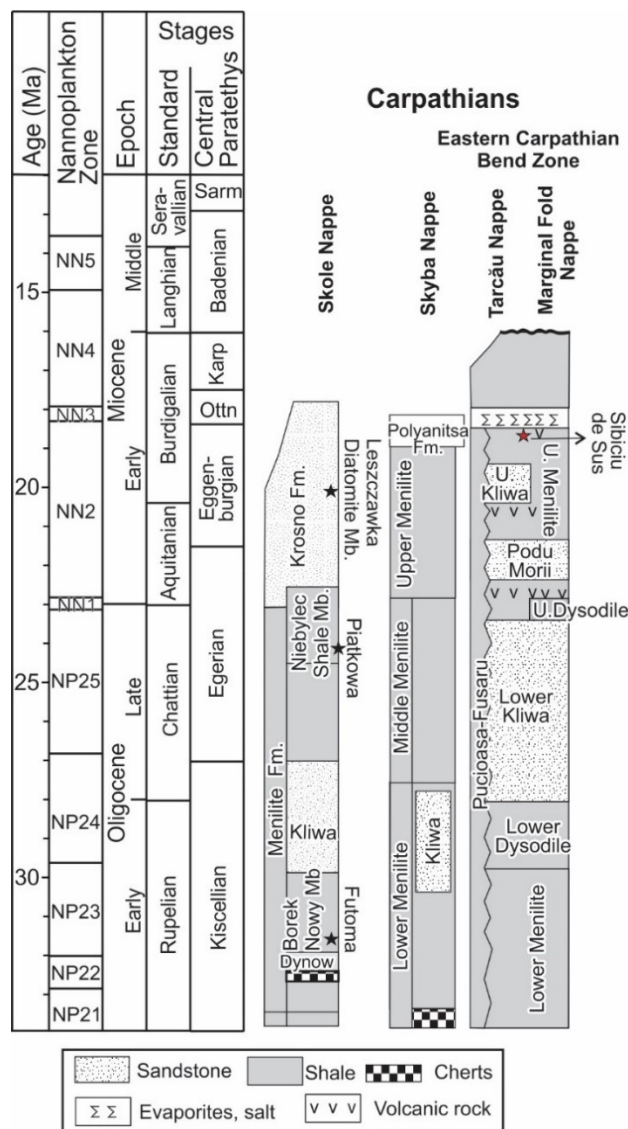


Figure 2.6. Stratigraphic position of diatomite occurrences (stars) within the Carpathian realm, plotted on a simplified stratigraphy of Oligocene to Miocene (compiled from Kotlarczyk and Kaczmarska, 1987; Rauball et al., 2019; Dumitrescu et al., 1970; Ștefănescu et al., 2000; Schleder et al., 2019). U.-upper; menilites-siliceous rocks; dysodile-shaly rocks.

The Upper Kliwa Formation is locally present and composed of friable quartz-rich sandstone. The uppermost part of the Bituminous Kliwa lithofacies is formed by the Upper Menilite Formation represented by menilites and diatomites. Rarely, supra-Menilites beds are observed and contain an alternation of quartz-rich sandstone, dysodiles and occasional tuffs (Dumitrescu et al., 1970).

Sedimentation continued with deposition of a regional evaporitic level during the early Burdigalian (e.g., Ștefănescu et al., 1978; Schleder et al., 2019). The Middle Miocene (Badenian to Middle Sarmatian) succession includes different lithologies: tuffs, marls, silts, locally salt and sandstones (Ștefănescu et al., 2000). The stratigraphic succession ends with a post-tectonic cover represented by Middle Sarmatian to Recent strata (Ștefănescu et al., 2000; Schleder et al., 2019).

The diatomites of the Upper Menilite Formation are exposed in an abandoned quarry (Figure 2.7). The quarry is known under several names, such as Sibiciu de Sus, Pătărlagele and Burdușoia Hill. In this thesis the name of Sibiciu de Sus when referring to the quarry. The quarry is located 2.5 km northeast from the Sibiciu de Sus city, in Buzău county (coordinates: 45°20'46.9"N, 26°22'15.3"E). Overall, the exposed rocks are part of a major NE-SW trending anticline, plunging to the SW. The diatomites are highly deformed both due to compressional tectonics and soft-sediment deformation. This complexity makes the lateral correlation of different layers very challenging. Vasiliu et al. (1996) and Frunzescu and Brănoiu (2004) divided the quarry into eight stratigraphic units, from bottom to top:

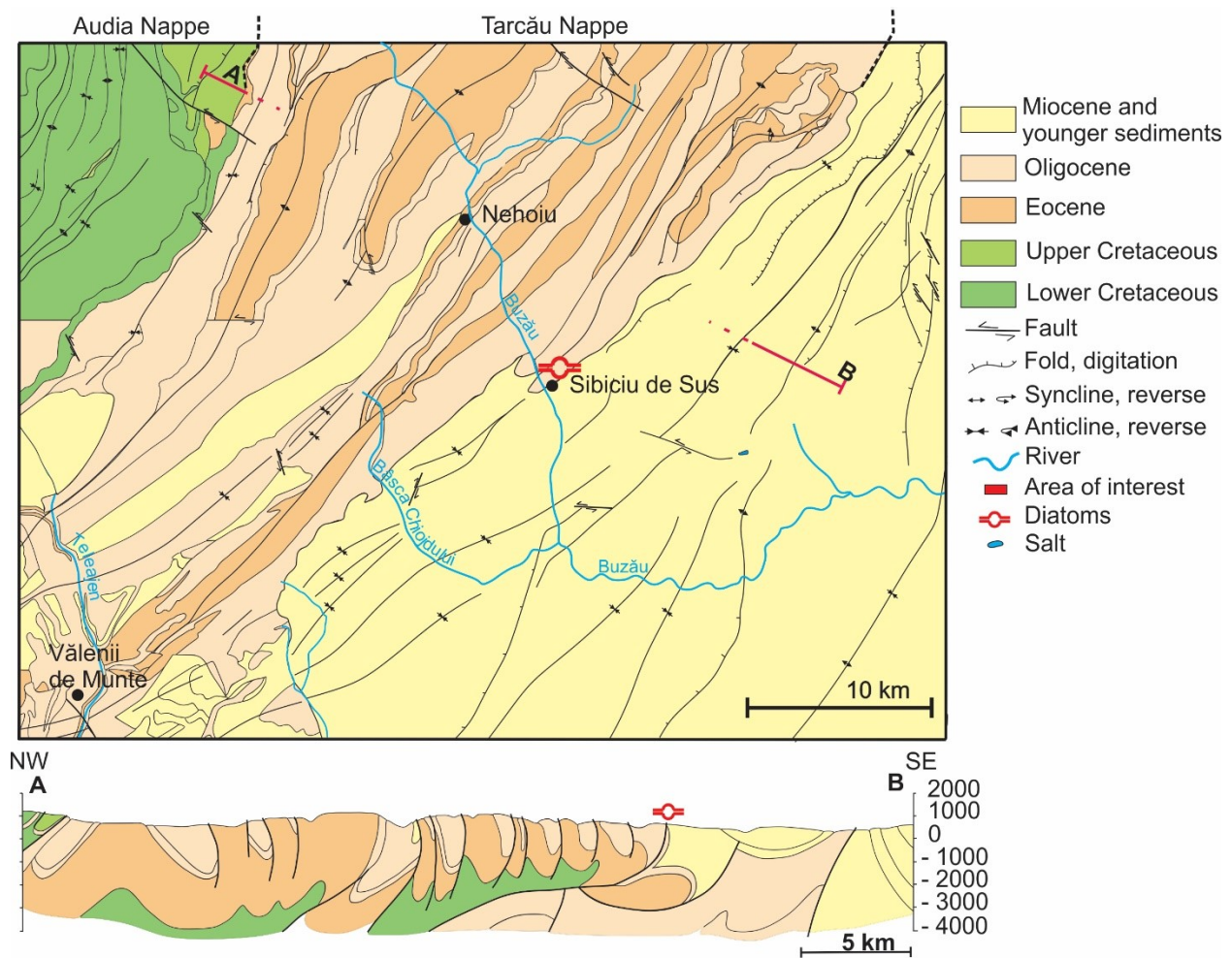


Figure 2.7. Simplified geological map and cross section of the studied area (redrawn after Dumitrescu et al., 1970, sheet 29 – Covasna; Motaș et al., 1968 sheet 36 – Ploiești).

**Alternation of Kliwa sandstone and dysodile-like rocks** made up of alternations of sandstones, dysodiles, and locally diatomaceous shales.

**Menilites** are represented by menilites, argillaceous diatomaceous shales transitioning into diatomite. Menilites have grey to black colour and are very compact with conchoidal and splintery fractures. These rocks tend to be heavier than diatomites. Two units, i.e. units i and ii, exposed in the core of the anticline, more than 30 m thick, are highly folded, faulted, and contain slumps and dykes.

**Alternation of white and black diatomite** is a unit characterized by thin layers of black, organic matter-rich and whitish, organic matter-poor diatomites, heavily faulted, and it has a thickness of about 8 m and 4 m, on the SE and NW limbs, respectively.

**Impure diatomites** are grey to blackish diatomites, with rare white laminae, with a thickness of 11 m on the SE limb and 6 m on the NW limb of the anticline.

**Pure diatomite** is represented on the SE limb by 8 m thick pure white diatomite. The pure diatomite is changing the colour to grey at the base of the unit. The rock is fine-grained, porous and forms conchoidal fractures. The unit can reach 30 m thickness in the NW limb of the anticline.

**Alternation of Kliwa sandstone with diatomite** is an approximately 20 m thick unit, and it is composed of quartz-rich sandstone beds, centimetres to metres thick and cm-thick argillaceous diatomites. Tuffaceous diatomite has been described from the NW limb. The tuffaceous diatomite has a beige-yellowish colour, is massive and has uneven fractures.

**Breccia zone** is an approximately 12 m thick layer with mudstones, tuffs, diatomites, sandstones and micas occurring at the SE limb of the anticline. Marls with radiolaria, and marls and tuffaceous rocks with foraminifer *Globigerina* were also described.

**Grey marls** is a unit with grey to blackish marls, about 15 m thick, and they are restricted to the SE part of the quarry. There are layers with sandstone with some rare tuffaceous laminae.

In this study, we follow the above described nomenclature of Vasiliu et al. (1996) and Frunzescu and Brănoiu (2004), making updates only where we found it necessary.

## 2.4 Gyöngyöspata Basin (Pannonian Basin)

### 2.4.1 Szurdokpüspöki, Hungary

The Szurdokpüspöki quarry is located about 50 km northeast of Budapest and 3.2 km SE from the Szurdokpüspöki locality at the southwestern slope of the Mátra Mountains, (Figure 2.8). The diatomaceous rocks of Szurdokpüspöki accumulated in the Gyöngyöspata Basin, a small sub-basin of the Pannonian Basin.

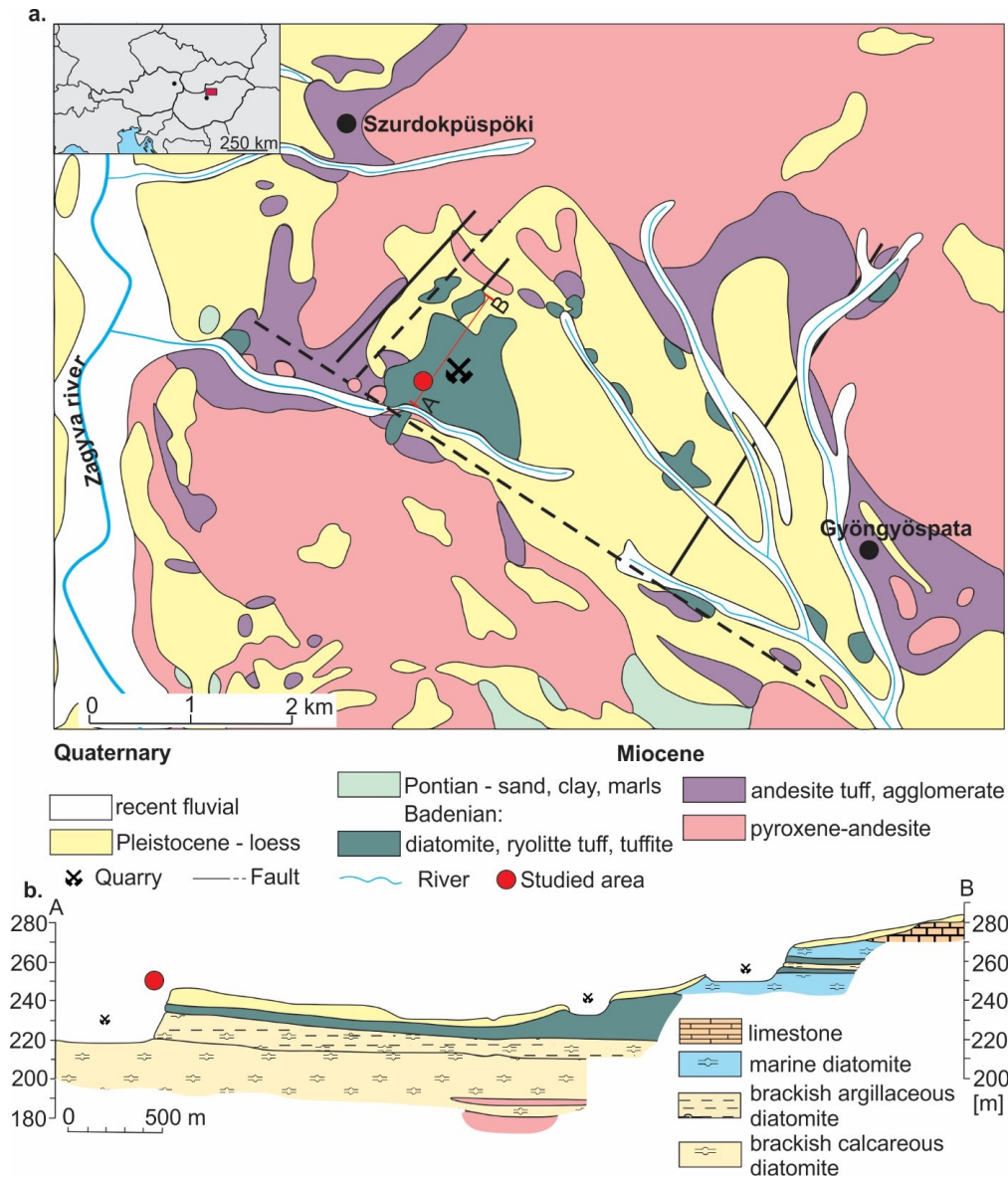


Figure 2.8. Geological map (a.) and geological cross-section (b.) of the Szurdokpüspöki quarry indicating the study area (after Hajós, 1986).

The basement of the Gyöngyöspata Basin is composed of Karpatian to Badenian (early to middle Miocene) pyroxene-andesite, andesite, rhyolite, dacite and tuff (Hajós, 1968, Varga et al., 1975). The irregular volcanic surface is covered by middle Miocene rocks, up to 300 m thick. The middle Miocene sediments in the Szurdokpüspöki quarry were described in detail by Hajós (1986) and include from base to top (a) an approximately 50-m-thick sequence with freshwater to oligohaline diatomite; (b) light greyish to white rhyolite tuff with pumice and mollusc shell remains, about 20 m thick; (c) brackish-marine calcareous and marly diatomite, approximately 90 m thick and 60 m of brackish-freshwater diatomite, which are overlain by (d) (“Leitha-“) limestone, 24 m thick. The Pliocene and the Quaternary cover are represented by andesitic tuffs (30 m) and tuffaceous clays (20 m).

## **2.5 Alpine-Carpathian Foredeep Basin**

### ***2.5.1 Parisdorf and Limberg, Austria***

Diatomaceous rocks of early Oligocene (mid-Burdigalian) age in the Alpine-Carpathian Foredeep accumulated along the south-eastern margin of the Bohemian Massif and are attributed to the Limberg Member of the Zellerndorf Formation (Roetzel et al., 2006; Grunert et al., 2010). Based on sedimentological and paleontological evidence, as well as foraminiferal stable isotope data and dinocyst assemblages, Grunert et al. (2010) suggested that the clay-diatomite succession of the Limberg Member accumulated along the steep escarpment of the Bohemian Massif due to upwelling.

In the study area, Paleozoic crystalline rocks of the Bohemian Massif are overlain by lower Miocene nearshore sands and gravels (upper Eggenburgian Burgschleinitz Formation) and sandy shallow marine limestones (lower Oligocene Zogelsdorf Formation), which laterally and vertically pass into deep-water pelitic sediments (Zellerndorf Formation), 25 to 100 m thick. The laminated diatomaceous sediments of the Limberg Member within the Zellerndorf Formation reach a maximum thickness of 5 to 7.5 m but pinch out laterally. The top of the Zellerndorf Formation is disconformably overlain by lower-middle Miocene marine and freshwater sediments covered by Pleistocene loess (Grunert et al., 2010). Diatomaceous sediments of the Limberg Member have been mined in small quarries, currently abandoned. The Parisdorf diatomite mine is located about 400 m SE of Parisdorf (Figure 2.9). Here, the diatomites are exposed at the base, followed by pelites of the Zellerndorf Formation. The Neogene sediments are covered by

Pleistocene deposits. The Limberg quarry is located 800 m NE of Limberg (Figure 2.9). Similar to the Parisdorf mine, the finely stratified diatomites of the Limberg Member are exposed at the base, followed by the pelites of the Zellerndorf Formation.

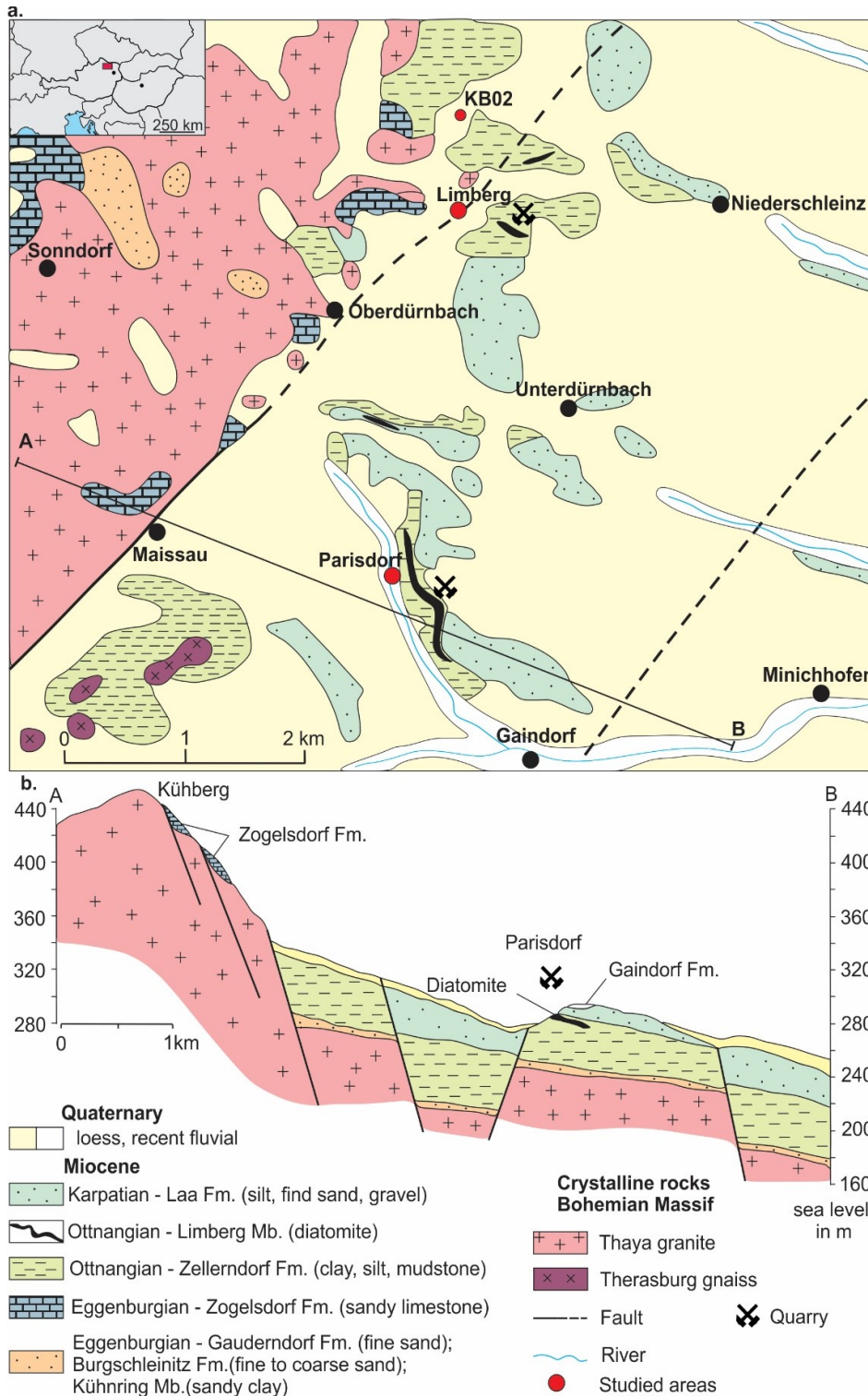


Figure 2.9. Geological map (a.) and cross section (b.) of the Limberg and Parisdorf study sites together with the position of the studied borehole (after Roetzel, 1999; 2004).



## Chapter III

This chapter describes all methods used for this study and all the references are cited accordingly. Moreover, some paragraphs written in this chapter are from articles published in peer-reviewed journals or currently submitted articles (see sub-chapter 4.1.1. for list of publications).

### 3.1 Samples and Methods

#### 3.1.1 Samples

For this study in total 185 samples were selected in several field campaigns as follows:

- 78 samples from *Karaburun, Turkey* have been collected in 2016 together with Jan Mayer, Aral Okay, Mike Simmons and Gabor Tari.
- 22 samples from *Sibiciu de Sus, Romania* have been collected in 2016 together with Alexandra Tamas and Dan M. Tamas.
- 29 samples from *Szurdokpüspöki, Hungary* have been collected in 2017 together with Jan Mayer, Prof. Reinhard F. Sachsenhofer and Gabor Tari.
- 13 samples from *Parisdorf* and 7 from *Limberg, Austria* have been collected in 2018 together with Jan Mayer, Prof. Reinhard F. Sachsenhofer and Gabor Tari. On the courtesy of Reinhard Roetzel and Patrick Grunert, 12 samples were provided from the Limberg-Hangbrücke (KB2/07) borehole drilled north of Limberg in 2007.
- 29 samples from *Karadere, Bulgaria* have been collected in 2018 together with Emanuil Kozuharov and Prof. Reinhard F. Sachsenhofer. On the courtesy of Prof. Reinhard F. Sachsenhofer was provided 6 samples from the P-79 borehole drilled nearshore Karadere.

#### 3.1.2 Methodology

The author of this thesis performed the following analysis (Table 3.1): Eltra Analysis (bulk parameters), Rock Eval Pyrolysis, petrography, XRD measurements, organic petrography (microscopy, vitrinite reflectance measurements), AAS (in cooperation with Prof. W. Prochaska), SEM analysis on the diatoms (some samples were done in cooperation with Aleksander Horvat at the Slovenian Institute of Paleontology).

Biomarker analysis, strontium isotopes and nannoplankton analysis were performed by cooperation partners and the results were interpreted by the author (biomarkers: Achim Bechtel

and Magdalena Pupp; strontium isotopes: Rachel Flecker, Vanessa Fairbank from University of Bristol and Ryan Ickert from SUERC, United Kingdom; nannoplankton: Stjepan Coric from Geologische Bundesanstalt für Österreich). Assistance was provided by Jakub Witkovski, Andrzej Witkowski from University of Szczecin, Poland and Aleksander Horvat from the Slovenian Institute of Paleontology for the identification of the fossil diatoms.

Table 3.1: Overview of the applied methods and sample numbers.

	Samples	Bulk param.	Rock Eval	XRD	Biomarkers	Petrography	VR	Strontium	Diatoms	FAAS
Karaburun, Tr.	78	78	78	78	10	17	10	34	*	*
Karadere, Bg.	29	29	29	29	11	10	*	*	11	29
<i>P-79, Bg. borehole</i>	6	6	6	*	*	*	*	*	*	6
Sibiciu de Sus, Ro.	22	22	22	22	12	10	4	*	10	22
Szurdokpüspöki, Hu.	24	24	24	24	*	3	*	*	13	15
Parisorf, At.	13	13	13	13	*	2	*	*	7	5
Limberg, At.	7	7	7	7	*	3	*	*	4	9
<i>Limberg, At. borehole</i>	12	12	*	*	*	*	*	*	*	*
<b>Total</b>	<b>191</b>	<b>191</b>	<b>179</b>	<b>173</b>	<b>33</b>	<b>45</b>	<b>14</b>	<b>34</b>	<b>45</b>	<b>86</b>

Bulk para.- bulk parameter, Rock Eval- Rock Eval pyrolysis, XRD- x-ray diffraction, VR- vitrinite reflectance measurements and organic petrography, Strontium- strontium isotopes, diatoms- preparation and scanning electron microscope imaging of diatom frustules, FAAS- flame atomic absorption spectroscopy; Tr. Turkey, Bg. Bulgaria, Ro. Romania, Hu. Hungary, At. Austria.

A short description of the analytical methods used for this thesis is given below.

### 3.1.2.1 Bulk parameter measurements

Total carbon (TC), total sulphur (S) and total organic carbon (TOC) contents were analysed using an ELTRA Elemental Analyzer for all samples. Samples for TOC measurements were decarbonised with concentrated phosphoric acid. Results are given in weight percent (wt. %). Total inorganic carbon (TIC) was determined ( $TIC = TC - TOC$ ) and used to calculate calcite equivalent percentages ( $TIC \times 8.333$ ).

### 3.1.2.2 Rock Eval Pyrolysis

Pyrolysis measurements were performed using a “Rock-Eval 6” instrument. The amount of free S1 hydrocarbons (mg HC/g rock) and the amount of S2 hydrocarbons generated during pyrolysis (mg HC/g rock) were determined and used to calculate the petroleum potential (S1 + S2

[mg HC/g rock]), and the production index ( $PI = S1 / (S1 + S2)$ ) (Lafargue et al., 1998), and the hydrogen index ( $HI = S2 / TOC \times 100$  [mg HC/g TOC]). Tmax was measured as a maturity indicator. The amount of hydrocarbons, which can be generated below 1 m<sup>2</sup> of surface area was calculated using the Source Potential Index [ $m =$  thickness;  $\delta =$  bulk density] of Demaison and Huizinga (1994).

### ***3.1.2.3 Geochemical analysis-Biomarkers***

Samples selected for biomarker analysis were extracted using dichloromethane in a Dionex ASE 200 accelerated solvent extractor at 75° C and 50 bar. Afterwards, asphaltenes were precipitated with a hexane-dichloromethane solution (ratio 80:1 according to volume) and separated by centrifugation. Medium-pressure liquid chromatography (MPLC) using a Köhnen-Willsch instrument was used to separate the hexane-soluble fractions into NSO compounds, saturated hydrocarbons and aromatic hydrocarbons (Radke et al., 1980).

The saturated and aromatic hydrocarbon fractions were analysed by a gas chromatograph equipped with a 30 m DB-5MS fused silica column (i.e. 0.25 mm; 0.25 mm film thickness), coupled to a ThermoFischer ISQ Dual-quadrupole mass spectrometer. Using Helium as a carrier gas, the oven temperature was programmed from 70° C to 300° C at 4° C/min increase, followed by an isothermal period of 15 min. With the injector temperature at 275° C, the samples were injected seamlessly. The spectrometer was operated in the EI (electron ionisation) mode over a scan range from m/z 50 to 650 at 0.7 s total scan time. The procession of the data happened with an Xcalibur data system. Individual compounds were identified by retention time in the total ion current (TIC) chromatogram and the comparison of the mass spectra with published data. Percentages and absolute concentrations of various compound groups in the saturated and aromatic hydrocarbon fractions were calculated using peak areas in the gas chromatograms and their relations to the internal standards (deuterated n-tetracosane and 1, 1'-binaphthyl, respectively). Concentrations were normalised to TOC.

### ***3.1.2.4 Organic petrography and vitrinite reflectance***

Polished blocks were prepared for ten samples. Semi-quantitative maceral analysis using reflected white light and fluorescence light and vitrinite reflectance measurements were performed using an incident light Leitz microscope and following established procedures (Taylor et al., 1998).

Vitrinite reflectance ( $R_r$ ), a maturity parameter, has been determined on 30 to 50 vitrinite particles and mean values have been calculated (with standard deviation). An Yttrium- Aluminium-Garnet has been used as standard ( $R_r = 0.899\%$ ).

### 3.1.2.5 Mineralogy – XRD

The bulk mineralogical composition was determined with a Bruker AXS D8 Advance X-ray diffraction spectrometer (copper radiation generated at 40 kV and 40 mA). The powdered samples have been placed carefully in sample holders to create a flat upper surface to achieve a random distribution of lattice orientation. To identify and quantify the different mineral phases, the software Diffrac.Eva and the method described by Schultz (1964), which is based on peak heights, were used. X-ray power diffraction (XRPD) is the main technique used to determine the type of silica phase (e.g. opal-A, opal-CT). The prominent diffraction responses for opal-A centred near  $\sim 4\text{\AA}$  ( $\sim 22.2^\circ 2\theta$ ) and for opal-CT centred at  $4.09\text{\AA}$  ( $\sim 21.75^\circ 2\theta$ ) (Jones and Segnit, 1971; Flörke et al., 1991; Smith, 1998) (Figure 3.1).

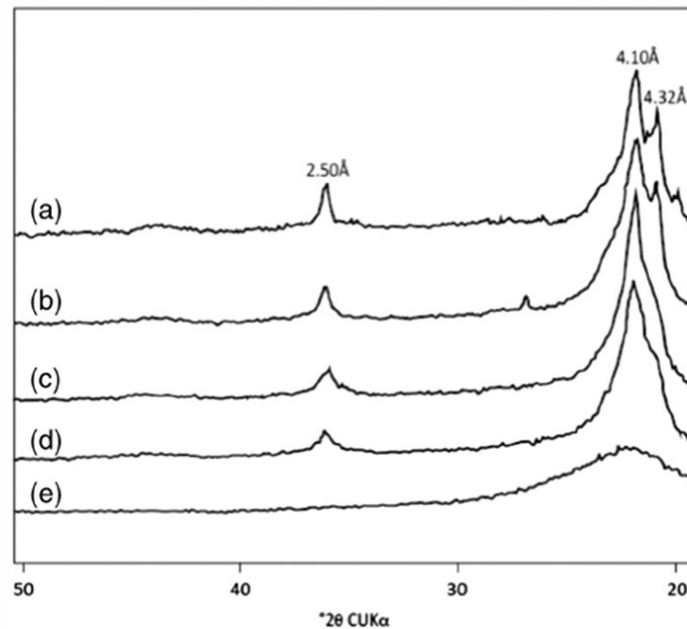


Figure 3.1. Typical XRD traces of opal-CT (a to d) and opal-A (e). Gradual increase of order from the bottom to the top is seen in the sharpening of the peak from  $4.32\text{\AA}$  to  $4.10\text{\AA}$  (Wilson, 2014, Jones and Segnit, 1971).

### ***3.1.2.6 Petrography***

Thin sections were prepared from the rock samples. They were studied using a Leica DM 2500P microscope and pictures were taken with a Leica DFC490 camera.

### ***3.1.2.6 Flame atomic absorption spectroscopy***

Flame atomic absorption spectroscopy was performed on selected samples to determine organic silica content using the methods described by Zolitschka (1988). Approximately 100 mg of sample material and 50 mL of 0.5 mol/L potassium hydroxide solution were boiled for 1 h to dissolve the opaline diatom valves. Afterwards, a 5-mL aliquot of the solution was diluted with distilled water (1:1). A PerkinElmer 3030 atomic absorption spectrometer was used for analysis and operated with a CH<sub>4</sub>-N<sub>2</sub>O flame to create free Si atoms in a gaseous state. A Si-hollow cathode lamp was used as a spectral line source. The AAS was calibrated using a Merck CertiPUR\* silicon-standard solution (#1.1231.0500).

### ***3.1.2.7 Strontium isotopes***

Strontium isotope data were determined at the University of Bristol. For strontium isotope analysis, foraminifera were separated from semi-consolidated sediment samples by covering with water in a plastic bottle and agitating until the sample disaggregated. This material was dried and sieved, and planktic foraminiferal tests were picked by hand under a binocular microscope. After picking, samples were cleaned using the clay removal technique of Barker et al. (2003), in which the picked foraminifera were lightly crushed and then agitated in water to flocculate and decant residual clay. Carbonate samples were weighed into PFA vials and leached in ammonium acetate to remove groundwater salts and displace contaminant Sr on exchangeable sites (e.g., Bailey et al., 2000). The remaining material was rinsed twice in deionised water, and then dissolved in dilute HCl. All HCl and HNO<sub>3</sub> were prepared by sub-boiling distillation in PFA (e.g., Mattinson, 1972). Sr was separated from matrix elements using Sr.Spec resin (Horwitz et al., 1991; 1992) using a nitric acid chemistry procedure adapted from Pin et al. (1994), where samples are loaded in 8M HNO<sub>3</sub>, cleaned in sequential steps of 8M HNO<sub>3</sub> and 3M HNO<sub>3</sub>, and Sr eluted in 0.01 M HNO<sub>3</sub>. After ion exchange chemistry, samples were loaded onto purified Re filaments in a Ta emitter solution (cf., Birck, 1986). Total procedural blanks yielded values ranging from 300-500 pg, which are negligible relative to the amount of sample run. Isotopic analyses were made on a VG-Sector-

54 thermal ionisation mass spectrometer using a three-cycle dynamic multicollector routine and an exponential mass fractionation correction relative to  $^{86}\text{Sr}/^{88}\text{Sr} = 0.1194$  (e.g., Nier, 1938; Moore et al., 1982; Steiger and Jager, 1977; Hans et al., 2013). Filaments were slowly heated to 2.4 A, and then focussing and filament current was adjusted to achieve a stable  $10^{-11}$  A ion beam on  $^{88}\text{Sr}$ . Analyses are typically run for 15-20 blocks of 10 cycles for approximately 1.5-2 hours. Rubidium interferences were monitored but were negligible. Typical precision on the  $^{87}\text{Sr}/^{86}\text{Sr}$  is  $\pm 20$ -30 ppm (2SE). Repeated measurements of reference material NBS987 at similar run conditions ( $0.5$ - $1.5 \times 10^{-11}$  A) during the period over which these analyses were made yielded a value of 0.710259 ( $\pm 0.000027$  2SD;  $n = 68$ ), within uncertainty of the convention value of 0.71025, and indicates that the measurement repeatability is commensurate with the within-run uncertainty.

### ***3.1.2.8 Micropaleontological analysis***

#### ***3.1.2.9 Diatoms***

For siliceous microfossil examination several methods were used in order to achieve the best result from the diatomite rock samples and they are described below. Each corresponding location of the analysed samples are mentioned here briefly, more details can be found in chapter IV.

- ***Samples, which yielded positive results for diatom identification***

*Sample locations: Szurdokpüspöki, Hungary; Parisdorf, Austria; Karadere, Bulgaria*

a). 1 g of dry sediment from the samples was treated for two days with 30 ml of 33% hydrochloric acid (HCl) and 30 ml of 33% hydrogen peroxide ( $\text{H}_2\text{O}_2$ ) (Schrader, 1973). After the reaction settled, the solution was heated to  $90^\circ\text{C}$  to finish the rest of the reaction. The samples were cooled and washed three times with 30 ml distilled water. The solution was then sieved through a  $50 \mu\text{m}$  sieve to concentrate the fine fraction. For microscope slides, 5 ml of solution was strewn on a glass slide. For the determination of the relative abundance of diatom genera, the first 300 valves were counted following the method by Schrader and Gersonde (1978). Siliceous microfossil slides were studied using a Leica DM 2500P microscope and pictures were taken with a Leica DFC490 camera.

b). 2 ml of the fine fraction (a.) was placed on an aluminium stub covered with conductive carbon tab and set for the water to evaporate in a fume hood. After the water evaporated, the stubs

were gold sputtered for maximum 20 seconds. Some of the diatom valves were examined and photographed using scanning electron microscope (SEM) Leo 1450EP.

*Sample locations: Sibiciu de Sus, Romania; Limberg, Austria*

Dry rock samples were examined under the scanning electronic microscope (SEM) JSM-IT100 and LEO1450P. An approximately 1×1 cm piece of dry sample sputter with gold was used. For the relative abundance of diatom genera, the first 300 valves were counted using the counting method described in Schrader and Gersonde (1978). Where possible, some of the diatom valves were counted using the SEM LEO1450P at 1000× magnification.

- ***Samples, which yielded negative results for diatom identification***

*Sample locations: Sibiciu de Sus, Romania; Limberg, Austria*

As diatomite samples examined were highly indurated, none of the commonly used methods (Schrader, 1973; Dumitrica, 1970) for siliceous microfossil extraction yielded positive results. The methods applied without success on 1g of sediment in different experiments were:

1. equal amounts of hydrochloric acid (HCl) 33% and hydrogen peroxide (H<sub>2</sub>O<sub>2</sub>) 33%;
2. saturated sulphuric acid (H<sub>2</sub>SO<sub>4</sub>) and potassium permanganate (KMnO<sub>4</sub>)
3. 1% of hydrofluoric acid (HF) solution
4. freezing and thawing the samples in distilled water

The samples were treated for different time periods ranging from hours to several days without yielding positive results. Therefore, no routine light microscope examination could be performed.

### ***3.1.2.10 Nannoplankton***

Smear slides for nannofossil identification were prepared at the Austrian Geological Survey from 10 Karadere, Bulgaria samples using the standard preparation method described by Perch-Nielsen (1985). Nannofossil identifications were made using light microscopy (LM) and scanning electron microscopy (SEM). In LM, all samples were investigated under 1000× magnification with parallel and crossed nicols. Biostratigraphic assignments were made in accordance with the nannoplankton zonation of Martini (1971).

## Chapter IV

### 4.1 Results and interpretation

In this chapter the findings of the study are described and interpreted and all the references are cited accordingly. Most of the results have been published in peer-reviewed journals or are submitted (see below). Moreover, parts of the work have been presented in conferences organized by the American Association of Petroleum Geologists (AAPG).

#### *4.1.1 List of published, accepted and submitted articles*

Tulan, E., Sachsenhofer, R.F., Tari, G., Flecker, R., Fairbank, V., Pupp, M., Ickert, R.B., 2020. Source rock potential and depositional environment of the Lower Oligocene İhsaniye Formation in NW Turkey (Thrace, Karaburun). *Turkish Journal of Earth Sciences*, 29, 64-84. doi:10.3906/yer-1906-14

Tulan, E., Sachsenhofer, R.F., Witkowski, J., Tari, G., Coric, S., Bechtel, A., 2020. Microfossil assemblages (diatoms, calcareous nannofossils, and silicoflagellates), paleoenvironment, and hydrocarbon source rock potential of the Oligocene Ruslar Formation at Karadere, Bulgaria. *Turkish Journal of Earth Sciences*, 29, 154-169. doi:10.3906/yer-1906-14

Tulan E., Radl M., Sachsenhofer R.F., Tari G., Witkowski J. (2020) Hydrocarbon source rock potential of Miocene diatomaceous sequences in Szurdokpüspöki (Hungary) and Parisdorf/Limberg (Austria). *Austrian Journal of Earth Science*, 131(1), 24-42. doi:10.17738/ajes.2020.0002

Tulan E., Sachsenhofer R.F., Tari G., Witkowski, Tămaş DM., Horvat A, Tămaş A (submitted). Hydrocarbon source rock potential and paleoenvironment of Lower Miocene diatomites in the Eastern Carpathians Bend Zone (Sibiciu de Sus, Romania).

#### *List of poster and oral conference presentations:*

Tulan E., Sachsenhofer R.F, Tari G., Pupp M. (2019). Hydrocarbon source rock potential of the Lower Oligocene İhsaniye Formation (Karaburun, Turkey) (poster), in Book of abstracts: Paratethys petroleum systems between the Central Europe and the Caspian Region, AAPG ERC conference, Vienna, 119.



Tulan E., Sachsenhofer R.F., Horvat A., Tari G., Olaru-Florea R.F. (2019). Hydrocarbon source rock potential of Oligo-Miocene diatomaceous rocks in Sibiciu de Sus, Romania (poster), in Book of abstracts: Paratethys petroleum systems between the Central Europe and the Caspian Region AAPG ERC conference, Vienna, 120.

Tulan E., Tari G., Sachsenhofer R.F., Witkowski J., Ćorić S., Bechtel A. (2019). Lower Oligocene fossil flora and fauna assemblages together with the hydrocarbon source rock potential at Karadere Ruslar Formation in Kamchia Basin, Bulgaria (presentation); in Book of abstracts: Exploration and Production in the Black Sea, Caucasus, and Caspian Region, AAPG GTW conference, Batumi.

## **4.2 Western Black Sea Basin**

### **4.2.1 Karaburun, Turkey**

#### **4.2.1.1 Sample and methods**

In total, 78 marl samples from of the İhsaniye Formation were collected west of Karaburun along the Black Sea coast (Figure 2.1). Samples 1 to 70 are from the Hanging Wall Section, whereas samples 71 to 78 were taken from the marly upper part of the Footwall Section (Figure 2.2). The following methods have been applied: bulk parameters measurements, Rock Eval pyrolysis, XRD on all 78 samples, biomarkers analysis on 11 samples, strontium isotopes on 34 samples, petrography on 17 sample and FAAS on 3 samples. Their results are presented below.

#### **4.2.1.2 Results**

#### **4.2.1.3 Lithology**

Two profiles within the İhsaniye Formation were investigated: The Hanging Wall Section and a part of the Footwall Section. Both of the sections are separated by a major fault normal fault (now an inverted fault, see Figure 2.2). The Hanging Wall Section is located west of the major fault and the Footwall Sections northeast of it. The Hanging Wall Section includes sediments approximately 70 m thick and is represented by samples 1 to 70. The section is well exposed (Figure 4.1), and only small parts are covered by vegetation or landslides. Non-exposed parts are marked by question marks in Figure 4.2. The studied composite section is represented by the alternation of light grey marl, carbonate-rich siltstone and sandstone as well as tuffaceous beds

between 56.8 and 58.0 m (Figure 4.2). The frequency of the siltstone layers generally decreases gradually upwards (Figure 4.1), but a few meters above the tuff level there is a gradual change from an argillaceous marlstone to a sandy marlstone (Figure 4.2) displaying a coarsening upwards trend. At about 68 m, the fine-grained sediments are overlain by a prominent mass transport deposit which has a channelized geometry and includes reworked Eocene limestones clasts from the underlying Soğucak Formation and Cretaceous volcanic and metamorphic clasts.

Marls are dark grey when freshly broken, compact and often contain macroscopically visible bioclasts (~2 mm), mostly foraminifera. Laminations are not visible, presumably because of complete bioturbation. Bioturbation structures are visible in a single sample (at 4.9 m of Hanging Wall Section). Under the microscope, the marls consist of a (micro-) sparitic to micritic matrix (Figure 4.3) with frequent foraminifera tests and a variety of detrital grains. The detailed microscopic description of the samples is listed in Table 4.1.

Siltstones and sandstones consist of carbonate and lithic grains and abundant bioclast components (Okay et al., 2019). In thin sections, the calcareous sandstones are dominated by a variety of bioclast: cryptostome bryozoan, echinoderm debris, coralline algae, coral fragments, mollusc debris and small indeterminate foraminifera (Figure 4.4). Angular quartz and lithic fragments are rare, although volcanoclastic fragments are present. Many clasts observed in the calcareous sandstone are reworked from the overlying Soğucak Formation and volcanoclastic basement, as well as the contemporaneous shelf.

Tuffaceous rocks are fine-grained and homogenous. They have a light grey to whitish colour and are very compact and much harder than the surrounding rocks. The microscopic observation reveals the presence of altered glass with an intersertal texture (Figure 4.3). In thin sections observation, the organic matter is more abundant in the lower part of the Hanging Wall Section (0.5-19.1 m), compared to the remaining part of the section and the Footwall Section, where organic matter is rare and frequently replaced by pyrite.

Selected XRD diffractograms are presented in Figure 4.4. According to XRD analysis, the major mineral constituents of the samples are calcite (48%) and clay minerals (24%), whereas quartz, feldspars, pyrite, ankerite, siderite, and dolomite occur as minor constituents (Figure 4.2). Aragonite occurs in significant amounts in the lower part of Hanging Wall Section, and a single

sample from the same section (46.9 m) contains gypsum (4%). In addition, the bSi for 4 selected samples are in average 5.06%.



Figure 4.1. a-d: Studied outcrop of the Hanging Wall Section of the İhsaniye Formation with detail pictures (selected sample locations are shown for reference). a, b) Lower part of the section represented by organic-rich marls intercalated with calcareous sandstones. c) upper part of the section represented by organic free marls with fewer calcareous sandstone layers; d) top of the studied section covered by the debris flow.

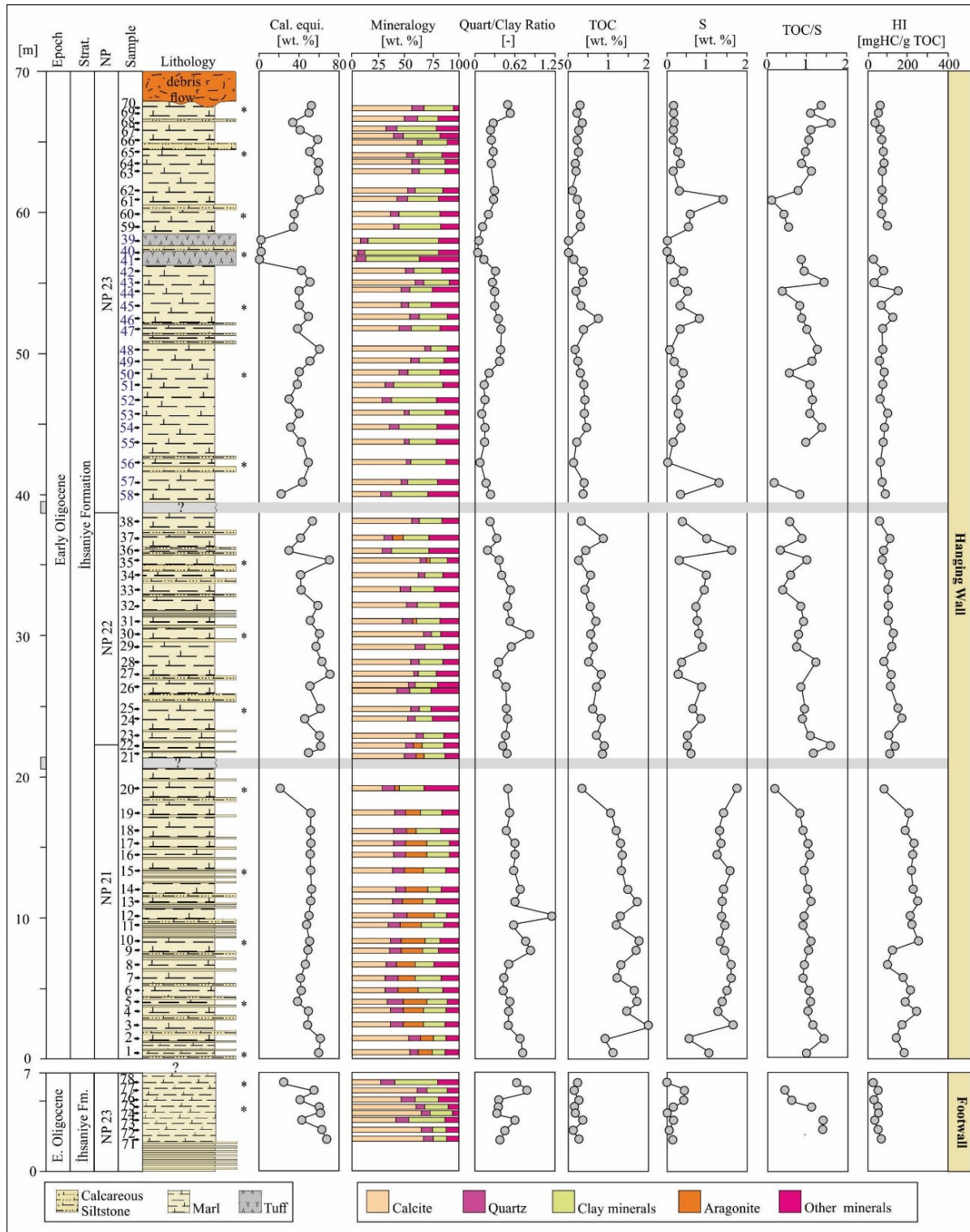


Figure 4.2. Bulk geochemical parameters and mineralogy of the İhsaniye Formation. Cal. equi.- calcite equivalent; TOC-total organic carbon; S-total Sulphur; HI-Hydrogen Index; Other minerals: pyrite, feldspar, ankerite, siderite, dolomite. \* position of thin sections.

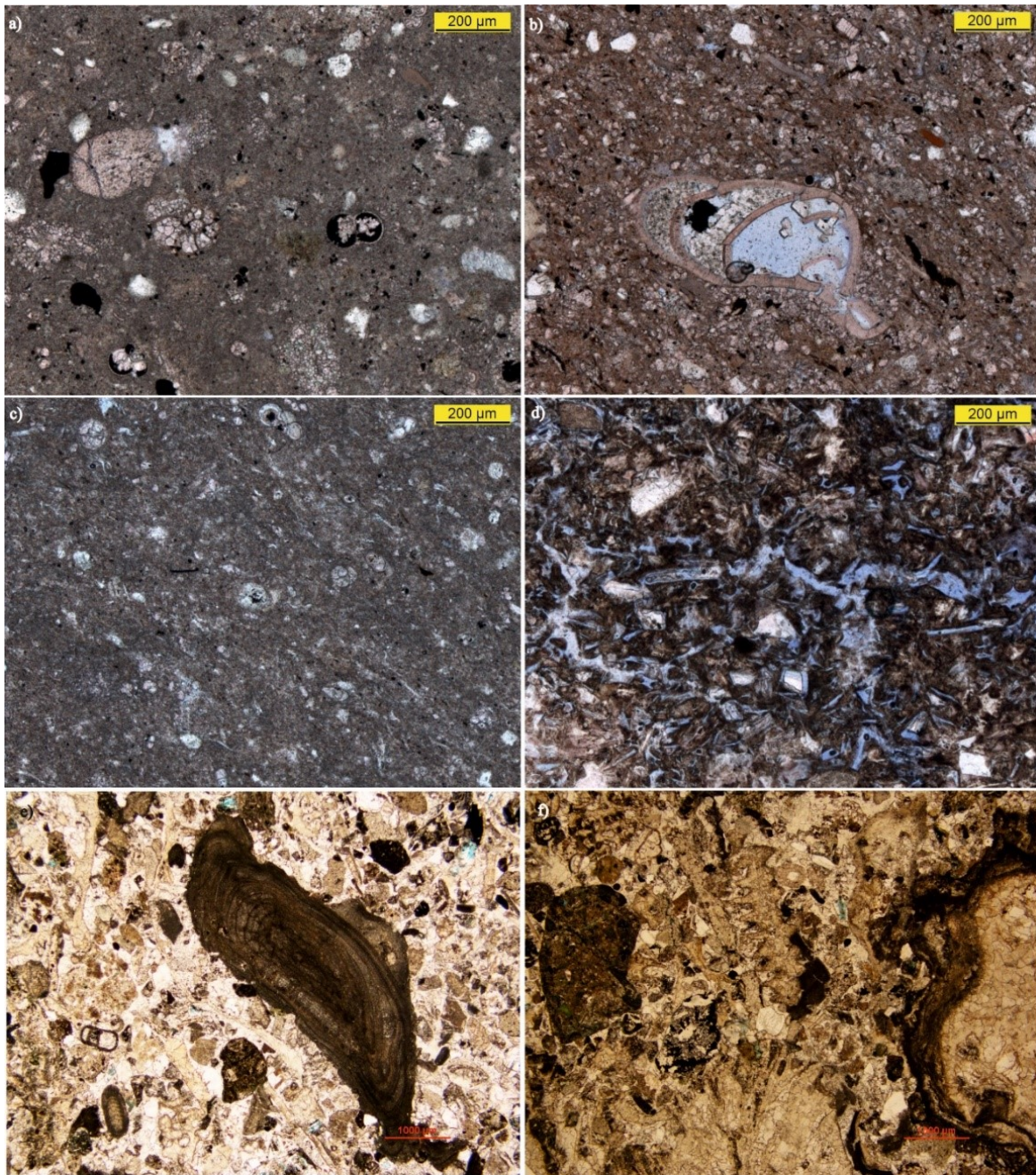


Figure 4.3. Thin section photographs. Footwall Section: a) Sample 75 (4.8 m)-Fossiliferous sandy marlstone with a matrix composed of micrite; Hanging Wall Section: b) Sample 1 (0.5 m)-Silty marlstone with a matrix composed of microsparite with few intraclasts and fossils; c) Sample 56 (42.2 m)-Marlstone with a matrix composed by microsparite and micrite with frequent foraminifera; d) Sample 40 (57.1 m)-Tuff consisting of altered volcanic glass with an intersertal texture; Calcareous sandstone (photographs by courtesy of Mike Simmons): e) Sample below 35 (34.8 m): bioclastic grainstone with a variety of fragmentary bioclasts: coralline algae (centre of image), mollusc debris and small indeterminate foraminifera; f) Sample below 66 (64.7 m) bioclastic grainstone with coral fragments some with algal or cyanobacterial encrustations.

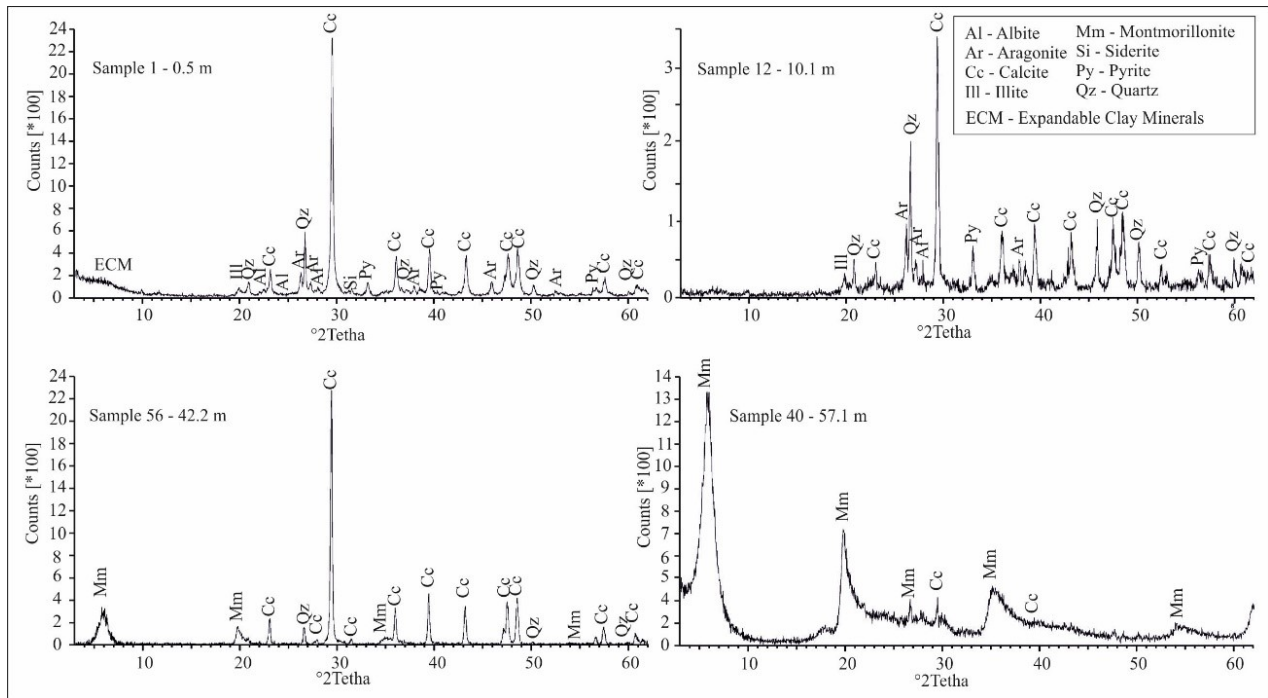


Figure 4.4. X-ray powder diffractograms of selected samples from the İhsaniye Formation (Hanging Wall Section): samples 1, 12, 56 and 40; (for samples position see Figure 2.2). Sample 40 represents the tuffaceous rock.

Based on mineralogy, the Hanging Wall Section can be subdivided into a lower part (0-19 m; samples 1-19) and an upper part (21.9-67.5 m; samples 20-70). The lower part is characterised by abundant aragonite (avg.: 18%) and with the exceptions of the lowermost samples, relatively uniform calcite (~40%) and quartz contents (~10%).

The upper part of the Hanging Wall Section is characterised by stronger compositional variations, and aragonite is present (in minor amounts) only below 36.9 m (samples 20-37; avg.: 3%). Samples from the tuff layer (56.8-58.0 m) are characterised by very high percentages of montmorillonite (avg.: 62%), which was formed by the alteration of volcanic glass (Figure 6). High percentages of clay minerals are also observed in mudstones between 42.2 and 47.8 m (samples 56-51), an interval, which contains low amounts of detrital quartz (3-9%). Consequently, the clay minerals/quartz ratio of these samples is very low (~0.1). Interestingly, there is a general upward decrease in clay minerals/quartz ratio, which starts in the lower part of the section (sample 9 at 7.9 m) and terminates in the middle part of the upper part (sample 56 at 42.2 m) (Figure 4.2).

Table 4.1. Thin section descriptions

Lithotype	Description	Env.	No.	
Argillaceous to sandy marlstone	Sandy marlstone with a micrite matrix; detritus grains (C), moderately sorted: feldspars (pl. (15-33 $\mu$ ) and ksp. (21-58 $\mu$ )), some of the feldspar. Are altered by chlorite or sericite, and few present inclusions; few sub-rounded to rounded quartz (11-45 $\mu$ ); biotite; glauconite. Fossils (C): globigerinid in intact condition; some are filled with framboidal pyrite.	basin	65,70	Hanging Wall Section
	Argillaceous marlstone; detritus grains (R): rounded quartz (5-13 $\mu$ ), ksp. (39 $\mu$ ) covered with sericite; framboidal pyrite. Fossils (F): planktonic foraminiferal tests; one worm tube filled with calcite.	distal/ outer shelf	60	
Tuff	Tuff consist of altered volcanic glass with an intersertal texture; detritus grains (R): biotite (10 $\mu$ ), ksp. (10 $\mu$ ) and angular quartz (13 $\mu$ ); Fossils (R): foraminifera tests; sponge spicules and broken shells.	basin	40	
Marlstone	Marlstone with a micrite-microsparite matrix; detritus grains (R), moderately to well sorted: feldspars (pl. (16 -36 $\mu$ ); ksp. (8 -21 $\mu$ )); some are altered by sericite; lithic fragments of pl. (59-100 $\mu$ ); angular to sub rounded quartz (5-25 $\mu$ ), some presents inclusions; biotite. Foraminiferal tests (F): globigerinid, gastropods and broken shells fragments. The organic matter is rare, and framboidal pyrite replaces some.		45, 50, 56	
	Marlstone with a microsparite and micrite matrix; detritus grains (R), poorly sorted: angular to rounded quartz (10-350 $\mu$ ), ksp. (8-26 $\mu$ ) few have inclusions, and some are altered by sericite; pl. (8 $\mu$ ); lithic fragment of pl. (16 $\mu$ ); biotite. Fossils (C): globigerinid, one test is destroyed and recrystallized; broken ostracods valves. The organic matter is rare, and some are replaced by pyrite or framboidal pyrite.	distal	30, 35, 25	

	Marlstone with a microsparite and micrite matrix; detritus grains (R): sub rounded quartz (10-50 $\mu$ ), pl. (14-25 $\mu$ ); sericitised ksp. (300 microns); lithic fragments composed of quartz and feldspar (33-160 $\mu$ ); some of the quartz have inclusions; Fossils (R): planktonic foraminifera, ostracods, gastropods, broken shells. The organic matter is frequent (sample 5) and can be observed a descending trend with height (sample 20).	basin	20, 15, 10, 5	
Silty marlstone	Silty marlstone with a microsparite matrix; detritus grains (C), well sorted: quartz sub rounded (7-10 $\mu$ ); ksp. (10 $\mu$ ); calcite (12 $\mu$ ). Foraminiferal tests (F), some have cherts or pyrite infills; globigerinid and ostracods valves; broken shells. The organic matter is scattered, some are replaced with framboidal pyrite.		1	
Sandy to silty marlstone	Fossiliferous sandy marlstone with a micrite matrix; detritus grains (F), poorly sorted: feldspars ksp. (10-42 $\mu$ ), some of them are altered by sericite; lithic fragments of ksp. (25-67 $\mu$ ); and pl. (50 $\mu$ ); quartz, chlorite/biotite. Fossils (A): globigerinid, one uniaxial foraminifera; one foraminifera filled with glauconite, two filled with chert; bryozoa; spicule; ostracods valves and shell fragments. The organic matter is scattered, and it is pyritized.		78, 75	Footwall Section

(A)-abundant, (F)-frequent, (C)-common, (R)-rare, ksp.-K-feldspar, pl.-Plagioclase, Env.-environment, No.-sample number.



The Footwall Section is represented by pebbly sandstones and marls which onlaps on the limestone of Soğucak Formation. Although the marly part of the Footwall Section is up to 30 m thick (Simmons et al., 2020), we study only 7 m of this succession (samples 71-78 in Figure 2.2, 4.2). In thin sections, the samples are characterised as fossiliferous sandy marlstones (Table 4.1). In the fine-grained part of the Footwall Section, the content of calcite minerals decreases upwards, whereas clay minerals increase in the same direction (Figure 4.2).

#### ***4.2.1.4 Bulk geochemical parameters and organic petrography***

Bulk parameters of the İhsaniye Formation are plotted versus vertical section position in Figure 4.2 and are listed in the Appendix 1 Table 1. The bulk parameters of the Hanging Wall Section support the subdivision into a lower (samples 1-19) and an upper part. The lower part is relatively rich in TOC (1.0-2.04%; avg.: 1.45%). In contrast, the upper part (samples 20-70) has an average of TOC of 0.38 wt.%. Within the upper part, the TOC contents decrease from 0.9% at 23.0 m (sample 23) to 0.2% at 62.2 m (sample 56). Above this height, the TOC content remains low (avg.: 0.3%). Unsurprisingly, the tuff layer is largely organic matter free. Sulphur contents typically follow the TOC trend, but a few organic-lean samples from the upper part of the succession contain high sulphur contents. TOC/S ratios are 2.0 and show upward decreasing trends between samples 21 (21.9 m) to 57 (40.8 m) and between 56 (42.2 m) to 61 (60.9 m). Also, an increasing upward trend is seen between 61 (60.9 m) and 70 (67.5 m). S<sub>2</sub> values reach a maximum of 4.48 mg HC/g rock (Figure 4.5) and HI values in the lower part of the succession vary between 140 and 252 mg HC/g TOC indicating the presence of type III-II kerogen, whereas HI values in the rest of the section (23-162 mg HC/g TOC) classify the organic matter as type III kerogen. A plot of HI versus T<sub>max</sub> (Figure 4.5) shows that the organic matter is immature. The fine-grained upper part of the Footwall Section contains very low organic matter (avg. TOC: 0.27 %) and a type III-IV kerogen (HI: 23-104 mgHC/gTOC).

Microscopic observations show that the organic matter is dominated by vitrinite (~90 vol.%), whereas inertinite and liptinite are present in small amounts. Vitrinite reflectance of samples from the lower part of Hanging Wall Section is about 0.3% R<sub>r</sub> (sample 1: 0.31% R<sub>r</sub>; sample 4: 0.30% R<sub>r</sub>; sample 12: 0.29% R<sub>r</sub>).

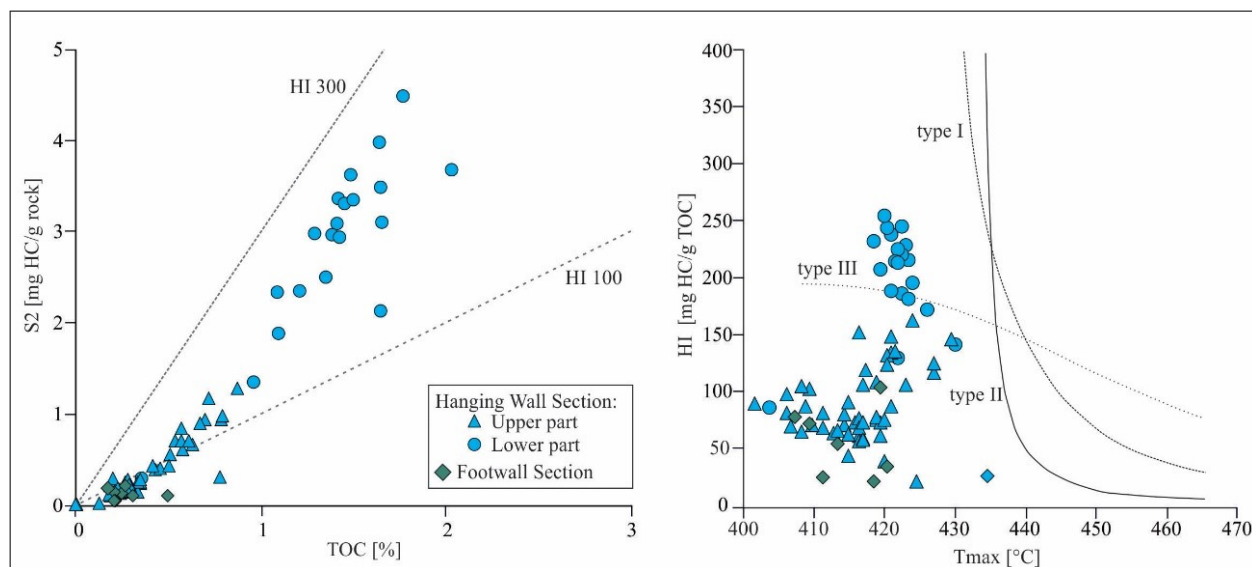


Figure 4.5. Plots of S2 vs TOC and Hydrogen Index (HI) vs Tmax for the İhsaniye Formation. The İhsaniye Formation contains type III and II kerogen.

### The molecular composition of hydrocarbons

Biomarker data have been determined for seven samples from the organic matter rich lower part of the Hanging Wall Section and four samples with moderately high TOC contents (0.6-0.9 wt.%) from its upper part. Typical ion traces are listed in Appendix 1 Table 2. The extractable organic matter (EOM) yields of the İhsaniye Formation vary between 1.12 and 2.82 mg/g TOC and are dominated by polar compounds (NSO, 62-83% of EOM). In contrast, hydrocarbons are rare. Consequently, only selected biomarker ratios could be determined.

**n-Alkanes and isoprenoids** - The extracts from the İhsaniye Formation are dominated by long-chain n-alkanes (n-C<sub>26-32</sub>: avg. 51.8%), which are characteristic for higher land plants (mainly plant waxes; Eglinton and Hamilton, 1967), and middle chain n-alkanes (n-C<sub>21-25</sub>: avg. 33.9%), which may originate from aquatic macrophytes (Ficken et al., 2000). In contrast, short chain n-alkanes, typically related to algae and microorganisms, are rare (n-C<sub>15-20</sub>: avg. 14.6%). There is a strong odd-even predominance with an average Carbon Preference Index (Bray and Evans, 1961) of 6.9, typical for terrestrial landplants with low maturity. Concentrations of pristane (Pr) and phytane (Ph) are very low, probably due to low maturity. Hence calculated Pr/Ph ratios (0.23-0.58) indicating anoxic conditions (Didyk et al., 1978) have to be treated with caution.

**Steroids** - The concentration of steroids is generally low ( $<2 \mu\text{g/g TOC}$ ).  $\text{C}_{27}$  and  $\text{C}_{29}$  are visible in low amounts,  $\text{C}_{28}$  steranes are missing. Sterenes, the immature precursor of steranes, are dominated by  $\text{C}_{29}$  sterenes with concentrations up to  $0.4 \mu\text{g/g TOC}$ . Similar to the steranes, the  $\text{C}_{28}$  sterenes are nearly missing. Steroids/hopanoids ratios range between 0.01-1.18. Values above 1 indicate organic matter input with a major contribution of marine algae, values below 1 point toward a dominantly land plant contribution (Moldowan and Wolfgang, 1985). Within the İhsaniye Formation, elevated values (1.18) are found only in one sample (7, 5.8m) in the lower part of the section, whereas the entire section is dominated by land plant contribution (0.01-0.83).

**Terpenoids** - Hopanes are non-aromatic cyclic triterpenoids that originate from precursors in bacterial membranes (Ourisson et al., 1979). Their concentration in the İhsaniye Formation is low ( $<2.6 \mu\text{g/g TOC}$ ). The  $\text{C}_{31} 22\text{S} / (22\text{S} + 22\text{R})$  hopane isomerization ratio varies widely between 0.0 and 0.42. Despite this variation, which may result from difficulties with quantification, the ratios indicate that the organic matter is immature (Peters et al., 2005). The ratio of  $\text{C}_{27} 18\alpha$ -trisorhopane (Ts) and  $\text{C}_{27} 17\alpha$ -trisorhopane (Tm) is a parameter both dependent on source and maturity (Moldowan and Fago, 1986). In the studied sample set, the Ts/Tm ratio ranges from 1.58 to 15.41.  $\beta\beta$ -hopanes are highly specific for immature to early oil generation source rocks (Seifert and Moldowan, 1980) and occur in concentrations up to  $1.4 \mu\text{g/g TOC}$ .

**(Methyl-)Phenanthrenes** - The phenanthrene concentration is  $<0.5 \mu\text{g/g TOC}$ . Except for two samples, the Methylphenanthrene Index (MPI-1) (Radke et al., 1980) is low ( $<0.28$ ), reflecting the low maturity of the section. Higher values ( $\sim 0.65$ ) are found in samples with very low concentrations of phenanthrene and methylphenathrenes.

**Land-plant related biomarkers** - Bi- and tricyclic diterpenes can be used to determine terrestrial organic matter input (Simoneit et al., 1986). Phyllocladane and retene are gymnosperm-derived biomarkers and occur in concentrations up to  $20.8 \mu\text{g/g TOC}$ , retene being the most abundant. Angiosperm derived biomarkers (triterpenoids) like perylene, and olea-12-ene ( $<1.23 \mu\text{g/g TOC}$ ) are far less abundant. A representative for land plant input is indicated by the sum of di- and triterpenoids and the di-/(di- + triterpenoids) ratio is representative for the ratio of gymnosperms to angiosperms (e.g. Bechtel et al., 2008). The sum of di- and triterpenoid is higher in the lower part of the section (max.  $32.1 \mu\text{g/g TOC}$ ) and lower in its upper part (max.  $1.1 \mu\text{g/g TOC}$ ).

TOC). Except sample 9, the di-/(di- + triterpenoids) ratio is high (0.52-0.93) indicating a significant contribution to gymnosperms to the terrestrial biomass.

#### ***4.2.1.5 Strontium isotope data***

Strontium isotope ( $\text{Sr}^{86}/\text{Sr}^{87}$ ) ratios have been determined on foraminifera from 34 samples and range from 0.707742 to 0.708071 (see Appendix 1 Table 3). Excluding sample 33, all data fall within a much smaller range of 0.707742 to 0.707926. Sr isotope data are commonly used to generate an age for open-marine sediments (McArthur et al., 2012). However, because there is evidence to suggest that at times the basin was not connected to the global ocean, in this paper, we use Sr isotope ratios combined with independent ages derived from the nannofossil assemblages, to identify whether or not the basin was isolated from the open ocean. Within this context, Sr isotope ratios that plot within error of coeval ocean water indicate that the basin was connected to the global ocean (Flecker and Ellam 2006). The Sr isotope ratios are therefore plotted against the estimated age of each sample (Figure 8) as determined by assuming constant sedimentation rates between the biostratigraphic tie points identified by Simmons et al. (2020). The more limited constraints on the exact stratigraphic position of the footwall samples mean that there is greater uncertainty in their age and hence the value of coeval ocean water Sr isotope ratio for these samples compared to for those from the Hanging Wall Section.

Comparison with the global ocean Sr isotope record for this period (McArthur et al., 2012) illustrates that only five of the 34 samples give Sr isotope ratios within the error of ocean water values (Figure 4.6). All but one of the remaining samples have ratios lower than coeval ocean water (Figure 4.6) suggesting that the connection with the open ocean was substantially restricted or closed during deposition of most of the İhsaniye Formation.

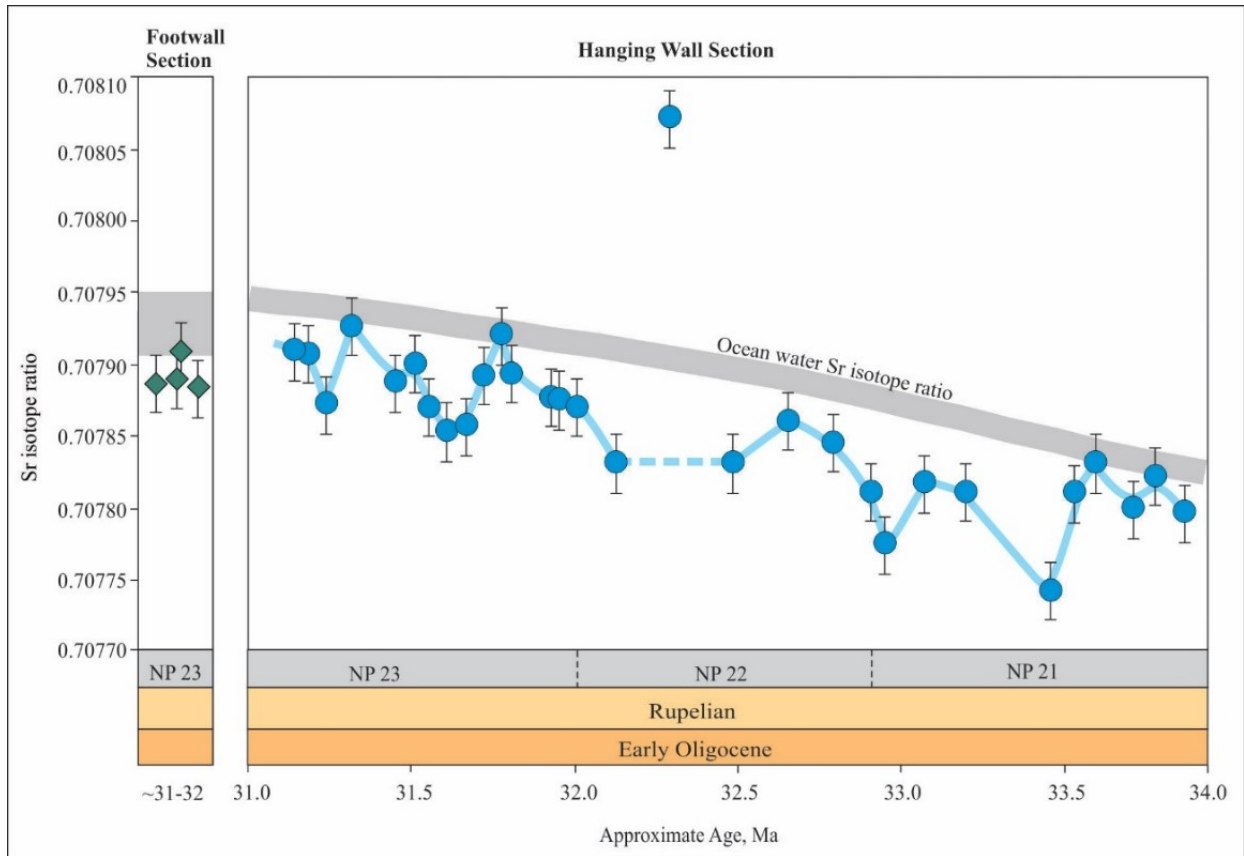


Figure 4.6. Variation of  $^{87}\text{Sr}/^{86}\text{Sr}$  in the İhsaniye Formation along the Hanging Wall and Footwall sections. Ages for the samples are calculated assuming constant sedimentation rates between biostratigraphic boundaries as determined by Simmons et al. (2020). The ocean water Sr isotope data is derived from McArthur et al. (2012). The thickness of the ocean water curve includes the analytical uncertainty.

## **4.2.2 Discussion and interpretation**

### **4.2.2.1 Maturity**

The low Tmax values (~418°C) in combination with vitrinite reflectance measurements (0.29-0.31% R<sub>r</sub>) show that the organic matter in the İhsaniye Formation is immature. This interpretation is supported by the occurrence of C<sub>29-31</sub> ββ-hopanes, low hopane isomerisation ratios (0.0-0.4) and low MPI-1 values (0.06-0.28).

### **4.2.2.2 Depositional environment**

Apart from the results of this study, the assessment of the depositional environment considers paleontological data from Hanging Wall Section published by Simmons et al. (2020). The presence of foraminifera in the entire section indicates a fully marine environment, which is also supported by the detected TOC/S values of İhsaniye Formation. The further discussion is focussed on the lower and upper part of the Hanging Wall Section.

#### **The lower part (0-19.5 m)**

According to Simmons et al. (2020), the lower part of the section has been deposited during NP21 in a shallowing bathyal to outer neritic environment. High percentages of quartz and land plant-derived macerals indicate strong detrital input. Simmons et al. (2020) described *Hoeglundina elegans*, an aragonite foraminifera species, which can tolerate low oxygen water with low nutrient conditions. We speculate that the high amount of aragonite in this part of the section reflects the presence of *H. elegans*. Low oxygen conditions are also supported by relatively high TOC contents. Petrographic and organic geochemical data prove that organic matter is dominated by higher land plants. Strong terrestrial input is also supported by the abundant presence of pollen derived from gymnosperms and angiosperms (Simmons et al., 2020). Hence, the relatively low amount of aquatic organisms may be caused by oligotrophic conditions.

#### **The upper part (19.5-68 m)**

Simmons et al. (2020) dated the upper part into the uppermost NP21 to lower NP23. Based on the ratio of planktonic and benthic foraminifera, these authors determined a deepening trend between samples 20 (19.1 m) and 55 (43.7 m). This trend is reflected by an upward decrease in quartz/clay minerals ratios (Figure 4) and an upward decrease in the size of lithic fragments (from

300 µm to 60 µm). The presence of micrite is an indication of a low-energy depositional environment (Flügel, 2004). An increasing distance to the shoreline is also indicated by the decrease in organic matter, dominated by land plants.

Above sample 55 (44.7 m) quartz/clay minerals ratios (Figure 4.2) and the percentage of planktonic foraminifera remain stable (Simmons et al., 2020). Only the uppermost two samples have high quartz/clay minerals ratios indicating stronger detrital input. Simmons et al. (2020) suggested that this part of the section has been deposited during a highstand systems tract. Organic matter contents remain very low (~0.3%) indicating a distal position to the shoreline as well as low productivity of aquatic organic matter and poor preservation conditions. Deposition of the tuffaceous rocks did not affect TOC contents indicating that the increased nutrient availability did not cause algal blooms.

#### ***4.2.2.3 Comparison to coeval sediments in the Western Black Sea and the Thrace Basin***

Typically, the Lower Oligocene succession in the Paratethys starts with marly sediments, which are overlain by thin carbonate-free shales or cherts (e.g. Sachsenhofer et al., 2018a, 2018b). Above this succession, a carbonate-rich layer forms a wide-spread marker horizon and represents the maximum of the isolation of the Paratethys (“Solenovian Event”) during the early NP23 (e.g. Voronina and Popov, 1984; Rusu, 1999). Above follow largely carbonate free shales. Marls representing the low salinity “Solenovian Event” have also been detected in the Western Black Sea (Sachsenhofer et al., 2009, 2018a, 2018b) including well Ropotamo-1 (Mayer et al., 2018; for the position of Ropotamo well see Figure 2.1).

Based on the age of the sediments, the Solenovian event is expected in the upper part of the Karaburun section dated as NP23 (40.0-67.5 m; samples 58-70; Figure 4.2). However, foraminiferal data (Simmons et al., 2020) and geochemical evidence (TOC/S ratio) exclude the presence of a major change in salinity. Although it cannot be completely excluded that the Solenovian event follows above the exposed succession in the Karaburun area.

Sr isotope data suggests that the connection was at best transient, and for most of the time, there can only have been a restricted connection. Hence, a closer look at the Oligocene successions in the Çatalca gap and the Thrace Basin is necessary. Within this context, it is intriguing that the Pınarhisar Formation deposited at the margin of the Çatalca gap (Figure 2.1) contains endemic

Solenovian mollusc faunas (Popov et al., 1985; Nevesskaja et al., 1987). Based on this mollusc fauna, Popov et al. (1985) and Nevesskaja et al. (1987) postulated brackish conditions. In contrast, based on the occurrence of Solenovian oolite shoals, İslamoğlu et al. (2010) assumed a marine and partially hypersaline environment with carbonate oversaturated waters. Nevertheless, all previous authors agree that the Pınarhisar Formation formed within the isolated Paratethys. However, as the Pınarhisar Formation accumulated at the shallow margin of the Çatalca gap, it is likely that it was restricted.

Gürgey and Batı (2018) studied the Lower Oligocene succession, up to 2500 m thick, in the centre of the Thrace Basin. They distinguished a Pshekhian(?) Lower Mezardere Formation (NP21-22) deposited in neritic normal marine environments and a Solenovian Upper Mezardere Formation (NP23/24), which represents a slightly shallower neritic environment. Based on the presence of marine dinocysts (e.g. *Wetzeliella gochtii*) and high amounts of green algae (e.g. *Pediastrum* spp.), Gürgey and Batı (2018) argued for a brackish-marine environment. Hence, it is not clear if a marine connection through the Thrace Basin existed in Solenovian time and more information on the Solenovian succession in the Thrace Basin is needed.

The Sr isotope data from our samples suggests that no permanent connection between this area and the open ocean existed. Rather, for much of the time during deposition of the İhsaniye Formation, the connection with the global ocean was highly restricted with only transient episodes of sufficient open-ocean water to cause the Sr isotope ratio of Thrace Basin water mirror that of coeval ocean water (Figure 4.6). The predominance of Sr isotope ratios lower than coeval ocean water suggest that fluvial or groundwater inputs had lower Sr isotope ratios. This is in line with more recent records from this area of the Black Sea where the fluvial Sr isotope data are substantially lower than these ocean water values (e.g. Major et al., 2002). However, evidence of limited and episodic oceanwater input does not necessarily equate to low salinity conditions since evaporation is driven by both freshwater dilution of ocean water and evaporation so that where the net evaporative flux is positive, normal marine or even higher salinities can prevail despite a preponderance of freshwater input (Flecker et al., 2002; Topper et al 2011).

#### ***4.2.2.4 Source rock potential***

Potential source rocks in the İhsaniye Formation are restricted to its lower part (NP21). Based on TOC contents, the source rocks may be classified as good (Figure 4.7). However, based



on petroleum potential (S1 + S2), they are classified only as poor to fair source rocks. This is also reflected in the Source Potential Index, which has been calculated according to Demaison and Huizinga (1994) ( $SPI = \text{thickness} \times (S1 + S2) \times \text{bulk density} / 1000$ ). For the calculation, only the lower organic matter rich part (samples 1-19), 17.5 m thick, is considered. The net mudstone thickness and the density are estimated as 15 m and of 2.55 g/cm<sup>3</sup>, respectively. Considering an average S1 of 0.07 mg HC/g rock and an average S2 of 2.99 mg HC/g rock, the SPI is calculated as 0.14 t HC/m<sup>2</sup>, which is a very low value. Hence, the source rock potential of the İhsaniye Formation is considered poor.

#### ***4.2.2.5 Comparison of the petroleum potential of Lower Oligocene rocks in the Western Black Sea and the Thrace Basin***

Mayer et al. (2018) studied the petroleum potential of Pshekhian and Solenovian (Early Oligocene) rocks in the Western Black Sea Basin, offshore Bulgaria. They showed that the average TOC contents of Pshekhian and Solenovian rocks are in the order 1.5 to 1.7 wt.%, but that HI values are higher in the Lower Solenovian (270 mg HC/g TOC) than in underlying (160 mg HC/g TOC) and overlying units (130 mg HC/g TOC). Consequently, the petroleum potential of Lower Solenovian rocks is better than that of Pshekhian and Upper Solenovian units (Figure 4.7). This is also the case for the Ropotamo well, located relatively near to the Karaburun area (Mayer et al., 2018). Gürgey and Batı (2018) observed a similar trend in deep wells in the central Thrace Basin. Here the Pshekhian Lower Mezardere Formation contains a lower hydrocarbon potential (avg. TOC: 0.88 wt.%; max. 1.50 wt.%; avg. HI: 136 mg HC/g TOC; max 345 mg HC/g TOC) than the Solenovian Upper Mezardere Formation (avg. TOC: 1.15 wt.%; max. 1.86 wt.%; avg. HI: 285 mg HC/g TOC; Figure 9). Remarkable are partly very high HI values (up to 744 mg HC/g TOC) in the Upper Mezardere Formation, which have not been observed in any other Oligocene succession in the Black Sea area (Sachsenhofer et al., 2018a, 2018b).

For the sake of completeness, it should be added that the best source rocks units in the Western Black Sea Basin are Lower Miocene diatom-rich rocks, which accumulated within shelf-break canyons (avg. 2.6 wt.% TOC, avg. HI: 400 mg HC/g TOC; Mayer et al., 2018; Figure 4.7). In contrast, the best source rocks in the Thrace Basin are found in the Middle to Upper Eocene Hamitabat Formation (avg. 0.78 wt.% TOC; max. 9.96 wt.%). Average S1 + S2 is 3.29 mg HC/rock (Figure 4.7), and the presence of type III kerogen classify the Hamitabat Formation as

gas-prone (Gürgey, 2009). The Oligocene Osmancık Formation (avg. 0.47 wt.% TOC, max. wt.% 1.75 wt.% TOC, S1 + S2 0.62 mg HC/rock) can locally reach fair hydrocarbon potential (Sarı and Savan, 2008; Şen, 2011; Figure 4.7). Although the İhsaniye Formation is located between the two basins, the majority of the samples analysed have a poor hydrocarbon potential (Figure 4.7). Only samples from the lower part of the Pshekhian succession (NP21; 0-19.5 m) have a fair potential, similar to that observed in coeval strata in the West Black Sea Basin and the Thrace Basin.

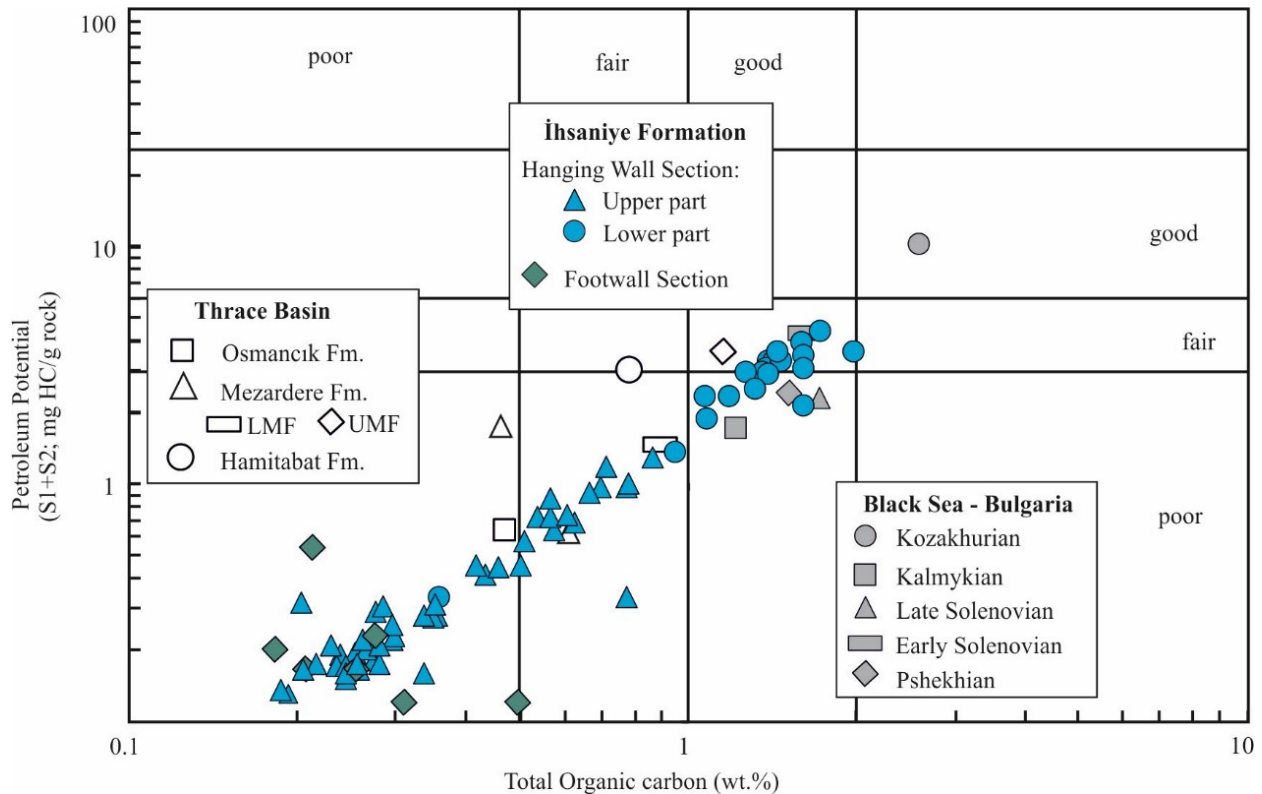


Figure 4.7. Petroleum Potential of the İhsaniye Formation. Mean values of the petroleum potential of sediments in the Thrace Basin and the Bulgarian part of the Black Sea are shown for comparison (data compiled from Sarı and Savan 2008; Gürgey 2009; Mayer et al., 2018; Gurgey and Batı 2018). LMF-Lower Mezardere Formation, UMF-Upper Mezardere Formation.

#### 4.2.2.6 Conclusions

The İhsaniye Formation is exposed along the Black Sea shore in 50 m high cliffs and includes fine-grained sediments overlain by thick mass transport sediments. The study is focused on fine-grained sediments deposited on the hanging wall side of a syn-sedimentary normal fault

(“Hanging Wall Section”), where the İhsaniye Formation is about 70 m thick. The results allow the following conclusions:

The fine-grained part of the İhsaniye Formation is represented by an alternation of marl, carbonate-rich siltstone, sandstone and tuffaceous beds and the frequency of the sandy layers intercalations is decreasing higher in the stratigraphy.

The TOC/S values of the İhsaniye Formation together with the continuous presence of the foraminifera in the studied section indicate a fully marine environment. The Hanging Wall Section is divided into two parts: the lower part (0-19.5 m) contains relatively high amounts of terrestrial organic matter deposited in oxygen-depleted conditions. The upper part (19.5-68 m) contains a prominent tuff layer. The succession below the tuff layer is low in organic matter (avg. TOC: 0.38%) and reveals a deepening trend in a low-energy depositional environment. The deepening trend is reflected by an upward decrease in detrital organic and inorganic matter.

In comparison with the coeval sediments in the Western Black Sea and the Thrace Basin, the İhsaniye Formation shows a different evolution, where the low salinity “Solenovian Event” is missing even though the Sr isotope record suggests that full connection with the Mediterranean occurred for relatively short periods during this interval. One possible explanation is that the “Solenovian Event” is hidden within the overlying mass transport sediments.

The studied succession is immature. The TOC content reaches a maximum of 2.04 wt.% in the lower part of the succession (0-19.5 m), which has some hydrocarbon potential even though it is poor. If mature, the section may generate 0.14 t HC/m<sup>2</sup>. The presence of type III-II kerogen indicates that the rocks are gas prone and may generate minor liquid hydrocarbons only.

### ***4.2.3 Karadere, Bulgaria***

#### ***4.2.3.1 Samples and methods***

In total, 29 samples from of the Ruslar Formation were collected near Karadere, along the Black Sea coast (Figure 2.3). The following methods have been applied the following analysis: bulk parameters measurements, Rock Eval pyrolysis, XRD and FAAS on all 29 samples; biomarkers analysis on 11 samples, petrography on 10 sample and micropaleontology analysis on 10 samples. Their results are presented below.

## **4.2.4 Results**

### **4.2.4.1 Lithology**

Approximately 20 m high cliffs of the Ruslar Formation are exposed along the Bulgarian Black Sea coast near Karadere (Black Cape; Figure 2.3). Neither the erosional base nor top of the Ruslar Formation are exposed. However, large blocks with coarse-grained Galata Formation at the northern end of the section indicate that the erosional surface at the base of the Miocene Galata Formation is very close, suggesting that the outcrop represents the upper part of the Ruslar Formation, which is reported to be about 70 m thick in the area.

The exposed part of the Ruslar Formation is dominated by laminated mudstones intercalated with sandstone layers and lenses. Sandy laminations are ubiquitous, but their frequency declines in the upper part between 11 m (sample 22) and 13 m (sample 26). At 11.5 m (between samples 23 and 24) a horizon with massive concretions is observed (Figure 4.8 and 4.9).

Thin section observations (Figure 4.10) indicate that organic matter-rich laminated argillaceous mudstone is the dominant lithology. The laminae are parallel, planar and continuous. Sometimes sandstone laminae are seen. Abundant diatom valves, well sorted angular quartz with subordinate feldspar, glauconite and (globigerinid) foraminifera are observed. In addition, the presence of intact diatom chains suggests that at the time of deposition the sediments were not disturbed. Based on XRD, the concretions (Figure 4.8) contain about 60% ankerite. Detrital grains (angular quartz and feldspar) within the concretions form a few continuous, parallel and planar layers. Diatom valves and foraminifera in concretions are very rare.

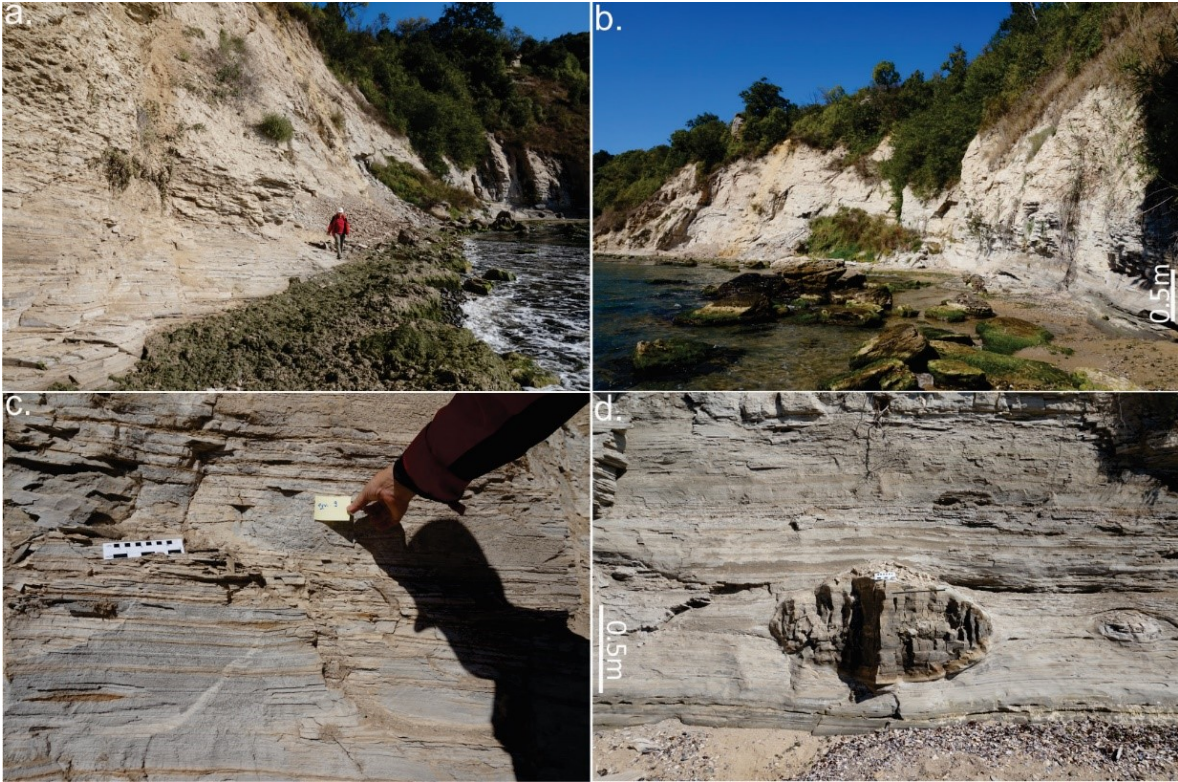


Figure 4.8. Karadere (Black Cape) section with Ruslar Formation. a. outcrop section from south; b. outcrop section from north; c. argillaceous mudstone alternating with sandstone laminations and sand lenses; d. concretions.

Based on the XRD analysis mudstones are composed on average of 57% clay minerals, 27% quartz and 6% calcite. The percentages of dolomite, feldspar, ankerite, siderite and pyrite do not exceed 2% (Figure 4.8).

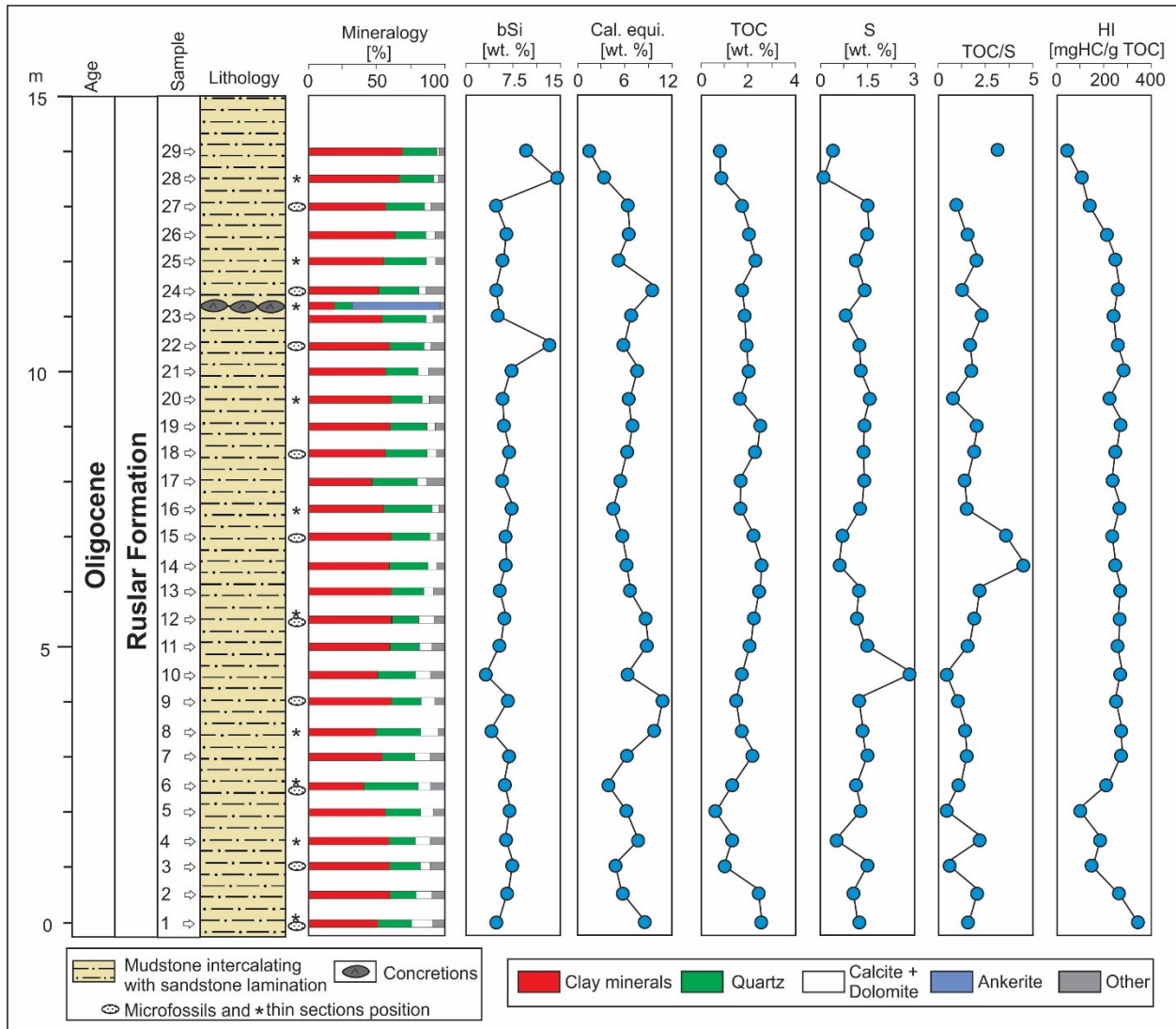


Figure 4.9. Bulk geochemical parameters and mineralogy of the Ruslar Formation beds exposed at Karadere. bSi-biogenic Silica; Cal. equi.-calcite equivalent; TOC-total organic carbon; S-total Sulphur; HI-Hydrogen Index; Other minerals: feldspar, pyrite ankerite, siderite.

Biogenic silica (bSi) contents are on average 6.5% (Figure 4.8) and do not show a clear depth trend. Two samples have relatively high biogenic silica contents (sample 22: 13% bSi; sample 28: 14.6% bSi). Similar biogenic silica contents (8.5-13.0% bSi) were measured for cuttings samples from the nearby borehole P-79.

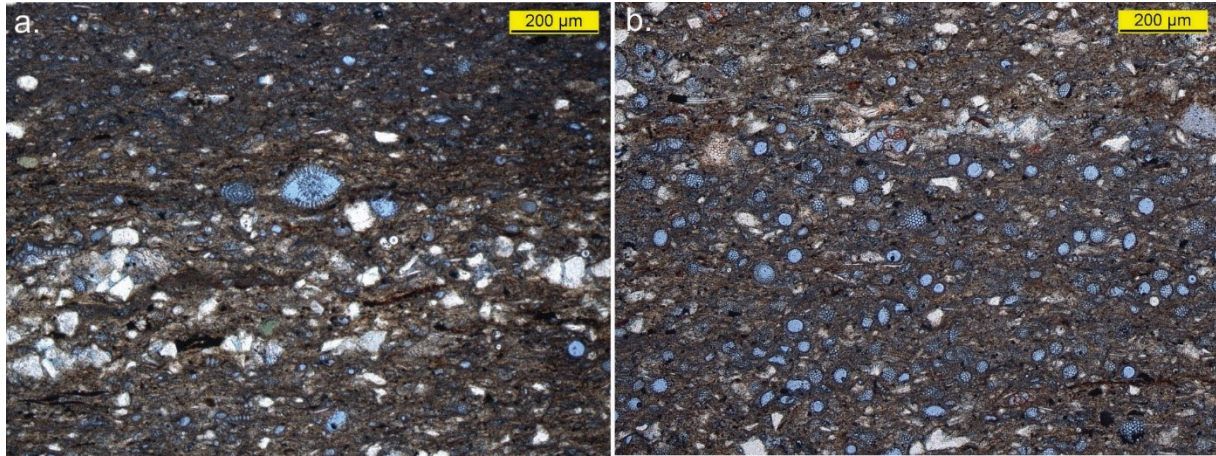


Figure 4.10. Selected thin sections photographs of Ruslar Formation exposed at Karadere. a. organic matter rich laminated argillaceous mudstone and angular quartz grains with common diatom valves (sample 6-3.0 m); b. diatom rich argillaceous mudstone with rare detritus (sample 12-6.0 m).

#### 4.2.4.2 Bulk parameters

Bulk parameters of the Ruslar Formation exposed at Karadere are plotted stratigraphically in Figure 4.9. and are listed in Appendix 1 Table 4. The average total organic carbon (TOC) content is 1.85% wt.. TOC contents below 1.5% wt. are restricted to samples 3 to 5 (1.5-2.5 m) and 28 to 29 (14-14.5 m). Sulphur (S) contents typically follow the TOC trend except sample 10 (5.0 m) where S content is 2.90% wt. (avg. 1.25% wt.). TOC/S ratios on average are 1.94 and show an increase in the middle of the section (samples 14-15; 7-7.5 m) due to low S contents (sample 14: 0.56% wt.; sample 15: 0.60% wt.). S<sub>2</sub> values reach a maximum of 8.48 mg HC/g rock (Figure 4.11) (avg. 4.51 mg HC/g rock) and the HI values range from 61 to 331 HC/g TOC indicating the presence of type II-III kerogen. T<sub>max</sub> varies between 421 and 436° C.

TOC and Rock-Eval data from cuttings samples from well P-79 (350-410 m depth; for location see Figure 2.3) are listed in Appendix 1 Table 4. The average TOC content is 1.77% wt. Sulphur contents are on average 1.08% wt. and TOC/S ratios vary between 1.35 and 1.94. S<sub>2</sub> values are on average 2.71 mg HC/g rock, reaching a maximum of 4.65 mg HC/g rock (400 m). HI values are between 102 and 206 HC/g TOC. According to plot of HI versus T<sub>max</sub>, the Ruslar Formation in P-72 is immature and contains predominantly type III kerogen (Figure 4.11).

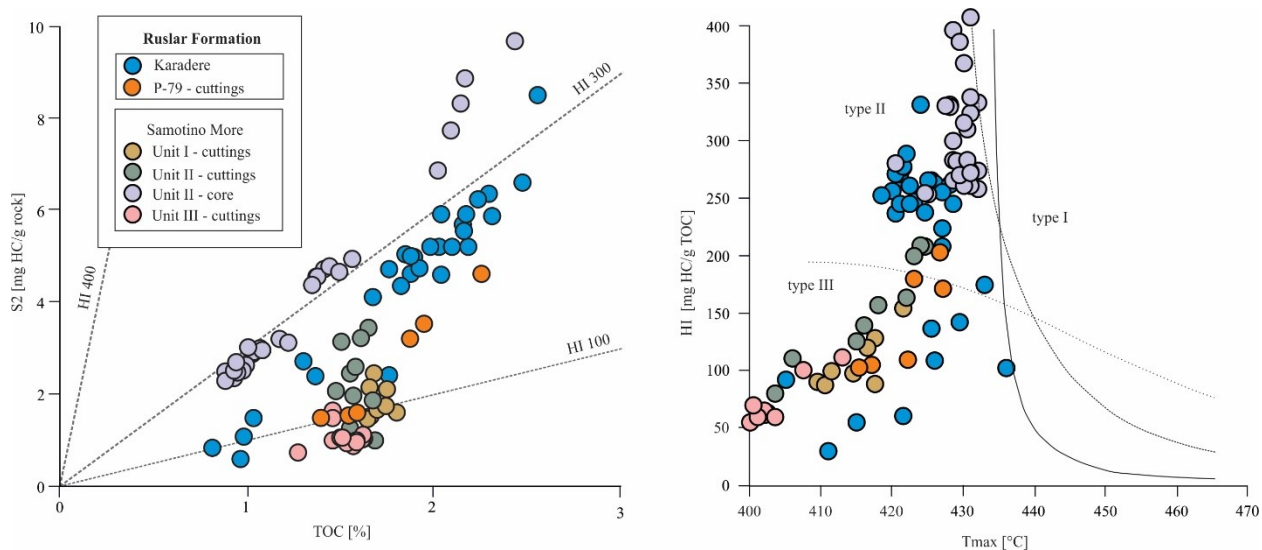


Figure 4.11. S2 vs TOC Hydrogen Index (HI) vs Tmax plots for the Ruslar Formation (Ruslar Formation at Karadere and Shkorpilovtsi P-79 relative to the offshore Ruslar Formation data from Samotino More - wells from Sachsenhofer et al., 2009). The Ruslar Formation contains type II and III kerogen.

#### 4.2.4.3 Biomarker data

Biomarker data have been determined for 11 samples from the Ruslar Formation at Karadere. The extractable organic matter (EOM) yields of the Ruslar Formation vary between 8.99 and 39.0 mg/g TOC and are dominated by polar NSO-compounds (62-76% of EOM; Appendix 1 Table 5). In contrast, saturated and aromatic hydrocarbons are very rare. Consequently, only some biomarker ratios could be determined.

**n-Alkanes and isoprenoids** - The saturated hydrocarbons are dominated by long-chain n-alkanes (n-C<sub>27-31</sub>: avg. 45%), which are characteristic for higher land plants (mainly plant waxes; Eglinton and Hamilton, 1967) and short chain n-alkanes, typically related to algae and microorganisms (n-C<sub>15-20</sub>: av. 30%). The middle chain n-alkanes are present as well (n-C<sub>21-25</sub>: av. 25%), which may originate from aquatic macrophytes (Ficken et al., 2000). Concentrations of pristane (Pr) and phytane (Ph) are variable with height. Pr/Ph ratios <1 may indicate anoxic conditions, while ratios between 1 and 3 indicate dysoxic conditions (Didyk et al., 1978). The calculated Pr/Ph ratios (0.67-1.29) indicate oxygen-depleted and partly anoxic conditions. The



low maturity of the section (avg. Tmax: 424° C) can affect the Pr/Ph ratios, therefore the values should be treated with caution.

**Steroids** - The concentration of steroids has a high range (2.1-64.1 µg/g TOC). Sterenes, the immature precursors of steranes, are dominated by C<sub>29</sub> sterenes (38-69%), whereas C<sub>27</sub> sterenes (14-36%) and C<sub>28</sub> sterenes (16-26%) are detected in low amounts.

**Terpenoids** - Hopanes are non-aromatic cyclic triterpenoids that originate from precursors in bacterial membranes (Ourisson et al., 1979). Their concentration in the Ruslar Formation ranges from 0.8 to 6.5 µg/g TOC. High steroids/hopanoids ratios (3.0-9.9) reflect a strong predominance of eu-caryotic (e.g., algal) over bacterial biomass (Moldowan and Fago, 1986). The presence of hop-17(21)-ene (0.04-1.17 µg/g TOC) supports the low maturity of the samples (Ten Haven, 1985). According to Bechtel et al. (2002; 2004; 2007), the biological source of hop-17(21)-enes can be related to anaerobic bacteria. 28,30-bisnorhopane is present in the Ruslar Formation with relative high concentrations (av.: 19.4 µg/g TOC). This compound has been suggested to indicate reworking of organic matter by chemoautotrophic bacteria (Noble et al., 1985; Watson et al., 2009).

**Diatom-related biomarkers** - The concentration of 24-norcholestane (ααα C<sub>26</sub> sterane), a possible biomarker for diatoms (Holba et al., 1998), is significant (av.: 2.68 µg/g TOC). C<sub>25</sub> HBI alkanes and thiophenes are also biomarkers indicating diatoms (Yon et al., 1982; Nichols et al., 1998; Kening et al., 1990; Volkman et al., 1994). Their concentrations are on average 8.46 µg/g TOC. High values (13-14 µg/g TOC) are seen in samples 4 (2.0 m), 14 (7.0 m) and 16 (8.0 m).

**Land-plant related biomarkers** - Aromatic triterpenoids (including oleanane/ursane types), indicative for the input of angiosperms (Bechtel et al., 2008 cum. lit.) occur in significant concentrations (up to 6.6 µg/g TOC). In contrast, diterpenoids, indicative for gymnosperms (Simoneit et al., 1986), have not been detected. Perylene occurs in high amounts (19.7 µg/g TOC). It may have different precursors including fungi (Marynowski et al., 2013 cum lit.).

#### **4.2.4.4 Diatom assemblages**

The positions of samples which were selected for the quantification of diatom assemblages are shown in Figure 4.9. The diatom assemblages are remarkably well-preserved with abundant

and identifiable diatom valves. The diatoms are present in nine samples, whereas samples 18 (9.0 m), 22 (11.0 m) and 27 (13.5 m) yielded less than 150 counts/sample.

The diatom genera found in Ruslar Formation at Karadere are shown in Plates I-III. Overall, 23 genera were recorded. Since Paleogene diatom assemblages of the West Black Sea Basin are poorly understood, the diatom identifications presented here are down to the genus level, and only few species-level identifications are given. The most common genera are *Paralia* (avg. 29%), *Distephanosira* (avg. 16%), and *Stephanopyxis* (avg. 15%). Less abundant genera include (avg. 9%), and *Coscinodiscus*, *Hemiaulus*, *Pseudopodosira*, *Rouxia*, *Xanthiopyxis* (<3% avg. each). The less abundant taxa include: *Actinoptychus*, *Azpeitia*, *Asterolampra*, *Delphineis*, *Diploneis*, *Distephanosira*, *Eunotogramma*, *Eurossia*, *Liradiscus*, *Lyrella*, *Plagiogramma*, *Pseudopodosira*, *Pseudotriceratium*, *Radialiplicata*, *Rouxia*, *Rutilaria*, *Saeptifera* and *Triceratium*.

A distinct up section change has been observed in the generic composition of the diatom assemblages (Figure 4.12). For instance, *Paralia* shows an up-section increase in abundance, reaching a peak (44%) in sample 25 (12.5 m). Further, *Distephanosira* (Plate I, Figure 1-3), decreases in abundance up section. *Stephanopyxis* is represented by a number of species (Plate I, Figure 7-14) and shows some cyclic variations with a maximum percentage of 20% (Figure 4.12). *Coscinodiscus* is extremely diverse (Plate I-Figure 15-23; Plate II-Figure 15-16). An up-section decrease has been observed for *Coscinodiscus*, *Hemiaulus* and the fossil resting spore genus *Xanthiopyxis* (Figure 4.12). *Hemiaulus* and *Xanthiopyxis* are present in most of the samples, except sample 27 (13.5 m) and, sample 12 (6.0 m) respectively. Raphid pennates are present with a significantly lower abundance, and they are represented by genera *Amphora* and *Lyrella*. Araphid pennates are represented by rare *Rhaphoneis*.

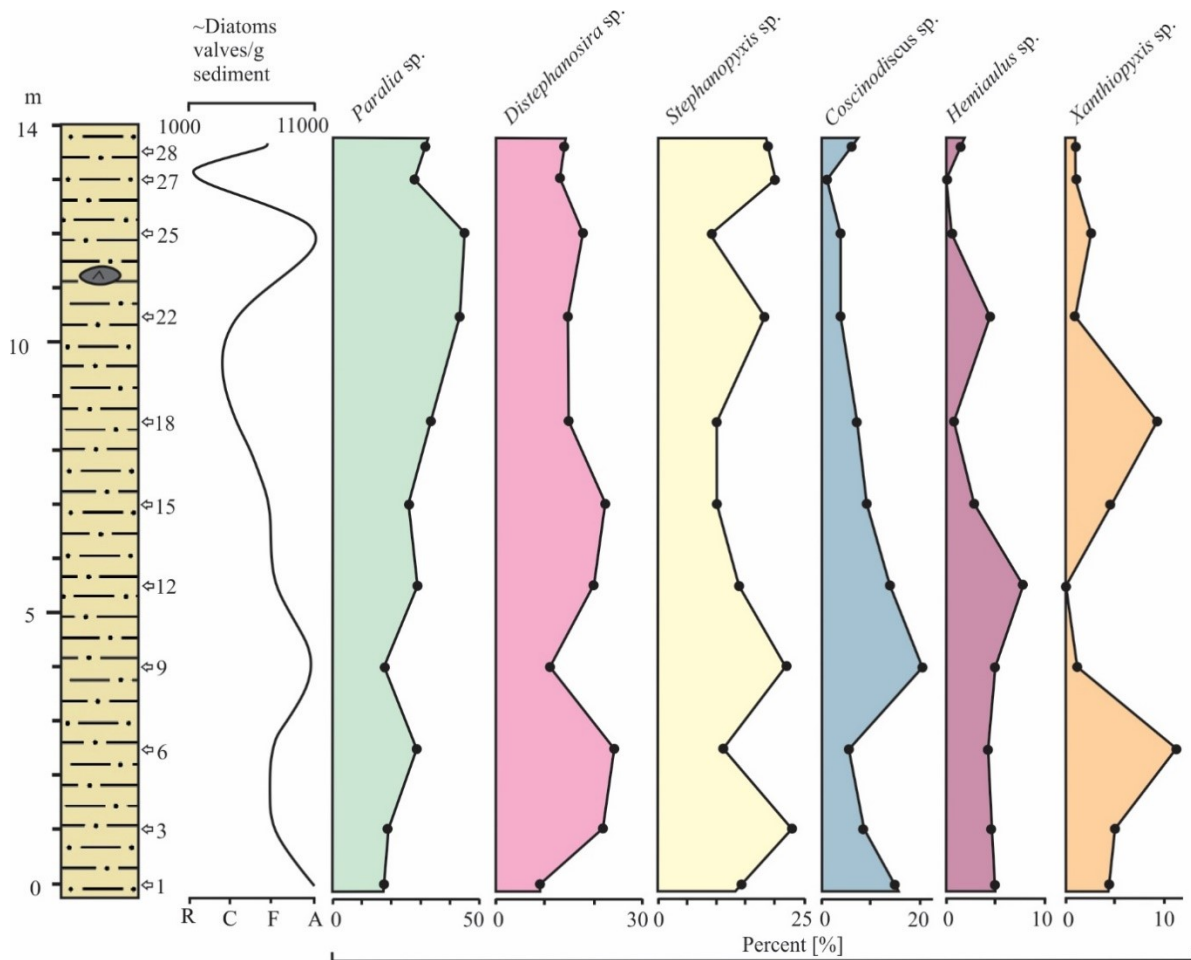


Figure 4.12. Variation in the relative abundance of the prevalent diatom genera with outcrop height observed at Karadere. R-rare, C-common, F-frequent, A-abundant.

#### 4.2.4.5 *Silicoflagellate assemblage*

Silicoflagellates are present in the Ruslar Formation at Karadere, but they are less common than diatoms. Four taxa were recorded: *Bachmannocena apiculata*, *Naviculopsis biapiculata*, *Distephanopsis crux* and *Corbisema regina* (Plate IV). In addition to silicoflagellates, we observed abundant synurophyte scales. *Macrora* is present in all samples, but is most frequent in samples 1 (0.5 m), 6 (3.0 m) and 9 (4.5 m), followed by *Corbisema regina*? and *Bachmannocena apiculata*?. *Naviculopsis biapiculata*? has been observed in only two samples: 3 (1.5 m) and 9 (4.5 m).

#### 4.2.4.6 *Calcareous nannofossils*

The investigated samples generally contain similar, exceptionally well-preserved and common calcareous nannofossil assemblages characterized by very low diversity (7-15 species;

Plate V). All samples are dominated by reticulofenestrids, predominately by *Reticulofenestra dictyoda* followed by *Reticulofenestra lockeri* and *Reticulofenestra minuta*. Regularly occur: *Coccolithus pelagicus*, *Cyclicargolithus floridanus*, *Coronocyclus nitescens*, *Dictyococcites bisectus*, *Dictyococcites hesslandii* and *Umbilicosphaera jafari*. *Helicoliths* are presented by *Helicosphaera recta* and *Helicosphaera perch-nielseniae*. Among muroliths regularly occur *Pontosphaera versa* and *Pontosphaera multipora*. Rare sphenoliths presented by *Sphenolithus moriformis* could be observed only in sample 1 (0.5 m). Discoasters are absent in all samples. Reworking from older sediments is very rare and presented by Upper Cretaceous species *Tetrapodorhabdus decorus* and *Watznaueria barnesiae*.

#### **4.2.5 Discussion and interpretation**

##### **4.2.5.1 Maturity and hydrocarbon source rock potential**

T<sub>max</sub> values of the Ruslar Formation (avg. 424° C) indicate that the Karadere section is immature. This statement is supported by the presence of hop-17(21)-enes (Luo et al., 2012). Whereas TOC contents classify the Ruslar Formation as good to very good source rocks (Figure 8), the petroleum potential suggests a fair to good quality. This discrepancy results from the presence of type II-III kerogen with relatively low hydrogen contents (avg. HI: 231 mgHC/gTOC) (Figure 6). Thus, the samples could generate gas, condensate and oil. Cuttings samples from borehole P-79 and unit I and III samples from Samotino More (Sachsenhofer et al., 2009) have an even lower petroleum potential, whilst unit II samples (NP23) have a comparable potential (Figure 4.13).

The Source Potential Index ( $SPI = \text{thickness} \times (S1 + S2) \times \text{bulk density} / 1000$ ; Demaison and Huizinga, 1994) gives an indication of the amount of hydrocarbons (in tons HC), which can be generated beneath 1 m<sup>2</sup> surface area. For the calculation the net mudstone thickness has been estimated as 15 m, because of the low percentage of sandstone layers. Taking into account the shallow burial depth and the high amount of diatoms, a density of only 2.0 g/cm<sup>3</sup> has been applied. Considering an average S1 of 0.12 mg HC/g rock and an average S2 of 4.51 mg HC/g rock, the SPI for the exposed part of the Ruslar Formation at Karadere is calculated as 0.14 t HC/m<sup>2</sup>.

Assuming that the measured values are representative for the entire Ruslar Formation and that the net mudstone thickness is 55 m, the SPI increases to 0.5 tHC/m<sup>2</sup>, which is slightly lower than that in the Ruslar Formation offshore Bulgaria (Sachsenhofer et al., 2018a; 2018b).

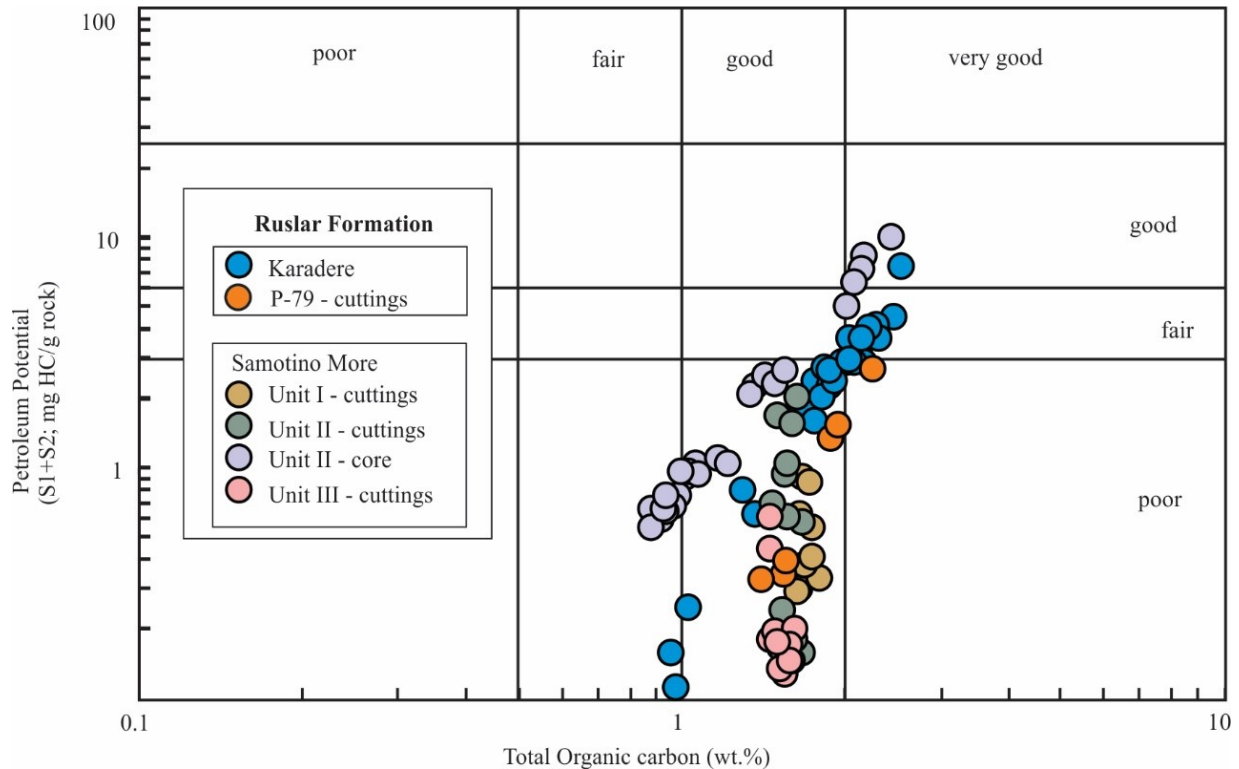


Figure 4.13. Petroleum Potential of the Ruslar Formation at Karadere versus the Ruslar Formation offshore (Samotino More well data from Sachsenhofer et al., 2009 and Shkorpilovtzi P-79).

#### 4.2.5.2 Age and depositional environment

Diatom data are insufficient to provide an independent age control for the study site. Hence, the age of the Ruslar Formation at Karadere is entirely relying on calcareous nannofossils. Samples contain *Pontosphaera versa*, which has its last occurrence (top) within NP23 (Bown, 2005) accompanied by *Helicosphaera recta* and *Helicosphaera perch-nielseniae* which both have its first occurrence within NP22 (de Kaenel and Villa, 1996, Boesiger et al., 2017). Based on the absence of *Reticulofenestra umbilicus*, all samples are attributed to Early Oligocene standard nannoplankton Zone NP23 (*Sphenolithus predistentus* Zone) of Martini (1971). This assignment is further supported by the absence of *Sphenolithus ciperoensis*, which first occurrence defines the NP23/NP24 boundary, and nannofossil species which typically occur in NP24-NP25 Zones. The absence of discoasters and low diversity assemblages indicate shallow marine conditions. This interpretation is supported by the common occurrence of small reticulofenestrids represented by *R. minuta* accompanied by helicoliths and muroliths which points to the near shore environment.

Diatoms occur in high abundance in the analysed samples and provide important insights on the depositional environment. Although most of the interpretation is based on the present-day diatom environmental preferences, the interpretation should be treated as tentative, since the diatom living preferences may change through time. For example, the modern *Paralia* is a tychopelagic species common in the North Sea (Gebühr et al., 2009) and can be found in both the plankton and benthos of modern temperate coastal environments (McQuoid and Nordberg, 2003). The extant *Paralia* is commonly associated with high primary productivity in coastal upwelling zones and strong physical mixing may play a crucial role in transporting cells into the plankton (e.g. Davies and Kemp, 2016). *Paralia* was found to be a common constituent of pelagic/hemipelagic deposits, such as the Cretaceous Marca Shale (Davies and Kemp, 2016). A global distribution has been observed for *Distephanosira*, especially *D. architecturalis*, which was described from coastal, neritic and pelagic middle Eocene to late Oligocene successions (Witkowski et al., 2014).

*Stephanopyxis* is a common planktonic genus. In the modern oceans it is found in tropical or warm waters regions (Round et al., 1990). It is also adapted to live in a stratified water column, and is capable of reproducing at rapid rates in low light conditions (Goldman, 1993; Kemp et al., 2006). Another planktonic diatom adapted to stratified waters, and often considered an indicator of oligotrophic conditions, is *Hemiaulus* (Kemp et al., 2006). The stratified-adapted species like *Stephanopyxis* and *Hemiaulus* are able to rapidly reproduce in conventional blooms, but they can also gradually accumulate in deep chlorophyll maxima (Kemp et al., 2006).

*Xanthiopyxis* is a fossil resting spore morpho-genus associated with the marine diatom genus *Chaetoceros* (Suto, 2004). When nutrient levels are depleted, many diatom species form thick-walled resting spores that sink to deeper levels or to the sea floor and wait for more favourable condition for vegetative growth (Suto, 2004). High abundance of *Xanthiopyxis* in at least two intervals in the studied succession likely points to a pronounced seasonality in nutrient levels during these periods.

In the Ruslar Formation at Karadere, *Stephanopyxis* abundance shows a series of fluctuations that generally parallel the percentage of *Hemiaulus*, which is generally low (<8%). *Xanthiopyxis* displays an opposite trend (Figure 4.12). This may indicate that a water column

stratification developed periodically, with intermittent periods of pronounced seasonality in nutrient supply, perhaps linked to invigorated vertical mixing.

Water column stratification resulted in oxygen-depleted bottom water conditions, which are indicated by low Pr/Ph ratios and the presence of hop-17(21)-ene (Luo et al., 2012). Considering the high amount of diatoms, the presence of diatom-related biomarkers (24-norcholestane; C<sub>25</sub>HBI alkanes and thiophenes) is not surprising. The presence of 28,30-bisnorhopane may indicate upwelling (e.g. Watson et al., 2009). However, bisnorhopane occurs in significant amounts in various anoxic settings (e.g. Pedersen et al., 2006). Moreover, upwelling is not supported by the observed calcareous nannofossil assemblages. These assemblages are characterized by high amounts of reticulofenestrads, whereas *Coccolithus pelagicus* occurs in very low amounts in all investigated samples. Assemblages with high amounts of *C. pelagicus* indicate marine environments with higher nutrient levels caused by upwelling conditions (Okada and McInyre 1979; Winter et al. 1994). In contrast to *C. pelagicus*, common occurrences of small reticulofenestrads among nannofossil assemblages indicate shallow, well stratified water column (Perch-Nielsen, 1985). Wade and Bown (2006) observed the co-occurrence of diatoms and abundant *Reticulofenestra minuta* in extreme palaeoenvironments during the Messinian salinity crises in the Polemi Basin (Cyprus) and concluded that this species tolerates brackish to hypersaline environments. Abundant *R. minuta* in low diversity assemblages occurs there before and after the deposition of evaporates (Wade and Bown 2006) caused by basin isolation. In analogy, the low diversity calcareous nannofossil assemblages accompanied by diatoms may point to sedimentation after the “Solenovian event”.

The detected calcareous nannoplankton assemblage and the abundance of plant debris agree with the postulated shallow marine environment. High amounts of terrestrial plants are also reflected by a relatively low HI and high amounts of C<sub>29</sub> steroids. The presence of triterpenoids and the absence of diterpenoids show that the terrestrial input is dominated by angiosperms.

Overall, it is concluded that the studied section of the Lower Oligocene Ruslar Formation was deposited in a neritic marine environment, away from the wave zone. The surface water was mostly well oxygenated, but at least periodic water column stratification resulted in oxygen-depleted bottom water. Evidence for major changes in salinity could not be observed.

#### ***4.2.5.3 Regional understanding***

As mentioned before, the Ruslar Formation typically contains from base to top calcareous shales (NP21-NP22), marlstones to limestone representing the low salinity Solenovian event (lower part of NP23) and overlying pelitic rocks with low carbonate contents (upper part of NP23 to NP24). Following the Solenovian event, the connection with the open ocean was partially restored during upper NP23 (Popov et al., 1993). Sachsenhofer et al. (2009) subdivided the Ruslar Formation offshore Bulgaria into six units (from bottom to top: unit I to VI, whereby the diatom-rich unit VI turned out to be part of the Kaliakra canyon fill and should not be considered part of the Ruslar Formation; Mayer et al., 2018a). Their unit II corresponds to the NP23 (Solenovian event and overlying rocks).

The fragment of the Ruslar Formation exposed at Karadere was deposited in a fully marine environment and probably represents the (marine) upper part of NP23 (upper part of unit II). Hence, it is assumed that the “Solenovian event” is hidden in the unexposed lower part of the Ruslar Formation. Within this context, it is important to note that the “Solenovian event” is probably missing at Karaburun along the Turkish Black Sea coast (İhsaniye Formation, Simmons et al., 2019; Tulan et al., 2019), located about 185 km SSE of Karadere. This may indicate that a connection between the Paratethys and the Mediterranean Sea remained open at the southwestern edge of the Black Sea.

The top of the Ruslar Formation in the Karadere area is formed by an erosional unconformity, and the uppermost part of the Ruslar Formation has been eroded. We speculate that the erosion is related to the incision of the Kaliakra canyon offshore Bulgaria, which has been described in detail by Mayer et al. (2018a). This implies that the base of the Galata Formation may be considered as part of the canyon fill.

#### ***4.2.6 Conclusions***

The fragment of the Ruslar Formation outcropping at Karadere along the western Black Sea shore exposes organic-rich, diatom-rich mudstones with sandstone intercalations, about 15 m thick, which have been dated as intra-Early Oligocene (biozone NP23). The lower part of the Ruslar Formation (including the “Solenovian event”) is not exposed. Stratigraphically higher parts have been removed by erosion.



The mudstones are characterized by well preserved, rich diatom assemblages, which are unique for sediments of this age in the Black Sea area. Diatom assemblages, frequent silicoflagellate skeletons as well as calcareous nannoplankton and rare foraminifera suggest a fully marine, neritic environment. Whereas the surface water was oxygenated, water column stratification caused oxygen-depleted bottom water conditions. Apart from oxygen depletion, biomarker data also provide evidence for strong input of terrestrial organic matter, dominated by angiosperms. Not surprisingly, diatom-related biomarkers occur in significant concentrations.

The hydrocarbon potential of the Oligocene rocks is fair to good, with an average TOC of 1.85% wt. and type II-III kerogen (avg. HI: 231 mg HC/g TOC), which may generate oil and gas. The organic matter is thermally immature. The SPI shows that the exposed section may generate about 0.2 tHC/m<sup>2</sup>, when mature. A rough estimate of the SPI for the entire Ruslar Formation at Karadere (incl. the non-exposed part) is 0.5 tHC/m<sup>2</sup>. This value is low, but in the order of other Oligocene sections offshore Bulgaria.

## **4.3 Eastern Carpathian Bend Zone**

### ***4.3.1 Samples and methods***

In total, 22 samples from of the Upper Menilites were collected in Sibiciu de Sus quarry, in Buzau county (Figure 2.5, 2.7). The following methods have been applied the following analysis: bulk parameters measurements, Rock Eval pyrolysis, XRD and FAAS on all 22 samples; petrography on X sample and micropaleontology analysis on 10 samples. Their results are presented below.

### ***4.3.2 Sibiciu de Sus, Romania***

### ***4.3.4 Results***

The stratigraphically lowermost rocks are exposed on the upper excavation level in the core of the anticline and include alternations of quartz-rich sandstone and menilites. These rocks are overlain by cherts, alternation of white and black diatomite, and pure diatomite (Figure 4.14). The lower excavation level is represented by impure diatomite (Figure 4.15). Higher stratigraphic units (e.g. breccia zone, grey marls) were not accessible during the sampling campaign in 2018. Because of strong tectonic deformation, it is impossible to determine the true thickness of the exposed units. Moreover, the relation between rocks exposed on both levels is hard to assess with confidence.

#### ***4.3.4.1 Lithological description***

The "alternation of quartz-rich sandstone and menilites" is a heavily folded and faulted unit that comprises thin quartz-rich sandstone beds (up to 30 cm thick) and menilites (5-30 cm thick) (Figure 4.14). The quartz-rich sandstone is fine-grained and poorly cemented. Sulphides are abundant. Thin sections reveal the presence of angular to subangular quartz grains, minor siliceous cement and abundant glauconite grains (Figure 4.16). Biotite is rare. As expected, the XRD diffractogram is dominated by quartz peaks (Figure 4.17).



Figure 4.14. Upper level of Sibiciu de Sus quarry. The white lines highlight the differences in lithology and complexity of the structure; a. composite picture with the position of the samples; b. core of the anticline represented by an alternation of quartz-rich sandstone and menilites; c. pure diatomite (cream colour); d. indistinguishable layering/structure of diatomite; e. pure diatomite (whitish colour) and alternation of white and black diatomite.



Figure 4.23. The lower level of the Sibiciu de Sus quarry exposing impure diatomite. The white lines highlight the complexity of the structure. Note the green-yellowish colour is caused by sulphides.

The menilites are splintery, have a dark grey to black colour when freshly broken and a strong smell of hydrocarbons. The XRD diffractogram indicates clay minerals and quartz as the main constituents (Figure 4.17). Vasiliu et al. (1996) and Frunzescu and Brănoiu (2004) described dysodile-like rocks instead of menilites. I suspect that the term dysodile was misused since our results indicate silica contents. The unit described as "alternation of white and black diatomite" is composed of white and black thin layers (cm to mm thick) which are heavily faulted (Figure 4.16a). The rock is compact, but relatively soft and has a very low weight. Microscopically, the rock is composed of a mass of diatom frustules embedded in the siliceous groundmass. The white layers include a lower amount of detrital grains and organic matter in comparison with the dark ones (Figure 4.16b). The detrital grains are represented by angular quartz, orthoclase feldspar and glauconite.



Figure 4.16. Selected samples and thin-section photographs from Sibiciu de Sus quarry. a, b-highly faulted alternation of white and black diatomite [a], the white layers contain significantly less organic matter compared with the black ones [b] (sample S17); c, d, e-impure diatomite highly deformed and faulted, covered with sulphides containing abundant organic matter [c], volcanic vacuolar glass [d] (sample S1) and intact diatoms frustules [e] (sample S10); f-pure diatomite with diatom mass and rare organic matter with few sandstone deformations present (sample S19); g- chert with few detrital grains: angular quartz, feldspars and glauconite (sample S21). h – quartz-rich sandstone containing angular quartz and glauconite with siliceous cement (sample S15).

The "pure diatomite" unit has a white-cream colour when freshly broken. Intercalations of white and cream diatomite laminae are visible, some of the laminae are fractured. In thin section, the pure diatomite is characterised by a mass of diatom frustules with siliceous groundmass. Some diatom frustules are intact. The detrital material is represented by angular quartz, feldspars, glauconite and volcanic glass. In thin sections, rare layers of sandy material are observed in the diatomite. The thickness of the sandy material is variable along the observed section (Figure 4.16f), indicating most probably syn-sedimentary deformation. The base of the unit is represented by strongly deformed layers represented by an alternation of white and black diatomites (>30 cm thick) (Figure 4.14e).

Cherts are fine-grained, very compact without visible stratification and exhibit splintering fractures. The colour is dark grey. In thin section (Figure 6g), the cherts show a siliceous mass with some detrital grains, including angular quartz, feldspar, sparse glauconite and rare volcanic glass.

The only lithology exposed on the lower excavation level (Figure 4.15) is impure diatomite (fresh cut colour dark grey) which is fine-grained and compact. The rock has a very light weight and a strong hydrocarbon smell. Intercalations with white diatomite laminae are observed. Soft-sediment deformations, small fractures/faults and folds are common (Figure 4.15). Sulphides are found on the surface of the samples due to weathering. In thin sections (Figure 4.16 d, e) abundant diatom frustules are present in a siliceous matrix. Some diatom frustules are intact and contain abundant organic matter. Detrital grains are represented by angular quartz, feldspar, glauconite and sponge spicules.

The unit designated as "Alternations of quartz-rich sandstone with diatomite" is exposed along the southern entrance in the quarry. It is separated by vegetation from the impure diatomites exposed at the lower level. In the field, it was hardly possible to correlate these units. The diatomaceous rock exposed here is 2 to 3 m thick and includes few sandstone layers (20 cm thick). The unit is also highly faulted, and we could not distinguish a typical depositional alternation between the sandstone and the diatomites. On a side note, Tămaş et al. (2020) demonstrated the presence of sand intrusions in a nearby outcrop of the underlying Upper Kliwa Formation. We presume that this zone might represent either a fault zone with thrusting of Upper Kliwa sandstone

onto the diatomites or by sand intrusions reaching this level (or a combination of both). Unfortunately, the quality of the outcrop prevented a clear determination of the nature of the contact.

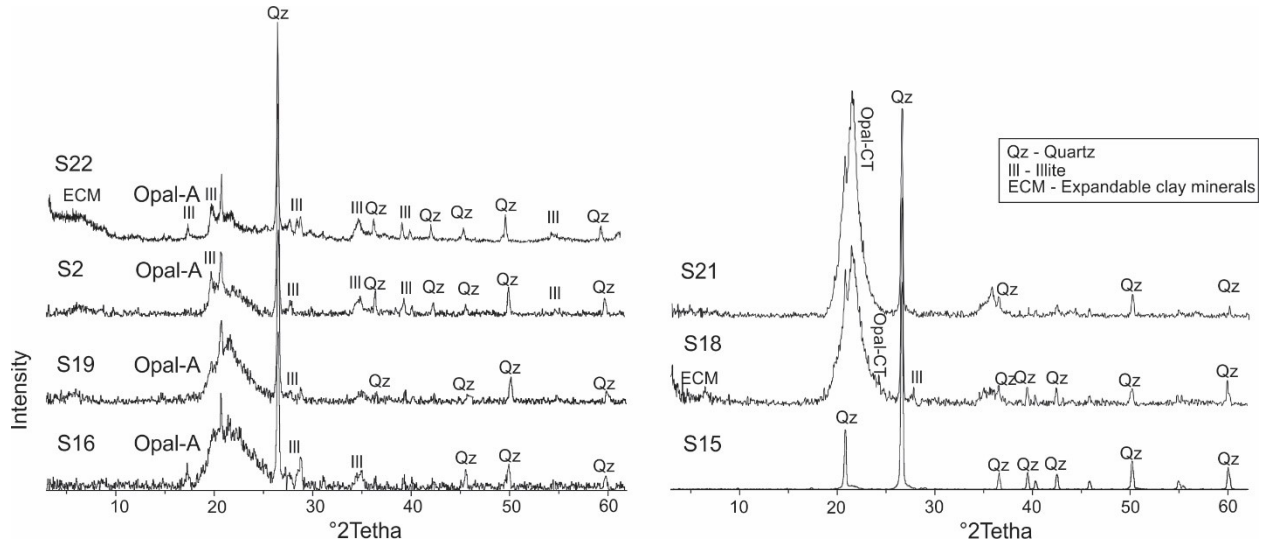


Figure 4.17. Representative XRD diffractograms showing different opal types in Sibiciu de Sus samples.

Based on XRD diffractograms, the mineral content of diatomites is rather uniform, but differences exist in opal types. Chert samples (S18, S21) contain opal-CT, whereas all other samples contain opal-A (Figure 4.17). Quartz and clay minerals are also present. As expected, in the analysed menilite sample (S22 in Figure 4.17) opal-A was recognized, and the quartz-rich sandstone sample (S15 in Figure 4.17) indicates quartz as the main mineral.

Biogenic silica (bSi) contents have been measured for all samples and are plotted in Figure 8. Diatomites contain, on average 51% bSi. Lower contents are seen in the quartz-rich sandstone (S15: 17% bSi) and the menilite (S22: 10% bSi) samples. Carbonate contents are low in all samples, and few samples exceed 2% wt. (Table 1, Figure 4.18).

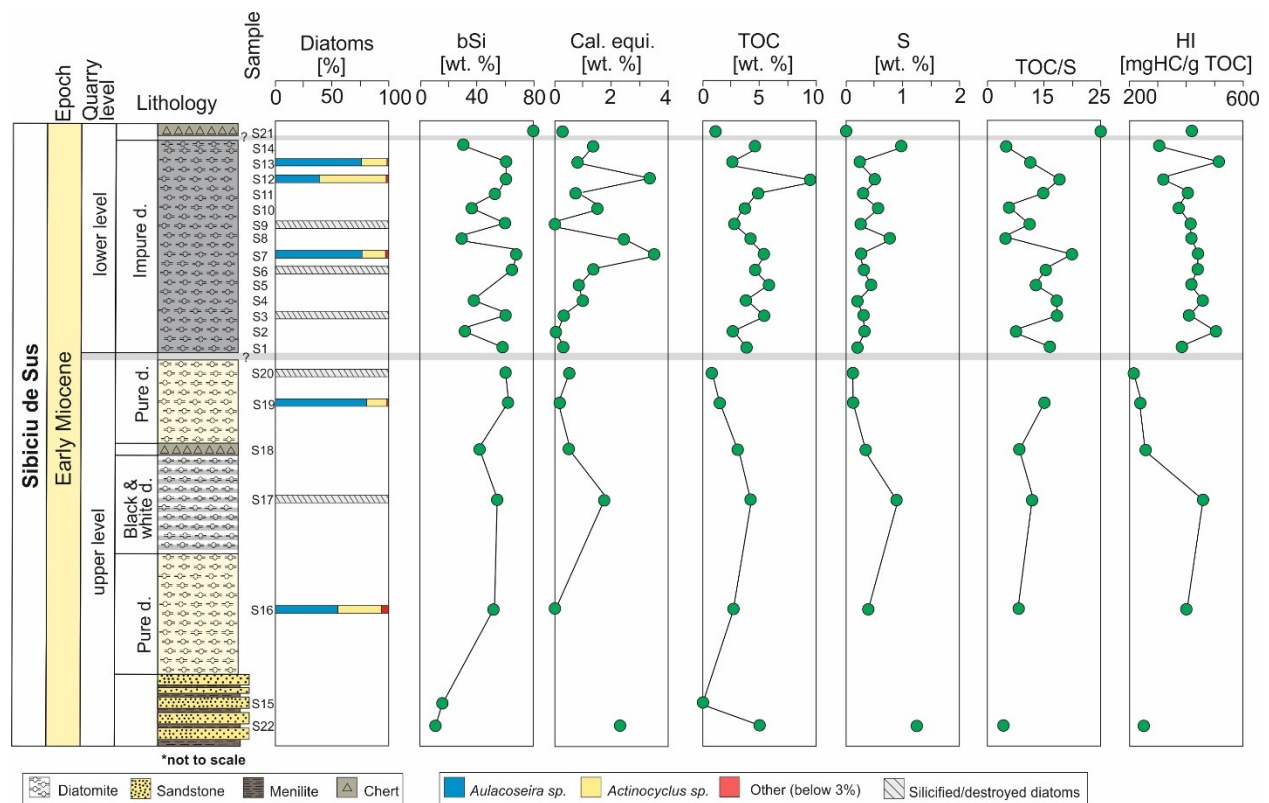


Figure 4.18. Bulk geochemical parameters and the relative abundance of the prevalent diatom genera of the diatomites exposed at Sibiciu de Sus. bSi-biogenic silica; Cal. equi. – calcite equivalent; TOC-total organic carbon; S-total sulfur; HI-hydrogen index.

#### 4.3.4.2 Bulk geochemical parameters

Bulk geochemical parameters measured in Sibiciu de Sus samples are listed in Appendix 1 Table 6 and plotted in Figure 4.18. The average TOC content for diatomite samples is 3.77% wt. Maximum TOC contents (up to 9.57 % wt.) are observed in impure diatomite samples. The menilite sample also has a high TOC content (5.01% wt.). As expected, the TOC content of the sample from quartz-rich sandstone is very low (0.36% wt.). The sulphur (S) content follows the TOC trend but is typically much lower (average 0.42 % wt.). Therefore, TOC/S ratios are high (4-25; Figure 4.18).

S2 values reach a maximum of 30.67 mg/HC g rock (Figure 4.19) (avg. 14.64 mg/HC g rock), and HI values range between 206 to 515 HC/g TOC, indicating the prevalence of type II kerogen. Tmax values do not exceed 424°C. Although Tmax values are low, the Production Index



is high (0.1-0.3; Table 1; Figure 4.20). This is clear evidence for the presence of migrated hydrocarbons (Figure 4.20).

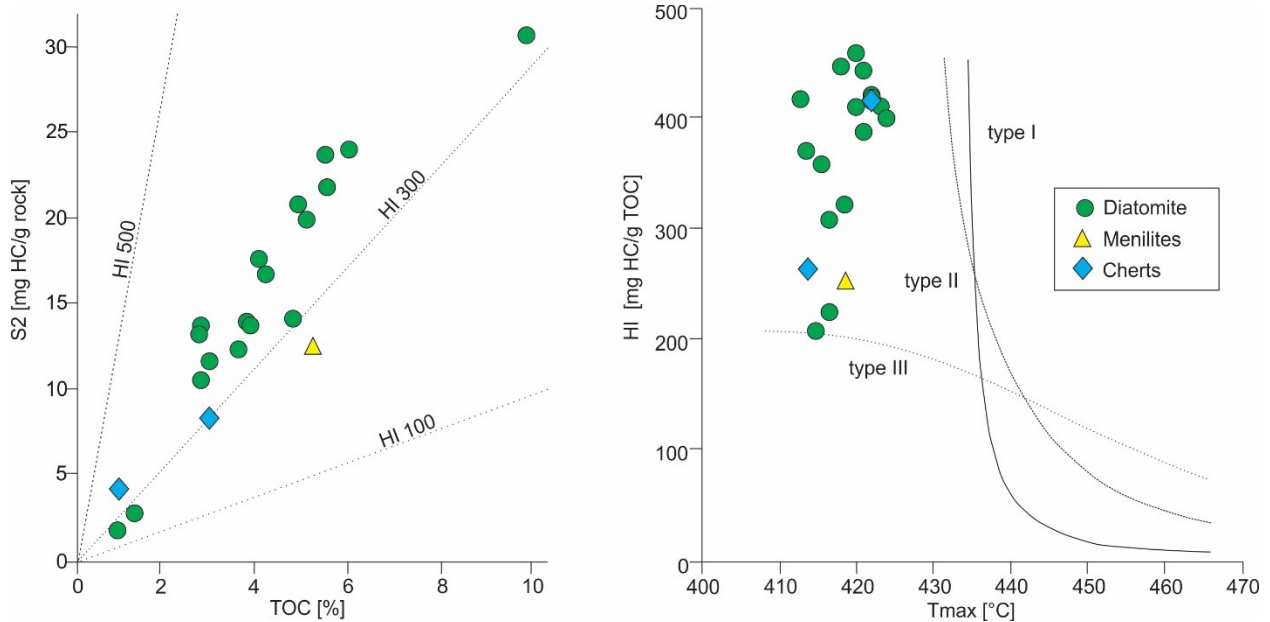


Figure 4.19. Plots of S2 vs TOC and Hydrogen Index (HI) vs Tmax for Sibiciu de Sus quarry samples.

#### 4.3.4.3 Diatom assemblages

Attempts to extract siliceous microfossils from diatomite samples were unsuccessful, but SEM examination enables an insight into the taxonomic composition of the fossil diatom assemblages. The rock surfaces of eleven samples were analysed. In six samples, the diatoms were broken or/and silicified beyond recognition (Figure 4.18). As light microscopic examination was impossible and literature on Neogene diatoms in the Eastern Carpathians is scarce, most of the identifications are to the genus level. Pictures of those diatoms for which we were able to provide a positive identification are presented in Plates VII-X. The average abundance of the diatom genera is plotted against the stratigraphic position of the samples examined for diatoms in Figure 4.18.

Paradoxically, despite common fragmentation of diatom valves and pervasive silicification, the preservation of valve fine structure is often pristine. Diatom valves are often linked in chains, and even the most delicate areolae occlusions (i.e., vela) are preserved intact.

Thus, the siliceous cement responsible for induration of the rock is unlikely to be derived from diatom dissolution.

Two genera seem to be especially abundant in the Sibiciu de Sus diatom assemblages based on the average of all analysed samples: *Aulacoseira* (66%) and *Actinocyclus* (31%). *Ellerbeckia*, *Opephora*, *Paralia*, *Rhaphoneis* and chrysophycean cysts have been recognized rarely, and they are represented on average below 3%.

A striking contrast is seen when plotting the results of the diatom genera against lithology (Figure 4.18). For example, in the impure diatomite, three samples (S3, S6, S9) are heavily silicified with unidentifiable diatoms, whereas three other samples (S7, S12, S13) yield good results. Samples S7 and S13 showed similar genera abundances: *Aulacoseira* (77% and 76%, respectively), *Actinocyclus* (21% and 19%, respectively). In contrast, *Aulacoseira* (36%) is less abundant in sample S12, which contains abundant *Actinocyclus* (61%). From three pure diatomite samples (S16, S19, S20), two yielded good results. Samples S16 and S19 are characterized by abundant *Aulacoseira* (56% and 84%, respectively) and *Actinocyclus* (39% and 16%, respectively).

Diatoms in sample S17 representing the black and white diatomite are too silicified for proper identification. However, our observations show that the black layers contain significantly more diatom frustules compared to white ones. As expected, diatoms could not be detected in the sample from the quartz-rich sandstone.

#### **4.3.5 Discussion and interpretation**

##### **4.3.5.1 Maturity, migrated bitumen and hydrocarbon source rock potential**

T<sub>max</sub> values of the diatomites from Sibiciu de Sus (max. 424°C) indicate that the studied section is immature. Nevertheless, S1 and PI values are high. This shows the presence of migrated bitumen (Figure 4.20), which is also responsible for the strong hydrocarbon smell of many diatomite samples.

In order to test the influence of the migrated bitumen on the Rock-Eval results, a cm-size piece and several mm-size fragments from sample S12 were washed with hexane. The obtained S1 values were reduced by 50% (cm-size sample; PI: 0.09) and 75% (mm-fragments; PI: 0.05), respectively. The S2 values decreased by a maximum of 5%, implying that the influence on S2

and HI is minor. Hence, the organic matter of most diatomite samples is classified as oil-prone type II kerogen (Figure 4.19). Only pure diatomite, chert and menilite contain a type III-II kerogen.

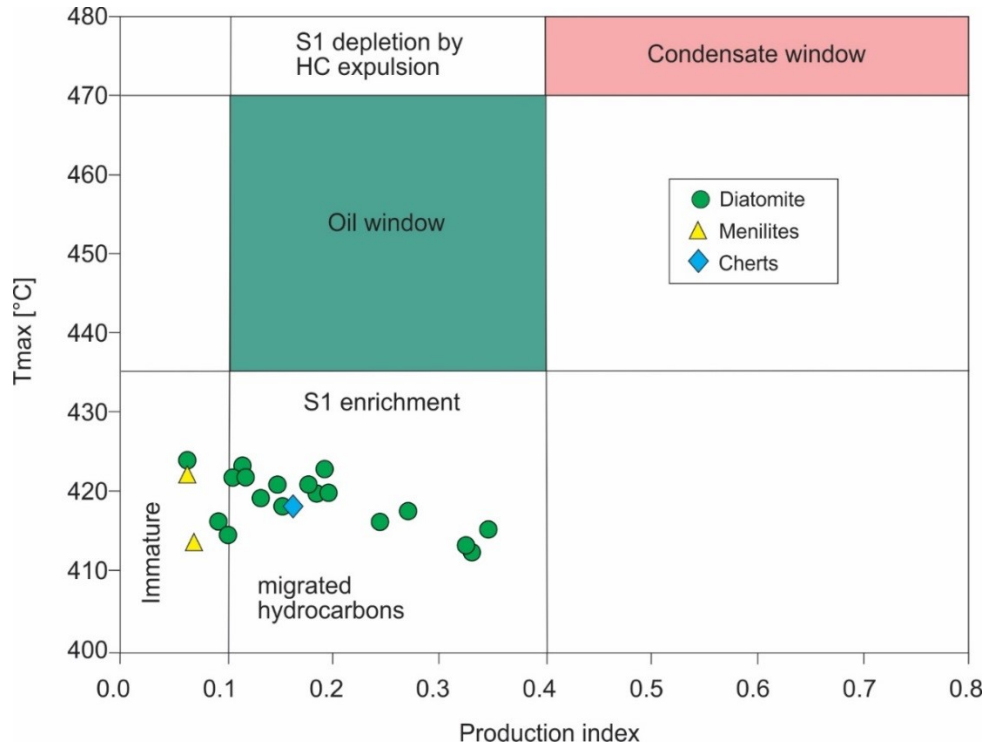


Figure 4.20. Plot of Tmax vs. Production Index which indicate that the samples from Sibiciu de Sus quarry are contaminated with migrated hydrocarbons.

The generative potential is determined based on TOC and the petroleum potential (S1+S2). Based on the TOC contents, all fine-grained Sibiciu de Sus samples, except for pure diatomite samples (S19, S20), may be classified as a very good source rock (Figure 14). Based on the petroleum potential, most samples are classified as good to very good source rocks (irrespective if original or corrected S1 values are taken into consideration).

In order to approximate amount of hydrocarbons (in tons HC) that can be generated beneath 1 m<sup>2</sup> of surface area is determined the source potential index ( $SPI = \text{thickness} \times (S1+S2) \times \text{bulk density} / 1000$ ; Demaison and Huizinga, 1994). Due to the highly deformed structure of the rock unit exposed at Sibiciu de Sus, we use a net thickness of the diatomite to 40 m, based on the measurements by Frunzescu and Branoiu (2004), for the calculation of the SPI. Considering the shallow burial depth, and the high amount of diatoms, a density of only 1.95 g/cm<sup>3</sup> has been

applied. The average S1 values (of 3.83 mg HC/g rock) is clearly influenced by migrated bitumen. For our calculation, we consider only 25% of it (0.96 mg HC/g rock) and the average S2 of 15.54 mg HC/g rock. Using these data, the SPI is calculated as 1.3 t HC/m<sup>2</sup>.

#### 4.3.5.2 Depositional environment

Diatoms can be excellent environment indicators. However, their proper identification is critical for a reliable assessment of the depositional environment. Frunzescu and Brănoiu (2004) documented *Actinocyclus*, *Coscinodiscus*, *Melosira* and *Stephanodiscus* from Sibiciu de Sus diatomites. *Melosira*, however, is a genus that has been undergoing taxonomic revision, and numerous taxa have been transferred elsewhere, including *Aulacoseira*, *Paralia*, *Orthoseira* and *Ellerbeckia* (Round et al., 1990). Especially the fossil taxa included in *Melosira* are in need of further revision. The taxa reported as *Melosira clavigera* and *M. granulata* tentatively identified by Frunzescu and Brănoiu (2004) from Sibiciu de Sus have been transferred to *Ellerbeckia* and *Aulacoseira*, respectively (Simonsen, 1979; Crawford and Sims, 2006). Apart from that, Sebe-Rădoi et al. (2017) reported *Actinocyclus*, *Coscinodiscus* and *Actinoptychus* as the dominant genera in the Sibiciu de Sus diatomite.

In the present study, the most abundant genus is *Aulacoseira*, a widespread taxon inhabiting lacustrine and lotic waters (Denys et al., 2003). The Holocene *Aulacoseira* can indicate shallow-water conditions with high wind exposure, which provides the turbulent, high-nutrient regime favourable for this taxon to flourish (Kociolek et al., 2015).

*Actinocyclus* is a primarily estuarine genus. However, it can occur in the plankton in salinified or eutrophic inland water. *Actinocyclus* is most abundant in wind-mixed shallow lakes and in estuaries or turbulent rivers (Stoermer and Julius, 2003). Round et al. (1990) characterized *Actinocyclus* as a marine genus that is becoming established in freshwater, mainly epiphytic on seaweeds but frequently met in the nearshore plankton. Moreover, *Actinocyclus* has been described co-occurring with *Ellerbeckia* in a fossil freshwater deposit in the United States (Kociolek and Spaulding, 2002). Nonetheless, a disagreement with this assessment has been raised by Crawford (2004). Marine diatoms are less abundant in Sibiciu de Sus, and they are represented by *Rhaphoneis* and *Opephora*; both genera are living attached to sand grains (Round et al., 1990).

Based on the diatom assemblage composition, Sebe-Rădoi et al. (2017) suggested a shallow marine depositional environment with freshwater contribution for the diatomites in Sibiciu de Sus. However, the large proportion of *Aulacoseira* suggests a more substantial freshwater input, which, together with the presence of *Actinocyclus*, may suggest a transitional environment like an estuary or a river mouth with highly eutrophic conditions. Furthermore, the high diatom production in Sibiciu de sus may be caused by river plumes, which are highly eutrophic areas (e.g., Lohrenz et al., 1990; Smith and Demaster, 1996). In addition, the high TOC/S ratio points toward a non-marine depositional environment.

The presence of the glauconite is usually an indication for shallow marine environment (Smith et al., 1987) and a slow rate of deposition (Triplehorn, 1965). However, the glauconite from the Sibiciu de Sus is most probably detrital since it is considered unlikely for the glauconite to form in estuaries or at water depths shallower than 15 m due to wave-induced turbulence (e.g., Cloud 1955; Rothwell, 1980).

#### **4.3.5.3 Regional significance**

##### **4.3.5.3.1 Diatom preservation**

The diatomites at Sibiciu de Sus represent a shallow marine depositional setting with strong freshwater input. The section contains abundant well-preserved diatoms, represented by several genera. The excellent preservation of the valve fine structure in the diatoms suggest that silica content was high, preventing the diatom frustules from getting dissolved. Hence, a volcanic activity in the area should not be excluded considering that tuffs have been previously described in the quarry (Vasiliu et al., 1996; Frunzescu and Brănoiu, 2004). After all, volcanic tephra helps significantly in diatom preservation (Harper et al., 2015), which might be the case in Sibiciu de Sus diatoms preservation.

The remarkably good preservation of the diatoms and the considerable thickness of the diatomite deposits make Sibiciu de Sus unique compared with other Oligo-Miocene diatomaceous successions in the Carpathian realm. For example, within the Skole Nappe in Poland diatomites are present in three horizons (e.g., Kotlarczyk and Kaczmarska, 1987): Futoma Member (Lower Oligocene; Menilite Formation), Piątkowa horizon (Upper Oligocene, Lower Miocene, at the transition between Menilite and Krosno Formations) and Leszczawka Diatomite Member (Lower Miocene; Strzyżow Formation; formerly Upper Krosno Formation) (Figure 2). The sedimentary

beds are largely represented by diatomites, diatomaceous shales, shales, sandstones, cherts and tuffite deposited in a shallow marine, neritic environment. The diatomite thickness varies significantly, from approximately 10 m in the Futoma Member, 3 to 25 cm intercalations in Piątkowa and a complex of up to 140 m in Leszczawka Diatomite Member (Kotlarczyk and Kaczmarek, 1987; Figarska-Warchoł et al., 2015 and references therein).

Although the diatomites from Menilite and Krosno formations contain more shale compared with Sibiciu de Sus, the diatoms are as strongly indurated as at Sibiciu de Sus. Kotlarczyk and Kaczmarek (1987) spent months on the preparation of the samples in order to achieve a positive identification of the diatoms. Later, Figarska-Warchoł et al. (2015) observed the rock samples using SEM, but the diatoms have mostly broken frustules. In both cases, a diatom-based age identification was not possible due to the lack of reference sections and the presence of long-ranging Paleogene-Neogene taxa.

#### ***4.3.5.3.2 Petroleum potential comparison***

In general, the Oligocene to Lower Miocene Menilite Formation comprises menilites, bituminous marls and black shales. It is widespread in the Carpathians, and it forms the most important hydrocarbon source rock (e.g. Kotarba and Koltun, 2006; Boote et al., 2018). Sachsenhofer et al. (2015) and Rauball et al. (2019) studied the vertical variation of the source potential of the Lower Menilites and the Upper Menilites in the Eastern Carpathians (Figure 2). An overview of the Menilite Formation is given by Sachsenhofer et al. (2018a, b).

In the ECBZ, the extent of Upper Menilites is limited, and they have been described mostly in the southern part (Slănicul de Buzău river valley; Mutihac and Ionesi, 1974). Overall, geochemical data from the Tarcău Nappe are insufficient for estimating the hydrocarbon potential of the Upper Menilites. For example, Grasu et al. (1988) provided a percentage ranging from 0 to more than 20% TOC, although no location for the analysed samples is provided. Țabără (2010) postulated only the TOC ranges (2.25-11.85% TOC) for the samples analysed in the north side of the Tarcău Nappe (near Gura Humorului, see Figure 1 for location). However, the data provided is still insufficient for a proper assessment of the Upper Menilites hydrocarbon potential within the Tarcău Nappe and additional studies are necessary.

It is worth mentioning that the Upper Menilites have been described in the northern part of the Carpathians, specifically in the Skyba Nappe in Ukraine (corresponding to Tarcău Nappe in Romania). Here, the TOC content of the Upper Menilites is moderately high (2-7% wt.; max. 15%) and the HI values are on average 440 mg HC/g TOC. On average, the values for S1 is 0.45 mg HC/g rock, S2 is 32.30 mg HC/g rock and Tmax is 425° C (Rauball et al., 2019). Overall, the petroleum potential of the Upper Menilites is good to very good (Figure 14). The organic matter is immature, however (Rauball et al., 2019). Sachsenhofer et al. (2015) studied the “Upper Dysodilic Shale Member”, representing the Upper Menilites in the Marginal Folds Nappe, and estimated the SPI as 1.82 tHC/m<sup>2</sup>.

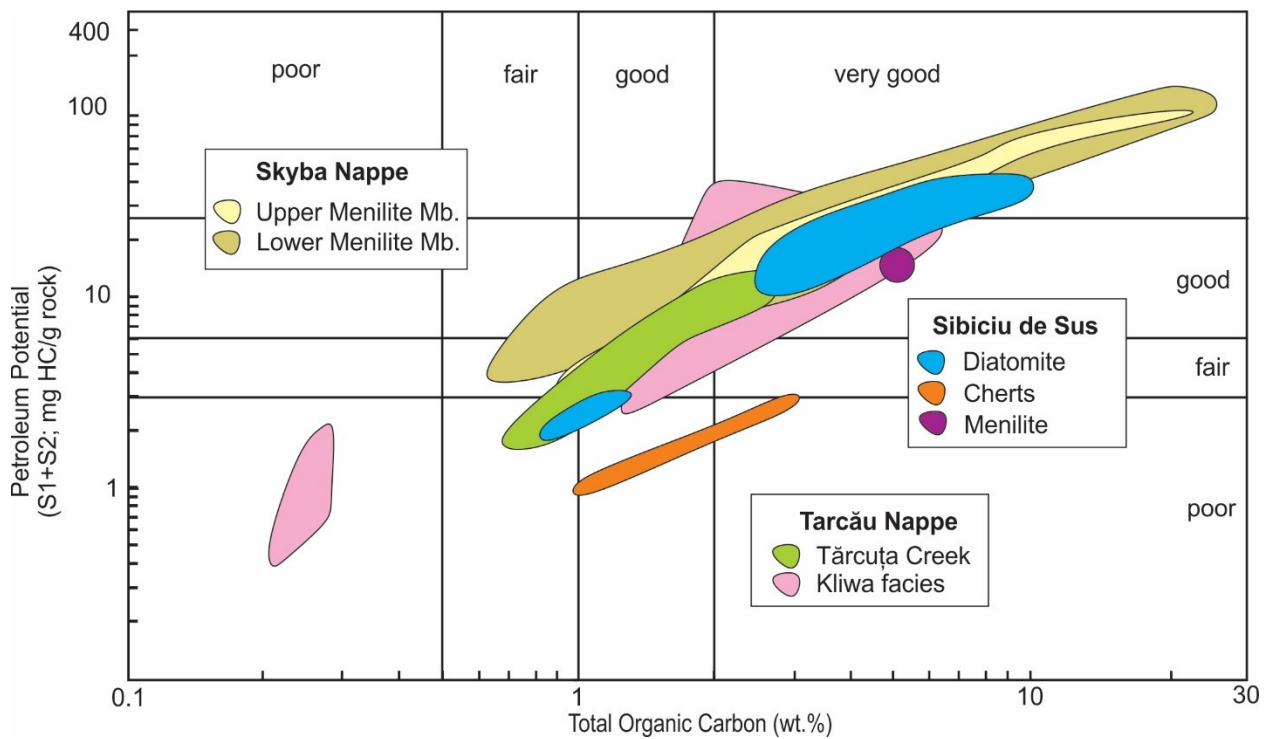


Figure 4.21. Petroleum potential of the diatomites from Sibiciu de Sus. Values of the petroleum potential of equivalent sediments in the Tarcău Nappe and Skyba Nappe (Ukraine) are shown for comparison (data compiled from Belayouni et al., 2007; Wendorff et al., 2017; Rauball et al., 2019).

In comparison, the Lower Menilites represented in the Tarcău Nappe have a very good hydrocarbon potential (Figure 4.21), and only a few samples display poor hydrocarbon potential. The samples from the Kliwa lithofacies presented by Belayouni et al. (2007) have a fair to good hydrocarbon potential, and the samples from Tărcuța Creek (Wendorff et al., 2017) have poor to good potential (Figure 4.21). The TOC maximum reached 10.99% wt. in the Kliwa lithofacies

(avg. 2.87% wt.), and in Tărcuța Creek it is 2.58 (avg. 1.74% wt.). The HI is on average 285 mgHC/gTOC for the Kliwa lithofacies (Belayouni et al., 2007) and 384 mgHC/g TOC for Tărcuța Creek (Wendorff et al., 2017). From the two sections, only the last one is thermally mature.

Moreover, Lower Menilites from the Skyba Nappe contain TOC which exceeds 20% wt. and the HI values are very high (up to 800 mg HC/g TOC). This highlights the excellent hydrocarbon potential of the thermally immature succession (Rauball et al., 2019).

#### ***4.3.5.3.3 Regional understanding***

During Early Miocene, the connection between the Central and Eastern Paratethys was closing (e.g., Rögl, 1999; Kováč et al., 2018). The tectonic movements and the uplift of the Carpathians caused changes in the sedimentary regimes. In the Carpathian Basin, the marine connection was obstructed and evaporites were deposited in the Romanian and Ukrainian sectors across the NN3/NN4 zones boundary (Rögl, 1998; Popov et al., 2004b; Gozhyk et al., 2015). The last anoxic event within the basin is represented by the Upper Kliwa and Upper Menilites, which indicates rapid changes between open marine and restricted marine anoxic conditions (Amadori et al., 2011). The Sibiciu de Sus diatomites display the depositional sequence during/after the marine connection was closed between the Eastern and Central Paratethys and before deposition of the evaporitic sequence. Besides, the sediments were deformed during the mid-Miocene tectonic stage resulting in strong deformation of the diatomites at Sibiciu de Sus. The deformation happened due to compressional tectonics and soft-sediment deformation.

The Oligocene and Lower Miocene in the Romanian Carpathians contain endemic fossil assemblages which makes the age determination constrained and uncertain (e.g., Melinte-Dobrinescu and Brustur 2008; Munteanu et al. 2014; Bercea et al. 2016, Tămaș 2018). For example, the Lower Kliwa is presumed to be Chattian (Oligocene) in age within the ECBZ (e.g., Dumitrescu et al., 1970; Săndulescu, 1984; Schleder et al., 2019) and in the northern part of the Tarcău Nappe, the formation age is proposed to be Aquitanian (Miocene) (Belayouni et al., 2007). Sibiciu de Sus outcrop represents another location within the ECBZ where a certain age cannot be provided. However, given the regional context, the Upper Menilites studied here are most probably Lower Burdigalian in age and cannot be younger than the evaporitic sequence above (i.e. intra-Burdigalian salt; Schleder et al., 2019).



#### **4.3.6 Conclusions**

The abandoned Sibiciu de Sus quarry provides one of the largest exposures of diatomites in the Eastern Carpathians. The exposed diatomites represent the upper part of the Upper Menilites in the ECBZ. The diatomites, represented here by several lithologies and are highly deformed due to soft-sediment deformation and subsequent compressional tectonics.

The Sibiciu de Sus diatomites are characterized by well-preserved diatom assemblages, where even the most delicate areolae occlusions are preserved intact. However, the samples are highly indurated and common diatoms extraction methods yielded no positive results. Therefore, diatom assemblages were examined using SEM techniques. Diatom assemblages are represented by two dominant genera (*Aulacoseira*, *Actinocyclus*) and four subordinate genera (*Ellerbeckia*, *Opephora*, *Paralia*, *Rhaphoneis*) and suggest deposition in a shallow marine environment with strong freshwater contribution.

The hydrocarbon potential of the Lower Miocene rocks is good to very good, with an average TOC of 3.77% wt. and type II–III kerogen (avg. HI: 384 mg HC/g TOC). The organic matter is thermally immature. However, high amounts of S1 hydrocarbons provide proof of the presence of migrated hydrocarbons. The SPI calculations indicate that the exposed section could generate about 1.3 t HC/m<sup>2</sup> if mature.

## **4.4 Gyöngyöspata Basin**

### ***4.4.1 Szurdokpüspöki, Hungary***

#### ***4.4.1.1 Sample and methods***

In total, 24 samples from of the diatomaceous earth were collected from Szurdokpüspöki quarry, (Figure 2.8). The following methods have been applied the following analysis: bulk parameters measurements, Rock Eval pyrolysis, XRD on all 22 samples, FAAS on 18 samples; petrography on X sample and micropaleontology analysis on 13 samples. Their results are presented below.

#### ***4.4.2 Results***

##### ***4.4.2.1 Lithology***

A 12-m thick section representing diatomaceous rocks has been studied in the abandoned Szurdokpüspöki quarry (Figures 2.8, 4.22). Unexposed parts are marked in Figure 4.22 with question marks. The diatomite is laminated (paper-like), very fragile, with dark grey to yellow-whitish colour when freshly broken. Few dark-grey chert layers have been observed intercalated with the diatomaceous rock. In thin section observation, the rock contains diatom valves masses in an argillaceous matrix with very rare detrital grains (Figure 4.23). The detritus is represented by angular quartz, plagioclase, volcanic clasts and volcanic glass. Few samples are heavily altered, but in sample III-Sp, the siliceous diatom valves are replaced by calcite or clay minerals.

In X-ray diffractograms, opal-A is present in the majority of the samples from Szurdokpüspöki. Opal-CT is present only in sample 6-Sp. The diffractograms show that clay minerals, biogenic silica and varying amounts of calcite are the major constituents of the studied rocks (Figure 4.24). A change in mineralogy with height is observed on XRD diffractograms. The base of the section (samples I-Sp to 9-Sp) is calcite dominated, whereas the upper part of the section (samples 10-Sp to 21-Sp) is dominated by clay minerals.

The same trend has been observed in the carbonate contents, where the lower 6-m-thick interval is characterized by high carbonate contents (samples I-Sp to 9-Sp; 10-70% wt.; Appendix 1 Table 7), whereas the rest of the section is largely carbonate-free (samples 10-Sp to 21-Sp). The percentage of biogenic silica ranges from 15 to 30 % and is typically higher in the carbonate-poor upper part than in the carbonate-rich lower part (Figure 4.22).

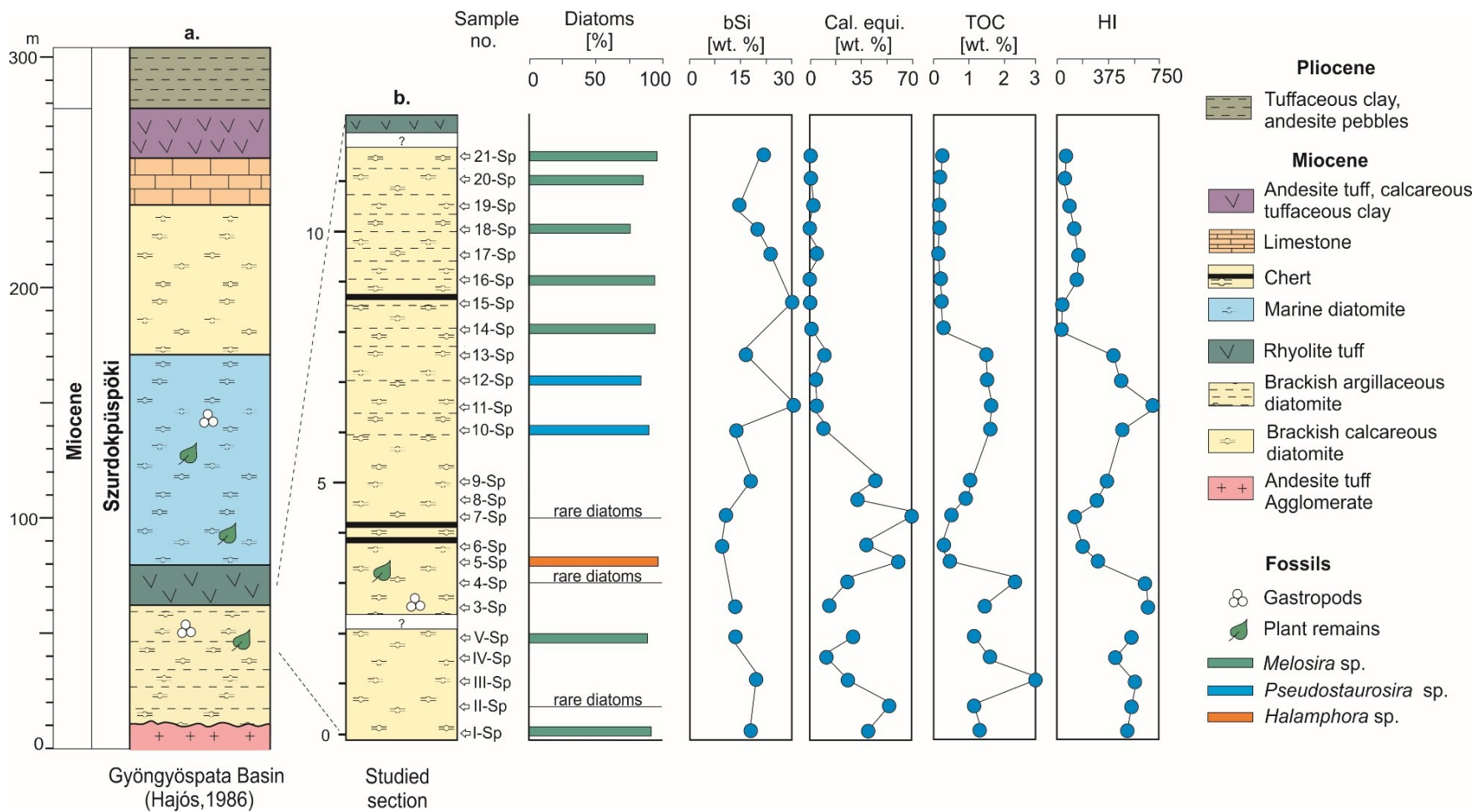


Figure 4.22 Szurdokpüspöki quarry, Hungary. a. lithology of the Gyöngyöspata Basin established on the Szurdokpüspöki quarry and the wells drilled in the area (after Hajós, 1986); b. lithology of the studied section with the geochemical parameters and the predominant diatom genera. bSi-biogenic silica; Cal. equiv.-calcite equivalent; TOC-total organic carbon; HI-hydrogen index.

Szurdokpüspöki quarry

Parisdorf quarry (Limberg)

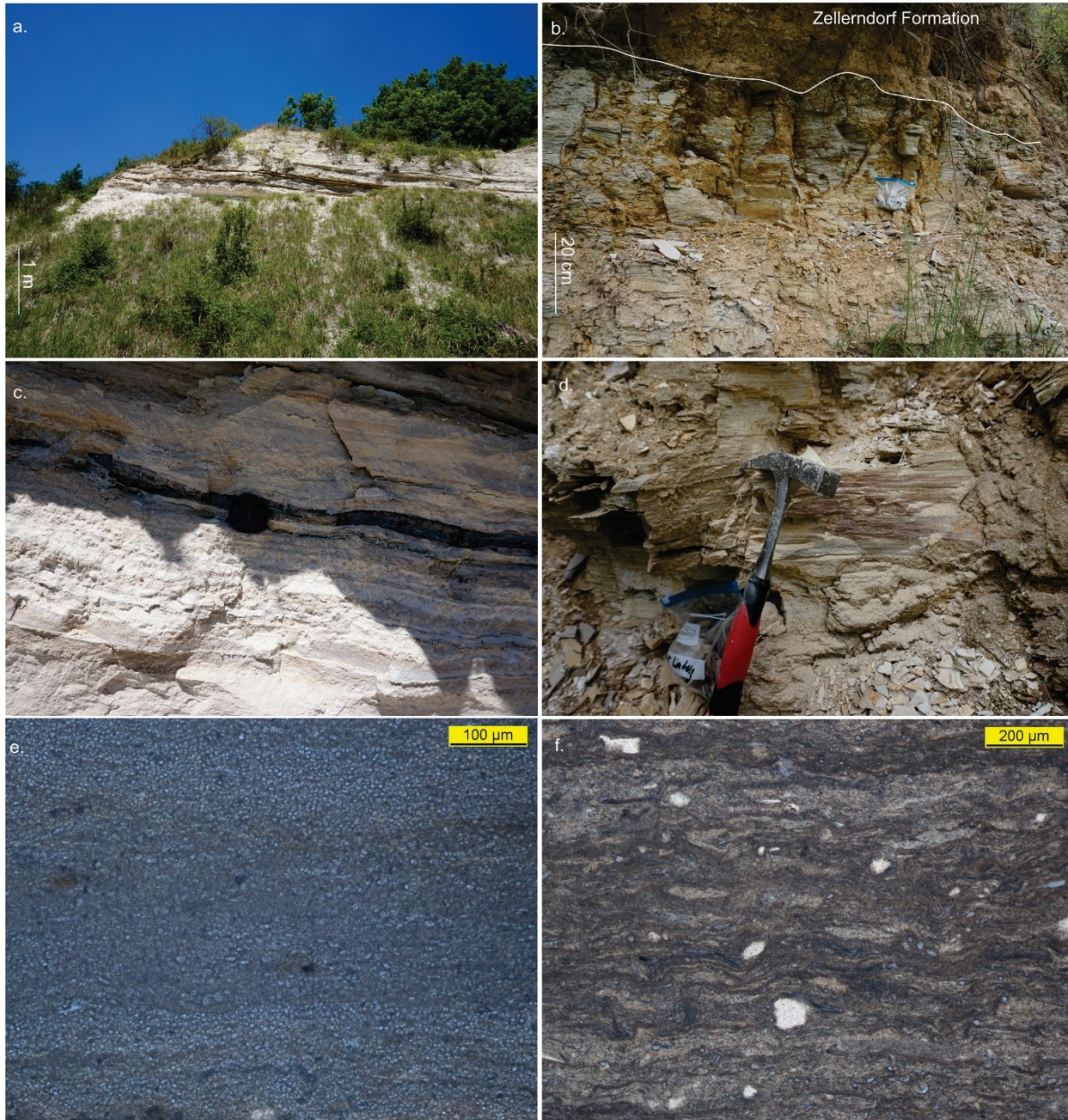


Figure 4.23. Photographs of diatomite at Szurdokpüspöki and Parisdorf quarries. a, b – Overview of studied sections; c-calcareous diatomite with chert intercalate (sample 7-Sp); d-argillaceous diatomite (sample 15-Li); e, f-thin section microphotographs; e-abundant diatom valves with argillaceous matrix (21-Sp); f-argillaceous diatomite with common diatom valves and relative large angular quartz grains (4-Pa).

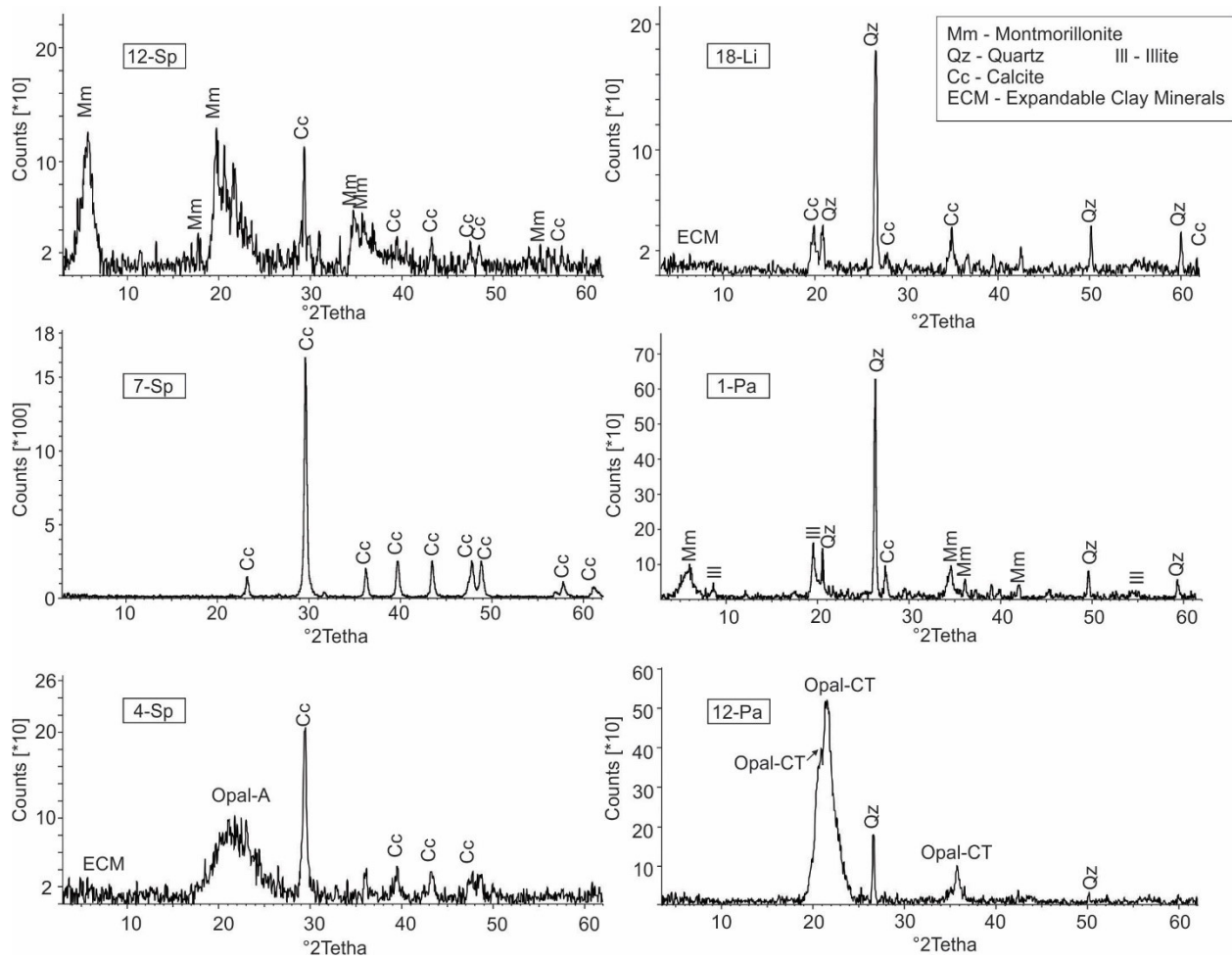


Figure 4.24. X-ray diffractograms of diatomaceous sediments at Szurdokpüspöki (4-Sp; 7-Sp; 12-Sp), Parisdorf (12-Pa; 1-Pa) and Limberg (18-Li).

Chert layers are found both in the carbonate-rich lower part (between samples 6-Sp and 7-Sp; Figure 4.22) and in the carbonate-free upper part (between samples 15-Sp and 16-Sp).

Based on the very low carbonate contents in the upper part and the presence of chert layers, this section can be correlated to the lower freshwater to oligohaline interval with diatomite described by Hajós (1986). The overlying andesite tuffs (Figure 4.22) are exposed in the south-eastern sector of the quarry.

#### 4.4.2.2 Bulk geochemical parameters

Bulk parameters for the Szurdokpüspöki sections are listed in Appendix 1 Table 7 and plotted versus height in Figure 4.22. TOC contents are high (0.2-3.0% wt.; average 1.28% wt.) in the lower part of the Szurdokpüspöki section (samples I-Sp to 13-Sp) and very low (average 0.14% wt.) in the carbonate-free upper part of the section (samples 14-Sp to 21-Sp). Within the organic matter-rich section, the interval around the lower chert layers is poor in TOC, but TOC contents increase upwards and are in the order of 1.5% wt. in the middle part (samples 10-Sp to 13-Sp). Sulphur (S) contents range up to 1.16% wt. TOC/S ratios are meaningful only for the organic matter-rich lower portion of the section. For samples with TOC contents exceeding 0.3% wt., TOC/S ratios range from 1 to 8 (Table 1) and show an upward decreasing trend. S<sub>2</sub> values reach a maximum of 14.4 mg HC/g rock and strongly relates to TOC contents. HI values in the lower organic matter-rich section range from 178 to 723 mg HC/g TOC. A plot of S<sub>2</sub> versus TOC suggests that the true HI is in the order of 640 mg HC/g TOC which suggests the prevalence of type I to II kerogen. T<sub>max</sub> is on average 406° C, indicating that the organic matter is immature.

#### 4.4.2.3 Diatom assemblages and depositional environment

Samples from the Szurdokpüspöki quarry contain diverse and abundant diatom assemblages, including numerous extant brackish and marine forms alongside fossil taxa that were likely brackish or freshwater. Fossil brackish and freshwater diatoms are generally poorly known, and therefore in the paleoenvironmental interpretation below, we focus on genus-level rather than species-level identifications. For the present, we generally follow the identifications by Hajós (1986) but make the necessary amendments where newer taxonomic concepts are involved. We also stress that further work is needed in order to obtain a proper understanding of Central Paratethys diatom assemblages.

The dominant diatom is represented by *Melosira bituminosa* Pantocsek following Hajós (1986). This species is morphologically dissimilar from *Melosira* sensu stricto, however, and certainly belongs in another genus. In SEM, we note that the valve structure of *M. bituminosa* generally resembles that of *Ehrenbergia granulosa* (Grunow) A. Witkowski, Lange-Bertalot and Metzeltin (2000), especially in the placement of the marginal processes, and the presence of

carinoportulae. However, a formal transference is beyond the scope of the present study. Hajós (1959) identified *Amphora* sp. Ehrenberg ex Kützing in the brackish section. Nevertheless, the genus *Amphora* was divided into several subgenera, one of them being *Halamphora* Cleve. In 2009, Levkov raised the subgenus *Halamphora* to the genus level and transferred many *Amphora* spp. which present all morphological features of the new genus to *Halamphora*. In our identification, the diatom from Szurdokpüspöki previously identified as *Amphora* presents the features of the new genus *Halamphora*. A similar case is represented by *Fragilaria* Lyngbye, from which Williams and Round (1988) separated the genus *Pseudostaurosira*.

Diatom assemblages from the Szurdokpüspöki quarry are often dominated by single genera. Seven samples (I-Sp, V-Sp, 14-Sp, 16-Sp, 18-Sp, 20-Sp, 21-Sp) are dominated (avg. 92%) by „*Melosira*” (see discussion below) and in two samples (10-Sp, 12-Sp) *Pseudostaurosira* (previously part of *Fragilaria*) is the most abundant (81%). *Halamphora* (previously a subgenus within *Amphora*) dominates only in sample 5-Sp (98%). Less frequent genera include *Brachysira* Kützing (including the extant *B. aponina* Kützing), *Cocconeis* Ehrenberg, *Cymbella* C. Agardh, *Diploneis* Ehrenberg ex Cleve, *Epithemia* Kützing, *Navicula* Bory, *Nitzschia* Hassall (including the extant *N. inconspicua*), *Planothidium* Round and Bukhtiyarova, *Podosira* Ehrenberg, *Seminavis* Mann and *Surirella* Turpin (Plate VI-VII), including the extant *S. striatula*. Only few samples (II-Sp, 4-Sp, 7-Sp) contained sparse diatoms (Figure 4.22).

Based on the valve structure similarity discussed above, we hypothesize that „*Melosira*” *bituminosa* must have occupied a similar ecological niche to *E. granulosa*, i.e., in littoral and often in tidal flats (Witkowski et al., 2000).

*Halamphora* is a relatively large, widely distributed genus, with most of the species being found in marine or brackish water habitats; some in coastal environment and only a few species occur in freshwater. Most of the genera found in Szurdokpüspöki are periphytic and benthic, some haptobenthic (*Cocconeis*), i.e., living in near-shore littoral brackish water. Few planktonic genera are found, represented by *Nitzschia*, and *Navicula*. This is generally consistent with previous interpretations (Hajós, 1986) of the paleoenvironment, which is mainly near-shore littoral brackish waters. In addition, we observe favourable conditions for single genera blooms (5-Sp: *Halamphora* sp.; 10;12-Sp: *Pseudostaurosira* sp.) which were most likely a result of the volcanic activity in the area. Thus, the diatom assemblage composition strongly indicates a brackish marine environment.

Modern taxa such as *Surirella striatula*, *Nitzschia inconspicua* and *Brachysira aponina* generally occur in salinities lower than 10 psu (e.g., Hajós, 1973; Gaiser et al., 2005; Rovira et al., 2015), for instance in modern-day Mediterranean lagoons, which perhaps could be viewed as an analogue for the depositional setting of the Szurdokpüspöki site.



## **4.5 Alpine-Carpathian Foredeep Basin**

### ***4.5.1 Parisdorf and Limberg, Austria***

#### ***4.5.1.1 Samples and methods***

In total 20 samples were analysed from two locations. 13 samples from Parisdorf and 7 samples from Limberg. The samples from the quarries are referred to in the text below as quarry samples. The second set consisting of 12 samples have been collected by P. Grunert and R. Roetzel from the Limberg-Hangbrücke (KB2/07) borehole drilled north of Limberg in 2007, and the samples are here referred as borehole samples.

#### ***4.5.2 Results***

##### ***4.5.2.1 Lithology***

Zellerndorf Formation below the diatomaceous Limberg Member has been studied in borehole KB 02. In the borehole, the Zellerndorf Formation is 19.3 m thick and contains a layer with well-rounded quartz gravels at its base. The main part of the formation is dominated by laminated silty clay, often with sea urchin spines and phytoclasts. Carbonate contents are low (1-8% wt.).

The diatomaceous sediments of the Limberg Member are exposed in Parisdorf (c. 6 m height) and in Limberg (<4 m height) (Figure 4.25). The exposed rocks are fine laminated diatomite with few clay intercalations. At Parisdorf the exposed section starts at the bottom with a chert layer. The carbonate content is very low. Both outcrops are overlain by pelitic rocks of the upper part of the Zellerndorf Formation. The Parisdorf outcrop is partly covered with vegetation and the missing section is marked in Figure 4.25 with question mark.

Clay minerals form the main component of most samples. Detrital quartz grains are rare. The average biogenic silica content is 9% wt. with higher contents in samples 12-Pa (23.7%), 8-Pa (15.4%), 16-Li (22.7%) and 17-Li (14.5%). In thin sections, the lithology is represented by an argillaceous mass with frequent diatom valves and rare detritus (Figure 4.23). X-ray diffractograms support that clay minerals, biogenic silica and calcite are the major constituents of diatomaceous rocks. In contrast to Szurdokpüspöki samples, diffractograms from the Limberg Member do not indicate opal-A in any of the samples, only two samples from Parisdorf show opal-CT (e.g. chert sample 12-Pa; Figure 4.24).

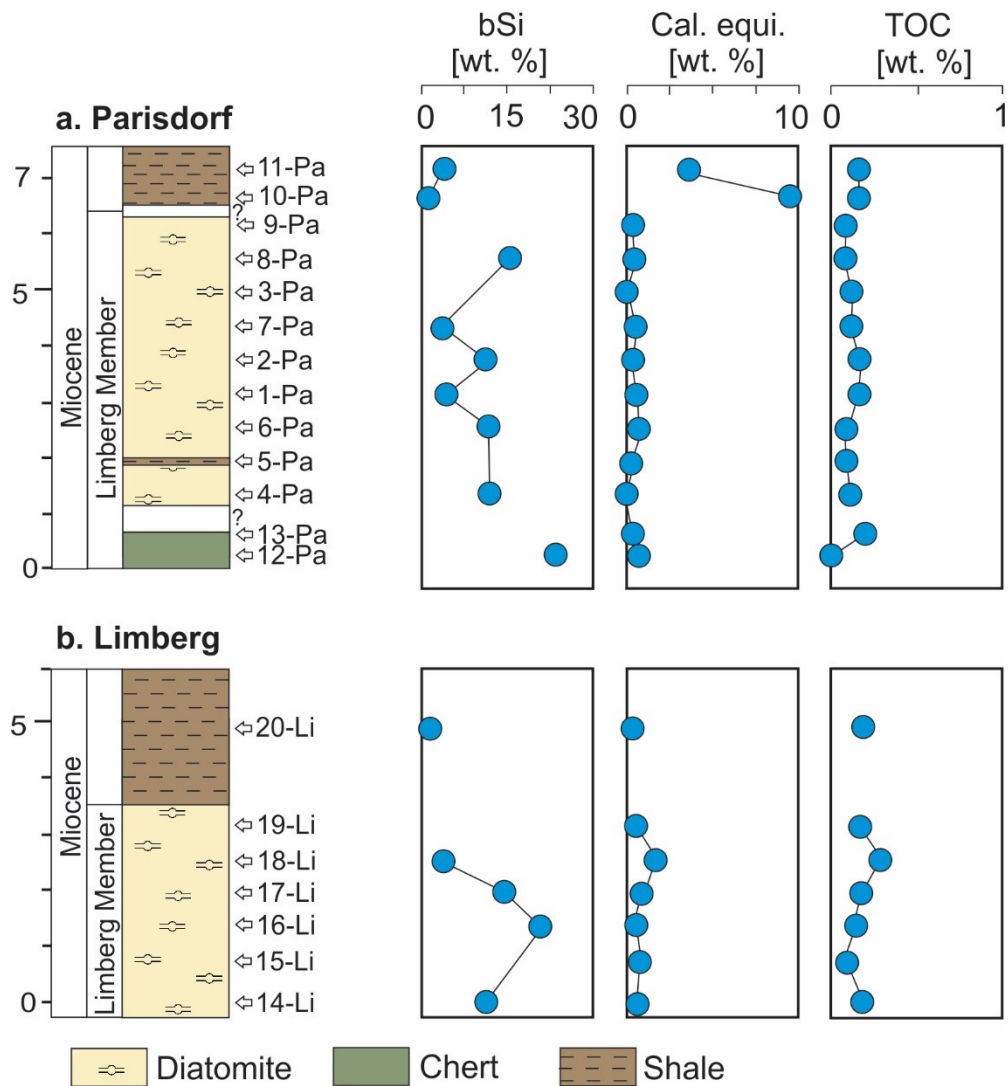


Figure 4.25. Outcrops of Limberg Member, Austria. a. lithology of the Limberg Member in Parisdorf quarry; b. lithology of the Limberg Member in Limberg. bSi-biogenic silica; Cal. equi.-calcite equivalent; TOC-total organic carbon.

#### 4.5.2.2 Bulk geochemical parameters

TOC contents in the Zellerndorf Formation borehole samples range from 0.58 to 0.91% wt. (Table 2). Sulfur contents are relatively high (0.48-1.38 w.%) resulting in low TOC/S ratios (0.57-1.73). Bulk parameters for the diatomaceous rocks in the Parisdorf and Limberg quarries are listed in Appendix 1 Table 8 and plotted versus height in Figure 4.25. TOC contents are very low (avg. 0.13% wt.) and the S content does not exceed 0.08 wt. %. S<sub>2</sub> values reach a maximum of 0.36 mgHC/gTOC, but are typically below 0.2 mgHC/gTOC. HI and TOC/S values are unreliable

due to low TOC contents. Tmax has to be considered with caution, because of low S2 values, but is typically in the order of 400 to 420° C.

#### **4.5.2.3 Diatom assemblages and depositional environment**

Samples from Parisdorf and Limberg contain a high amount of broken diatom valves (Figure 4.26). Very rare, small diatoms valves and cryophyte scales have been preserved. Two samples were barren (2-Pa from Limberg Member and 20-Li from Zellerndorf Formation). Therefore, diatom genera identification and quantification were impossible. Previous work in the area yielded better results. Řeháková (1994) and Roetzel et al. (2006) described 46 diatom genera from Parisdorf sediments, the most common genera being *Thalassionema*, *Chaetoceros*, *Coscinodiscus*, *Rhizosolenia*, *Stephanopyxis* and *Thalassiosira*, and noticed a lack of shallow-water benthic taxa. Hence, Řeháková (1994) postulated a sublittoral deeper marine depositional environment with neritic and pelagic marine plankton.

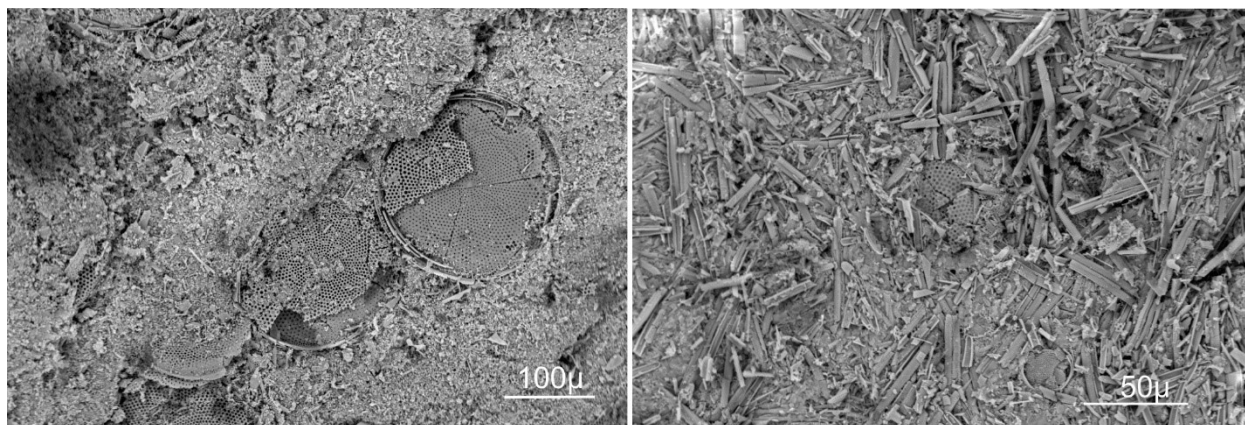


Figure 4.26. SEM photographs of broken diatoms observed on the rock surface of Parisdorf diatomite.

#### **4.5.3 Discussion and interpretation**

Below, the discussion will concentrate the two diatom-rich sediments from Szurdokpüspöki and Parisdorf / Limberg by examine each diatom occurrence and compare it to each other.

#### ***4.5.3.1 Maturity and hydrocarbon potential of diatomite at Szurdokpüspöki and Parisdorf / Limberg***

None of the studied successions experienced deep burial. Therefore, as expected, very low Tmax values (Appendix Tables 7, 8) show that all studied rocks are immature. For Szurdokpüspöki samples this is also proven by the presence of opal-A. With TOC contents up to 3.0% wt. and partially high HI values, the lower part of the diatomaceous succession at Szurdokpüspöki contains a good hydrocarbon potential (Figure 4.27).

In contrast, the hydrocarbon potential of the upper part of the studied section is very low. The average hydrocarbon potential (S1+S2) of the lower part is 6.8 mg HC/g rock. The thickness of the exposed organic matter-rich succession is 7.5 m, but because the base of the succession is not exposed, it is likely that its thickness is significantly higher (see also Figure 4 based on Hajós, 1986) and may be as high as 20 m. The density of diatomite is typically low. Assuming a density of 1.8 g/cm<sup>3</sup> and applying the approach of Demaison and Huizinga (1994), it is suggested that the succession may generate about 0.25 tons of hydrocarbons per square meter, if mature.

The diatomites of the Limberg Member at Parisdorf and Limberg do not hold any hydrocarbon potential. This is valid also for the under- and overlying pelitic rocks of the Zellerndorf Formation.

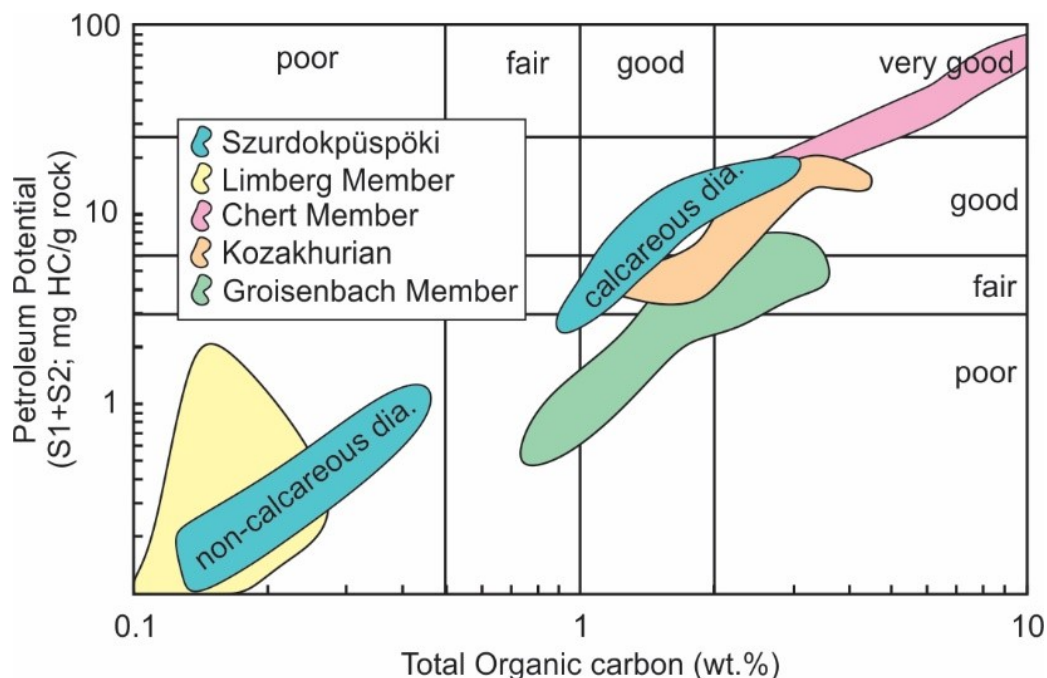


Figure 4.27. Petroleum potential of Szurdokpüspöki and Limberg Member in comparison with that of different Oligocene to middle Miocene siliceous sediments. Data are from: Jirman et al. (2019)-Chert Member of the Oligocene Menilite Formation (Western Carpathians); Mayer et al. (2018)-lower Miocene (Kozakhurian) from the Kaliakra Canyon (West Black Sea Basin); Sachsenhofer et al. (2003)-middle Miocene Groisenbach Member (Aflenz Basin). dia. – diatomite.

#### 4.5.3.2 Comparison of hydrocarbon potential of different diatomaceous rocks within Paratethys

In this section, we briefly review the depositional environment and geodynamic setting of some Oligocene to middle Miocene diatomaceous rocks in the Paratethys area and compare their hydrocarbon potential with that of the studied sections. Their stratigraphic position is shown in Figure 4.28.

Similar to the middle Miocene Limberg Member, the **Oligocene Menilite Formation** represents a foreland basin setting. In the Western Carpathians (Czech Republic) the Menilite Formation comprises from base to top: Subchert Member, Chert Member, Dynów Marlstone and Šitbořice Member. The lower Oligocene Chert Member is represented by laminated cherts and non-calcareous siliceous shales, which were deposited in an anoxic bathyal environment with limited influx of detritus (Krhovský, 1981). High silica contents are due to diatom blooms. Pícha and Stráník (1999) postulated that cherty rocks were deposited due to high siliceous

bioproductivity caused by upwelling. In contrast, based on fish and trace fossil assemblages, Kotlarczyk and Uchman (2012) argued that lower Oligocene cherts accumulated in a silled, anoxic basin with a stratified water column. Jirman et al. (2019) investigated the Menilite Formation exposed in the Loučka section of the Silesian Unit (Western Carpathians, Czech Republic) and found that the best source rocks occur within the Chert Member (TOC 1.51-16.5% wt.; avg.: 5.9% wt.; type II-I kerogen; HI up to 725 mg HC/g TOC). The very good petroleum potential (see Figure 11) is mainly caused by excellent organic matter preservation caused by strictly anoxic conditions in a silled basin.

Upwelling locally enhanced by the geometry of a shelf-break canyon (e.g. Kaempfer, 2007), has been postulated for the **lower Miocene (Kozakhurian)** diatomaceous sediments in the **Kaliakra Canyon** in the West Black Sea Basin (Mayer et al., 2018; Sachsenhofer et al., 2018a). Here, Kozakhurian rocks contain high biogenic opal (up to 87% wt.) and TOC contents (1.2-4.3% wt.). HI values (180-530 mg HC/g TOC) show the presence of type II kerogen (Mayer et al., 2018). Their petroleum potential is good but not as high as in the Chert Member (Figure 4.27). In case of the Kozakhurian rocks, high TOC contents and moderately high HI values reflect high bioproductivity typical for upwelling settings and deposition in an oxygen-depleted environment (Mayer et al., 2018) which facilitated the preservation of the organic matter.

This is in major contrast to the roughly coeval (Ottomanian) Limberg Member, where poor organic matter preservation caused very low TOC contents. According to Roetzel et al. (2006), the Limberg Member accumulated in a pelagic, deep-neritic zone. Maybe depositional depth was still not deep enough to reach the Oxygen Minimum Zone (0.2-1.5 km).

In addition to the marine diatomaceous sediments, the lacustrine **middle Miocene Groisenbach Member** in the Aflenz pull-apart basin (Sachsenhofer et al., 2003) is worth mentioning. The pelitic Groisenbach Member forms the lower part of the Göriach Formation. It was deposited in shallow fresh to oligosaline waters (Hajós, 1972) within an anoxic water column (Sachsenhofer et al., 2003) and contains high biogenic silica contents (~30%). Sachsenhofer et al. (2003) assumed that volcanic ashfalls provided both nutrients and the high dissolved-silica content in the lake water stimulating diatom productivity. The rocks contain an average TOC of 1.78% wt. and mixed type III and type II kerogen (80-330 mg HC/g TOC; Sachsenhofer et al., 2003). Its

petroleum potential is similar to that of Szurdokpüspöki, although relatively low HI values may reflect a high contribution of landplants transported into the relatively small basin from its margins.

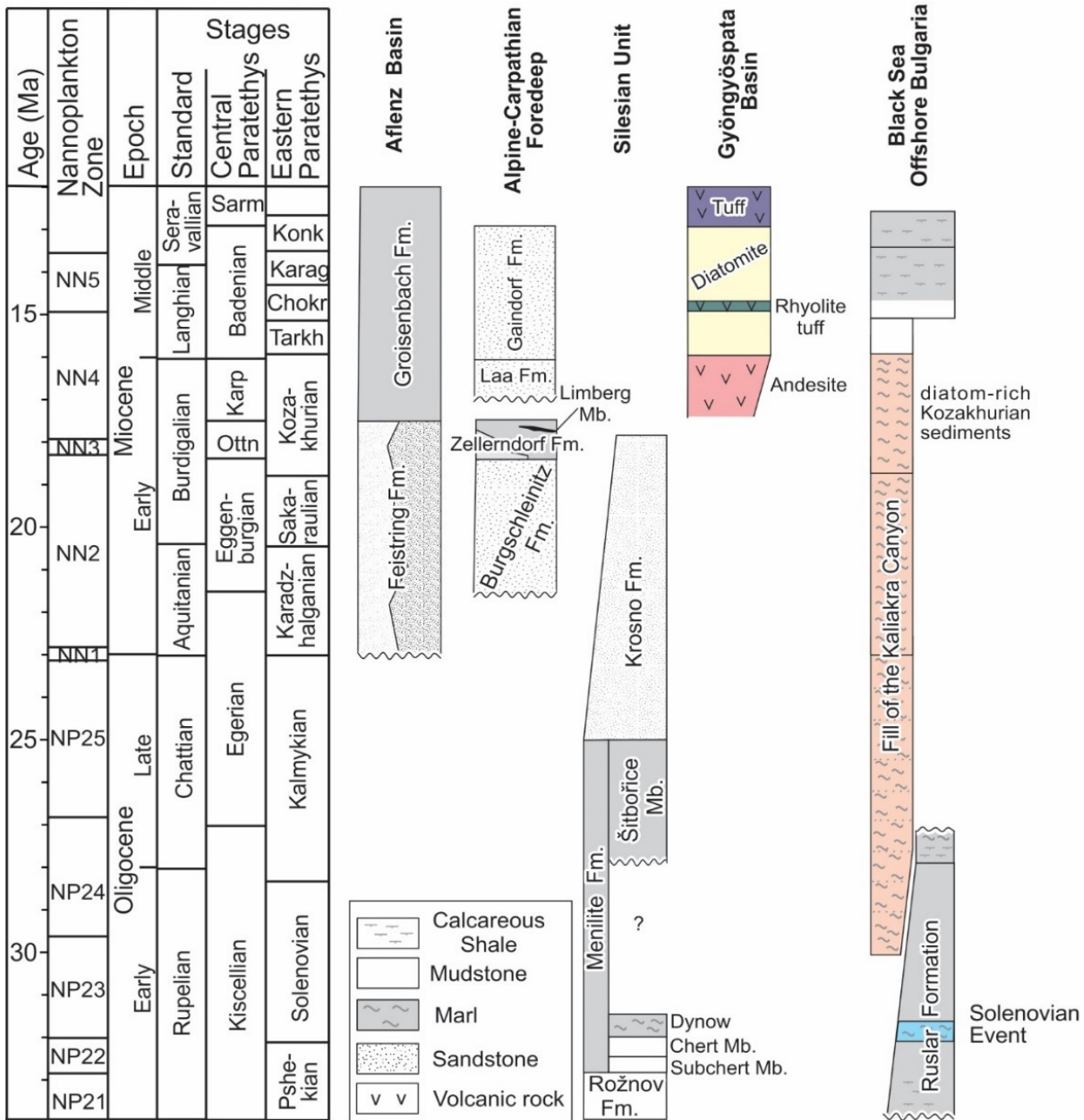


Figure 4.28. Stratigraphy of Oligocene to Miocene sediments within the Paratethys (compiled from Jirman et al., 2019; Hajós, 1986; Roetzel, 1999; Sachsenhofer et al., 2003; Sachsenhofer et al., 2018).

Overall, the compilation in Figure 4.27 shows that diatomaceous rocks may contain largely varying petroleum potential. Nevertheless, anoxic events play one of the sea biggest roles in preservation of the organic matter as seen in the Chert Member, Groisenbach Member and Kozakhurian sediments. In the Limberg Member, even though bioproductivity was probably high

due to upwelling, TOC contents are very low due to poor preservation of organic matter in a high energy environment. In the Szurdokpüspöki sediments, the organic matter preservation at first glance seems to be controlled by the calcite content although there is no clear causal relation. The presence of periphytic and benthic diatoms suggests that anoxic conditions were not present. Probably, excellent organic matter preservation in the lower part of the Szurdokpüspöki quarry was caused by other factors (e.g. high rates of deposition).

#### ***4.5.3.3 Comparison of diatom preservation at Szurdokpüspöki and Parisdorf / Limberg***

The Szurdokpüspöki diatomite yields abundant and unusually well-preserved diatom frustules (Plates VI-VII). The fact that even the most fragile raphid diatoms are well preserved makes Szurdokpüspöki one of the best sites for studying fossil diatoms. This was realised early on in the history of diatom study, as a cleaned sample from this locality has been distributed among early 20th-century European diatom researchers under the name „Castel” (e.g., Ross, 1995). The excellent preservation testifies to an unusual mode of biogenic silica preservation. Nowadays, a direct relationship of the volcanic activity and diatom blooms is accepted (i.e. volcanic ash weathering provides silica supplies and nutrients (Cressman, 1962)). Nevertheless, a discussion on the relationship between volcanic activity and diatom preservation has emerged. Harper et al. (2015) demonstrated an excellent relationship between the volcanic tephra and the diatom preservation in Quaternary sediments, as well as the change of the environment caused by volcanism. In Szurdokpüspöki, the tuff layers are present in between the diatomaceous layers (Figure 4.22) which, besides providing silica supplies, act as a barrier in diatom valves preservation.

In contrast to Szurdokpüspöki, frustules at Parisdorf/Limberg are heavily broken (Figure 4.26). The siliceous exoskeleton of the diatom valves is usually tough, and they can resist decaying (Weckström et al., 2017). Dissolution and physical fragmentation are the two main damages on diatom valves. The dissolution of the diatom valves appears when there is a shortage in biogenic silica (Olli et al., 2008), however, this is not the case in Parisdorf/Limberg. The physical fragmentation can be caused by high energy environments (i.e. friction with sand grains) or racking by zooplankton (Flower 1993; Flower and Ryves, 2009). As observed on the rock surface, the diatoms were not broken before settling down to the substratum since their shape is still



recognisable (Figure 4.26). The breakage to the diatom valves in Parisdorf and Limberg were probably caused by a high-energy environment in the coastal upwelling condition (Roetzel et al., 2006). Wave action may have also contributed to poor diatom preservation. Furthermore, fragmentation due to sediment compaction cannot be excluded.

#### **4.5.4 Conclusions**

Diatomaceous sediments in the abandoned Szurdokpüspöki, Parisdorf and Limberg quarries have been studied for their hydrocarbon potential. The results indicate a fair-good potential for the lower part of the middle Miocene Szurdokpüspöki succession. In contrast, the upper part of the Szurdokpüspöki succession and the lower Miocene Limberg Member contain very poor potential. At both locations the sediments are thermally immature. If mature the Szurdokpüspöki succession may generate about 0.25 tons of hydrocarbons per square meter.

The detected diatom assemblage in the Szurdokpüspöki succession, deposited in a restricted basin, supports a near-shore littoral brackish depositional environment. The preservation of diatom valves in Szurdokpüspöki is excellent, probably due to the presence of tuff layers providing silica. In contrast, diatom frustules at Parisdorf, deposited in a sublittoral deeper marine setting, are severely broken, probably because of a high energy environment related to upwelling currents.

The comparison of Oligocene to Middle Miocene diatomaceous rocks in different environmental and geodynamic settings reveals major differences in petroleum potential varying from excellent source rocks (e.g. Chert Member of the Maikop Formation) to very poor source rocks (Limberg Member).

## Summary

This thesis provides insight into the presence of Oligocene and Miocene diatoms in the Paratethys realm, as well as indications for potential diatom-bearing hydrocarbon source rocks. In the chapter IV Results and interpretation, the conclusions of each studied outcrop are given at the end. For an overview of the sections discussed in the thesis see Figure 4.29. In the summary below, a short overview of the studied sections is given, as well as an assembly of the findings related to the Paratethyan realm.

### 5.1 Oligocene

In the *Western Black Sea Basin*, two Oligocene outcrops (equivalent of the Maykop Suite) have been studied (Karaburun, Turkey and Karadere, Bulgaria). The Lower Oligocene rocks of the *İhsaniye Formation*, exposed near Karaburun (Thrace, NW of İstanbul) are exposed over 70 m-thick in two sections. The sections are divided by an inverted fault (Simmons et al., 2020) into Hanging Wall Section and Footwall Section. Here, the composite section is represented by the alternation of light grey marl, carbonate-rich siltstone, sandstone and tuffaceous beds. However, in the studied sections the diatoms are not present, but instead an outstanding foraminifera assemblage is to be found and studied in detail by Simmons et al. (2020). The studied Karaburun section was deposited in a fully marine environment. Moreover, based on foraminifera and the nannoplankton, the studied lower part (0-19.5 m) of the Hanging Wall section is deposited during NP21 in a shallowing bathyal to outer neritic environment and the upper part (19.5-68 m) was deposited in the uppermost NP21 to lower NP23 (Simmons et al., 2020), in a deepening trend with a low-energy environment.

Karadere, is located 185 km NNE of Karaburun. Here, the *Ruslar Formation* is exposed in a 20 m-thick outcrop which is dominated by laminated mudstones intercalated with sandstone layers and lenses. In contrast with Karaburun, the exposed rocks contain a rich siliceous assemblage (Plate I-IV). Based on the nannoplankton fossils, the exposed section was dated as intra-Early Oligocene (NP23) and the sediments were deposited in a fully marine, neritic environment. Moreover, the surface water was oxygenated and water column stratification caused oxygen-depleted bottom water conditions.

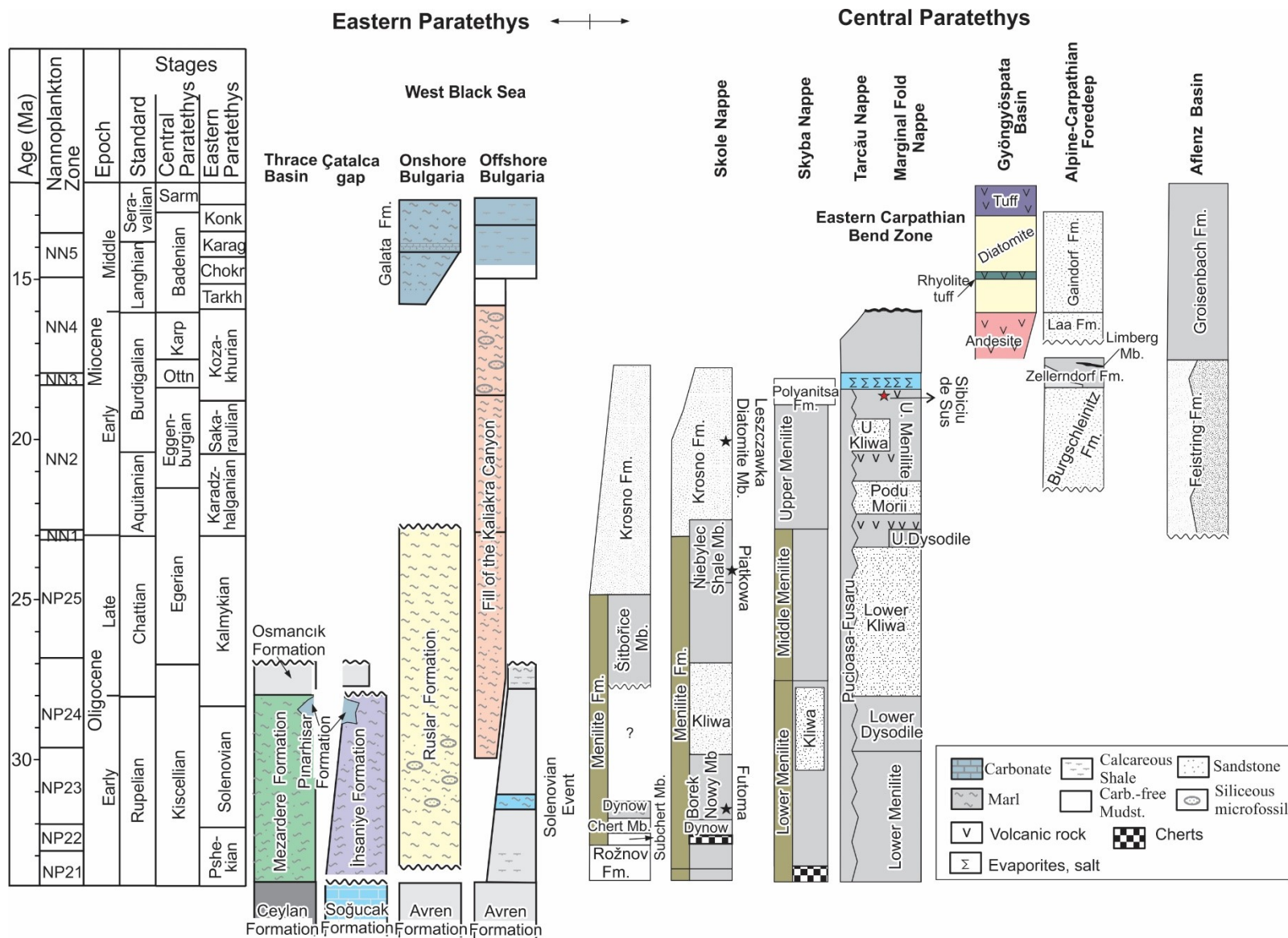


Figure 4.29. Overview of the studied and the discussed sections in the thesis.

At the beginning of nannoplankton zone NP23 (early Rupelian) the connection between the Paratethys and the world ocean was lost (Voronina and Popov, 1984; Rusu, 1999). The event, known as “Solenovian Event”, is represented by a carbonate-rich layer which forms a wide-spread marker horizon and represents the maximum of the isolation of the Paratethys (e.g. Voronina and Popov, 1984; Rusu). Later, the connection with the Mediterranean Sea was later partially restored in the upper NP23 (Late Rupelian) (Popov et al., 1993).

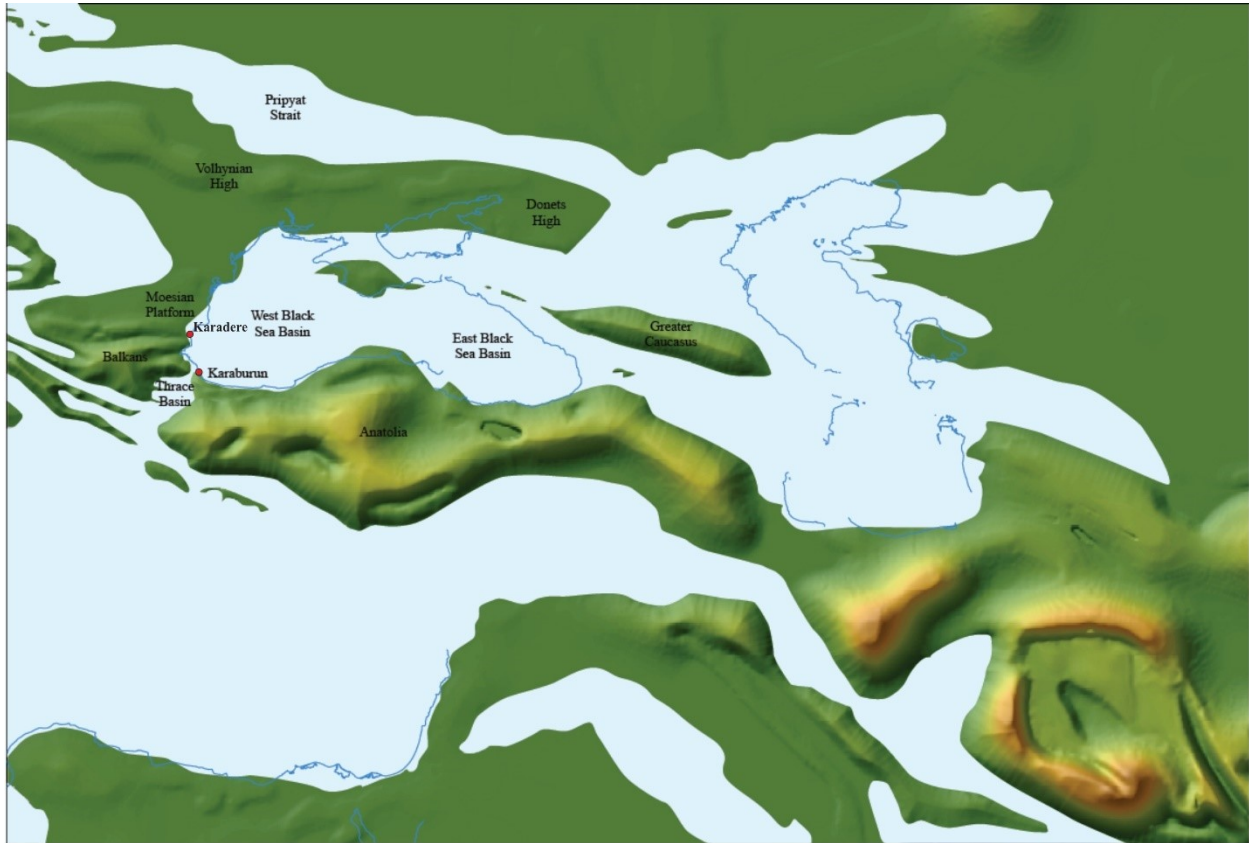


Figure 4.30. Simplified regional paleogeographic setting of the Early Oligocene of Eastern Paratethys (from Simmons et al., 2000 modified after Popov et al., 2004b).

During Late Eocene and Early Oligocene time a marine connection formed between the West Black Sea Basin and the Thrace Basin through Çatalca gap (Okay et al., 2019). The Solenovian event is expected in the upper part of the Karaburun section dated as NP23. Nevertheless, foraminiferal data (Simmons et al., 2020) and geochemical evidence (TOC/S ratio) exclude the presence of a major change in salinity. Also, Sr isotope data suggests that the connection was at best transient only, and for most of the time, there can only have been a restricted

connection. However, the Solenovian event may follow above the exposed succession in the Karaburun area. In addition, the fragment of the Ruslar Formation exposed at Karadere was deposited in a fully marine environment and probably represents the (marine) upper part of NP23. Presumably, the “Solenovian event” is hidden in the unexposed lower part of the Ruslar Formation. All the above may indicate that a connection between the Paratethys and the Mediterranean Sea remained open at the southwestern edge of the Black Sea (Figure 4.30).

## 5.2 Miocene

During Early Miocene, the connection between the Central and Eastern Paratethys was closing (e.g., Rögl, 1999; Kováč et al., 2018) and the tectonic movements, plus the uplift of the Carpathians caused changes in the sedimentary regimes. In the Carpathian Basin, the marine connection was obstructed and evaporites were deposited in the Romanian and Ukrainian sectors across the NN3/NN4 zones boundary (i.e., Early Miocene, Burdigalian) (Rögl, 1998; Popov et al., 2004; Gozhyk et al., 2015). However, it's important to mention that in the Romanian Carpathians, the Oligocene and Lower Miocene contain endemic or very limited fossil assemblages and the age determination is constrained and uncertain (e.g., Melinte-Dobrinescu and Brustur 2008; Munteanu et al. 2014; Bercea et al. 2016; Tămaş 2018).

In the ***Eastern Carpathian Bend Zone***, one of the largest diatomite occurrences is exposed over several hundred meters in the abandoned Sibiciu de Sus quarry (Buzău county). The quarry is divided into two levels and is providing an excellent outcrop of the upper part of the ***Upper Menilites***. Here are exposed several diatomite lithologies about 100 m thick, however, the rocks are deformed into a NW-SE orientated anticline which makes correlating different lithologies challenging. The findings from Sibiciu de Sus diatomites indicate that the depositional sequence was deposited during or after the marine connection was closed between the Eastern and Central Paratethys, and before the deposition of the evaporitic sequence (NN3/NN4 zones). In addition, the sediments were deformed during the mid-Miocene tectonic stage resulting in strong deformation of the diatomites at Sibiciu de Sus. The deformation is a result of compressional tectonics and soft-sediment deformation.

Two diatomaceous outcrops were studied further. One is represented by diatomaceous rocks of Early ***Ottangian*** (mid-Burdigalian) age from the ***Alpine-Carpathian Foredeep***. The sediments were accumulated along the south-eastern margin of the Bohemian Massif and attributed to the

**Limberg Member** of the Zellerndorf Formation (Roetzel et al., 2006; Grunert et al., 2010). Here, the diatomaceous sediments are exposed in Parisdorf (c. 6 m height) and in Limberg (<4 m height) the exposed rocks are fine laminated diatomite with few clay intercalations.

The second outcrop is represented by **Middle Miocene** diatomite from **Szurdokpüspöki (Pannonian Basin)** deposited in a restricted basin, near a volcanic silica source. The diatom-rich succession is separated by a rhyolitic tuff into a lower non-marine and an upper marine layer deposited in Gyöngyöspata Basin. An approximately 12-m thick section has been investigated, represented by laminated (paper-like) and very fragile diatomite. The studied section, based on diatom assemblage composition, indicates a brackish marine depositional environment which place the studied section in the lower non-marine section of the Gyöngyöspata Basin.

During Miocene time, the Pannonian Basin System was covered entirely by the Miocene Central Paratethys Sea (e.g., Kováč, et al., 2007). The system was bordered by the mountains chains such as the Alps, the Carpathians and the Dinarides. The epicontinental sea spread and flooded the Alpine-Carpathian Foredeep (Kováč et al., 2007), which is observed in the Limberg Member (Early Oligocene) through the deposition of the diatoms in coastal upwelling conditions setting (Roetzel et al., 2006).

At the time of Badenian, the majority of the “Pannonian back-arc basin” was subsiding. However, in the north, a narrow belt was represented by few uplift areas (Kováč, et al., 2007). Sub-basins within the North Hungarian Range, as the case of Gyöngyöspata Basin, were subject to stress field, from NE-SW to ESE-WNW oriented tension (Csontos et al., 1991; Fodor et al. 1999). Here, around the fringes of volcanoes, the dominating depositional environment was shallow marine (Kováč et al., 2007). Further in time, as mentioned before, the isolation of eastern parts of the Central Paratethys at the end of middle Miocene (late Langhian) period resulted in the “Middle Badenian” salinity crisis, which is seen in the Carpathian Foredeep and Transylvanian Basin through a thick evaporite sediments (e.g., Rögl, 1998; Popov et al., 2004a; Kováč et al., 2007; Gozhyk et al., 2015).

### **5.3 Hydrocarbon potential of the studied diatomaceous rocks**

Diatomaceous sediments may be prolific hydrocarbon source rocks in many basins worldwide, however not all the diatom-rich sediments can hold a significant hydrocarbon

potential. From five studied sections, only one did not contain diatom frustules and it is represented by the Karaburun section (İhsaniye Formation).

In Karaburun, only the lower part of the studied Hanging Wall Section (samples 1-19; 17.5-m thick) contains up to 2% wt. TOC contents and a type III-II kerogen, which is mainly gas prone and may generate minor liquid hydrocarbons only. Considering an average S1 of 0.07 mg HC/g rock and an average S2 of 2.99 mg HC/g rock, the Source Potential Index ( $SPI = \text{thickness} \times (S1 + S2) \times \text{bulk density} / 1000$ ; Demaison and Huizinga, 1994) is calculated as 0.14 t HC/m<sup>2</sup>, which is a very low value. In comparison with the age equivalent surrounding rocks (Figure 4.31) and the above results the source rock potential of the İhsaniye Formation is considered poor.

Further north from Karaburun, the Ruslar Formation exposed at Karadere contain on average 1.85 % wt. TOC. The HI values range from 61 to 331 HC/g TOC and is indicating the presence of type II-III kerogen. The samples could generate gas, condensate and oil. Considering a thickness of 15 m, an average S1 of 0.12 mg HC/g rock and an average S2 of 4.51 mg HC/g rock, the SPI for the exposed part of the Ruslar Formation at Karadere is calculated as 0.14 t HC/m<sup>2</sup>. If the values are representative for the entire Ruslar Formation and if the net mudstone thickness is 55 m, the SPI increases to 0.5 tHC/m<sup>2</sup>. Even though the studied section has diatoms frustules the hydrocarbon potential is poor to good (Figure 4.31).

The Sibiciu de Sus samples contain in average 3.77% wt. TOC and the maximum is reach at 9.57% wt. TOC. S2 values reach a maximum of 30.67 mg/HC g rock (avg. 14.64 mg/HC g rock), and HI values range between 206 to 515 HC/g TOC, indicating the prevalence of type II kerogen. However, the Production Index is high (0.1-0.3; Appendix 6), this is a clear evidence for the presence of migrated hydrocarbons. Based on the petroleum potential, most samples are classified as good to very good source rocks. For the SPI calculations was consider only 25% of it (0.96 mg HC/g rock) and the average S2 of 15.54 mg HC/g rock. Using these data, the SPI is calculated as 1.3 t HC/m<sup>2</sup>.

The diatomites exposure of Limberg Member have very low TOC contents (avg. 0.13% wt.) and the S content does not exceed 0.08 wt. %. S2 values reach a maximum of 0.36 mgHC/gTOC, but are typically below 0.2 mgHC/gTOC. Therefore, the diatomites here have a very poor hydrocarbon potential.

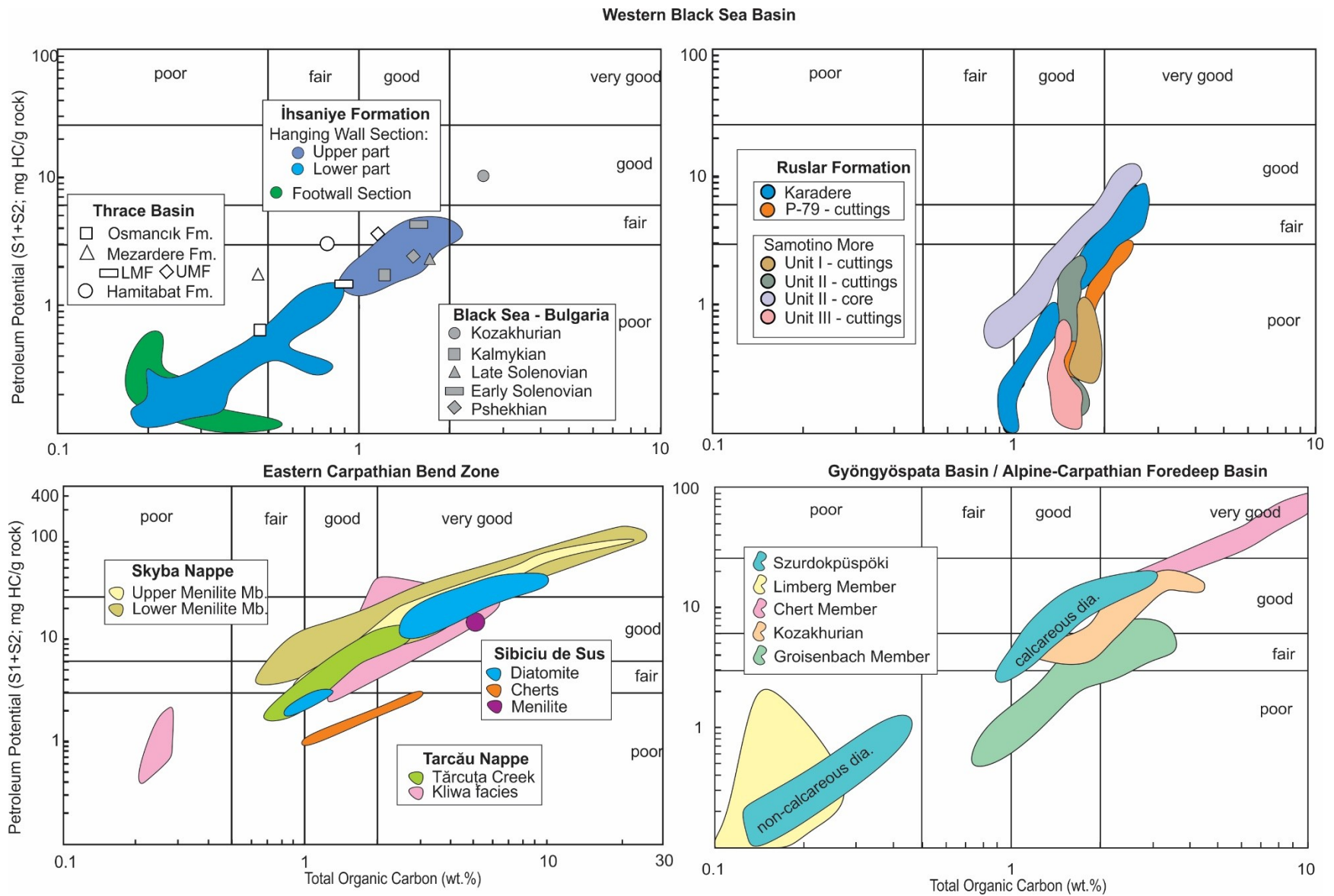


Figure 4.31. Petroleum potential versus total organic carbon (TOC) for all investigated Oligo-Miocene source rocks.



In Szurdokpüspöki sections the TOC contents are high (0.2-3.0% wt.; average 1.28% wt.) in the lower part and very low (average 0.14% wt.) in the carbonate-free upper part of the section. S<sub>2</sub> values reach a maximum of 14.4 mg HC/g rock and strongly relates to TOC contents. HI values in the lower organic matter-rich section range from 178 to 723 mg HC/g TOC. According to SPI calculations it is suggested that the succession may generate about 0.25 tons of hydrocarbons per square meter. The diatomites exposed are separated in non-calcareous diatomite with poor petroleum potential and the calcareous diatomites with fair to good hydrocarbon potential (Figure 4.31).

However, all the analysed samples did not experience deep burial and they are thermally immature.

#### ***5.4 Diatom preservation***

Diatoms are documented in Plate I-X where diatom identification was possible. More diatom pictures without identification are provided in Appendix 4 from the external storage device.

In my findings, the Ruslar Formation mudstones from Karadere are characterized by well-preserved diatom-rich assemblages, which are unique for Oligocene sediments the Black Sea area. The diatom assemblages are remarkably well preserved with abundant and identifiable diatom valves. Besides diatom assemblages, frequent silicoflagellate skeletons, and calcareous nannoplankton, and rare foraminifera are observed. The microfossil assemblages suggest a fully marine, neritic environment.

The Sibiciu de Sus section contain abundant and well-preserved diatoms indicating a shallow marine depositional setting with strong freshwater input. However, several samples had the diatoms valves broken beyond recognition due to pervasive silicification, but where the diatoms valves were recognised, the preservation of valve fine structure was pristine. The siliceous cement responsible for induration of the rock is unlikely to be derived from diatom dissolution. Hence, a volcanic activity in the area should not be excluded. After all, volcanic tephra helps significantly in diatom preservation (Harper et al., 2015), which might be the case in Sibiciu de Sus diatoms preservation.

Another place where the diatoms are well preserved is Szurdokpüspöki, where even the most fragile raphid diatoms are well preserved. The excellent preservation testifies to an unusual mode of biogenic silica preservation, which was achieved most probably due to volcanic tephra presence (i.e. tuff layers in between the diatomites). In contrast to Szurdokpüspöki, frustules at Parisdorf/Limberg are heavily broken. The physical fragmentation can be caused by high energy environments (i.e. friction with sand grains) or racking by zooplankton (Flower 1993; Flower and Ryves, 2009). However, the observation on the the rock surface, the diatoms were not broken before settling down to the substratum since their shape is still recognisable. The breakage to the diatom valves in Parisdorf and Limberg were probably caused by a high-energy environment in the coastal upwelling condition (Roetzel et al., 2006). Wave action may have also contributed to poor diatom preservation. Furthermore, fragmentation due to sediment compaction cannot be excluded.

To conclude, the perfect environment for diatom preservation would be one away from waves or upwelling currents, plus a volcanic activity near, which can bring more silica in the environment and help the diatoms valves not to get dissolved. Moreover, the sedimentation rate does not have a significant impact on diatom preservation, as seen in Sibiciu de Sus where is predominantly composed of diatoms valves and siliceous mass and rare detrital grains, or in Karadere where a significant argillaceous input is present.

## **Conclusions and outlook**

In this thesis a total of five outcrops have been studied to determine the source rock hydrocarbon potential of diatom rich sediments. Apart from one outcrop in Karaburun, Turkey all the studied sediments were diatom-rich. Below are noted the conclusions for each studied outcrop.

Along the Black Sea shore, the **İhsaniye Formation** fine-grained part is represented by an alternation of marl, carbonate-rich siltstone, sandstone and tuffaceous beds and the frequency of the sandy layers intercalations is decreasing higher in the stratigraphy. The TOC/S values for the İhsaniye Formation together with the continuous presence of the foraminifera in the studied section indicate a fully marine environment. The studied Hanging Wall Section is divided into two parts: the lower part (0-19.5 m)

contains relatively high amounts of terrestrial organic matter deposited in oxygen-depleted conditions. The upper part (19.5-68 m) contains a prominent tuff layer. The succession below the tuff layer is low in organic matter (avg. TOC: 0.38%) and reveals a deepening trend in a low-energy depositional environment. The deepening trend is reflected by an upward decrease in detrital organic and inorganic matter. The studied succession is immature. The TOC content reaches a maximum of 2.04 wt.% in the lower part of the succession (0-19.5 m), which has some hydrocarbon potential even though it is poor. If mature, the section may generate 0.14 t HC/m<sup>2</sup>. The presence of type III-II kerogen indicates that the rocks are gas prone and may generate minor liquid hydrocarbons only.

The studied fragment of the **Ruslar Formation** outcropping at Karadere exposes organic-rich, diatom-rich mudstones with sandstone intercalations, about 15 m thick, which have been dated as intra-Early Oligocene (biozone NP23). The mudstones are characterized by well preserved, rich diatom assemblages, which are unique for sediments of this age in the Black Sea area. Diatom assemblages, frequent silicoflagellate skeletons as well as calcareous nannoplankton and rare foraminifera suggest a fully marine, neritic environment. Whereas the surface water was oxygenated, water column stratification caused oxygen-depleted bottom water conditions. Apart from oxygen depletion, biomarker data also provide evidence for strong input of terrestrial organic matter, dominated by angiosperms. Not surprisingly, diatom-related biomarkers occur in significant concentrations. The hydrocarbon potential of the Oligocene rocks is fair to good, with an average TOC of 1.85% wt. and type II-III kerogen (avg. HI: 231 mg HC/g TOC), which may generate oil and gas. The organic matter is thermally immature. The SPI shows that the exposed section may generate about 0.2 tHC/m<sup>2</sup>, when mature. A rough estimate of the SPI for the entire Ruslar Formation at Karadere (incl. the non-exposed part) is 0.5 tHC/m<sup>2</sup>. This value is low, but in the order of other Oligocene sections offshore Bulgaria.

In comparison with the coeval sediments in the Western Black Sea and the Thrace Basin, the İhsaniye Formation shows a different evolution, where the low salinity “Solenovian Event” is missing even though the Sr isotope record suggests that full connection with the Mediterranean occurred for relatively short periods during this interval. One possible explanation is that the “Solenovian Event” is hidden within the

overlying mass transport sediments. Moreover, in the the lower part of the Ruslar Formation, which includes the “Solenovian event” is not exposed at Karadere and stratigraphically higher parts have been removed by erosion.

The abandoned **Sibiciu de Sus** quarry provides one of the largest exposures of diatomites in the Eastern Carpathians. The exposed diatomites represent the upper part of the Upper Menilites in the ECBZ. The diatomites, represented here by several lithologies and are highly deformed due to soft-sediment deformation and subsequent compressional tectonics. The Sibiciu de Sus diatomites are characterized by well-preserved diatom assemblages, where even the most delicate areolae occlusions are preserved intact. However, the samples are highly indurated and common diatoms extraction methods yielded no positive results. Therefore, diatom assemblages were examined using scanning electron microscope techniques. Diatom assemblages are represented by two dominant genera (*Aulacoseira*, *Actinocyclus*) and four subordinate genera (*Ellerbeckia*, *Opephora*, *Paralia*, *Rhaphoneis*) and suggest deposition in a shallow marine environment with strong freshwater contribution. The hydrocarbon potential of the Lower Miocene rocks is good to very good, with an average TOC of 3.77% wt. and type II–III kerogen (avg. HI: 384 mg HC/g TOC). The organic matter is thermally immature. However, high amounts of S1 hydrocarbons provide proof of the presence of migrated hydrocarbons. The SPI calculations indicate that the exposed section could generate about 1.3 t HC/m<sup>2</sup> if mature.

Diatomaceous sediments in the abandoned **Szurdokpüspöki**, **Parisdorf** and **Limberg** quarries have been studied for their hydrocarbon potential. The results indicate a fair-good potential for the lower part of the middle Miocene Szurdokpüspöki succession. In contrast, the upper part of the Szurdokpüspöki succession and the lower Miocene Limberg Member contain very poor potential. At both locations the sediments are thermally immature. If mature the Szurdokpüspöki succession may generate about 0.25 tons of hydrocarbons per square meter. The detected diatom assemblage in the Szurdokpüspöki succession, deposited in a restricted basin, supports a near-shore littoral brackish depositional environment. The preservation of diatom valves in Szurdokpüspöki is excellent, probably due to the presence of tuff layers providing silica. In contrast, diatom frustules at Parisdorf, deposited in a sublittoral deeper marine setting, are severely broken, probably because of a high energy environment related to upwelling currents. The comparison of Oligocene to Middle Miocene diatomaceous rocks in different

environmental and geodynamic settings reveals major differences in petroleum potential varying from excellent source rocks (e.g. Chert Member of the Maikop Formation) to very poor source rocks (Limberg Member). The studied sections proved that not all the diatom-rich rocks can be considered prolific hydrocarbon source rock, and that the depositional environment is playing an important role in organic matter preservation.

Overall, the analyzed Oligo-Miocene samples in the Paratethys showed that most of the diatom-rich sediments can have a large extent when it comes to petroleum potential. From the analyzed samples the ranges can vary from a very good petroleum potential to a poor one, which indicate that not all diatom-rich sediments can be considered hydrocarbon source rocks. Moreover, all the analysed samples did not experience deep burial and they are thermally immature, if mature they could generate on average 0.5 t/m<sup>2</sup>, which is a low number when compared with other hydrocarbon source rocks in the Paratethys.

Furthermore, additional studies are necessary to understand the extent of the rich-diatom bearing sediments within the Oligocene and Miocene interval in the Paratethys. However, studying diatoms is rather tough, since they have a small size, require special extraction treatments and expensive equipment, which make this kind of studies often overlooked by scientist. With a proper technique to extract the diatom frustules or when is not possible to observe the rock surface, can increase significantly the accuracy of the depositional environment. Besides, biostratigraphic studies on diatoms is crucial within the Paratethys, as is observed in the Romanian Eastern Carpathians, where the age determination is critical to understand the geological evolution of the Carpathians.

## **Acknowledgements**

I wish to express my sincere appreciation to my supervisors and mentor: Professor Reinhard Sachsenhofer for his continuous teaching efforts, patience and guidance, your advices, discussions and constructive criticism shaped me to become a better person and a better geologist; Gabor Tari is thanked for his encouragements which always pushed me further, for his guidance and fruitful discussions; Professor Frank Melcher is appreciated for his continuous support and mentorship. I say to you Mulțumesc din suflet!

I am extremely grateful to OMV Group - Technology project, this work would not be possible without their support. I am thanking especially Leo Bräuer for his unceasing support and efforts to make this project possible. Many thanks to Linda Kirchberger for allowing me to work on this project in OMV TECH Center and Lab, as well as the staff from the lab who was very patient when introduced me to the equipment required. Thank you, Robert Muggleton for teaching me to use the SEM, and for picking up my calls even in the times when you were out of office. Thank you, Ales Vrsic for your great patience and passion for sliced rocks, I have learned a lot from you. Many thanks to Wolfgang Hujer and Elias Mekonnen for being always helpful and have great conversations.

I would like to show my appreciation to the Chair of Petroleum Geology staff for being always there for me. Many thanks to my fellow PhD colleagues, Magdalena Pupp and Johannes Rauball for their fun conversations and insights into geochemistry methods.

I am grateful to the Institute of Paleontology, Research Centre of the Slovenian Academy of Sciences and Arts and its staff for granting me access to their laboratory and use the SEM. Especially, I would like to thank Aleksander Horvat, for being very helpful, kind and gave me valuable insights in diatom preparation. Also, I want to show my appreciation to Jakub Witkowski from University of Szczecin, your passion for diatoms touch me deeply and inspired me to enjoy studying the diatoms.

I would like to show my appreciation to my fieldtrip colleagues Jan Mayer, Mike Simmons, Aral Okay, Dan and Alexandra Tamas and Emanuil Kozhuharov.

Last but not least, I wish to acknowledge the support and great love of my family, my life partner, Andreas Poldlehner; my brother, Emanuel Tulan and my parents Ghiță and Gina Tulan. You kept me going and I have learned from you to be patient and pushed me to always do a little more.

## References

- Akartuna M., 1953. Geology of Çatalca-Karacaköy Region. University of Istanbul, Istanbul Üniversitesi Fen Fakültesi Monografileri 13:88 (in Turkish).
- Alizadeh, A.A., Guliyev, I.S., Kadirov, F.A., Eppelbaum, L.V., 2016. Geosciences of Azerbaijan. Stuttgart, Springer, 340 pp.
- Allen, M.B. and Armstrong, H.A., 2008. Arabia–Eurasia collision and the forcing of mid-Cenozoic global cooling. *Palaeogeography, Palaeoclimatology, Palaeoecology*, 265(1-2), pp.52-58.
- Amadori M. L., Belayouni H., Guerrera F., Martín-Martín M., Martín-Rojas I., Miclăuş C. and Raffaelli G., 2012: New data on the Vrancea Nappe Moldavidian Basin, Outer Carpathian Domain, Romania: paleogeographic and geodynamic reconstructions. *International Journal of Earth Sciences*, 101, 6, 1599-1623. <https://doi.org/10.1007/s00531-011-0744-1>
- Aoyagi, K. and Iijima, A., 1987. Petroleum occurrence, generation, and accumulation in the Miocene siliceous deposits of Japan. In *Siliceous sedimentary rock-hosted ores and petroleum*, pp. 117-137.
- Aoyagi, K. and Omokawa, M., 1992. Neogene diatoms as the important source of petroleum in Japan. *Journal of Petroleum Science and Engineering*, 7(3-4), pp.247-262.
- Bailey TR, McArthur JM, Prince H, Thirlwall MF, 2000. Dissolution methods for strontium isotope stratigraphy: whole rock analysis. *Chemical Geology* 167 (3-4): 313-319. doi: 10.1016/s0009-2541(99)00235-1.
- Báldi T., 1984. The terminal Eocene and Early Oligocene events in Hungary and the separation of an anoxic, cold Paratethys. *Eclogae Geologicae Helveticae*, 77(1):1-27.
- Barker S, Greaves M, Elderfield H., 2003. A study of cleaning procedures used for foraminiferal Mg/Ca paleothermometry. *Geochemistry, Geophysics, Geosystems* 4 (9): 1-20, doi: 10.1029/2003gc000559.
- Barron, J. A., 1987. Diatomite: environmental and geological factors affecting its distribution. In *Siliceous Sedimentary Rock-Hosted Ores and Petroleum*, ed. J. R. Hein, New York: Van Nostrand Reinhold Co., pp. 164-78



- Basistová, P., 2007. Diatomaceae in the sediments of the Carpathian Foredeep (locality Brno-Královo Pole), Brno, Bachelor thesis. Masaryk University, Faculty of Science, pp 37. <https://is.muni.cz/th/rnscx>
- Bazhenova O.K., 2002: Oil and gas source rock potential and the presence of oil and gas in Sakhalin. In: Gladenkov Y.B., Bazhenova O.K., Grechin V.I., Margulis L.S. and Salnikov B.A., 2002 (eds.): The Cenozoic geology and the oil and gas presence in Sakhalin. Moscow, GEOS, 137-194 (in Russian).
- Bechtel A, Gratzner R, Sachsenhofer RF, Gusterhuber J, Lücke A, et al., 2008. Biomarker and carbon isotope variation in coal and fossil wood of Central Europe through the Cenozoic. *Palaeogeography, Palaeoclimatology, Palaeoecology* 262(3-4):166-175.
- Bechtel A, Markic M, Sachsenhofer RF, Jelen B, Gratzner, et al, 2004. Paleoenvironment of the Upper Oligocene Trbovlje coal seam (Slovenia). *International Journal of Coal Geology*. 57(1):23-48. doi:10.1016/j.coal.2003.08.005.
- Bechtel A, Sachsenhofer RF, Kolcon I, Gratzner R, Otto A et al., 2002. Organic geochemistry of the Lower Miocene Oberdorf lignite (Styrian Basin, Austria): Its relation to petrography, palynology and the palaeoenvironment. *International Journal of Coal Geology*. 51(1):31-57. doi:10.1016/s0166-5162(02)00079-4.
- Bechtel A, Widera M, Sachsenhofer RF, Gratzner R, Lücke A, et al., 2007. Biomarker and stable carbon isotope systematics of fossil wood from the second Lusatian lignite seam of the Lubstow deposit (Poland). *Organic Geochemistry*. 38(11):1850-1864. doi:10.1016/j.orggeochem.2007.06.018.
- Belayouni H., Di Staso A., Guerrera F., Martín Martín M., Miclăuş C., Serrano F. and Tramontana M., 2007: Stratigraphic and geochemical study of the organic-rich black shales in the Tarcău Nappe of the Moldavidian Domain Carpathian Chain, Romania. *International Journal of Earth Sciences*, 981, 157–176. <https://doi.org/10.1007/s00531-007-0226-7>
- Bercea R., Balc R., Filipescu S., Zaharia L. and Pop S., 2016: Middle Miocene micropaleontological and sedimentary aspects within a piggy-back basin, Pucioasa section, Carpathian Bend Zone, Romania. AAPG European regional conference and exhibition, Bucharest, Abstract Book, 50.
- Berger, W. H., 1970. Biogenous deep-sea sediments – fractionation by deep-sea circulation. *Geological Society of America Bulletin*, 81, 1385–401.

- Boesiger TM, de Kaenel E, Bergen JA, Browning E, Blair SA., 2017. Oligocene to Pleistocene taxonomy and stratigraphy of the genus *Helicosphaera* and other placolith taxa in the circum North Atlantic Basin, *Journal of Nannoplankton Research*, 37(2-3): 145-175.
- Boote D.R.D., Sachsenhofer R.F., Tari G. and Arbouille, D., 2018. Petroleum provinces of the Paratethyan region. *Journal of Petroleum Geology*, 41, 247-298.
- Bown, P. R., 2005. Palaeogene calcareous nannofossils from the Kilwa and Lindi areas of coastal Tanzania (Tanzania Drilling Project 2003-4). *Journal of Nannoplankton Research*. 27(1): 21-95.
- Bramlette, M. N., 1946. The Monterey Formation of California and the origin of its siliceous rocks, US Geological Survey Professional Paper, 212, 1–57.
- Bray EE, Evans ED., 1961. Distribution of n-paraffins as a clue to recognition of source beds. *Geochimica et Cosmochimica Acta* 22 (1): 2-15. doi: 10.1016/0016-7037(61)90069-2.
- Chatalov GA., 1988. Recent developments in the geology of the Strandzha Zone in Bulgaria. *Bulletin of the Technical University of Istanbul* 41: 433-465.
- Cheshitev G, Kancev I., 1989. Geological map of People's Republic of Bulgaria. 1:500.000. Committee of Geology, Department of Geophysical Prospecting and Geological Mapping, Sofia, Bulgaria.
- Cloud P.E. 1955: Physical limits of glauconite formation. *Bulletin of the American Association of Petroleum Geologists*, 39, 484-92.
- Codrea, V., Barbu, O., Bedelea, H., 2018. Middle Miocene diatomite-bearing formations from western Romania. *Bulletin of the Geological Society of Greece*, 40/1, 21. <http://doi.org/10.12681/bgsg.16329>
- Crawford R. and Sims P.A., 2006: The diatoms *Radialiplicata* sol (Ehrenberg) Glezer and *R. clavigera* (Grunow) Glezer and their transfer to *Ellerbeckia* Crawford, thus a genus with freshwater and marine representatives. *Nova Hedwigia*, Beiheft 130,137-162.
- Crawford R.M., 2004: The diatom genera *Ellerbeckia* and *Actinocyclus*: an appraisal of Kociolek and Spaulding. *Journal of Phycology*, 402, 432-434. <https://doi.org/10.1111/j.1529-8817.2004.03187.x>

- Cressman, E.R., 1962. Nondetrital siliceous sediments. In: Fleischer M. (ed.) Data of Geochemistry. Geological survey professional paper, 1-23. <http://doi.org/10.3133/pp440t>
- Csontos L., Nagymarosy A., Horváth F. and Kováč M., 1992: Tertiary evolution of the intra-Carpathian area: a model. *Tectonophysics* 208, 221-241.
- Dachev C, Stanev V, Bokov P., 1988. Structure of the Bulgarian Black Sea area. *Bullettino di Geofisica Teorica ed Applicata* 30: 79-107.
- Davies A and Kemp AES., 2016. Late Cretaceous seasonal palaeoclimatology and diatom palaeoecology from laminated sediments. *Cretaceous Research*, 65, 82-111. doi:10.1016/j.cretres.2016.04.014.
- Demaison G, Huizinga BJ., 1994. Genetic classification of petroleum systems using three factors: charge, migration and entrapment. *AAPG Memoirs* 60: 73-92.
- Denys L, Muylaert K, Krammer K, Joosten T, Reid M. and Rioual P., 2003: *Aulacoseira subborealis* stat. nov. Bacillariophyceae: a common but neglected plankton diatom. *Nova Hedwigia*. 773-4, 407-427.
- Dicea O., 1996: Tectonic setting and hydrocarbon habitat of the Romanian external Carpathians. In Ziegler P.A. and Horvath F. (eds.): Peri-Tethys Memoir 2. Structure and prospects of Alpine basins and forelands, *Memoires du Museum National d'Histoire Naturelle Paris*, 170, 403-425.
- Didyk BM, Simoneit BR, Brassell ST, Eglinton G., 1978. Organic geochemical indicators of paleoenvironmental conditions of sedimentation. *Nature* 272 (5650): 216-222. doi:10.1038/272216a0.
- Dill H.G., Sachsenhofer, R.F., Grecula, P., Sasvári, T., Palinkas, L. A., Borojevic-Šostarić, S., Strmic-Palinkas, S., Prochaska, W., Garuti, G., Zaccarini, F., Arbouille, D., Schulz, H.-M., 2008. Fossil fuels, ore and industrial minerals. In: McCann, T. (eds.), *The Geology of Central Europe. Volume 2: Mesozoic and Cenozoic*, Geological Society, London, 1341-1449. <https://doi.org/10.1144/cev2p.9>
- Dumitrescu I., Săndulescu M., Bandrabur T. and Săndulescu J., 1970: Harta geologică L-35-XV, foaia 29 Covasna 1:200.000. Institutul Geologic al României, București.

- Dumitrica P., 1970: Cryptocephalic and cryptothoracic Nassellaria in some Mesozoic deposits of Romania. *Revue Roumaine de geologie, geophysique, et geographie, Ser. Geol.*, 14,45-124.
- Eglinton G, Hamilton RJ., 1967. Leaf epicuticular waxes. *Science* 156(3780): 1322-1335. doi:10.1126/science.156.3780.1322.
- Espitalie, J., Marquis, F., Barsony, I., 1984. Geochemical logging. In: Voorhess, K.J. (Eds.): *Analytical Pyrolysis*. Butterworths, Boston, 53-79.
- Ficken KJ, Li B, Swain DL, Eglinton G., 2000. An n-alkane proxy for the sedimentary input of submerged/floating freshwater aquatic macrophytes. *Organic Geochemistry* 31(7-8): 745-749. doi:10.1016/s0146-6380(00)00081-4.
- Figarska-Warchoł B., Stańczak G., Rembiś M. and Tobała T., 2015: Diatomaceous rocks of the Jawornik deposit the Polish Outer Carpathians - petrophysical and petrographical evaluation. *Geology, Geophysics and Environment*, 414, 311. <https://doi.org/10.7494/geol.2015.41.4.311>
- Flecker R, De Villiers S, Ellam RM., 2002. Modelling the effect of evaporation on the salinity -  $^{87}\text{Sr}/^{86}\text{Sr}$  relationship in modern and ancient marginal-marine systems: the Mediterranean Messinian Salinity Crisis. *Earth and Planetary Science Letters* 203 (1): 221-233. doi: 10.1016/s0012-821x(02)00848-8.
- Flecker R, Ellam RM., 2006. Identifying Late Miocene episodes of connection and isolation in the Mediterranean-Paratethyan realm using Sr isotopes. *Sedimentary Geology* 188-189: 189-203. doi: 10.1016/j.sedgeo.2006.03.005.
- Flörke O.W., Graetsch H., Röller K., Martin B. and Wirth R., 1991: Nomenclature of micro- and non-crystalline silica minerals. *Neues Jahrbuch für Mineralogie, Abhandlungen*, 163, 19-42.
- Flower, R.J., 1993. Diatom preservation: experiments and observations on dissolution and breakage in modern and fossil material. In *Twelfth International Diatom Symposium* pp. 473-484. Springer, Dordrecht. [https://doi.org/10.1007/978-94-017-3622-0\\_48](https://doi.org/10.1007/978-94-017-3622-0_48)
- Flower, R.J., Ryves, D.B., 2009. Diatom preservation: differential preservation of sedimentary diatoms in two saline lakes. *Acta Botanica Croatica*, 68/2, 381-399.

- Flügel E., 2004. *Microfacies of carbonate rocks: analysis, interpretation and application*. Springer Science and Business Media, Berlin, pp. 586. doi: 10.5860/choice.42-3437.
- Fodor L., Csontos L., Bada G., Györfi I. and Benkovics L. 1999: Tertiary tectonic evolution of the Pannonian basin system and neighbouring orogens: a new synthesis of paleostress data. In: Durand B., Jolivet L., Horváth F. and Séranne M. (Eds.): *The Mediterranean Basins: Tertiary extension within the Alpine Orogen*. Geol. Soc. London, Spec. Publ. 156, 295-334.
- Frunzescu, D., Brănoiu, G., 2004. *Monografia geologică a Bazinului râului Buzău*. Editura Universității din Ploiești, pp. 309.
- Gaiser, E., Wachnicka, A., Ruiz, P., Tobias, F. and Ross, M., 2005. Diatom indicators of ecosystem change in subtropical coastal wetlands. In: Bortone, S.A. (ed.) *Estuarine Indicators*. CRC Press Marine Science Series, Boca Raton, pp. 599.
- Gebühr C, Wiltshire K, Aberle N, van Beusekom J, Gerds G, 2009. Influence of nutrients, temperature, light and salinity on the occurrence of *Paralia sulcata* at Helgoland Roads, North Sea. *Aquatic Biology*, 7: 185-197. doi:10.3354/ab00191.
- Gedik İ, Timur E, Umut M, Bilgin AZ, Pehlivan Ş, et al., 2014. Geological Maps of Turkey, 1:50.000 scale Istanbul F21-a sheet and explanatory notes. Maden Tetkik ve Arama Genel Müdürlüğü, Ankara, pp. 40.
- Georgiev G., 2011. Geology and hydrocarbon systems in the Western Black Sea. *Turkish Journal of Earth Sciences*, 21(5):723-754. doi:10.3906/yer-1102-4.
- Georgiev G, Dabovski C., 1997. Alpine structure and petroleum geology of Bulgaria. *Geology and Mineral Resources* 8/9, 3-7 (in Bulgarian). doi:10.1306/3b05b0b0-172a-11d7-8645000102c1865d.
- Glushko W.W. and Kruglov S.S., 1986: Tectonic map of the Ukrainian Carpathians: Kiev, Ministerstvo Geologii, scale 1:200,000, 6 sheets.
- Goldman JC., 1993. Potential role of large oceanic diatoms in new primary production. *Deep Sea Research Part I: Oceanographic Research Papers*, 40(1), 159-168. doi:10.1016/0967-0637(93)90059-c.
- Gozhyk P., Semenenko V., Andreeva-Grigorovich A. and Maslun N., 2015: The correlation of the Neogene of Central and Eastern Paratethys segments of Ukraine

- with the International Stratigraphic Chart based on planktonic microfossils. *Geol. Carpath.* 66, 3, 235–244.
- Grasu C., Catană C. and Grinea D., 1988: Flișul Carpatic - Petrografie și considerații economice. Editura Tehnică. București, pp 8.
- Grasu C., Miclăuș C., Florea F. & Șaramet M., 2007: Geology and economic use of bituminous rocks of Romania. Univ.Al. I. Cuza, Iași, pp. 253.
- Grigoraș N., 1955: Studiul comparativ al faciesurilor Paleogenului dintre Putna și Buzău. *An. Com. Geol.*, 28, 99-220.
- Grunert, P, Soliman A, Harzhauser M, Müllegger S, Piller W, Roetzel R, Rögl F., 2010. Upwelling conditions in the Early Miocene Central Paratethys Sea. *Geologica Carpathica.* 61/2, 129-145.
- Gürgey K., 1999. Geochemical characteristic and thermal maturity of oils from the Thrace basin (western Turkey) and western Turkmenistan. *Journal of Petroleum Geology* 22 (2): 167-189. doi: 10.1111/j.1747-5457.1999.tb00466.x.
- Gürgey K., 2009. Geochemical overview and undiscovered gas resources generated from Hamitabat petroleum system in the Thrace Basin, Turkey. *Marine and Petroleum Geology* 26 (7): 1240-1254. doi: 10.1016/j.marpetgeo.2008.08.007.
- Gürgey K, Batı Z., 2018. Palynological and petroleum geochemical assessment of the Lower Oligocene Mezardere Formation, Thrace Basin, NW Turkey. *Turkish Journal Earth Sciences* 27 (5): 349-383. doi: 10.3906/yer-1710-24.
- Gürgey K, Philp RP, Emiroglu H, Siyako M, Uygur E, et al., 2003. Geochemical characterization of natural gas; n-alkane carbon isotope approach and its implication to source, maturity, migration, and mixing deductions. *Proceedings of the 14th International Petroleum Congress and Exhibition of Turkey*, pp. 174.
- Gürgey K, Philp RP, Emiroglu H, Siyako M, Uygur E, et al., 2005. Geochemical and isotopic approach to maturity/source/mixing estimations for natural gas and associated condensates in the Thrace basin, Turkey. *Applied Geochemistry* 20 (11): 2017-2037. doi: 10.1016/j.apgeochem.2005.07.012.
- Haczewski G., 1989: Coccolith limestone horizons in the Menilite- Krosno series (Oligocene, Carpathians)—identification, correlation and origin. *Ann. Soc. Geol. Pol.*, 59, 435–523.

- Hajós, M.A., 1959. Szurdokpüspöki kovaföldrétegek algái (Die Algen des Kieselgurschichten von Szurdokpüspöki). *Földtani Közlöny*. 89/2, 155-169.
- Hajós, M.A., 1968. Die Diatomeen der Miozanen Ablagerungen des Matravorlandes. *Geologica Hungarica*. 37, 1-401.
- Hajós, M.A., 1973. The Mediterranean diatoms. Initial Reports of the Deep-Sea Drilling Project, 13 (Part 2), 944-951.
- Hajós, M.A., 1986. Magyarországi miocén diatomás képződmények rétegtana / Stratigraphy of Hungary's miocene Miocene diatomite deposits. *Institutum Geologicum Hungaricum Series Paleontologica*, 49, 1-339.
- Halássová E., Hudáčková N., Holcová K., Vass D., Elečko M. and Pereszlenyi M., 1996: Sea ways connecting the Fiakovo/Petervasara Basin with the Eggenburgian/Burdigalian open sea. *Slovak Geol. Mag.*, 2, 125–136.
- Hans U, Kleine T, Bourdon B., 2013. Rb-Sr chronology of volatile depletion in differentiated protoplanets: BABI, ADOR and ALL revisited. *Earth and Planetary Science Letters* 374: 204-214. doi: 10.1016/j.epsl.2013.05.029.
- Harper, M.A., Pledger, S.A., Smith, E.G.C., Van Eaton, A.R., Wilson, C.J.N., 2015. Eruptive and environmental processes recorded by diatoms in volcanically dispersed lake sediments from the Taupo Volcanic Zone, New Zealand. *Journal of Paleolimnology*, 54/4, 263-277. <https://doi.org/10.1007/s10933-015-9851-5>.
- Harwood D.M, 2010: Diatomite, in: Smol, J.P. and Stoermer, E.F. eds., 2010. *The diatoms: applications for the environmental and earth sciences*. Cambridge University Press.
- Hilgen, F. J., Lourens, L. J., Van Dam, J. A., Beu, A. G., Boyes, A. F., Cooper, R. A., Wilson, D. S., 2012. The Neogene Period. *The Geologic Time Scale*, 923–978. doi:10.1016/b978-0-444-59425-9.00029-9.
- Holba AG, Dzou LI, Masterson WD, Hughes WB, Huizinga BJ, et al., 1998. Application of 24-norcholestanes for constraining source age of petroleum. *Organic Geochemistry*. 29(5-7): 1269-1283. doi:10.1016/s0146-6380(98)00184-3.
- Holba AG, Dzou LIP, Masteron WD, Hughes WB, Huizinga BJ, Singletary MS, Moldowan JM, Mello MR, Tegelaar E., 1998a. Application of 24-norcholestanes for constraining source age of petroleum. *Org Geochem* 29:1269–1283

- Holba AG, Tegelaar EW, Huizinga BJ, Moldowan JM, Singletary MS, McCaffrey MA, Dzou LIP., 1998b. 24-norcholestanes as age-sensitive molecular fossils. *Geology* 26:783–786
- Horsfield B and Rullkötter J, 1994. Diagenesis, Catagenesis, and Metagenesis of Organic Matter. *The petroleum system from source to trap*, pp. 189-200. doi:10.1306/m60585c10.
- Horvat, A., 2004. Middle Miocene siliceous algae of Slovenia. *Narodna in univerzitetna knjižnica, Ljubljana*, pp. 255.
- Horwitz Philip E, Chiarizia R, Dietz ML., 1992. A novel Strontium-Selective extraction chromatographic resin. *Solvent Extraction and Ion Exchange* 10 (2): 313-336. doi: 10.1080/07366299208918107.
- Horwitz Philip E, Dietz ML, Fisher DE., 1991. Separation and preconcentration of strontium from biological, environmental, and nuclear waste samples by extraction chromatography using a crown ether. *Analytical Chemistry* 63 (5): 522-525. doi: 10.1021/ac00005a027.
- Iijima, A. and Tada R. 1981. Silicadiagenesis of Neogene diatomaceous and volcaniclastic sediments in northern Japan. *Sedimentology*, 28, 185–200.
- Iijima, A., 1988. Diagenetic transformations of minerals as exemplified by zeolites and silica minerals—a Japanese view. In *Developments in sedimentology*, vol. 43, pp. 147-211). Elsevier.
- Isaacs, C. M., 1983. Compositional variation and sequence in the Monterey Formation, Santa Barbara coastal area, California. *Pacific Section, SEPM Special Publication*, 28, 117–32
- Isaacs, C.M., Rullkötter, J. (eds.), 2001. *The Monterey Formation: From Rocks to Molecules*. Columbia University Press, New York 268-295. <https://doi.org/10.1017/S0016756802246506>
- Isaacs C. M., 1981. Porosity reduction during diagenesis of the Monterey Formation, Santa Barbara Coastal area, California. In *The Monterey Formation and Related Siliceous Rocks of California*, ed. R. E. Garrison, and R. G. Douglas, Los Angeles, CA: Pacific Section, Society of Economic Paleontologists and Mineralogists, pp. 257-72.



- İslamoğlu Y, Harzhauser M, Gross M, Jiménez-Moreno G, Ćorić S, et al., 2010. From Tethys to Eastern Paratethys: Oligocene depositional environments, paleoecology and paleobiogeography of the Thrace Basin (NW Turkey). *International Journal of Earth Science*. 99 (1): 183-200. doi: 10.1007/s00531-008-0378-0.
- Jirman, P., Geršlová, E., Bubík, M., Sachsenhofer, R. F., Bechtel, A., Więclaw, D., 2019. Depositional environment and hydrocarbon potential of the Oligocene Menilite Formation in the Western Carpathians: A case study from the Loučka section (Czech Republic). *Marine and Petroleum Geology*, 107, 334–350. <https://doi.org/10.1016/j.marpetgeo.2019.05.034>
- Jones J.T. and Segnit E.R., 1971: The nature of opal. Nomenclature and constituent phases. *Journal of the Geological Society of Australia*. 1, 181, 57-68.
- Kaempf, J., 2007. On the magnitude of upwelling fluxes in shelf-break canyons. *Continental Shelf Research*, 27, 2211–2223. <https://doi.org/10.1016/j.csr.2007.05.010>
- Kaenel de E and Villa G., 1996. Oligocene-Miocene calcareous nannofossil biostratigraphy and paleoecology from the Iberian Abyssal Plain. *Proceedings of the Ocean Drilling Program. Scientific Results*. 149: 79-145. doi:10.2973/odp.proc.sr.149.208.1996.
- Kemp AES, Pearce RB, Grigorov I, Rance J, Lange CB, et al., 2006. Production of giant marine diatoms and their export at oceanic frontal zones: Implications for Si and C flux from stratified oceans. *Global Biogeochemical Cycles*, 20 (4), 1-13. doi:10.1029/2006gb002698.
- Kociolek J.P. and Spaulding S.A. 2002: Morphological variation, species concepts, and classification of an unusual fossil centric diatom bacillariophyta from Western North America, *Journal of Phycology*, 384, 821-833. <https://doi.org/10.1046/j.1529-8817.2002.02009.x>
- Kociolek J.P., Theriot E.C., Williams D.M., Julius M., Stoermer E.F. and Kingston J.C. 2015: Centric and Araphid Diatoms. In *Freshwater Algae of North America*, Academic Press, 653-708. <https://doi.org/10.1016/b978-0-12-385876-4.00015-3>
- Kotarba, M.J., Koltun, Y.V., 2006. The origin and habitat of hydrocarbons of the Polish and Ukrainian parts of the Carpathian Province. In: Golonka, J. and Pícha, F.J. (eds.) *The Carpathians and Their Foreland: Geology and Hydrocarbon Resources*.

- American Association of Petroleum Geologists Memoirs, 84, 395–442.  
<https://doi.org/10.1306/985614m843074>
- Kotlarczyk J. and Kaczmarek I. 1987: Two diatom horizons in the Oligocene and ?Lower Miocene of the Polish Outer Carpathians. *Annales Societatis Geolorum Poloniae*, 57, 142-188.
- Kotlarczyk, J., Uchman, A., 2012. Integrated ichnology and ichthyology of the Oligocene Menilite Formation, Skole and Subsilesian nappes, Polish Carpathians: a proxy to oxygenation history. *Palaeogeography, Palaeoclimatology, Palaeoecology*, 331, pp.104-118. <https://doi.org/10.1016/j.palaeo.2012.03.002>
- Kováč M., Halássová E., Hudáčková N., Holcová K., Hyžný M., Jamrich M. and Ruman A. 2018: Towards better correlation of the Central Paratethys regional time scale with the standard geological time scale of the Miocene Epoch. *Geol. Carpath.*, 693, 283-300. <https://doi.org/10.1515/geoca-2018-0017>
- Kováč M., Hudáčková N., Halássová E., Kováčová M., Holcová K., Oszczytko-Clowes M., Báldi K., Less Gy., Nagymarosy A., Ruman A., Klučiar T. and Jamrich M. 2017a: The Central Paratethys palaeoceanography: a water circulation model based on microfossil proxies, climate, and changes of depositional environment. *Acta Geologica Slovaca* 9, 2, 75–114.
- Kováč M., Márton E., Oszczytko N., Vojtko R., Hók J., Králiková S., Plašienka D., Klučiar T., Hudáčková N. and Oszczytko-Clowes M. 2017b: Neogene palaeogeography and basin evolution of the Western Carpathians, Northern Pannonian domain and adjoining areas. *Global Planet. Change* 155, 133–154.
- Kováč, M., Andreyeva-Grigorovich, A., Bajraktarević, Z., Brzobohatý, R., Filipescu, S., Fodor, L., Harzhauser, M., Nagymarosy, A., Oszczytko, N., Pavelić, D. and Rögl, F., 2007. Badenian evolution of the Central Paratethys Sea: paleogeography, climate and eustatic sea-level changes. *Geologica Carpathica*, 58(6).
- Kováč, M., Halássová, E.V.A., Hudáčková, N., Holcová, K., Hyžný, M., Jamrich, M. and Ruman, A., 2018. Towards better correlation of the Central Paratethys regional time scale with the standard geological time scale of the Miocene Epoch. *Geologica Carpathica*, 69(3), pp.283-300.

- Krebs, W.N., Gladenkov, A.Y. and Jones, G.D., 2010. Diatoms in oil and gas exploration. In Smol, J.P. and Stoermer, E.F. (eds.), *The diatoms: applications for the environmental and earth sciences*. Cambridge University Press, 402–412.
- Krhovský J., 1995. Early Oligocene palaeoenvironmental changes in the West Carpathian Flysch belt of Southern Moravia. *Proc. XV Congr. Carp.-Balk. Geol. Ass.*, Sept. 1995, Geol. Soc. Greece, Spec. Publ., 4, 209–213.
- Krhovský J., Adamová M., Hladíková J. and Maslowská H., 1991: Paleoenvironmental changes across the Eocene/Oligocene boundary in the Zdánice and Pouzdrany Units (Western Carpathians, Czechoslovakia): The long-term trend and orbitally forced changes in calcareous nannofossil assemblages. In: Hamršík B. and Young J.R. (Eds.): *Nannoplankton research. Proceedings, 4th Internat. Nannoplankton Assoc. Conference, II*. Knihovnička ZPN, 14b, 105–187.
- Krhovský J., Asdamova J., Hladíková J. and Maslowská H. 1992. Paleoenvironmental changes across the Eocene/Oligocene boundary in the Zdanice and Pouzdrany units Western Carpathians, Czechoslovakia: the long-term trend and orbitally forced changes in calcareous nannofossil assemblages. *INA conference, Nannoplankton research*, 105-187.
- Krhovský, J., 1981. Stratigraphy and palaeoecology of the Menilite Formation of the Ždánice unit and of the diatomites of the Pouzdrany unit (the western Carpathians, Czechoslovakia) (in Czech with English summary). *Zemny Plyn. a Nafta* 26, 45–62.
- Lafargue E., Marquis F., Pillot D., 1998. Rock-Eval 6 applications in hydrocarbon exploration, production, and soil contamination studies. *Revue de l'institut français du pétrole* 53 (4): 421-437. <https://doi.org/10.2516/ogst:1998036>
- Larter, S.R., 1984. Application of analytical pyrolysis techniques to kerogen characterization and fossil fuel exploration/exploitation. In *Analytical pyrolysis* (pp. 212-275), Butterworth-Heinemann.
- Less G, Özcan E, Okay AI., 2011. Stratigraphy and larger foraminifera of the Middle Eocene to Lower Oligocene shallow-marine units in the northern and eastern parts of the Thrace Basin, NW Turkey. *Turkish Journal of Earth Sciences* 20 (6): 793-845. doi: 10.3906/yer-1010-53.

- Levkov, Z., 2009. Amphora sensu lato. In: Lange-Bertalot, H. (ed.) *Diatoms of Europe*, Volume 5. A.R.G. Gantner, pp. 916.
- Lohrenz S.E., Dagg M.J. and Whitledge T.E., 1990: Enhanced primary production at the plume/oceanic interface of the Mississippi River, *Continental Shelf Research*, 10, 7, 639-664. [https://doi.org/10.1016/0278-4343\(90\)90043-1](https://doi.org/10.1016/0278-4343(90)90043-1)
- Luo Q, Yu S, Liu Y, Zhang Y, Han H, et al., 2012. Existence and implications of hop-17 (21)-enes in the lower cretaceous of the Saihantala Sag, Erlian Basin, China. *Petroleum Science*. 9(2):154-160. doi:10.1007/s12182-012-0195-8.
- Magoon, L. B., Dow, W. G., 1994. *The Petroleum System*. In Magoon, L. B., Dow, W. G (Eds.): *The Petroleum System- from source to trap*. AAPG Memoir 60. ISBN: 0-89181-338-1
- Major CO, Ryan WBF, Lericolais G, Hajdas I., 2002. Constraints on Black Sea outflow to the Sea of Marmara during the last glacial-interglacial transition. *Marine Geology* 190 (1-2): 19-34. doi:10.1016/s0025-3227(02)00340-7.
- Martini E., 1971. Standard Tertiary and Quaternary calcareous nannoplankton zonation. *Proceedings of the II Planktonic Conference*. Ed. Tecnoscienza, Roma, 739-785.
- Marynowski L, Smolarek J, Bechtel A, Philippe M, Kurkiewicz S, et al., 2013. Perylene as an indicator of conifer fossil wood degradation by wood-degrading fungi. *Organic Geochemistry* 59:143-151. doi:10.1016/j.orggeochem.2013.04.006.
- Mattinson JM., 1972. Preparation of hydrofluoric, hydrochloric, and nitric acids at ultralow lead levels. *Analytical Chemistry* 44 (9): 1715-1716. doi: 10.1021/ac60317a032.
- Mayer J, Rupprecht BJ, Sachsenhofer RF, Tari G, Bechtel A et al., 2018a. Source potential and depositional environment of Oligocene and Miocene rocks offshore Bulgaria. *Geological Society, London, Special Publications* 464(1): 307-328. doi:10.1144/sp464.2.
- Mayer J, Sachsenhofer RF, Ungureanu C, Bechtel A, Gratzner R, et al., 2018b. Petroleum charge and migration in the Black Sea: insights from oil and source rocks geochemistry. *Journal Petroleum Geology* 41: 337-35. doi:10.1111/jpg.12706.
- McArthur JM, Howarth RJ, Shields GA., 2012. Strontium isotope stratigraphy. In: Gradstein FM, Ogg JG, Schmitz M, Ogg G (editors). *The geologic time scale*. Elsevier, pp. 127-144. doi: 10.1016/b978-0-444-59425-9.00007-x.

- McCarthy, K., Rojas, K., Niemann, M., Palmowski, D., Peters, K. and Stankiewicz, A., 2011. Basic petroleum geochemistry for source rock evaluation. *Oilfield Review*, 23(2), pp.32-43.
- McQuoid M and Nordberg K., 2003. The diatom *Paralia sulcata* as an environmental indicator species in coastal sediments. *Estuarine, Coastal and Shelf Science*, 56(2), 339-354. doi:10.1016/s0272-7714(02)00187-7.
- Melinte-Dobrinescu M. and Brustur T., 2008. Oligocene-Lower Miocene events in Romania. *Acta Palaeontologica Romaniaae* 6, 203-215.
- Moldowan JM, Fago FJ., 1986. Structure and significance of a novel rearranged monoaromatic steroid hydrocarbon in petroleum. *Geochimica et Cosmochimica Acta*, 50(3): 343-351. doi:10.1016/0016-7037(86)90188-2.
- Moldowan MJ, Wolfgang K., 1985. Relationship Between Petroleum Composition and Depositional Environment of Petroleum Source Rocks. *AAPG Bulletin* 69 (8): 1255. doi: 10.1306/ad462bc8-16f7-11d7-8645000102c1865d.
- Moore LJ, Murphy TJ, Barnes IL, Paulsen PJ., 1982. Absolute isotopic abundance ratios and atomic weight of a reference sample of strontium. *Journal of Research of the National Bureau of Standards* 87 (1): 1. doi: 10.6028/jres.087.001.
- Moțaș I., Bandrabur T., Ghenea C. and Săndulescu M., 1968: Harta geologică L-35-XXVII, foaia 36 Ploiești la 1:200.000. Institutul Geologic al României, București.
- Munteanu I., Popescu D., Borosi V., Dobre S., Maioru V, and Iusco G., 2014: Stratigraphic re-evaluation of the Oligocene-Lower Miocene formations in the Diapiric Fold Zone, Eastern Carpathian, Romania. *Search and Discovery Article 90192*, European Regional Conference and Exhibition, Barcelona, Spain.
- Murata, K. J. and Larson, R. R., 1975. Diagenesis of Miocene siliceous shale, Temblor Range, California. *US Geological Survey Journal of Research*, 3, 553–66.
- Mutihac V. and Ionesi L., 1974: *Geology of Romania*. Editura Tehnică, Bucharest, pp. 655.
- Natal'in B, Say AG., 2015. Eocene - Oligocene stratigraphy and structural history of the Karaburun area, southwestern Black Sea coast, Turkey: transition from extension to compression. *Geological Magazine* 152: 1104-1122. doi:10.1017/s0016756815000229.

- Neveeskaja LA, Goncharova IA, Iljina LB, Paramonova NP, Popov SV, et al., 1987. History of the Paratethys. *Ann Instituti Geologici Publici Hungarici* 70: 337-342.
- Nichols PD, Volkman JK, Palmisano AC, Smith GA, White DC., 1988. Occurrence of an isoprenoid C<sub>25</sub> diunsaturated alkene and high neutral lipid content in Antarctic sea-ice diatom communities. *Journal of Phycology*, 24(1): 90-6. doi:10.1111/j.1529-8817.1988.tb04459.x.
- Nier AO., 1938. The isotopic constitution of strontium, barium, bismuth, thallium and mercury. *Physical Review* 54 (4): 275-278. doi: 10.1103/physrev.54.275.
- Nikishin AM, Okay AI, Tüysüz O, Demirer A, Amelin N, et al., 2015. The Black Sea basins structure and history: New model based on new deep penetration regional seismic data. Part 1: Basins structure and fill. *Marine and Petroleum Geology* 59:638-655. doi:10.1016/j.marpetgeo.2014.08.017.
- Noble R, Alexander R, Kagi RI., 1985. The occurrence of bisnorhopane, trisnorhopane and 25-norhopanes as free hydrocarbons in some Australian shales. *Organic Geochemistry*. 8(2):171-176. doi:10.1016/0146-6380(85)90035-x.
- Ognjanova-Rumenova N.G. and Crawford R.M., 2012: Morphology and ultrastructure of the fossil freshwater diatom *Aulacoseira temperei*. *Diatom research*, 273, 107-19.
- Ognjanova-Rumenova, N., and Radovan P., 2015. Stratigraphic and taxonomic significance of siliceous microfossils collected from the Turiec Basin, Western Carpathians (Slovakia). *Acta Botanica Croatica* 74/ 2, 345-361. <https://doi.org/10.1515/botcro-2015-0023>
- Okada H and McIntyre A., 1979. Seasonal distribution of the modern Coccolithophores in the western North Atlantic Ocean. *Marine Biology*, 54, 319-328.
- Okay A, Özcan E, Hakyemez A, Siyako M, Sunal G, et al., 2019. The Thrace Basin and the Black Sea: the Eocene-Oligocene marine connection. *Geological Magazine*: 156 (23): 39-61. doi: 10.1017/S0016756817000772.
- Okay A, Şengör AM, Görür N., 1994. Kinematic history of the opening of the Black Sea and its effect on the surrounding regions. *Geology* 22 (3): 267-270. doi: 10.1130/0091-7613(1994)022<0267:KHOTOO>2.3.CO;2.
- Okay AL, Satır M, Tüysüz O, Akyüz S, Chen F., 2001. The tectonics of the Strandja Massif: late-Variscan and mid-Mesozoic deformation and metamorphism in the northern Aegean. *International Journal of Earth Sciences*. 90 (2): 217-33.

- Oktay F, Eren RH, Sakıncı M., 1992. Sedimentary geology of eastern Thrace Oligocene Basin around Karaburun-Yeniköy. In Proceedings of the 9th Petroleum Congress of Turkey. Ankara: Turkish Association of Petroleum Geologists 92-101 (in Turkish).
- Olli, K., Clarke, A., Danielsson, Å., Aigars, J., Conley, D.J., Tamminen, T., 2008. Diatom stratigraphy and long-term dissolved silica concentrations in the Baltic Sea. *Journal of Marine Systems*, 73/3-4, 284-299. <https://doi.org/10.1016/j.jmarsys.2007.04.009>
- Ourisson G, Albrecht P, Rohmer M., 1979. The Hopanoids: palaeochemistry and biochemistry of a group of natural products. *Pure and Applied Chemistry* 51 (4): 709-729. doi: 10.1351/pac197951040709.
- Pantocsek, J., 1889. Beiträge zur Kenntnis der Fossilen Bacillarien Ungarns. Teil II. Brackwasser Bacillarien. Anhang: Analyse de marine Depots von Bory, Bremia, Nagy-Kurtos in Ungarn; Ananio und Kusnetzki in Russland. Nagy-Tapolcsány, Buchdruckerei von Julius Platzko pp. 123.
- Paraschiv D. and Olteanu G., 1970. Oil fields in Mio-Pliocene zone of eastern Carpathians District of Ploiesti. *AAPG Bulletin*. 399-427. <https://doi.org/10.1306/5d25c395-16c1-11d7-8645000102c1865d>
- Patruș D., Ștefănescu M., Popa E. and Popescu I., 1968: Geology of the Inner Zones of the Carpathian Bend. Geological Institute, Romania, pp. 50.
- Pătruș I., 1955: Geologia și tectonica regiunii Vălenii de Munte-Cosminele-Buștenari. *An. Com. Geol.*, 28, 5-98.
- Peaboy and Cameron, 2010: Forensic science and diatoms in: Smol, J.P. and Stoermer, E.F. eds., 2010. *The diatoms: applications for the environmental and earth sciences*. Cambridge University Press, 534 to 539.
- Pedersen JH., Karlsen DA, Backer-Owe K, Lie JE, Brunstad H., 2006. Two geochemistry of two unusual oils from the Norway North Sea: implications for new source rock and play scenario. *Petroleum Geoscience* 12: 85-96.
- Perch-Nielsen K., 1985. Cenozoic calcareous nannofossils, in *Plankton stratigraphy* (eds. Bolli HM, Saunders JB and Perch-Nielsen K) Cambridge University Press, 427-554.

- Peters KE, Walters CC, Moldowan JM (2005). The Biomarker Guide Volume 1: Biomarkers and isotopes in the environment and human history. Geological Magazine 143, pp. 361. doi: 10.1017/s0016756806212056.
- Peters, K.E. and Cassa, M.R., 1994. Applied source rock geochemistry: American Association of Petroleum Geologists Memoir 60.
- Pícha, F.J., Stráník, Z., 1999. Late Cretaceous to early Miocene deposits of the Carpathian foreland basin in southern Moravia. *Int. J. Earth Sci.* 88, 475–495.
- Pin C, Briot D, Bassin C, Poitrasson F., 1994. Concomitant separation of strontium and samarium-neodymium for isotopic analysis in silicate samples, based on specific extraction chromatography. *Analytica Chimica Acta* 298 (2): 209-217. doi: 10.1016/0003-2670(94)00274-6.
- Pisciotta, K. A., 1983. Diagenetic trends in the siliceous facies of the Monterey Shale in the Santa Maria region, California. *Sedimentology*, 28, 547–71.
- Popescu B.M., 1995. Romania's petroleum systems and their remaining potential. *Petroleum Geoscience*. 14; 337-350.
- Popov N, Kojumdjieva E., 1987. The Miocene in northeastern Bulgaria (lithostratigraphic subdivision and geologic evolution). *Review of the Bulgarian Geological Society* 38, 15-33 (in Bulgarian).
- Popov S.V., Rögl F., Rozanov A.Y., Steininger F.F., Shcherba I.G. Kováč M. (eds.), 2004. Lithological–Paleogeographic maps of Paratethys. 10 Maps Late Eocene to Pliocene. *Courier Forschungsinstitut Senckenberg*, 250, 1-46.
- Popov SV, Iliana LB, Nikolayeva YA, 1985 . Molluscs and ostracods from the Oligocene Solenovian horizon of the Eastern Paratethys. *Paleontological Journal* 1: 28-41 (in Russian).
- Popov SV, Voronina AA and Gontcharova IA., 1993. Stratigraphy and bivalves of the Oligocene-Lower Miocene of the Eastern Paratethys. *Publications of the Paleontological Institute*, 256, Russian Academy of Sciences, Moscow, 206 pp (in Russian).
- Popov, S.V., Bugrova, E.M., Amitrov, O.V., Andreeva-Grigorovich, A.S., Akhmetiev M.A., Zaporozhets, N.I., Nikolaeva, I.A., Sychevskaja, E.K. and Shcherba I.G., 2004a. Biogeography of the Northern Peri-Tethys from the Late Eocene to the Early Miocene.



- Popov, S.V., Rögl, F., Raznov, A.Y, Steininger, F.F., Shcherba, I.G. and Kovac, M. 2004b. Lithological Paleogeographic maps of Paratethys. 10 Maps Late Eocene to Pliocene, Volume 250. Courier Forschungsinstitut Senckenberg.
- Professor Lampadius 1809: XXI. Analysis of the schist that accompanies the menilite near Paris. The Philosophical Magazine, 33, 13, 134-136.
- Pupp M, Bechtel A, Ćorić S, Gratzer R, Rustamov J, et al., 2018. Eocene and Oligo-Miocene Source Rocks in the Rioni and Kura basins of Georgia: depositional environment and petroleum potential. *Journal of Petroleum Geology* 41 (3): 367-392. doi: 10.1111/jpg.12708.
- Radke M, Willsch H, Welte DH., 1980. Preparative Hydrocarbon Group Type Determination by Automated Medium Pressure Liquid Chromatography. *Analytical Chemistry*, 52(3): 406-411. doi:10.1021/ac50053a009.
- Rampen SW, Abbas BA, Schouten S, Sinninghe Damsté JS (2010) A comprehensive study of sterols in marine diatoms (Bacillariophyta): implications for their use as tracers for diatom productivity. *Limnol Oceanogr* 55(1):91–105.
- Rauball J.F., Sachsenhofer R.F., Bechtel A., Coric S. and Gratzer R., 2019: The Oligocene-Miocene Menilite Formation in the Ukrainian Carpathians: A world-class source rock. *Journal of Petroleum Geology*, 424, 393–415. <https://doi.org/10.1111/jpg.12743>
- Řeháková, Z., 1997. Bericht 1997 über mikropaläontologische Untersuchungen der diatomeenführenden Sedimente auf Blatt 22 Hollabrunn. — unveröffentlichter Bericht, Archiv der Geologischen Bundesanstalt, Inv.Nr. ALK-022REH/97, pp. 5, Wien.
- Rice, D. D., and G. E. Claypool, 1981, Generation, accumulation, and resource potential of biogenic gas: *AAPG Bulletin*, v. 65, p. 5-25.
- Roetzel, R., 1999. Arbeitstagung der Geologischen Bundesanstalt 1999, Geologische Karten ÖK 9 Retz und ÖK 22 Hollabrunn, Geogenes Naturraumpotential der Bezirke Horn und Hollabrunn, Retz, Wien.
- Roetzel, R., Ćoric, S., Galovic, I., Rögl, F., 2006. Early Miocene (Ottangian) coastal upwelling conditions along the southeastern scarp of the Bohemian Massif (Parisdorf, Lower Austria, Central Paratethys). *Beiträge zur Paläontologie*, 30, 387-413.

- Rögl F., 1997. Palaeogeographic considerations for Mediterranean and Paratethys seaways (Oligocene to Miocene). *Annalen des Naturhistorischen Museums in Wien. Serie A für Mineralogie und Petrographie, Geologie und Paläontologie, Anthropologie und Prähistorie*, 279-310.
- Rögl F. 1999: Mediterranean and Paratethys. Facts and hypotheses of an Oligocene to Miocene paleogeography short overview. *Geol. Carpath.*, 504, 339-349.
- Rögl, F. 1997. Mediterranean and Paratethys. Facts and hypotheses of an Oligocene to Miocene paleogeography (short overview). *Geologica Carpathica*, 50, 339-349.
- Ross, R., 1995. Revision of *Rutilaria* Greville (Bacillariophyta). *Bulletin of the Natural History Museum. Botany Series*. Cambridge university press, pp 747.
- Rothwell R.G., 1989: Minerals and mineraloids in marine sediments; an optical identification guide. Elsevier Science Publishers, 55, 379, 293-294. <https://doi.org/10.1180/minmag.1991.055.379.23>
- Round F.E., Crawford R.M. and Mann D.G. 1990: *Diatoms: biology and morphology of the genera*. Cambridge University Press, pp. 176.
- Rovira, L., Trobajo, R., Sato, S., Ibáñez, C., Mann, D.G., 2015. Genetic and physiological diversity in the diatom *Nitzschia inconspicua*. *Journal of Eukaryotic Microbiology*, 62/6, 815-832.
- Rubinstein, I. and Goad, L.J., 1974. Occurrence of (24S)-24-methylcholesta-5, 22E-dien-3 $\beta$ -ol in the diatom *Phaeodactylum tricornutum*. *Phytochemistry*, 13(2), pp.485-487.
- Rusu, A., 1999. Rupelian mollusk fauna of Solenovian type found in Eastern Carpathians (Romania). *Acta Palaeontologica Romaniae*, 2: 449-452.
- Sachsenhofer R.F., Hentschke J., Bechtel A., Coric S., Gross D., Horsfield B., Rachetti A. and Soliman A. 2015: Hydrocarbon potential and depositional environments of Oligo-Miocene rocks in the Eastern Carpathians (Vrancea Nappe, Romania), *Mar. Petr. Geol.*, 68, 269-290.
- Sachsenhofer R.F., Popov S.V., Bechtel A., Coric S., Francu J., Gratzner R., Grunert P., Kotarba M., Mayer J., Pupp M. Ruprecht B.J. and Vincent S.J. 2018a: Oligocene and Lower Miocene source rocks in the Paratethys: Palaeogeographical and stratigraphic controls. In Simmons M. et al. (eds.): *Geological Society London Special Publication*, 464, 267-306. <https://doi.org/10.1144/SP464.1>

- Sachsenhofer R.F., Popov S.V., Ćorić S., Mayer J., Misch D., Morton M.T., Pupp M., Rauball J.F. and Tari G. 2018b: Paratethyan petroleum source rocks: an overview. *Journal of Petroleum Geology*, 413, 219-245. <https://doi.org/10.1111/jpg.12702>
- Sachsenhofer RF, Stummer B, Georgiev G, Dellmour R, Bechtel A et al., 2009. Depositional environment and hydrocarbon source potential of the Oligocene Ruslar Formation (Kamchia Depression; western Black Sea). *Marine and Petroleum Geology*, 26(1): 57-84. doi:10.1016/j.marpetgeo.2007.08.004.
- Sachsenhofer, R.F., Bechtel, A., Reischenbacher, D., Weiss, A., 2003. Evolution of lacustrine systems along the Miocene Mur-Mürz fault system (Eastern Alps, Austria) and implications on source rocks in pull-apart basins. *Marine and Petroleum Geology* 20, 83–110. [https://doi.org/10.1016/s0264-8172\(03\)00018-7](https://doi.org/10.1016/s0264-8172(03)00018-7)
- Sakıncı M., 1994. Karaburun (B İstanbul) denizel oligoseninin stratigrafisi ve paleontolojisi, *Maden Tetkik ve Arama Dergisi* 116: 9-14.
- Sancay HR, Batı Z, 2020. Late Eocene to Early Oligocene palynostratigraphy of the Western Black Sea, Eastern Paratethys. *Turkish Journal of Earth Sciences*, 29(SI-1), pp.115-138.
- Săndulescu M. 1984: *Geotectonica României*, Editura Tehnica, București, pp. 280.
- Săndulescu M., Popescu G. and Mărunțeanu M. 1995: Facies and stratigraphy of the Lower and Middle Miocene formations of the Slănic Syncline. *Romanian Journal of Stratigraphy*, 76, 6, 3-11.
- Săndulescu M., Ștefănescu M., Butac A., Patrut I. and Zaharescu P. 1981: Genetical and structural relations between flysch and Molasse The Eastern Carpathians Model. Guide to Excursion A5. Guide-book series No. 19. *Romanian Journal Stratigraphy*.
- Sarı A, Savan AK., 2008. Organic Geochemical Investigations of the Tertiary Units in the Thrace Basin (Edirne, Turkey). *Petroleum Science and Technology* 6 (3): 322-345. doi: 10.1080/10916460600809485.
- Schleder Z., Tămaș D.M., Krezsek C., Arnberger K. and Tulucan A., 2019: Salt tectonics in the Bend Zone segment of the Carpathian fold and thrust belt, Romania. *International Journal of Earth Sciences*, 1085, 1595-1614. <https://doi.org/10.1007/s00531-019-01721-x>
- Schrader H. and Gersonde R., 1978: Diatoms and silicoflagellates. In Zachariasse et al.: *Microplaeontological counting methods and techniques, an exercise on an eight*

- meters section of the lower Pliocene of Capo Rossello. Sicily. Utrecht Micropal. Bull. 17, 129-176.
- Schrader H.J., 1973. Proposal for a standardized method of cleaning diatoms-bearing deep-sea and land-exposed marine sediments. In: Simonsen, R. (eds.) Seconds symposium on recent and fossil diatoms. Nova Hedwigia, supplement 45, 409.
- Schrader, H., Gersonde R., 1978. Diatoms and silicoflagellates. In: Zachariasse et al. Microplaeontological counting methods and techniques-an exercise on an eight metres section of the lower Pliocene of Capo Rossello. Sicily. Utrecht Micropaleontological Bulletin 17, 129-76.
- Schultz L., 1964. Quantitative interpretation of mineralogical composition from X-ray and chemical data for the Pierre Shale. U.S. Geolical Survey Profesional Paper, 391-C. doi:10.3133/pp391c.
- Schulz HM, Bechtel AC, Rainer TH, Sachsenhofer RF, Struck UL., 2004. Paleooceanography of the Western Central Paratethys during early Oligocene nannoplankton Zone NP23 in the Austrian Molasse Basin. *Geologica Carpathica*. 55(4):311-23.
- Schwartz, D. E., 1987. Lithology, petrophysics, and hydrocarbons in cyclic Belridge Diatomite, south Belridge oil field, Kern Co., California. Fourth International Congress on Pacific Neogene Stratigraphy, Berkeley, CA, July 29–31, abstract volume, 102.
- Sebe-Radoi O.G., Dumitras D.G., Marincea S., Calin N., Birgoanu D., and Barbu O.C. 2017: Preliminary paleontological and mineralogical study of the diatomites from Pătârlagele, Romania. Goldschmidt Abstract volume.
- Seifert WK, Moldowan JM., 1980. The effect of thermal stress on source-rock quality as measured by hopane stereochemistry. *Physics and Chemistry of the Earth* 12: 229-237. doi: 10.1016/0079-1946(79)90107-1.
- Şen Ş., 2011. Petroleum Source Rock Assessment of the Southwestern Thrace Basin, NW Turkey. *Energy Sources, Part A: Recovery, Utilization, and Environmental Effects*, 33 (11): 1005–1017. doi:10.1080/15567036.2010.485177.
- Simmons, M.D., Bidgood, M.D., Connell, P.G., Ćorić, S., Okay, A.I., Shaw, D., Tulan, E., Mayer, J. and Tari, G.C., 2020. Biostratigraphy and palaeoenvironments of the

- Oligocene succession (İhsaniye Formation) at Karaburun (NW Turkey). *Turkish Journal of Earth Sciences*, 29(1), pp.28-63.
- Simmons MD, Tari GC, Okay AI (2018). Petroleum geology of the Black Sea: introduction. Geological Society, London, Special Publication 464 (1): 1-18. doi: 10.1144/sp464.15.
- Simoneit BR, Grimalt JO, Wang TG, Cox RE, Hatcher PG, et al., 1986. Cyclic terpenoids of contemporary resinous plant detritus and of fossil woods, ambers and coals. *Organic Geochemistry*, 10(4-6): 877-889. doi:10.1016/s0146-6380(86)80025-0.
- Simonsen R., 1979: The diatom system: ideas on phylogeny. *Bacillaria*, 2, pp.9-71.
- Sinclair HD, Juranov SG, Georgiev G, Byrne P, Mountney NP., 1997. The Balkan thrust wedge and foreland basin of Eastern Bulgaria: structural and stratigraphic development. In: Robinson AG (editor), *Regional and Petroleum Geology of the Black Sea and Surrounding Region*. American Association of Petroleum Geologists Memoir 68:91-114.
- Sinninghe Damsté, J. S., Schouten, S., Rijpstra, W. I. C., Hopmans, E. C., Peletier, H., Gieskes, W. W. C., & Geenevasen, J. A. J., 1999. Structural identification of the C25 highly branched isoprenoid pentaene in the marine diatom *Rhizosolenia setigera*. *Organic Geochemistry*, 30(12), 1581–1583. doi:10.1016/s0146-6380(99)00140-0
- Ślączka A., Kruglov S., Golonka J., Oszczytko N. and Popadyuk I., 2006: Geology and hydrocarbon resources of the Outer Carpathians, Poland, Slovakia, and Ukraine: general geology. *The Carpathians and their foreland: Geology and hydrocarbon resources: AAPG Memoir*, 84, 221-258. <https://doi.org/10.1306/985610M843070>.
- Smith S.A. and Hiscott R.N. 1987: Latest precambrian to Early Cambrian basin evolution, Fortune Bay, Newfoundland fault–bounded basin to platform. *Canadian Journal of Earth Sciences* 21, 1379-1392.
- Smith W. O. and Demaster D.J. 1996: Phytoplankton biomass and productivity in the Amazon River plume: correlation with seasonal river discharge. *Continental Shelf Research*, 16,3, 291-319. [https://doi.org/10.1016/0278-4343\(95\)00007-n](https://doi.org/10.1016/0278-4343(95)00007-n).
- Smol, J.P. and Stoermer, E.F. eds., 2010. *The diatoms: applications for the environmental and earth sciences*. Cambridge University Press, pp. 469.

- Ștefănescu M., 1978. Stratigraphy and structure of Cretaceous and Paleogene Flysch deposits between Prahova and Ialomița Valleys. Faculty of Geology. University of Bucharest, Bucharest.
- Ștefănescu M., Dicea O. and Tari G. 2000: Influence of extension and compression on salt diapirism in its type area, East Carpathian Bend area, Romania. In: Vendeville B.C., Mart Y. and Vigneresse J.L. (eds): Salt, shale and igneous diapirs in and around Europe. Geological Society, London, 131-147. <https://doi.org/10.1144/GSL.SP.1999.174.01.08>.
- Ștefănescu M., Radan S., Micu M., Mărunțeanu M, Ștefănescu M. 1978; Slanic Prahova Harta Geologică 129b, scara 1:50000.
- Steiger RH, Jäger E., 1977. Subcommittee on geochronology: Convention on the use of decay constants in geo- and cosmochronology. Earth and Planetary Science Letters 36 (3): 359-362. doi: 10.1016/0012-821x(77)90060-7.
- Suto I., 2004. Fossil marine diatom resting spore morpho-genus Xanthiopyxis Ehrenberg in the North Pacific and Norwegian Sea. Paleontological Research. 8(4):283-310. doi:10.2517/prpsj.8.283.
- Suttil, H.L., 2009. Sedimentological Evolution of the Emine and Kamchia Basins, Eastern Bulgaria. MPhil thesis, University of Edinburgh, 239 pp.
- Țabără D., 2010. Palynology, palynofacies and thermal maturation of the kerogen from the Moldavidian Domain Gura Humorului area. Analele Științifice de Universității AI Cuza din Iași, secțiunea. 2, Geologie, 562, 53.
- Tada, R. and Iijima, A., 1983. Petrology and diagenetic changes of Neogene siliceous rocks in northern Japan. Journal of Sedimentary Petrology, 53, 911–30.
- Tămaș A., Tămaș D.M., Krezsek C., Schleder Z., Palladino G. and Bercea R., 2020: The nature and significance of sand intrusions in a hydrocarbon-rich fold and thrust belt: Eastern Carpathians Bend Zone, Romania. Journal of the Geological Society. <https://doi.org/10.1144/jgs2019-107>
- Tămaș D.M. 2018: Salt tectonics in the Eastern Carpathian Bend Zone, Romania. PhD Thesis, Babes-Bolyai University, Cluj-Napoca, Romania, pp. 146.
- Tarek A (2000). Reservoir engineering handbook. Gulf Professional Publishing, pp.1526.
- Tari GC, Simmons MD., 2018. History of deepwater exploration in the Black Sea and an overview of deepwater petroleum play types. In: Simmons M, (editor) Petroleum

- Geology of the Black Sea. Geological Society Special Publication 464: 439-475. doi:10.1144/sp464.16.
- Tari, G., Horváth, F., 2006. Alpine evolution and hydrocarbon geology of the Pannonian Basin: an overview. In: Golonka J., Pícha F. (eds.), The Carpathians and their Foreland: Geology and Hydrocarbon Resources. AAPG Memoir 84, 605-618. <https://doi.org/10.1306/985733m843141>
- Taylor GH, Teichmüller M, Davis A, Diessel CFK, Littke R, et al., 1998. Organic petrology. Gebrüder Borntraeger, Berlin, pp. 704.
- Tissot, B. P., and D. H. Welte, 1984, Petroleum formation and occurrence: New York, Springer-Verlag, 699 p.
- Topper RPM, Flecker R, Meijer PT, Wortel MJR., 2011. A box model of the Late Miocene Mediterranean Sea: Implications from combined  $^{87}\text{Sr}/^{86}\text{Sr}$  and salinity data. *Paleoceanography* 26 (3) PA. doi: 10.1029/2010pa002063.
- Triplehorn D.M. 1965: Origin and significance of glauconite in the geologic sequence. *Tulsa Geological Society Digest*, 33, 282-283.
- Tulan E, Sachsenhofer RF, Tari G, Flecker R, Fairbank V, et al. (2020). Source rock potential and depositional environment of Lower Oligocene rocks in the Karaburun area, Turkey. *Turkish Journal of Earth Sciences*, 29(1), pp.64-84.
- Tulan E., Sachsenhofer R.F., Horvat A., Tari G., Olaru-Florea R.F. (2019). Hydrocarbon source rock potential of Oligo-Miocene diatomaceous rocks in Sibiciu de Sus, Romania (poster), in Book of abstracts: Paratethys petroleum systems between the Central Europe and the Caspian Region AAPG ERC conference, Vienna, 120.
- Valchev B, Sachkov D, Juranov S., 2018. 3D lithostratigraphic model of the Paleogene of the onshore part of the Moesian Platform (Northeast Bulgaria). *Geologica Balcanica* 47(1): 23-36.
- Varga, G., Csillag-Teplánszky, E., Félégyházi, Z., 1975. Geology of the Mátra Mountains (in Hungarian). Annual Report of the Hungarian Geological Institute 57/1, pp. 575.
- Vasiliu V.E., Frunzescu D. and Cehlarov A. 1996: Studiul mineralogic, petrografic și geochemic al diatomitelor de la Sibiciu Pătărlagele, *Revista Română de Petrol*, 3-1, 62-66, Câmpina.

- Volkman JK, Barnett SM, Dunstan GA, Jeffrey SW (1994). C25 and C30 highly branched isoprenoid alkenes in laboratory cultures of two marine diatoms. *Organic Geochemistry*, 21(3-4):407-13. doi:10.1016/0146-6380(94)90202-x.
- Volkman, J.K., 1986. A review of sterol markers for marine and terrigenous organic matter. *Organic geochemistry*, 9(2), pp.83-99.
- Voronina AA and Popov SV (1984). Solenovian horizon from Eastern Paratethys. *Bulletin of the Academy of Sciences of the USSR. Ser Geology* 9: 41-53 (In Russian).
- Wade BS and Bown PR., 2006. Calcareous nannofossils in extreme environments: The Messinian Salinity Crisis. Polemi Basin, Cyprus. *Palaeogeography, Palaeoclimatology, Palaeoecology*, 233, 271-286. doi:10.1016/j.palaeo.2005.10.007.
- Watson JS, Jolley DW, Kelley SP., 2009. High concentration of 28,30-bisnorhopane and 25,28,30-trisnorhopane at the PETM in the Faroe-Shetland basin. In: 24th International Meeting on Organic Geochemistry, 6-11 Sep 2009, Bremen, Germany.
- Weckström, K., Saunders, K.M., Gell, P.A., Skilbeck, C.G. (eds.), 2017. Applications of Paleoenvironmental Techniques in Estuarine Studies. *Developments in Paleoenvironmental Research*. <https://doi.org/10.1007/978-94-024-0990-1>
- Wehner, H., Kuckelkorn, K., 1995. Zur Herkunft der Erdöle im nördlichen Alpen-Karpatenvorland. *Erdöl, Erdgas, Kohle*, 111, 508–514.
- Wendorff M., Rospondek M.J., Kluska B. and Marynowski L., 2017. Organic matter maturity and hydrocarbon potential of the Lower Oligocene Menilite facies in the Eastern Flysch Carpathians Tarcău and Vrancea Nappes, Romania. *Applied Geochemistry*, 78, 295-310. <https://doi.org/10.1016/j.apgeochem.2017.01.009>
- Williams, D.M., Round, F.E., 1987. Revision of the genus *Fragilaria*. *Diatom research*, 2/2, 267-288.
- Wilson, M. J., 2014. The structure of opal-CT revisited. *Journal of Non-Crystalline Solids*, 405, 68-75.
- Winter A, Jordan R, Roth P., 1994. Biogeography of living Coccolithophores in ocean waters. In: Winter A and Siesser W (eds.): *Coccolithophores*. Cambridge University Press, Cambridge, 13-37.



- Witkowski J, Bohaty SM, Edgar KM, Harwood DM., 2014 Rapid fluctuations in mid-latitude siliceous plankton production during the Middle Eocene Climatic Optimum (ODP Site 1051, western North Atlantic), *Marine Micropaleontology*, 106, 110–129. doi:10.1016/j.marmicro.2014.01.001.
- Witkowski, A., Lange-Bertalot, H., Metzeltin, D., 2000. Diatom flora of marine coasts I. *Iconographia Diatomologica* 7. ARG Gantner Verlag KG, Ruggell, 7, pp. 950.
- Yon DA, Maxwell JR, Rybach, G., 1982. 2,6,10-Trimethyl-7-(3-methylbutyl)-dodecane, a novel sedimentary biological marker compound. *Chemischer Informationsdienst*, 13(43). doi:10.1002/chin.198243163.
- Yücel AO, Özcan E, Erbil Ü., 2020. Latest Priabonian larger benthic foraminiferal assemblages at the demise of the Soğucak Carbonate Platform (Thrace Basin and Black Sea shelf, NW Turkey): implications for shallow marine biostratigraphy. *Turkish Journal of Earth Sciences*, 29(1), pp.85-114.
- Yurtsever A, Çağlayan A., 2002. Geological maps of Turkey, 1:100.000 scale, Istanbul F21 and G21 sheet and explanatory text. Ankara: Maden Tetkik ve Arama Genel Müdürlüğü, Ankara, pp. 30.
- Zolitschka B., 1998. Paläoklimatische Bedeutung laminiertes Sedimente. Holzmaar (Eifel, Deutschland), Lake C2 (Nordwest-Territorien, Kanada) und Lago Grande di Monticchio (Basilicata, Italien). *Bornträger*, Berlin, 176 S.
- Zurzolo C., Bowler C., 2001. Exploring bioinorganic pattern formation in diatoms. A story of polarized trafficking. *Plant physiology*, 127 (4), pp.1339-1345.

## **Plates**

## Plate I – Diatoms from Ruslar Formation

Figure 1-5: *Distephanosira* sp.; Figure 5 view in LM of Figure 4 and Figure 1

Figure 6: *Paralia* sp.

Figure 7: resting spore

8-13: *Stephanopyxis* spp.

Figure 14: *Azpeitia* sp.

Figure 15: *Actinocyclus?* Sp.

Figure 16: *Azpeitia* sp.

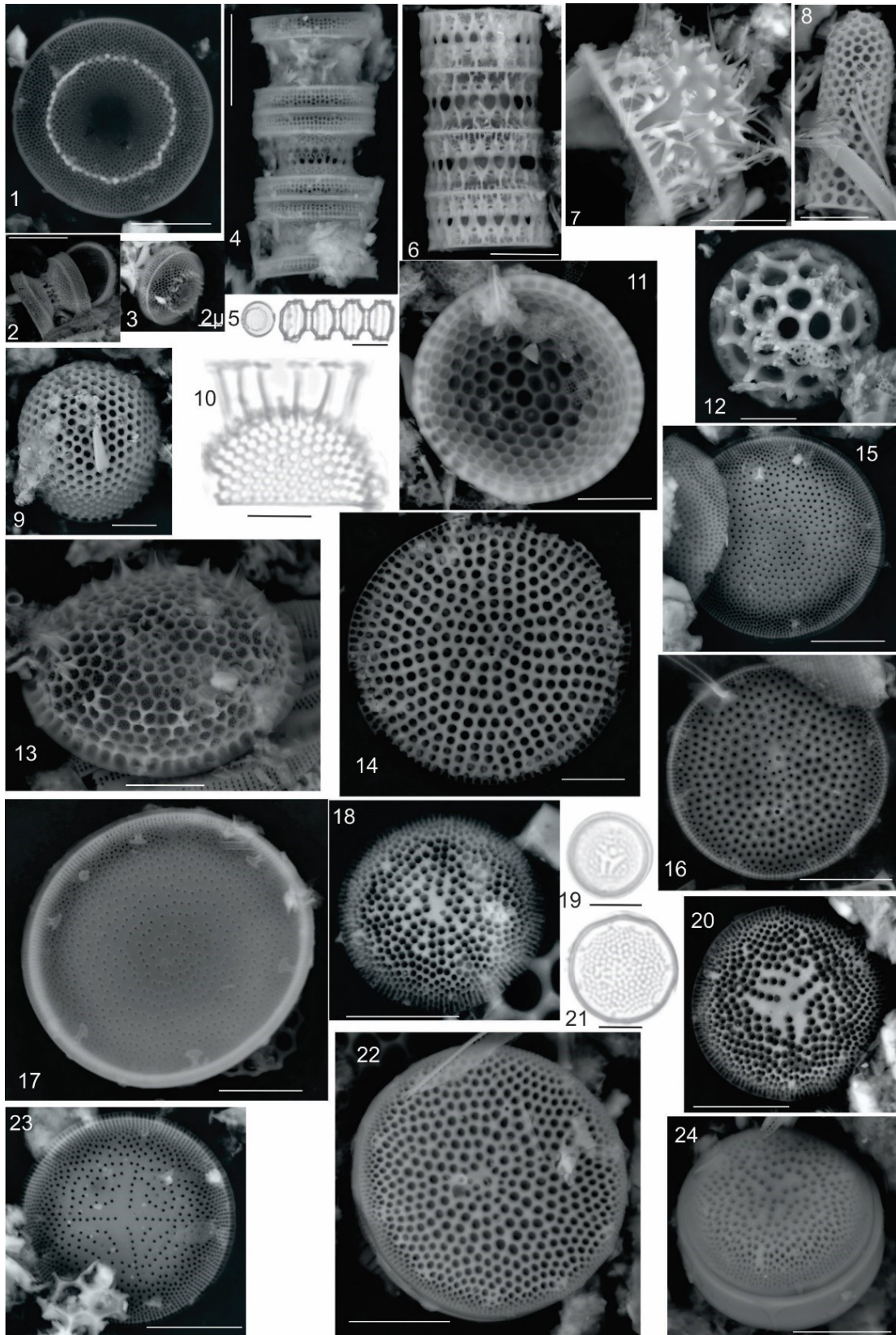
Figure 17 – 20: *Coscinodiscus* spp.; Figure 19 LM view of Figure 18;

Figure 21 22: *Azpeitia* sp.; Figure 21 LM view of Figure 22

Figure 24: *Coscinodiscus?* Sp.

\*Scale bar is 10  $\mu\text{m}$  unless specified otherwise. LM-light microscope.

Plate I – Diatoms from Ruslar Formation



## Plate II – Diatoms from Ruslar Formation

Figure 1-5: *Hemiaulus* spp.

Figure 6-11: *Asterolampra* spp.

Figure 12-13: *Pseudopodosira* sp. Figure 12 LM view of Figure 13

Figure 14-15: *Actinoptychus 154renaria154* (Bailey) Ralfs, in Pritchard (1861)

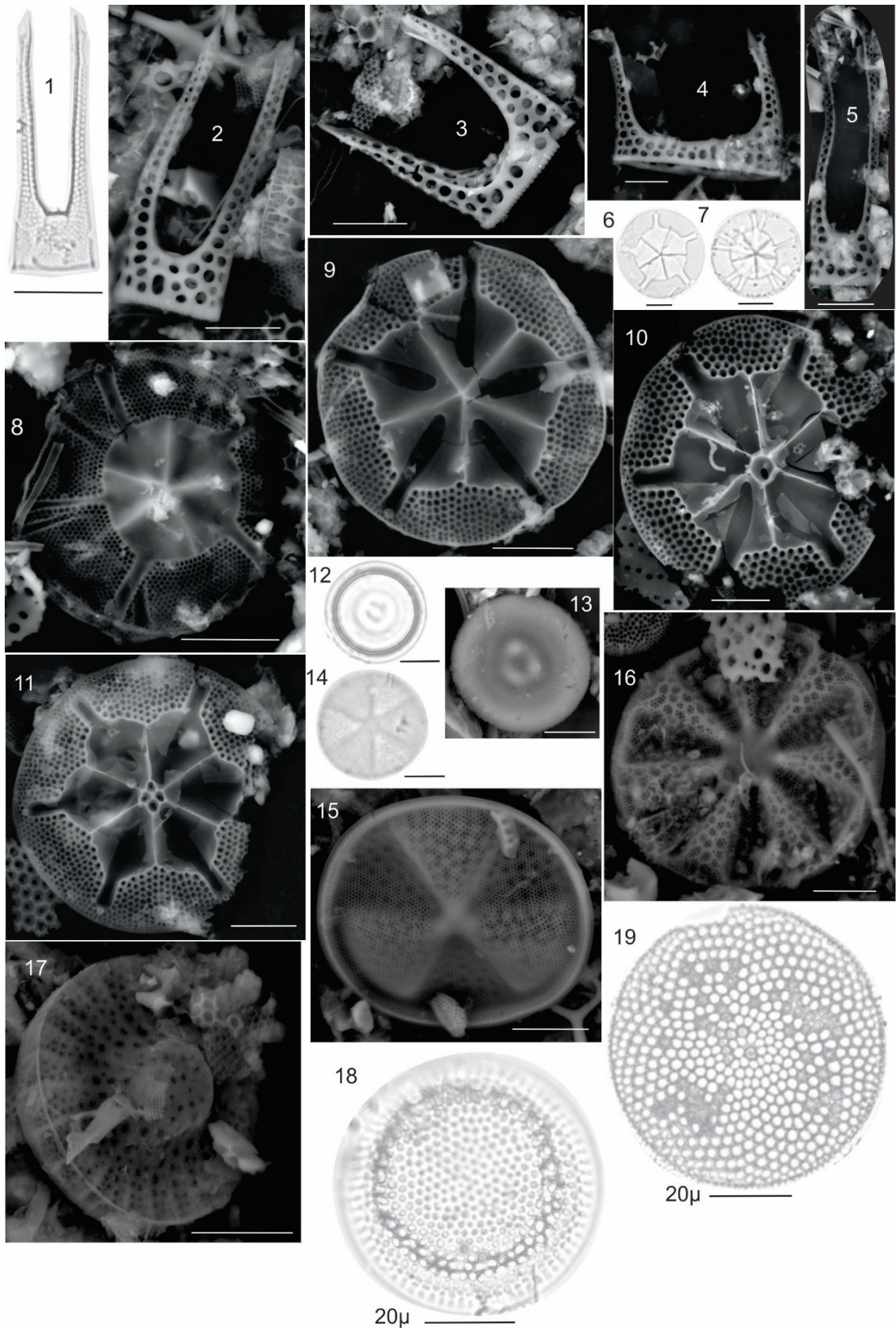
Figure 16: *Actinoptychus* sp. cf. *A. maculatus* Grove and Sturt 1887

Figure 17: *Pseudostictodiscus?* Sp.

Figure 18-19: *Coscinodiscus?*

\*Scale bar is 10  $\mu\text{m}$  unless specified otherwise. LM-light microscope.

Plate II – Diatoms from Ruslar Formation



### Plate III – Diatoms from Ruslar Formation

Figure 1- 2: *Triceratium* sp. cf. *T. dictyotum*? Sims and Ross (1990)

Figure 3: *Eurossia irregularis* (Greville) P.A.Sims (1993)

Figure 4: *Pseudotriceratium* Grunow (1884)

Figure 6-8: *Lyrella* sp.

Figure 9: *Rouxia* sp. (*Rouxia naviculoides*? Schrader)

Figure 10: *Diploneis ornata*? Schmidt in Schmidt et al. (1881)

Figure 11: *Lyrella*? Sp.

Figure 12: *Liradiscus*? Sp.

Figure 13-14: *Xanthiopyxis* sp. cf. *X. oblonga*

Figure 15-16: LM of *Xanthiopyxis* sp.

Figure 17: internal view of an unrecognizable pennate diatom

Figure 18: unidentified resting spore of *Chaetoceros* sp.

Figure 19: *Radialiplicata* sp.

Figure 20: *Saeptifera* sp.

Figure 21: *Delphineis 156renaria156*? (Ehrenberg) G.W. Andrews (1981)

Figure 22: *Plagiogramma* sp.

Figure 23: *Radialiplicata* sp.

Figure 24: internal view of an unrecognizable diatom

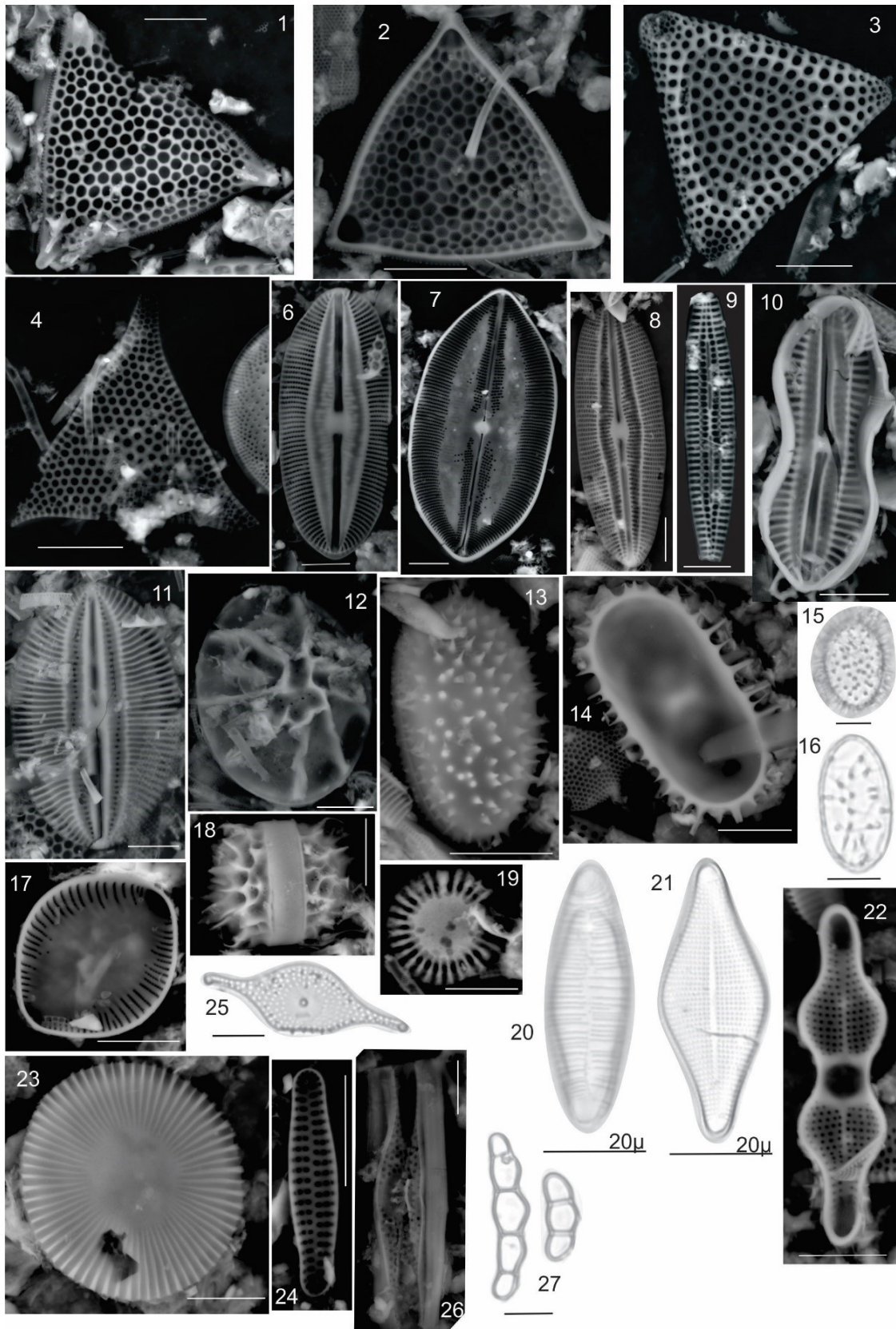
Figure 25: *Rutilaria 156renaria* Sheshukova-Poretskaya in Sheshukova-Poretskaya and Gleser 1964

Figure 26: *Rutilaria* sp. cf. *R. 156renaria156* Ross 1990

Figure 27: *Eunotogramma* sp.

\*Scale bar is 10  $\mu$ m unless specified otherwise. LM-light microscope.

Plate III – Diatoms from Ruslar Formation





**Plate IV – Silicoflagellates and other siliceous microfossils from Ruslar Formation**

Figure 1: *Bachmannocena* sp. (Locker, 1974) Burky (1987)

Figure 2-3: *Distephanopsis crux* (Ehrenberg) P. Dumitrica

Figure 4: *Corbisema regina?* D. Burky

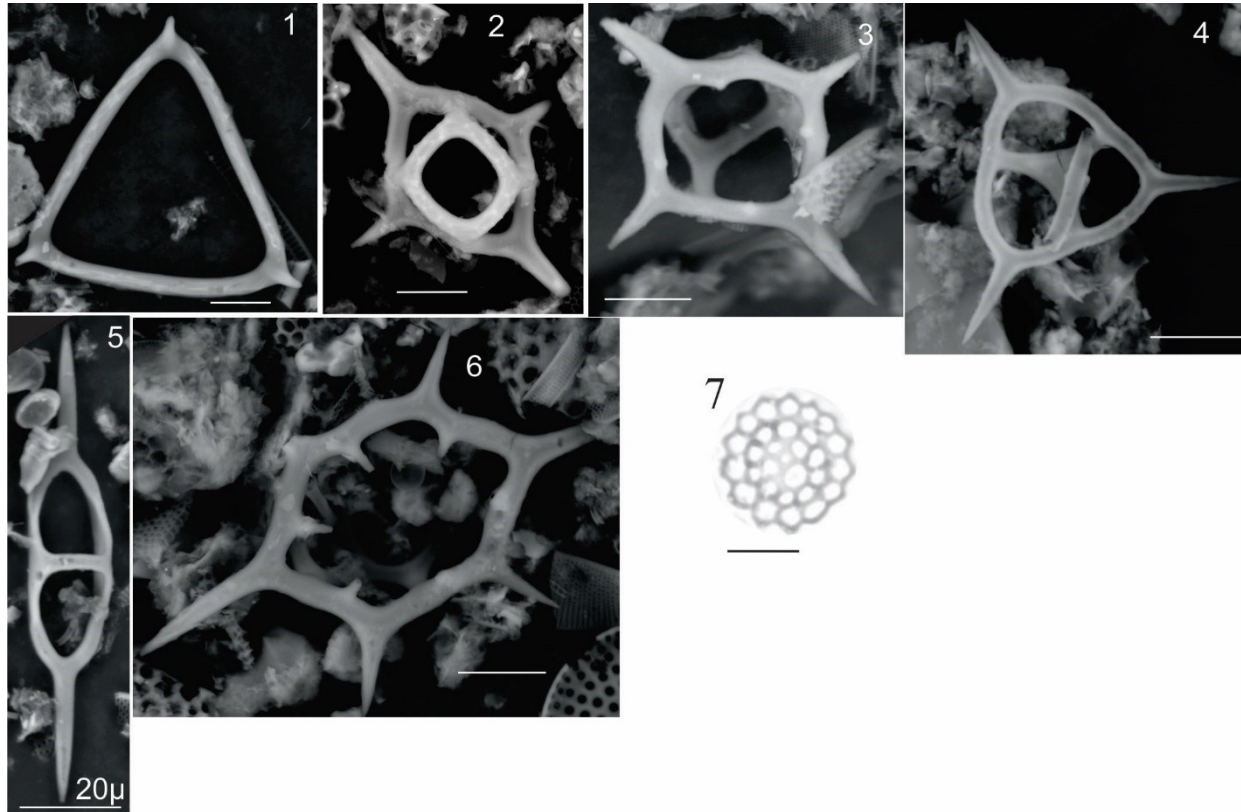
Figure 5: *Naviculopsis biapiculata* (Lemmermann) Frenguelli

Figure 6: *Stephanocha speculum* (Ehrenberg 1837) Jordan and McCartney 2015

Figure 7: *Macrora* sp. in LM

\*Scale bar is 10  $\mu\text{m}$  unless specified otherwise. LM-light microscope.

**Plate IV – Silicoflagellates and other siliceous microfossils from Ruslar Formation**



## Plate V- Calcareous nanofossils from Ruslar Formation

Figure 1-2: *Coccolithus pelagicus* (Wallich 1877) Schiller, 1930

Figure 3-4: *Reticulofenestra dictyoda* (Deflandre in Deflandre and Fert, 1954) Stradner in Stradner and Edwards, 1968

Figure 5: *Dictyococcites hesslandii* Haq 1971

Figure 6: *Reticulofenestra 160renar* Müller, 1970

Figure 7-8: *Pontosphaera versa* (Bramlette and Sullivan, 1961) Sherwood, 1974

Figure 9: *Reticulofenestra minuta* Roth, 1970

Figure 10: *Pontosphaera multipora* (Kamptner, 1948 ex Deflandre in Deflandre and Fert, 1954) Roth, 1970

Figure 11-13: *Helicosphaera recta* (Haq, 1966) Jafar and Martini, 1975

Figure 14: *Sphenolithus* sp.

Figure 15: *Umbilicosphaera* cf. *160renar* Muller, 1974

Figure 16-17: *Helicosphaera perch-nielseniae* (Haq 1971) Jafar and Martini (1975)

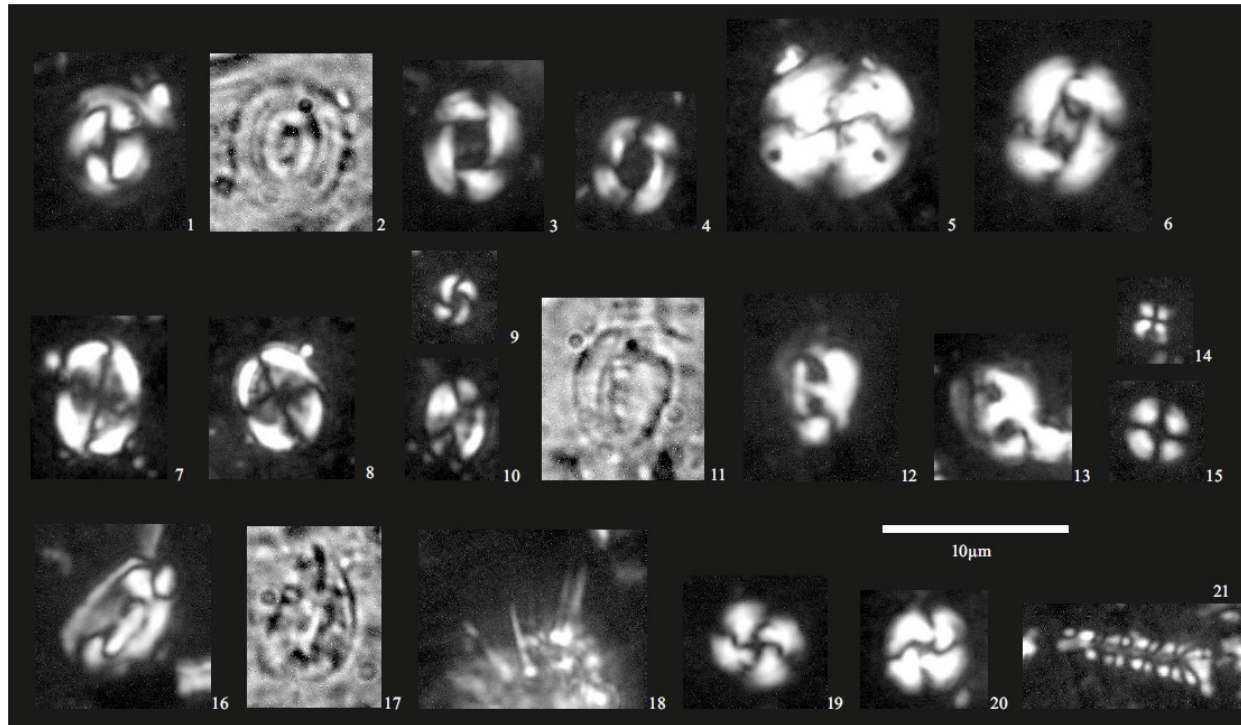
Figure 18: *Rhabdosphaera* sp.

Figure 19-20: *Cyclicargolithus floridanus* (Roth and Hay, in Hay et al., 1967) Bukry, 1971

Figure 21: *Tetrapodorhabdus decorus* (Deflandre in Deflandre and Fert, 1954) Wind and Wise 1983

\*Scale bar is 10  $\mu\text{m}$  unless specified otherwise. LM-light microscope.

Plate V- Calcareous nanofossils from Ruslar Formation



**Plate VI – Diatoms from Szurdokpüspöki quarry**

Figure: 1-3 tentative identification *Melosira bituminosa* Pantocsek

Figure: 4-6 tentative identification: *M. nuda?* Hajós

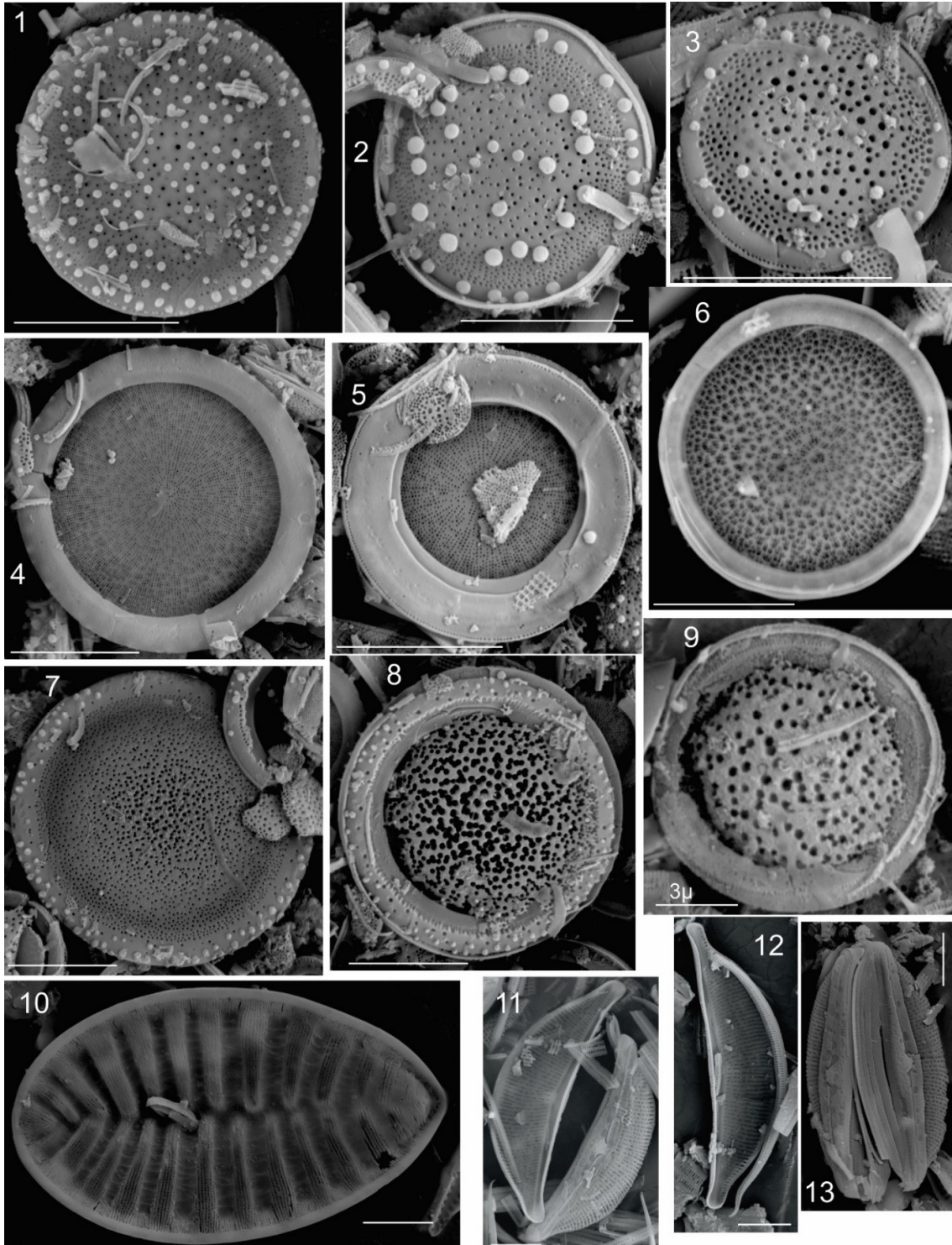
Figure: 7-9 tentative identification: *Melosira bituminosa* Pantocsek

Figure:10 *Surirella striatula* Turpin

Figure:11-13 *Halamphora* sp. (Kützing) Levkov

\*Scale bar is 10 µm unless specified otherwise.

Plate VI – Diatoms from Szurdokpüspöki quarry



**Plate VII – Diatoms from Szurdokpüspöki quarry**

Figure: 1-2 *Surirella* sp. Turpin

Figure: 3 *Cocconeis californica?* Grun

Figure: 4-6 *Epithemia turgida?* (Ehrenberg) Kützing

Figure: 7-9 *Pseudostaurosira* sp. Williams and Round

Figure: 10-11 *Nitzschia frustulum* (Kützing) Grunow

Figure: 12 *Brachysira* Kützing

Figure: 13 *Cymbella* sp. Agardh

Figure: 14 *Seminavis* sp. Mann

Figure: 15 *Planothidium* sp. Round and Bukhtiyarova

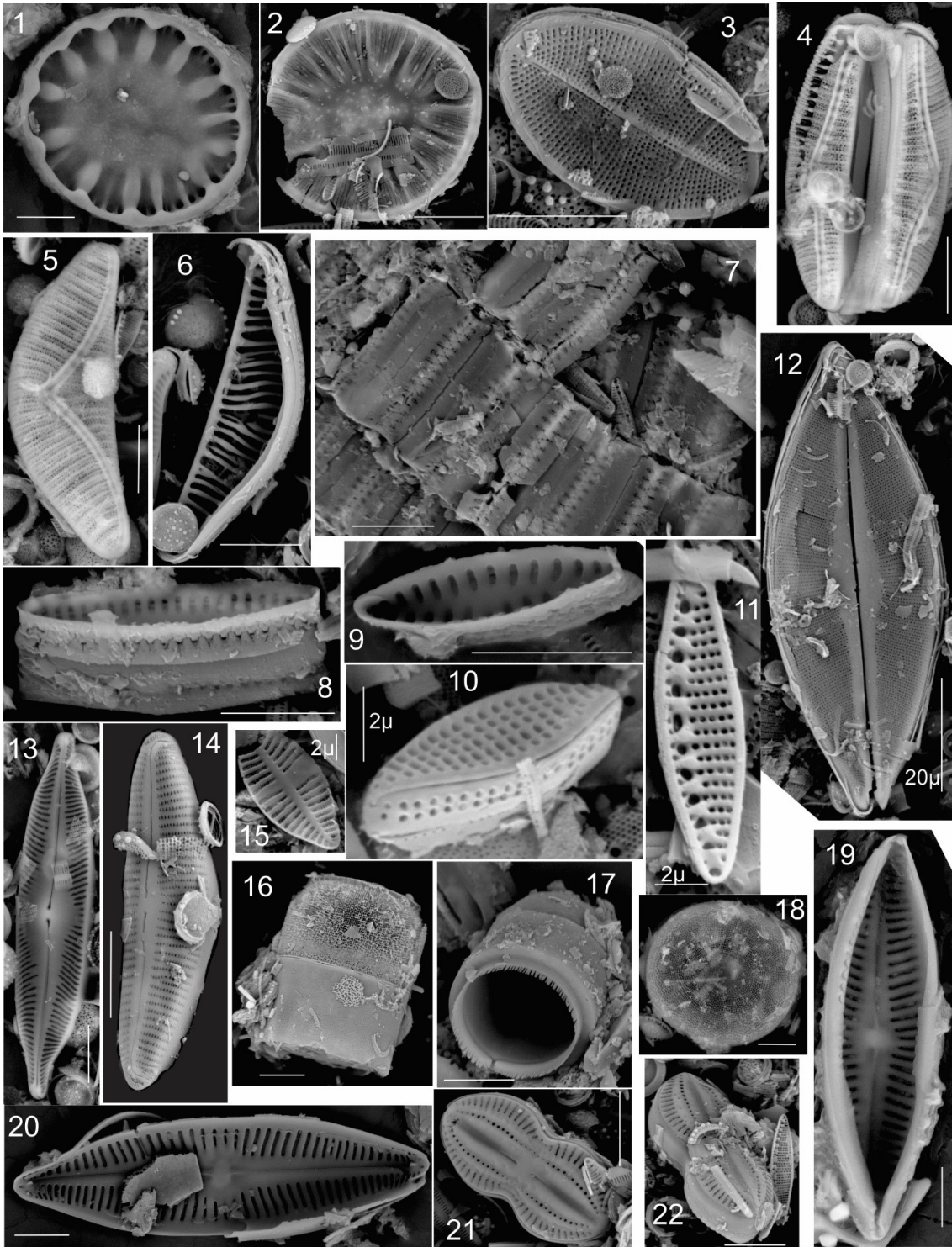
Figure: 16-18 *Podosira robusta* Pantocsek

Figure: 19 *Seminavis* sp. Mann; 20-*Navicula* sp.

Figure: 21-22 *Diploneis* sp. Ehrenberg ex Cleve.

\*Scale bar is 10  $\mu$ m unless specified otherwise.

Plate VII – Diatoms from Szurdokpüspöki quarry





**Plate VIII – Diatoms from Sibiciu de Sus quarry**

Figure: a, b-*Aulacoseira temperei*? Ognjanova-Rumenova and Crawford (2012)

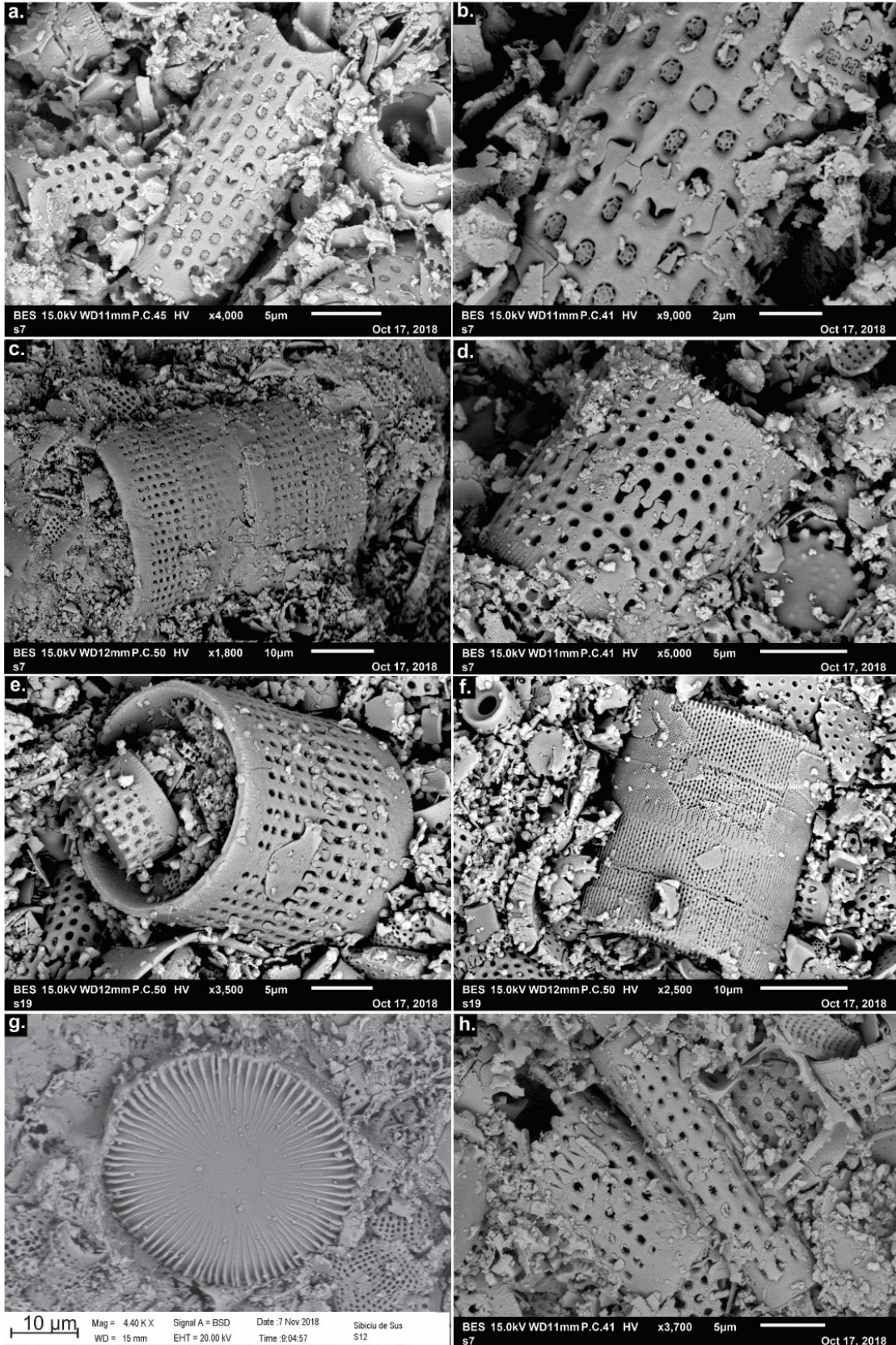
Figure: c, d, e *Aulacoseira* sp.

Figure: f, g *Ellerbeckia 166renaria*? (Moore ex Ralfs) Crawford (1988)

Figure: h *Aulacoseira* sp.

\*Scale bar is 10  $\mu\text{m}$  unless specified otherwise.

Plate VIII – Diatoms from Sibiciu de Sus quarry



**Plate IX – Diatoms from Sibiciu de Sus quarry**

Figure: a – h a variety of *Actinocyclus* spp.

\*Scale bar is 10  $\mu\text{m}$  unless specified otherwise.

Plate IX – Diatoms from Sibiciu de Sus quarry

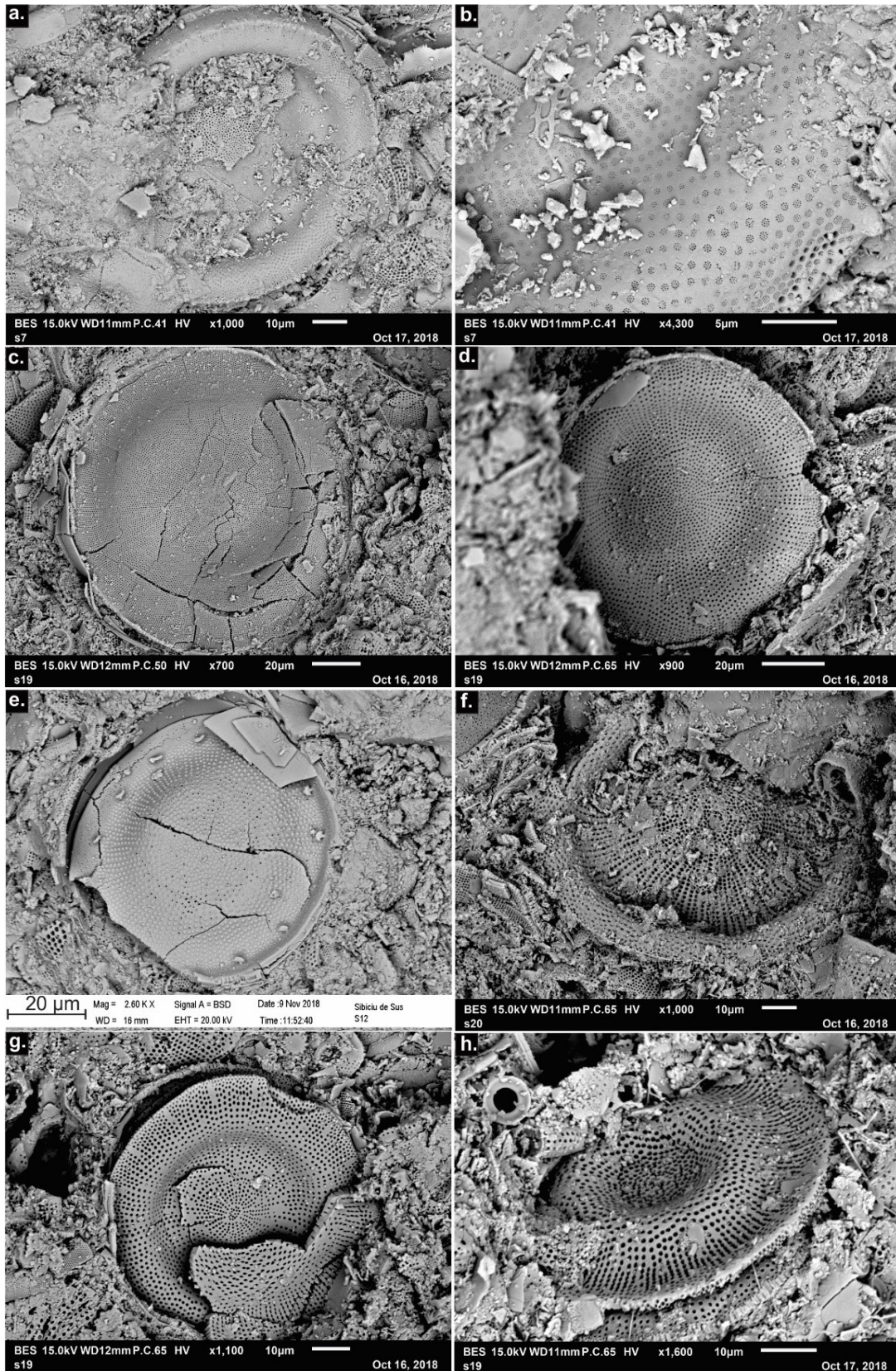


**Plate X – Diatoms from Sibiciu de Sus quarry**

Figure: a, b *Actinocyclus* sp.

Figure: c unidentified diatom

Figure: d, e chrysophyte cysts

Figure: f, g, h unidentified diatom

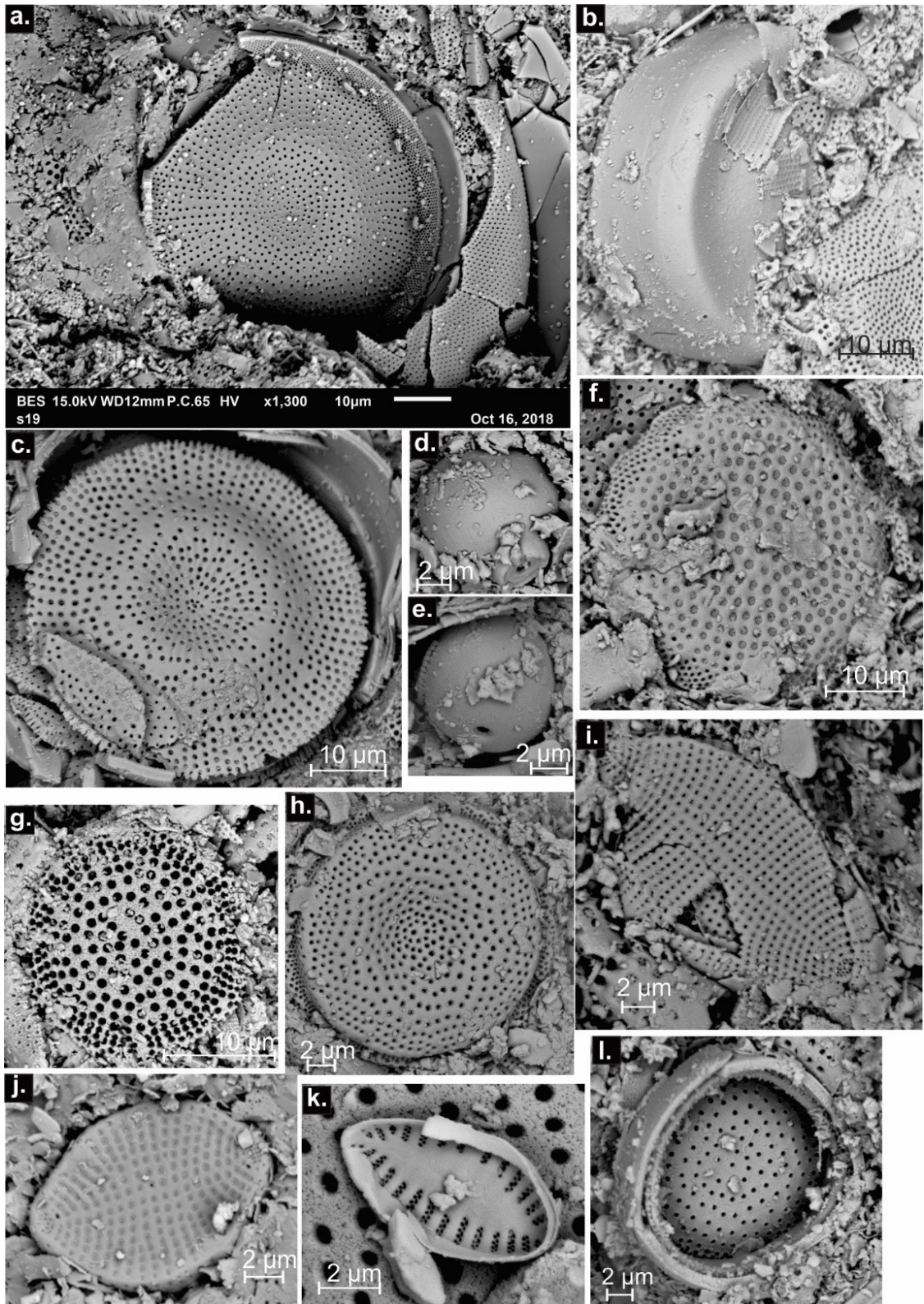
Figure: I, j *Rhaphoneis* cf. *Rh. Amphiceros*

Figure: k *Opephora* sp.

Figure: l unidentified diatom.

\*Scale bar is 10  $\mu\text{m}$  unless specified otherwise.

Plate X - Diatoms from Sibiciu de Sus quarry



## **Appendix**

*Appendix 1*

Table 1: Bulk parameters of the İhsaniye Formation

NP	Sample no.	Height	S1	S2	Tmax	TOC	S	PI	HI	TOC/S	Calc.equ.
		[m]	[mg HC/g rock]	[mg HC/g rock]	[°C]	[%]	[%]	[-]	[mgHC/gTOC]	[-]	[%]
<b>Hanging Wall Section</b>											
NP23	70	67.5	0.01	0.17	416	0.27	0.19	0.06	62	1.40	53.0
	69	67.0	0.01	0.14	416	0.24	0.21	0.07	58	1.17	48.8
	68	66.2	0.03	0.26	414	0.36	0.22	0.09	72	1.63	34.7
	67	65.8	0.01	0.16	417	0.26	0.20	0.06	60	1.27	41.2
	66	65.1	0.01	0.18	419	0.24	0.20	0.05	76	1.18	58.7
	65	64.3	0.01	0.19	416	0.25	0.26	0.05	73	0.95	49.2
	64	63.1	0.01	0.17	416	0.22	0.30	0.06	77	0.71	57.5
	63	62.9	0.01	0.16	416	0.23	0.20	0.06	69	1.17	57.1
	62	61.6	0.01	0.12	415	0.19	0.26	0.08	63	0.73	59.0
	61	60.9	0.01	0.16	408	0.24	1.47	0.06	66	0.17	40.7
	60	59.9	0.02	0.19	407	0.27	0.58	0.08	70	0.46	35.2
	59	59.0	0.02	0.27	406	0.27	0.51	0.07	98	0.54	33.1
	39	58.0	0.02	0.03	452	0.01	0.00	0.38			0.9
	40	57.1	0.01	0.02	408	0.00	0.01	0.33		0.79	0.6
	41	56.8	0.01	0.03	424	0.13	0.17	0.25	23	0.78	0.0
	42	55.9	0.02	0.26	419	0.35	0.43	0.05	74	0.82	42.5
	43	55.0	0.01	0.15	415	0.34	0.23	0.06	44	1.47	51.5
	44	54.5	0.02	0.31	416	0.20	0.51	0.05	152	0.39	40.1
	45	53.5	0.01	0.17	413	0.26	0.33	0.06	65	0.77	40.5
46	52.5	0.03	0.95	421	0.71	0.79	0.03	134	0.90	54.0	
47	51.7	0.02	0.27	419	0.34	0.34	0.05	79	1.00	38.4	
48	50.4	0.01	0.16	420	0.20	0.16	0.06	76	1.27	61.6	
49	49.5	0.01	0.15	419	0.24	0.21	0.06	62	1.16	53.1	



	50	48.6	0.01	0.21	414	0.26	0.41	0.05	81	0.64	42.7
	51	47.8	0.02	0.29	406	0.35	0.32	0.06	82	1.10	29.9
	52	46.9	0.02	0.21	411	0.30	0.25	0.07	69	1.17	30.9
	53	45.8	0.02	0.29	409	0.28	0.26	0.05	102	1.10	43.1
	54	44.8	0.02	0.40	415	0.44	0.31	0.05	91	1.42	34.3
	55	43.7	0.01	0.20	409	0.23	0.23	0.05	88	0.98	44.2
	56	42.2	0.01	0.13	413	0.19	0.07	0.07	67		48.5
	57	40.8	0.01	0.22	417	0.30	1.32	0.04	74	0.22	44.1
	58	40.0	0.02	0.24	411	0.29	0.38	0.06	81	0.77	24.4
NP22	38	38.1	0.01	0.17	417	0.28	0.43	0.06	59	0.65	55.5
	37	36.9	0.04	0.95	417	0.79	1.00	0.04	119	0.79	41.2
	36	36.1	0.03	0.42	402	0.46	1.64	0.07	90	0.28	29.5
	35	35.5	0.01	0.20	410	0.28	0.28	0.05	71	0.99	72.4
	34	34.4	0.03	0.62	417	0.58	1.00	0.05	106	0.58	42.2
	33	33.3	0.02	0.44	408	0.42	0.95	0.04	105	0.44	44.9
	32	32.1	0.02	0.56	419	0.52	0.69	0.03	109	0.75	58.5
	31	31.0	0.03	0.68	423	0.63	0.73	0.04	106	0.88	52.6
	30	30.1	0.03	0.72	420	0.54	0.76	0.03	132	0.72	60.9
	29	29.2	0.03	0.71	420	0.57	0.83	0.03	123	0.69	54.0
	28	28.2	0.02	0.45	421	0.51	0.38	0.03	88	1.33	62.6
	27	27.2	0.02	0.32	420	0.79	0.28	0.04	41		67.6
	26	26.5	0.03	0.91	421	0.68	0.82	0.03	135	0.82	52.8
	25	24.9	0.03	0.85	421	0.57	0.61	0.03	148	0.94	60.6
	24	24.1	0.03	1.17	424	0.72	0.85	0.03	162	0.85	45.6
23	23.0	0.03	0.72	427	0.62	0.52	0.03	117	1.18	59.4	
NP21	22	22.2	0.04	1.29	429	0.88	0.52	0.03	146	1.69	59.3
	21	21.9	0.03	0.99	427	0.80	0.65	0.03	124	1.23	47.8
	20	19.1	0.03	0.31	404	0.36	1.76	0.07	86	0.20	28.1

	19	17.5	0.06	2.34	423	1.10	1.45	0.02	213	0.75	52.4
	18	16.2	0.05	2.35	424	1.21	1.38	0.02	193	0.88	49.3
	17	15.3	0.07	3.36	421	1.43	1.39	0.02	235	1.02	53.0
	16	14.6	0.07	3.31	423	1.46	1.30	0.02	226	1.12	51.5
	15	13.3	0.08	3.09	422	1.42	1.53	0.03	218	0.93	51.6
	14	12.0	0.08	3.35	422	1.50	1.46	0.02	223	1.03	52.6
	13	11.1	0.09	3.98	420	1.64	1.44	0.02	242	1.14	51.7
	12	10.1	0.09	2.96	421	1.39	1.43	0.03	213	0.97	48.5
	11	9.5	0.09	2.98	418	1.29	1.47	0.03	230	0.88	47.3
	10	8.3	0.10	4.48	420	1.78	1.38	0.02	252	1.29	50.5
	9	7.9	0.06	2.13	422	1.65	1.47	0.03	129	1.12	48.9
	8	6.8	0.07	2.94	419	1.43	1.59	0.02	206	0.90	46.8
	7	5.8	0.08	2.50	422	1.36	1.59	0.03	184	0.85	41.3
	6	4.9	0.09	3.48	422	1.65	1.50	0.02	211	1.10	43.2
	5	4.1	0.09	3.10	421	1.66	1.44	0.03	187	1.15	38.6
	4	3.4	0.09	3.62	422	1.49	1.37	0.02	243	1.09	48.1
	3	2.6	0.08	3.67	423	2.04	1.67	0.02	180	1.22	47.0
	2	1.6	0.03	1.36	430	0.97	0.53	0.02	140	1.81	64.7
1	0.5	0.05	1.88	426	1.10	1.10	0.03	170	1.00	59.3	
<b>Footwall Section</b>											
NP 23	78	6.5	0.02	0.14	413	0.25	0.07	0.10	55	3.71	25.7
	77	5.9	0.02	0.15	409	0.21	0.45	0.09	73	0.46	55.6
	76	5.4	0.02	0.22	407	0.27	0.40	0.07	78	0.68	41.9
	75	4.8	0.01	0.06	434	0.22	0.18	0.14	27	1.19	59.2
	74	4.1	0.01	0.06	411	0.21	0.08	0.08	26	2.56	61.7
	73	3.3	0.01	0.11	420	0.31	0.17	0.08	36	1.85	43.2
	72	2.5	0.01	0.19	419	0.18	0.10	0.05	104	1.83	59.5
	71	1.7	0.01	.12	418	0.50	0.17	0.04	23	2.87	66.9

TOC - total organic carbon, S-Sulphur, HI-hydrogen index, PI-production index, calc. equi.-calcite equivalent.

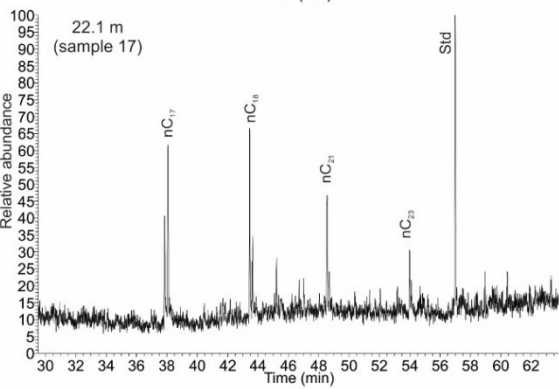
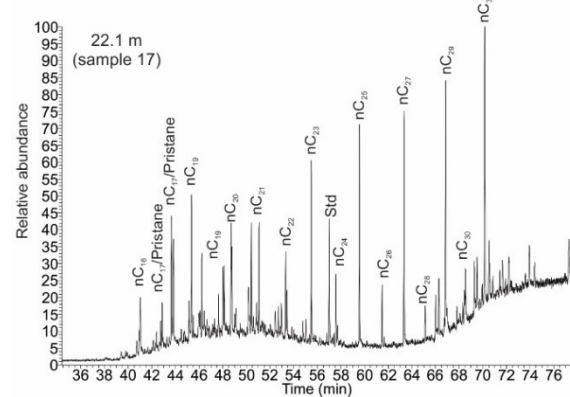
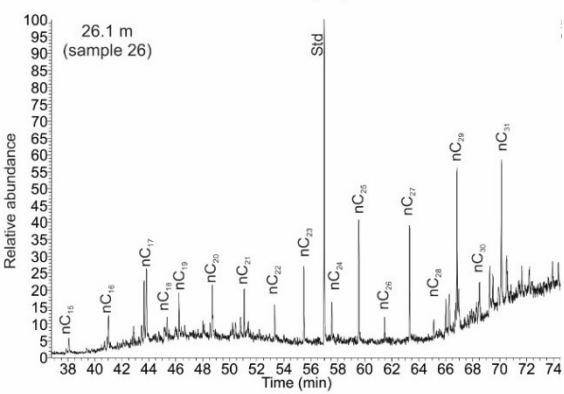
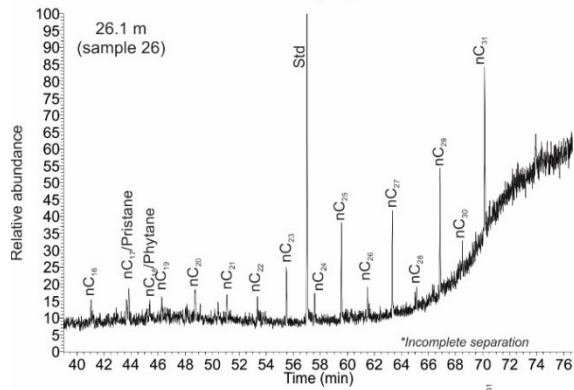
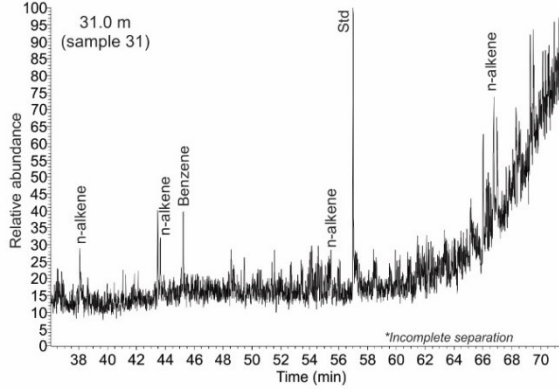
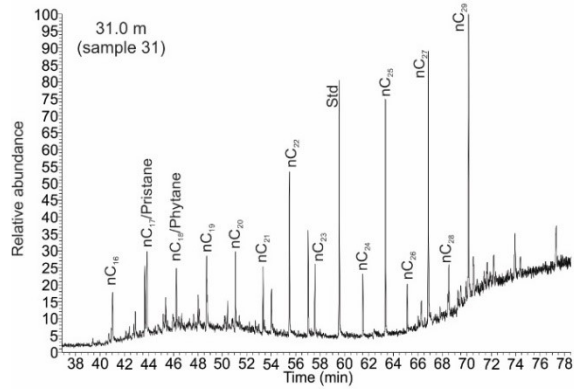
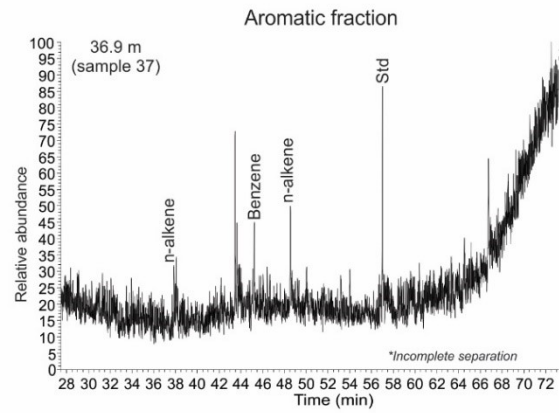
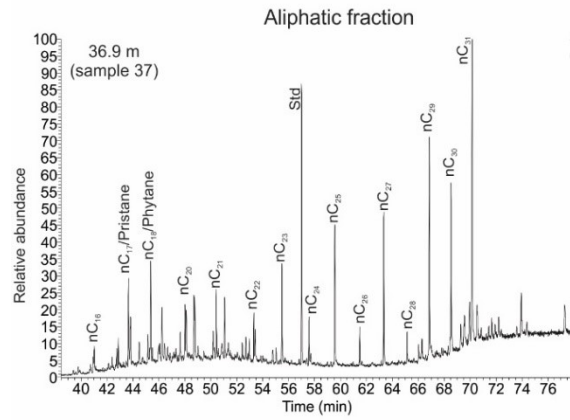
Table 2. Organic geochemical data of the İhsaniye Formation

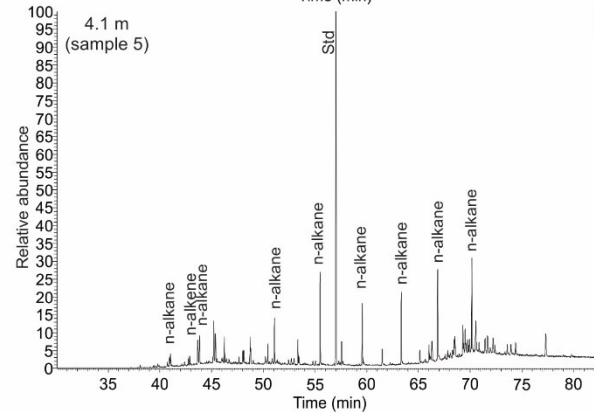
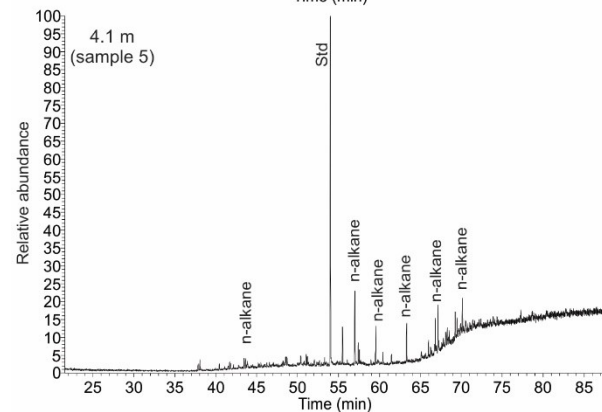
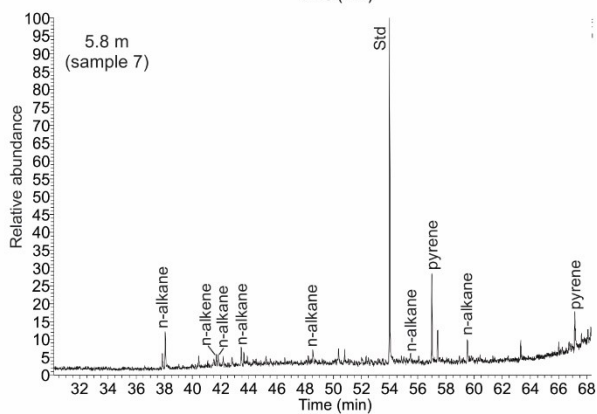
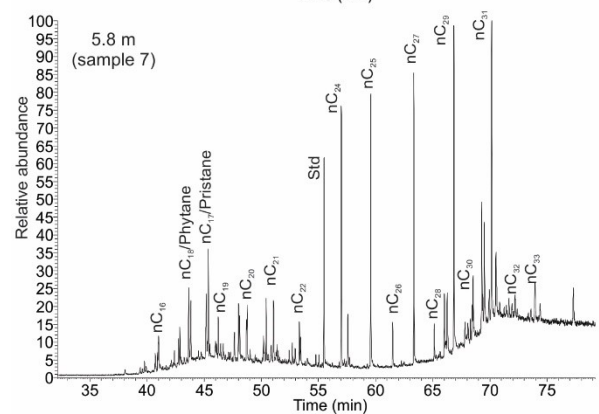
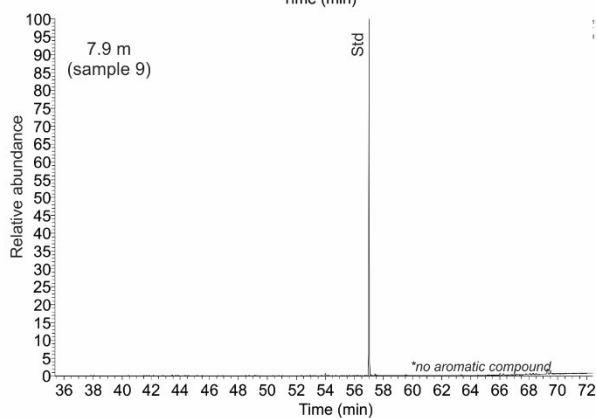
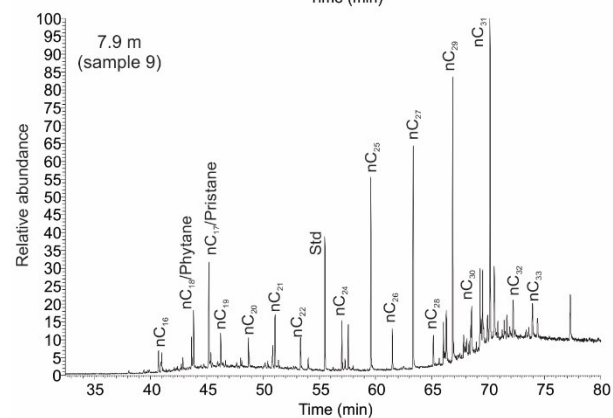
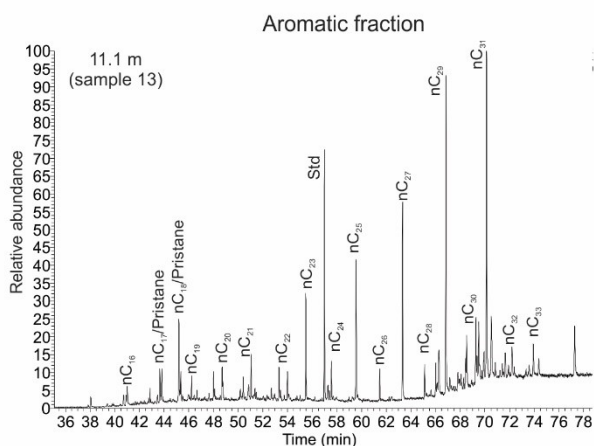
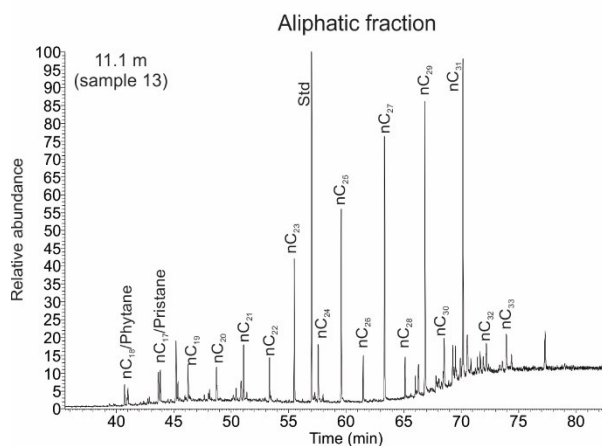
Sample no.	Height	TOC	HI	EOM	HC	NSO	Asph.	n-C <sub>15-20</sub>	n-C <sub>21-25</sub>	n-C <sub>26-32</sub>	Pr/Ph	Ts/Tm	Steroids/	22S/(22S+22R)	Di/(Di+Tri) terpeno.	Di+Tri-terpeno.	MPI index
	[m]	[wt %]	[mg/g TOC]	[mg/g TOC]				[%]					hopanoids C <sub>31</sub> -Hopanes				
37	36.9	0.79	119	1.54	7	73	19	15	29	56	0.33	3.55	0.41	0.16	0.67	1.00	0.19
31	31.0	0.63	106	1.28	2	81	17	14	35	52	0.43	5.14	0.54	0.20	0.77	0.49	0.10
26	26.5	0.68	135	1.32	5	81	14	11	31	59	0.58	1.78	0.33	0	0.93	0.05	[0.49]
22	22.2	0.88	146	1.12	8	83	10	19	36	45	0.40	15.41	0.01	0	0.72	1.10	0.24
17	15.3	1.43	235	1.45	24	62	14	18	32	50	0.69	1.58	0.27	[0.42]	0.88	4.12	0.06
13	11.1	1.64	242	2.82	3	73	14	7	31	63	0.43	9.52	0.27	0.35	0.52	32.12	0.28
9	7.9	1.65	129	2.31	13	74	13	8	30	62	0.23	12.42	0.64	0.24	0.06	0.76	0.24
7	5.8	1.36	184	2.16	5	79	16	11	34	55	0.49	8.07	1.18	0.26	0.75	15.19	0.20
5	4.1	1.66	187	2.33	7	81	11	14	37	49	0.45	5.90	0.62	0.35	0.73	24.93	0.28
3	2.6	2.04	180	2.60	7	81	12	11	42	48	0.58	5.71	0.83	0.29	0.88	26.03	0.22
1	0.5	1.10	170	1.60	13	73	14	33	36	31	0.42	4.51	0.10	0.30	0.85	9.64	0.17

TOC-total organic carbon, HI-hydrogen index, EOM-extracted organic matter, HC-hydrocarbons yields, NSO-polar compounds, Asph.-asphaltene, n-C<sub>15-20</sub>-short-chain alkanes, n-C<sub>21-25</sub>-medium-chain alkanes, n-C<sub>26-32</sub>- long-chain alkanes; Pr/Ph-Pristane/Phytane ratio; Di/(Di+Tri) terpeno.-Diterpenoids/triterpenoids ratio.

# GC-MS traces of the İhsaniye Formation

Karaburun, Turkey - Hanging Wall Section





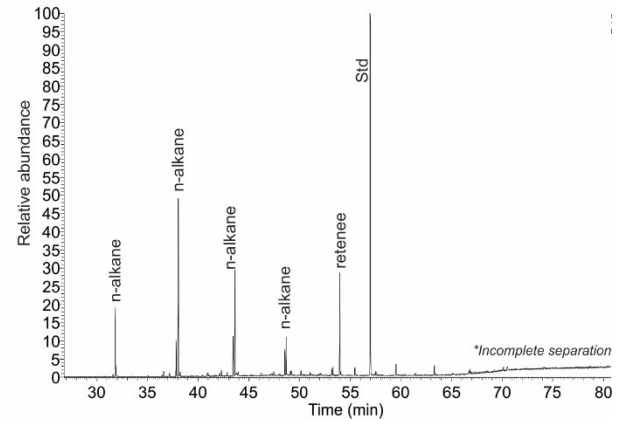
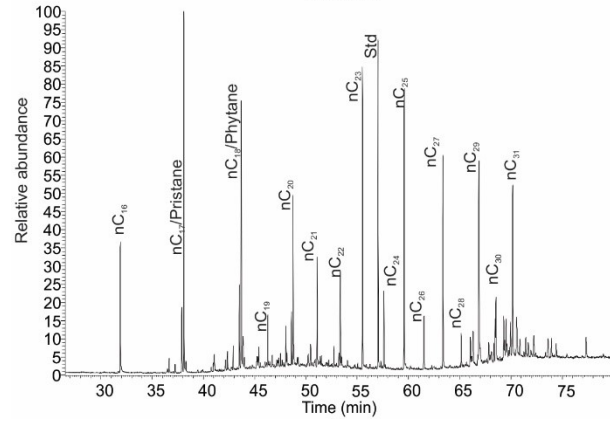
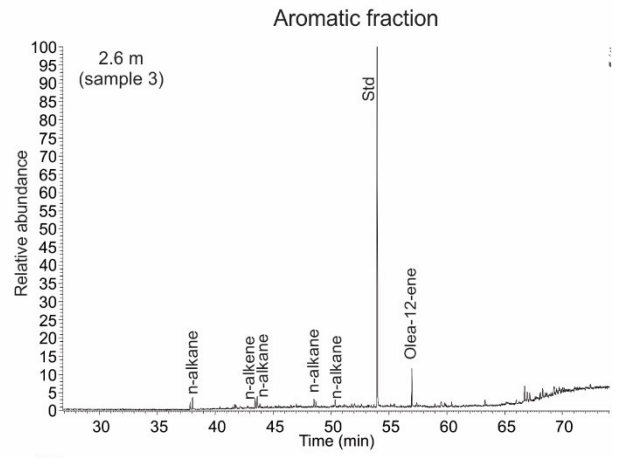
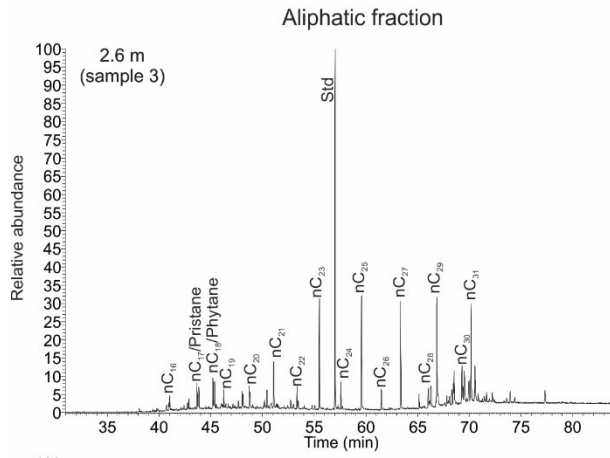


Table 3. Strontium isotopes results of the İhsaniye Formation

NP	Height (m)	Sample	Approximate age	$^{87}\text{Sr}/^{86}\text{Sr}$	$2\sigma$
<b>Hanging Wall Section</b>					
NP 23	67.5	70	31.16	0.707909	0.000020
	66.2	68	31.20	0.707907	0.000023
	64.3	65	31.25	0.707872	0.000020
	61.6	62	31.33	0.707926	0.000020
	57.1	40	31.46	0.707887	0.000020
	55.0	43	31.53	0.707900	0.000020
	53.5	45	31.57	0.707870	0.000020
	51.7	47	31.62	0.707853	0.000020
	49.5	49	31.69	0.707857	0.000018
	47.8	51	31.74	0.707892	0.000020
	45.8	53	31.79	0.707920	0.000018
	44.8	54	31.82	0.707893	0.000020
	40.8	57	31.94	0.707877	0.000020
	40.0	58	31.96	0.707875	0.000020
NP 22	38.1	38	32.02	0.707870	0.000020
	36.1	36	32.14	0.707831	0.000021
	33.3	33	32.31	0.708071	0.000020
	30.1	30	32.50	0.707831	0.000020
	27.2	27	32.67	0.707860	0.000020
	24.9	25	32.80	0.707845	0.000016
	23.0	23	32.92	0.707811	0.000020
NP 21	21.9	21	32.96	0.707774	0.000020
	19.1	20	33.08	0.707817	0.000021
	16.2	18	33.21	0.707811	0.000020
	10.1	12	33.47	0.707742	0.000020
	8.3	10	33.54	0.707810	0.000017
	6.8	8	33.61	0.707831	0.000020
	4.1	5	33.72	0.707799	0.000020
	2.6	3	33.79	0.707822	0.000020
	0.5	1	33.88	0.707796	0.000018
<b>Footwall Section</b>					
NP 23	5.9	77		0.707886	0.000020
	4.8	75		0.707889	0.000020
	3.3	73		0.707908	0.000020
	1.7	71		0.707884	0.000020

Table 4. Bulk parameters for Ruslar Formation

	Sample no.	Height	S1	S2	Tmax	TOC	S	PI	HI	TOC/S	Calc.eq
		[m]	[mg HC/g rock]		[°C]	[%]	[%]	[-]	[mgHC/gTOC]	[-]	[%]
Karadere	29	14.5	0.1	0.6	422	0.96	0.3	0.1	61	2.8	1.7
	28	14	0.1	1.1	426	0.98	0.1	0.1	110	9.59	3.65
	27	13.5	0.1	2.4	426	1.76	1.5	0	137	1.17	6.53
	26	13	0.1	4.6	427	2.04	1.5	0	224	1.36	6.6
	25	12.5	0.2	5.5	427	2.17	1.1	0	256	1.96	5.42
	24	12	0.2	5	425	1.88	1.5	0	266	1.29	9.55
	23	11.5	0.1	4.7	423	1.93	0.8	0	246	2.4	6.65
	22	11	0.1	5.2	423	1.99	1.3	0	261	1.5	5.91
	21	10.5	0.1	5.9	422	2.04	1.4	0	289	1.52	7.79
	20	10	0.1	4.4	425	1.83	1.7	0	238	1.1	6.29
	19	9.5	0.1	6.2	422	2.24	1.4	0	278	1.58	6.68
	18	9	0.1	5.2	423	2.1	1.4	0	247	1.52	6.46
	17	8.5	0.1	4.6	421	1.88	1.4	0	245	1.35	5.91
	16	8	0.1	5	421	1.85	1.3	0	272	1.41	4.42
	15	7.5	0.1	5.2	421	2.19	0.6	0	237	3.66	5.89
	14	7	0.2	5.9	419	2.31	0.6	0	253	4.13	6.7
	13	6.5	0.1	6.4	422	2.3	1.3	0	276	1.74	7.25
	12	6	0.1	5.9	421	2.18	1.3	0	271	1.73	8.19
	11	5.5	0.1	5.2	420	2.03	1.5	0	256	1.37	8.76
	10	5	0.1	4.7	421	1.76	2.9	0	267	0.61	6.99
	9	4.5	0.1	4.1	429	1.67	1.4	0	246	1.19	10.48
	8	4	0.1	5	428	1.89	1.4	0	262	1.32	9.73
	7	3.5	0.2	5.7	426	2.16	1.5	0	263	1.45	6.2
6	3	0.1	2.7	427	1.3	1.1	0	208	1.16	4.15	
5	2.5	0.1	0.8	436	0.82	1.4	0.1	102	0.6	6.75	
4	2	0.1	2.4	433	1.37	0.6	0	175	2.31	8.26	
3	1.5	0.1	1.5	430	1.03	1.5	0.1	143	0.69	5.5	
2	1	0.2	6.6	426	2.48	1.2	0	265	2.01	5.92	
1	0.5	0.2	8.5	424	2.56	1.4	0	331	1.84	8.5	
P-79	1	350	0.3	1.6	415	1.4	1.2	0.1	102	1.3	2
	2	360	0.3	1.7	417	1.88	0.9	0.2	107	1.7	2.92
	3	370	0.3	1.6	422	1.26	0.7	0.1	100	2.2	1.75
	4	380	0.4	3.3	427	1.95	1.1	0.1	210	1.4	5.25
	5	400	0.6	4.7	427	1.43	1.4	0.1	300	1.1	11.58
	6	410	0.4	3.6	423	1.6	1.1	0.1	229	1.4	11.33

TOC-total organic carbon, S-Sulphur, HI-hydrogen index, PI-production index, calc.eq.-calcite equivalent



Table 5. Organic geochemical data of the Ruslar Formation at Karadere.

Sample no.	Height	TOC	HI	EOM	HC	NSO	Asph.	n-C <sub>15-19</sub>	n-C <sub>21-25</sub>	n-C <sub>26-31</sub>	Steroids/hopanoids	Hop-17(21)-ene	28, 30-Bisnorhopane	ααα C <sub>26</sub> sterane	C <sub>25</sub> HBI	Pr/Ph	MPI index
	[m]	[wt%]	[mg/gTOC]	[%]							[μg/gTOC]						
28	14.5	0.98	97	39	14	34	52	29	27.1	44.6	9.9	1.2	53.7	9.8	9.6	1	0.9
25	12.5	2.17	271	21	15	71	14	45	24	32.7	7.1	0.2	0.3	4	9	0.8	1
22	11	1.99	261	19.5	12	72	16	29	25.3	47	5.4	0.8	12.6	2.8	8.8	0.8	0.9
19	9.5	2.24	278	17.9	17	74	8	19	28.8	52.6	6.3	0	2.4	0.6	5.6	0.7	1
16	8	1.85	272	25.8	19	71	9	35	23.9	42.4	4.6	0.9	34.5	2.6	13.9	1.1	1
14	7	2.31	253	20.4	16	76	8	20	27.6	53.3	4.4	0.4	40.6	2.5	13.8	1.3	1
12	6	2.18	271	15.3	16	71	13	25	24.4	51.5	3	0.3	16.5	0.7	7.7	0.8	1
9	4.5	1.67	246	17.3	11	72	17	51	18.1	30.8	8.4	0.1	8.9	0.9	3.4	0.8	1
7	3.5	2.16	263	17.9	11	73	16	38	21.8	41	9	0.2	7.7	2	5.6	0.7	1
4	2	1.37	175	32.8	11	75	14	31	28.2	43.4	4.2	0.6	29.8	2.7	13.6	0.9	1
1	0.5	2.56	331	9	14	62	24	22	26.7	52.6	5.3	0.1	6.3	0.9	2.1	0.7	0.9

TOC-total organic carbon, HI-hydrogen index, EOM-extracted organic matter, HC-hydrocarbons yields, NSO-polar compounds, Asph.-asphaltene, n-C<sub>15-19</sub>-short-chain alkanes, n-C<sub>21-25</sub>-medium-chain alkanes, n-C<sub>26-32</sub>-long-chain alkanes; Pr/Ph-Pristane/Phytane ratio.

# GC-MS traces of the Ruslar Formation

Karadere - Bulgaria

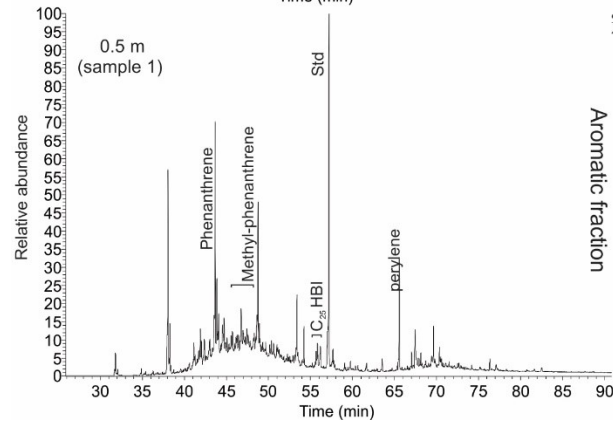
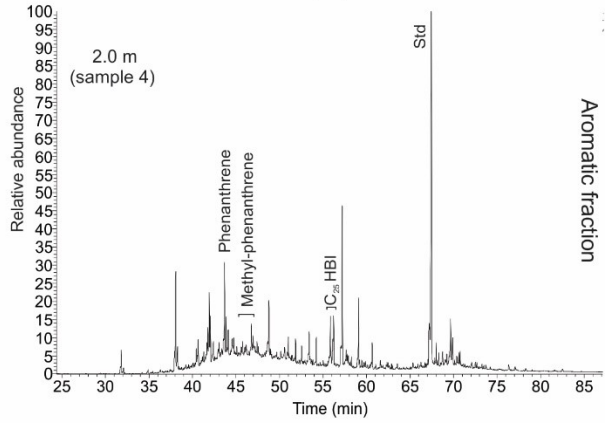
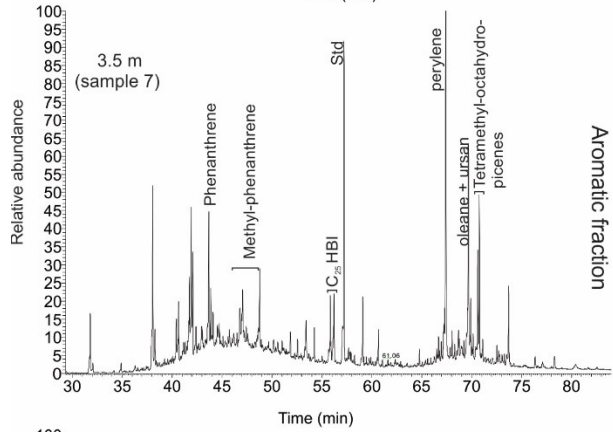
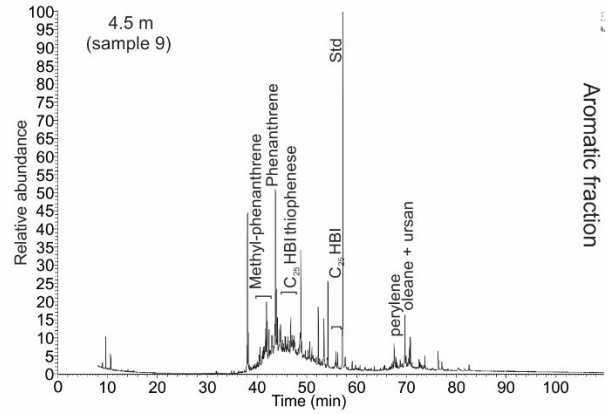
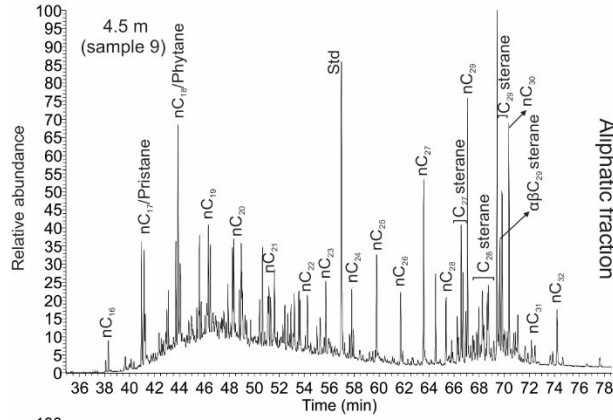


Table 6. Bulk parameters for analysed samples from Sibiciu de Sus quarry.

Sample	S1	S2	Tmax	TOC	S	PI	HI	TOC/S	Calc. Equiv.
	[mg HC/g]		[°C]	[%]	[%]		[mg HC/g TOC]		[%]
Impure diatomite									
S21	0.3	4.35	422	1.04	0.04	0.06	419	24.8	0.39
S14	4.57	14.07	417	4.59	0.92	0.25	307	5	1.33
S13	3.29	13.69	423	2.66	0.24	0.19	515	11	0.78
S12	5.56	30.67	419	9.57	0.52	0.15	320	18.5	3.36
S11	2.61	19.95	423	4.88	0.33	0.12	409	14.8	0.72
S10	6.59	13.71	414	3.7	0.59	0.32	370	6.3	1.69
S9	1.39	11.67	422	2.81	0.25	0.11	415	11.1	0.03
S8	8.29	16.69	413	4.01	0.72	0.33	417	5.6	2.33
S7	8.84	23.64	418	5.3	0.26	0.27	446	20.1	3.41
S6	4.46	20.75	421	4.69	0.3	0.18	443	15.5	1.35
S5	3.28	24.03	422	5.78	0.42	0.12	416	13.7	0.97
S4	4.02	17.65	420	3.85	0.22	0.19	458	17.2	1
S3	5.33	21.8	420	5.33	0.31	0.2	409	17.2	0.31
S2	2.02	13.19	420	2.61	0.34	0.13	505	7.7	0.05
S1	2.45	13.96	421	3.61	0.23	0.15	387	15.6	0.35
Pure diatomite and chert									
S20	0.2	1.77	415	0.86	0.1	0.1	206	8.4	0.52
S19	0.28	2.73	417	1.22	0.1	0.09	224	12.6	0.11
S18	0.58	7.68	414	2.9	0.34	0.07	265	8.5	0.5
Black and white diatomite									
S17	6.5	12.27	416	3.43	0.85	0.35	358	4,1	1.8
Pure Diatomite									
S16	0.72	10.55	424	2.64	0.38	0.06	400	7	0
Quartz-rich sandstone and menilite									
S15				0.36	0.22				
S22	2.44	12.58	419	5.01	1.42	0.16	251	3.5	2.18

TOC-total organic carbon, S – Sulphur, HI – hydrogen index, PI – production index, calc. equi.- calcite equivalent.

Table 7. Bulk parameters of Szurdokpüspöki quarry

	Sample	Height	Calc. Equiv.	TOC	Sulphur	S1	S2	Tmax	PI	HI	TOC/S
		[m]	[%]			[mg HC/g]		[°C]	[-]	[mg HC/g TOC]	[-]
Szurdokpüspöki quarry	21-Sp	11.4	0	0.31	0.05	0.09	0.27	379	0.24	88	5.8
	20-Sp	11	0.24	0.2	0.1	0.07	0.15	384*	0.3	74	2
	19-Sp	10.5	0.71	0.14	0.13	0.03	0.15	403	0.17	102	1.1
	18-Sp	10	0.32	0.13	0.06	0.03	0.19	403	0.14	143	2
	17-Sp	9.5	1.42	0.1	0.03	0.01	0.15	407	0.06	158	3.2
	16-Sp	9	0.36	0.13	0.11	0.05	0.19	387	0.21	146	1.1
	15-Sp	8.6	0.05	0.14	0.48	0.02	0.08	399*	0.2	59	0.3
	14-Sp	8.9	0.3	0.19	0.63	0.04	0.12	413	0.26	61	0.3
	13-Sp	7.5	4.62	1.42	1.12	0.28	5.68	415	0.05	399	1.3
	12-Sp	7	3.4	1.39	1.16	0.33	6.18	415	0.05	445	1.2
	11-Sp	6.5	3.4	1.53	0.83	0.48	11.05	418	0.04	723	1.8
	10-sp	6	5.13	1.47	0.8	0.2	6.61	416	0.03	450	1.8
	9-Sp	5	37.05	1.03	0.91	0.2	3.45	402	0.05	336	1.1
	8-Sp	4.5	28.55	0.91	0.74	0.17	2.39	387	0.06	261	1.2
	7-Sp	4.2	70.89	0.44	0.33	0.05	0.78	412	0.05	178	1.3
	6-Sp	3.8	33.62	0.22	0.44	0.02	0.43	422	0.04	193	0.5
	5-Sp	3.5	59.94	0.37	0.14	0.06	1.11	407	0.05	298	2.6
	4-Sp	3	18.88	2.31	0.52	0.96	14.4	405	0.06	623	4.5
	3-Sp	2.5	10.36	1.41	0.44	0.46	9.71	404	0.05	689	3.2
V-Sp	2	25.79	1.11	0.14	0.23	6.05	402	0.04	544	7.7	
IV-Sp	1.5	10.59	1.47	1	0.27	6.18	406	0.04	421	1.5	
III-Sp	1	22.16	2.95	0.73	1.67	16.25	418	0.09	551	4.1	
II-Sp	0.5	47.44	1.2	0.63	0.35	6.49	412	0.05	540	1.9	
I-Sp	0	34.5	1.22	0.75	0.32	6.35	407	0.05	519	1.6	

TOC-Total organic carbon, S-sulfur, HI-hydrogen index, PI-production index, calc. equi.-calcite equivalent. \* Tmax is unreliable, because of low S2 peak.

Table 8. Bulk parameter of the Limberg Member and the Zellerndorf Formation

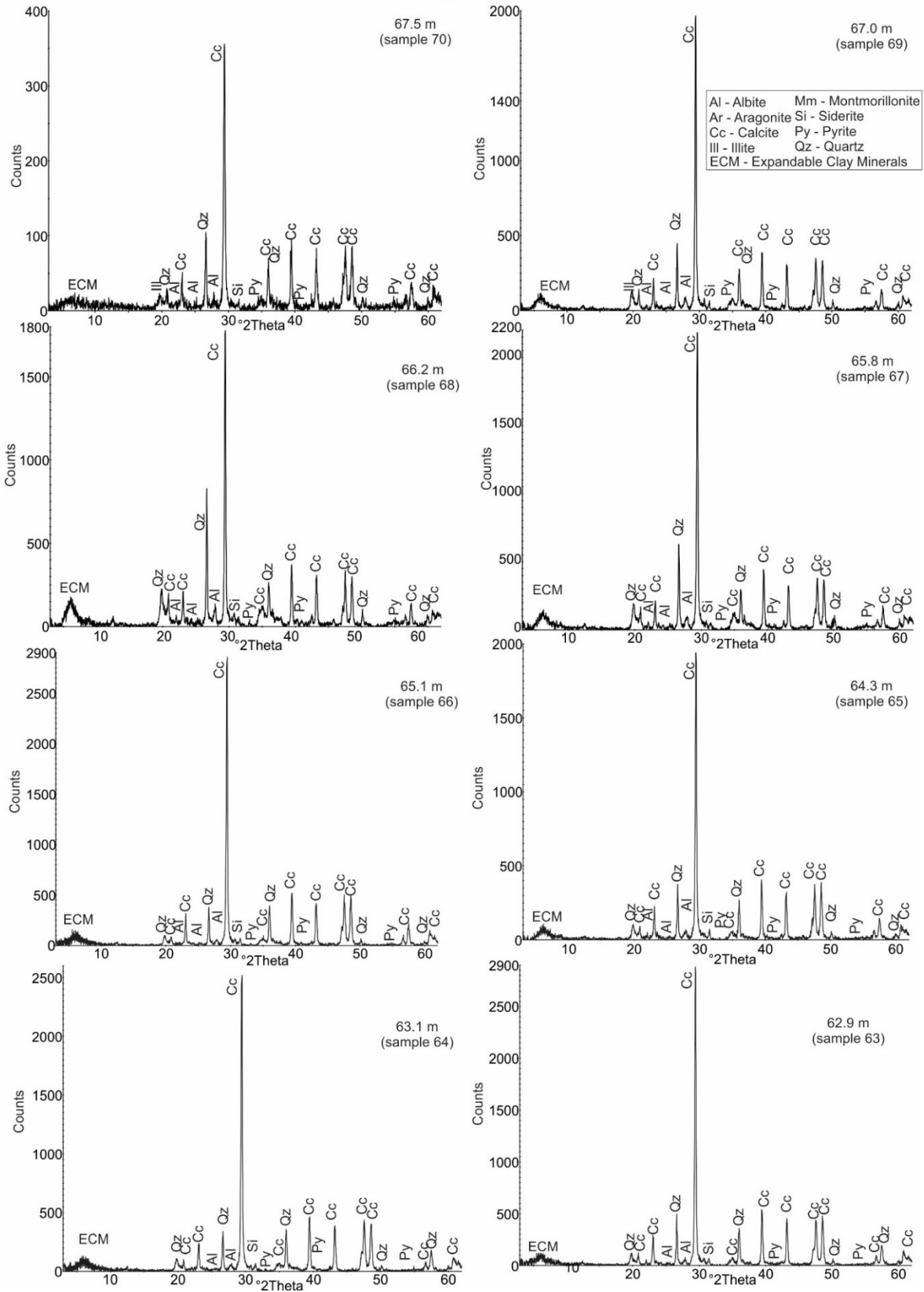
	Sample	Height	Calc. equ.	TOC	S	S1	S2	Tmax	PI	HI	TOC/S
		[m]	[%]	[%]	[%]	[mg HC/g]	[°C]	[-]	[mg HC/g TOC]	[-]	
<b>Parisdorf quarry</b>	Zellerndorf Formation (above Limberg Member)										
	11-Pa	7	3.82	0.16	0.01	0.02	0.04	*	0.33	25	20.6
	10-Pa	6.5	9.67	0.16	0.01	0.01	0.03	*	0.25	19	11.4
	Limberg Member										
	9-Pa	6.2	0.21	0.11	0	0.02	0.12	401*	0.14	106	26.2
	8-Pa	5.5	0.32	0.11	0.01	0.03	0.17	408	0.15	151	20.7
	3-Pa	5	0.09	0.13	0.01	0.02	0.08	396*	0.17	58	20.7
	7-Pa	4.2	0.31	0.13	0.01	0.02	0.09	403*	0.19	68	20.8
	2-Pa	3.5	0.13	0.15	0.08	0.03	0.1	386*	0.2	67	1.9
	1-Pa	3	0.28	0.15	0.11	0.02	0.08	395*	0.2	54	1.3
	6-Pa	2.5	0.33	0.11	0.01	0.03	0.09	402*	0.25	85	20.1
	5-Pa	2	0.17	0.1	0.01	0.01	0.03	*	0.29	25	11.7
	4-Pa	1.2	0	0.13	0.01	0.02	0.08	*	0.2	61	15.7
13-Pa	0.5	0.16	0.21	0.01	0.04	0.12	*	0.23	56	24.6	
12-Pa	0	0.43	0.07	0.01	0.02	0.16	420	0.11	236	8.1	
Zellerndorf Formation (above Limberg Member)											
<b>Limberg</b>	20-Li	4.9	0.19	0.16	0.01	0.02	0.06	423*	0.25	0	11.1
	Limberg Member										
	19-Li	3.1	0.29	0.17	0.32	0.02	0.13		0.25	34	0.5
	18-Li	2.4	1.44	0.3	0.02	0.03	0.25	379*	0.13	43	12.7
	17-Li	1.9	0.45	0.18	0.07	0.03	0.29	414	0.11	135	2.6
	16-Li	1.2	0.32	0.16	0.01	2.06	0.31	436	0.1	174	14.4
	15-Li	0.5	0.56	0.13	0.01	1.03	0.36	421	0.87	233	13.4
14-Li	0	0.29	0.18	0.18	0.04	0.11		0.74	205	1	
Zellerndorf Formation (below Limberg Member)											
<b>Limberg KB02 (Hangbrücke)</b>	KB 02/1	-16.05 to -16.15	7.08	0.85	0.57						1.5
	KB 02/2	-16.55 to -16.60	4.58	0.82	0.69						1.2
	KB 02/3	-17.00 to -17.10	6.06	0.83	0.48						1.7
	KB 02/4	-17.50 to -17.55	5.13	0.84	1.48						0.6
	KB 02/5	-18.10 to -18.15	5.54	0.8	0.86						0.9

KB 02/6	-18.55 to -18.60	4.65	0.73	0.92						0.8
KB 02/7	-19.00 to -19.10	5.48	0.75	0.86						0.9
KB 02/8	-19.55 to -19.60	7.04	0.58	0.87						0.7
KB 02/9	-20.10 to -20.15	6.31	0.64	0.72						0.9
KB 02/10	-20.55 to -20.60	4.81	0.74	0.74						1
KB 02/11	-21.10 to -21.15	2.66	0.91	0.73						1.2
KB 02/12	-21.45 to -21.55	1.75	0.86	0.76						1.1

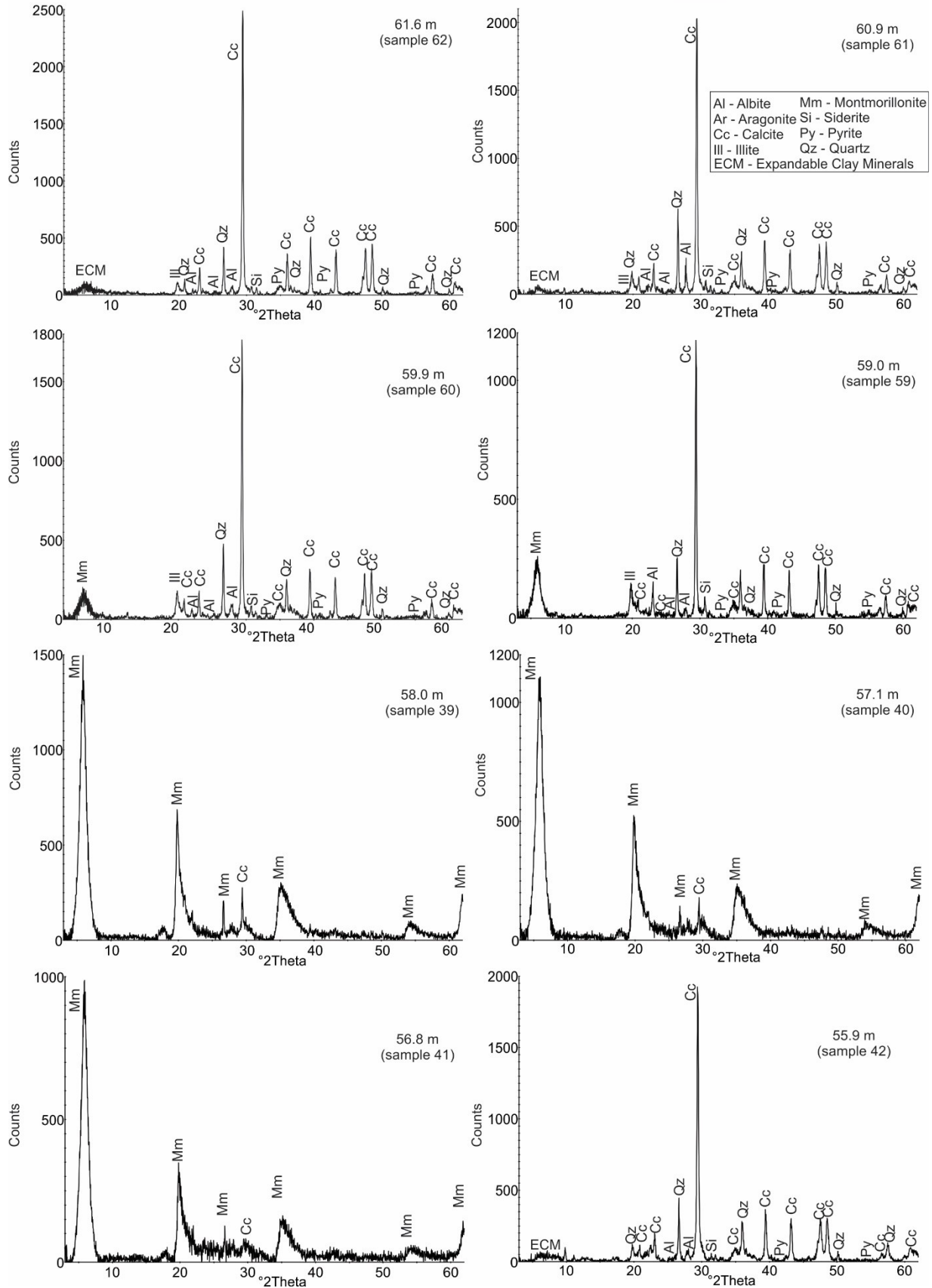
TOC-Total organic carbon, S-sulfur, HI-hydrogen index, PI-production index, calc. equi.-calcite equivalent. \*Tmax is unreliable, because of low S2 peak.

**Appendix 2 - XRD diagrams**

**Karaburun, Turkey - Hanging Wall Section**

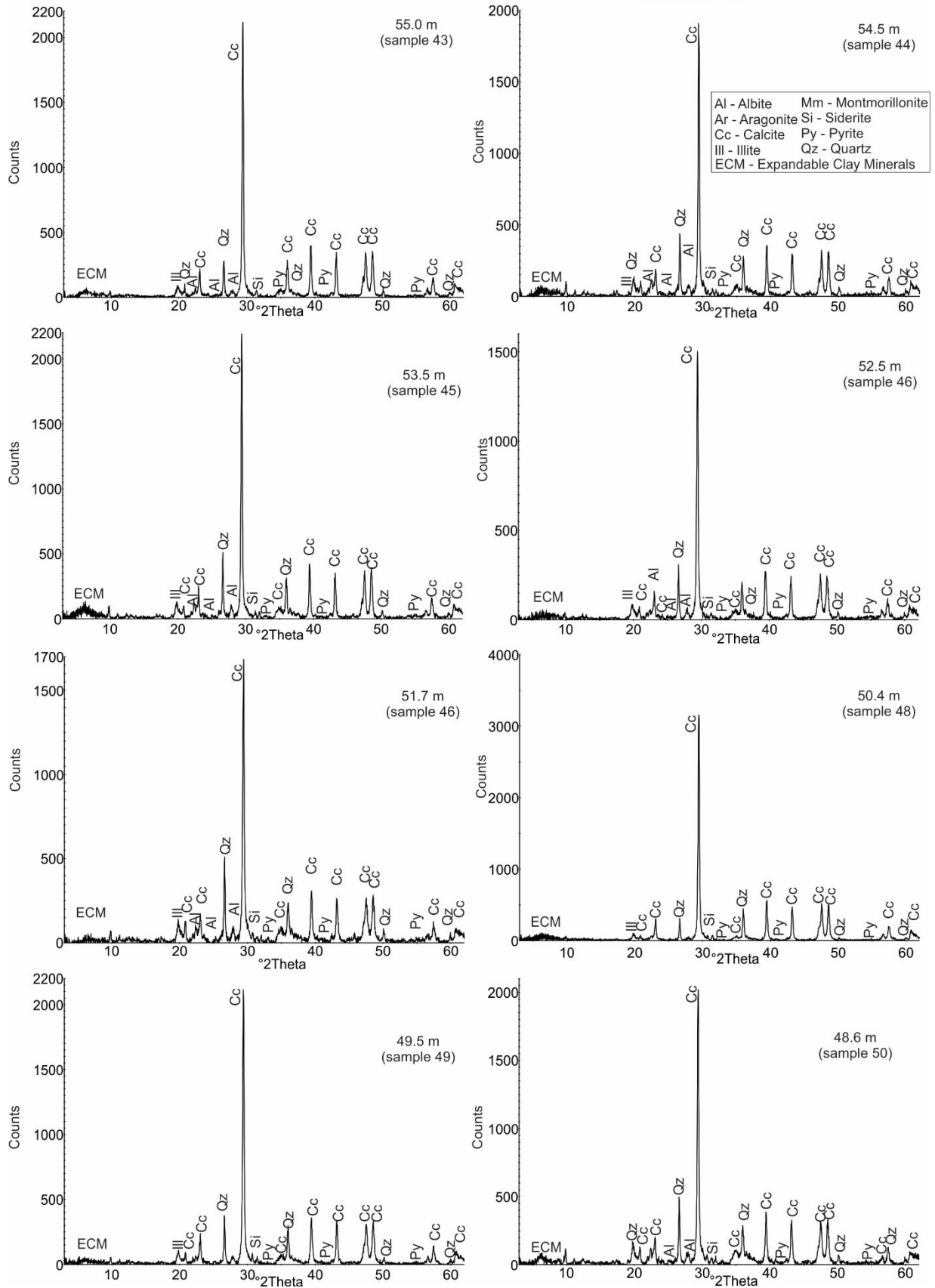


Karaburun, Turkey - Hanging Wall Section

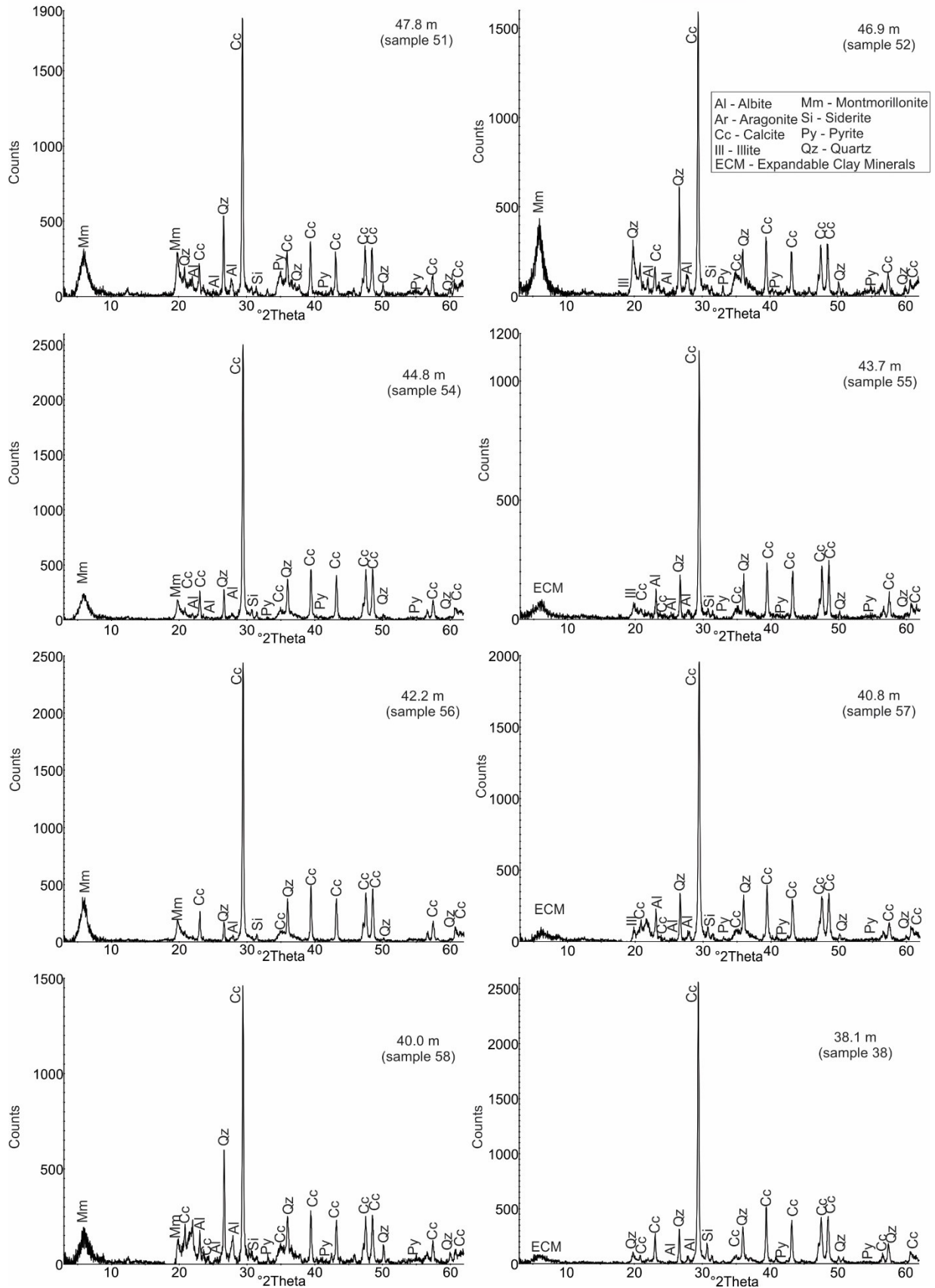




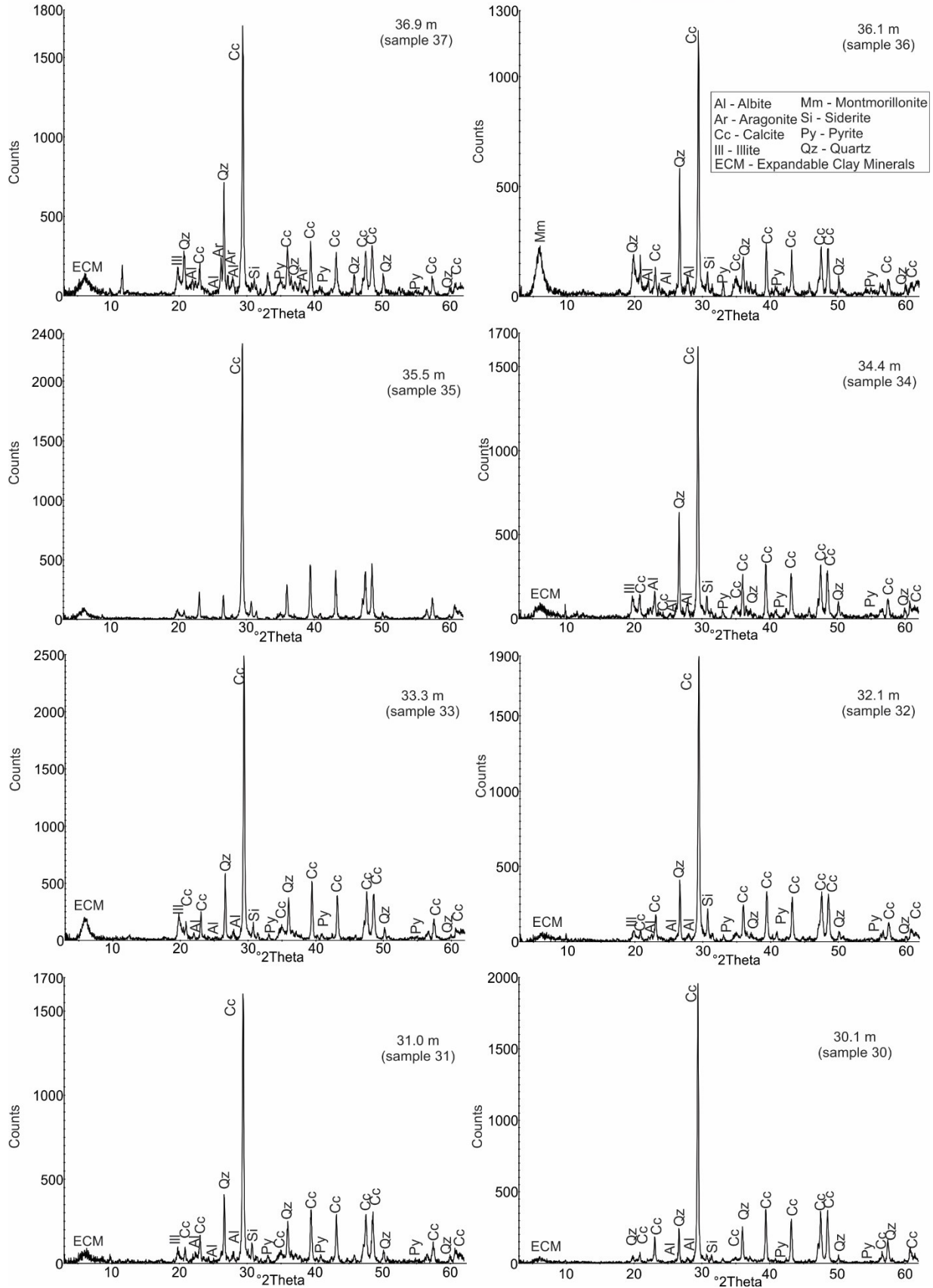
Karaburun, Turkey - Hanging Wall Section



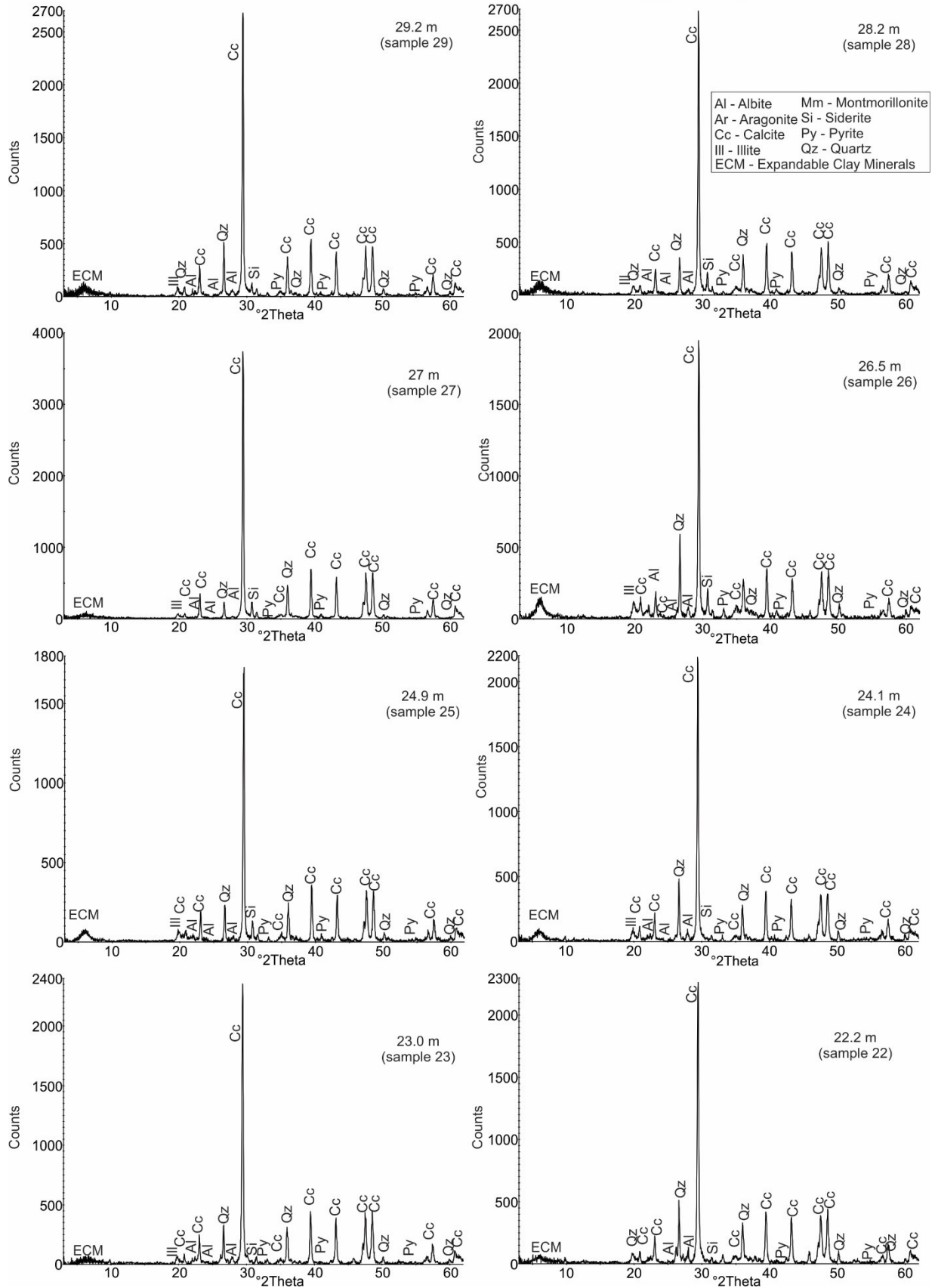
Karaburun, Turkey - Hanging Wall Section



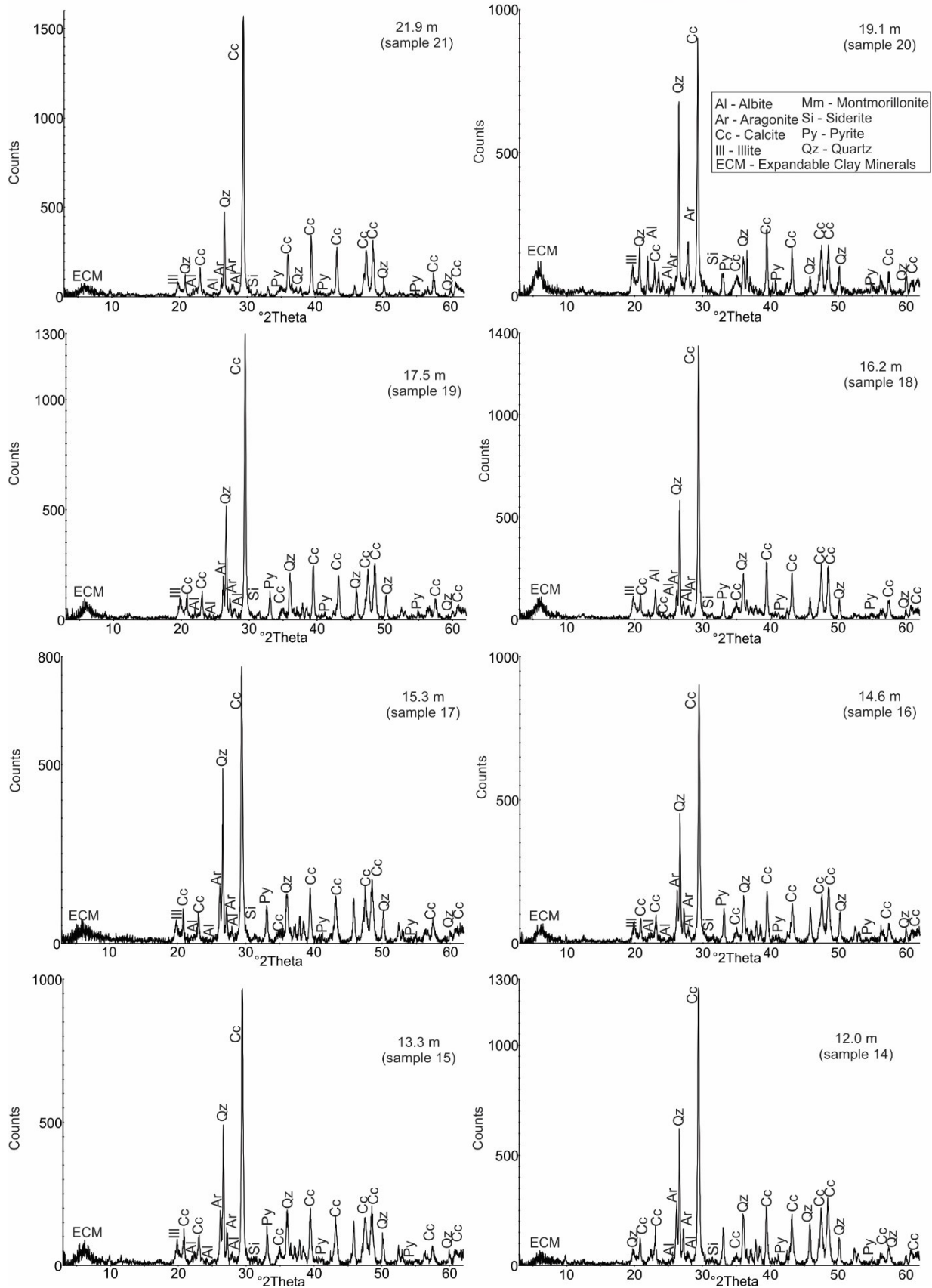
Karaburun, Turkey - Hanging Wall Section



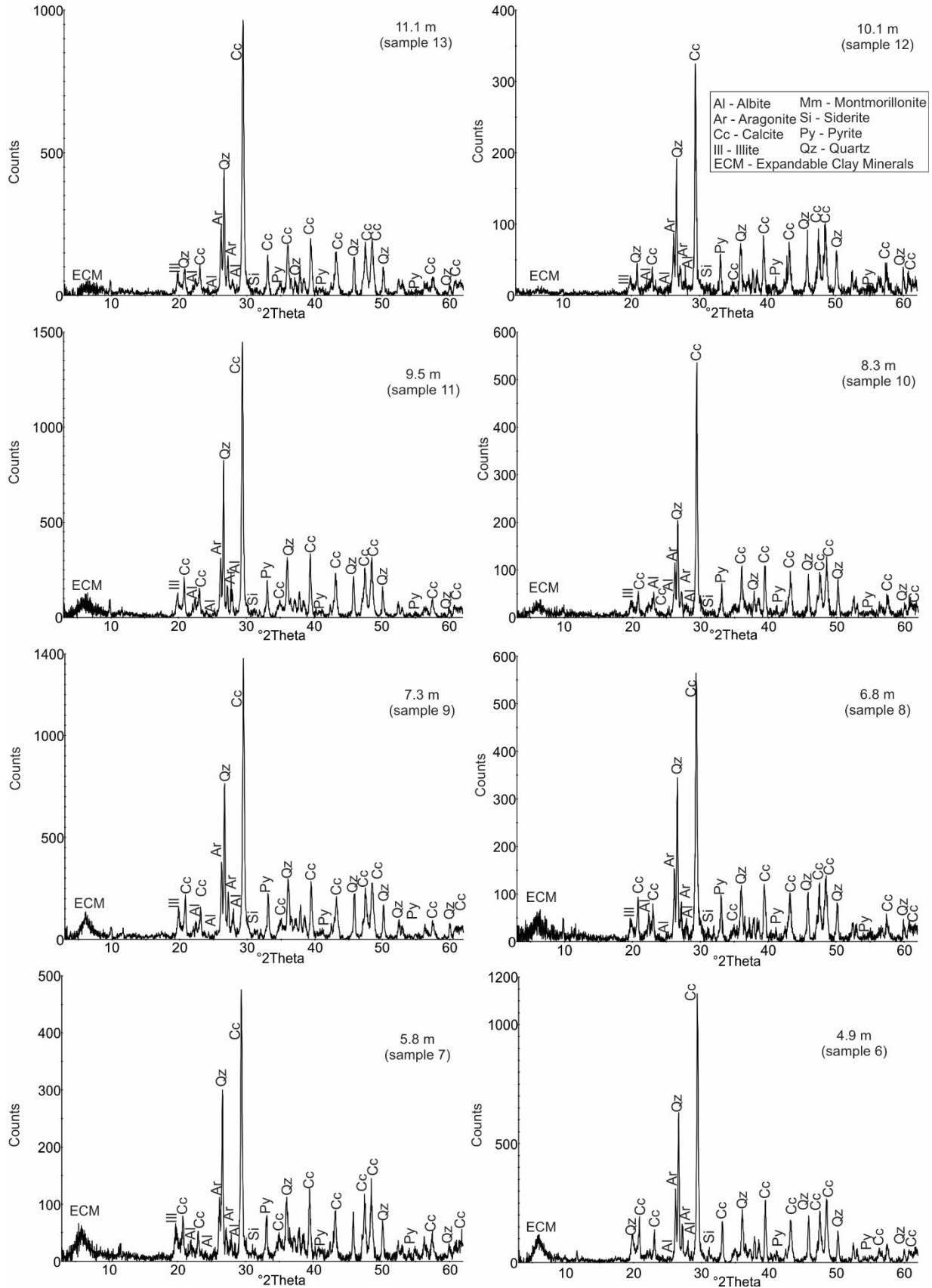
Karaburun, Turkey - Hanging Wall Section



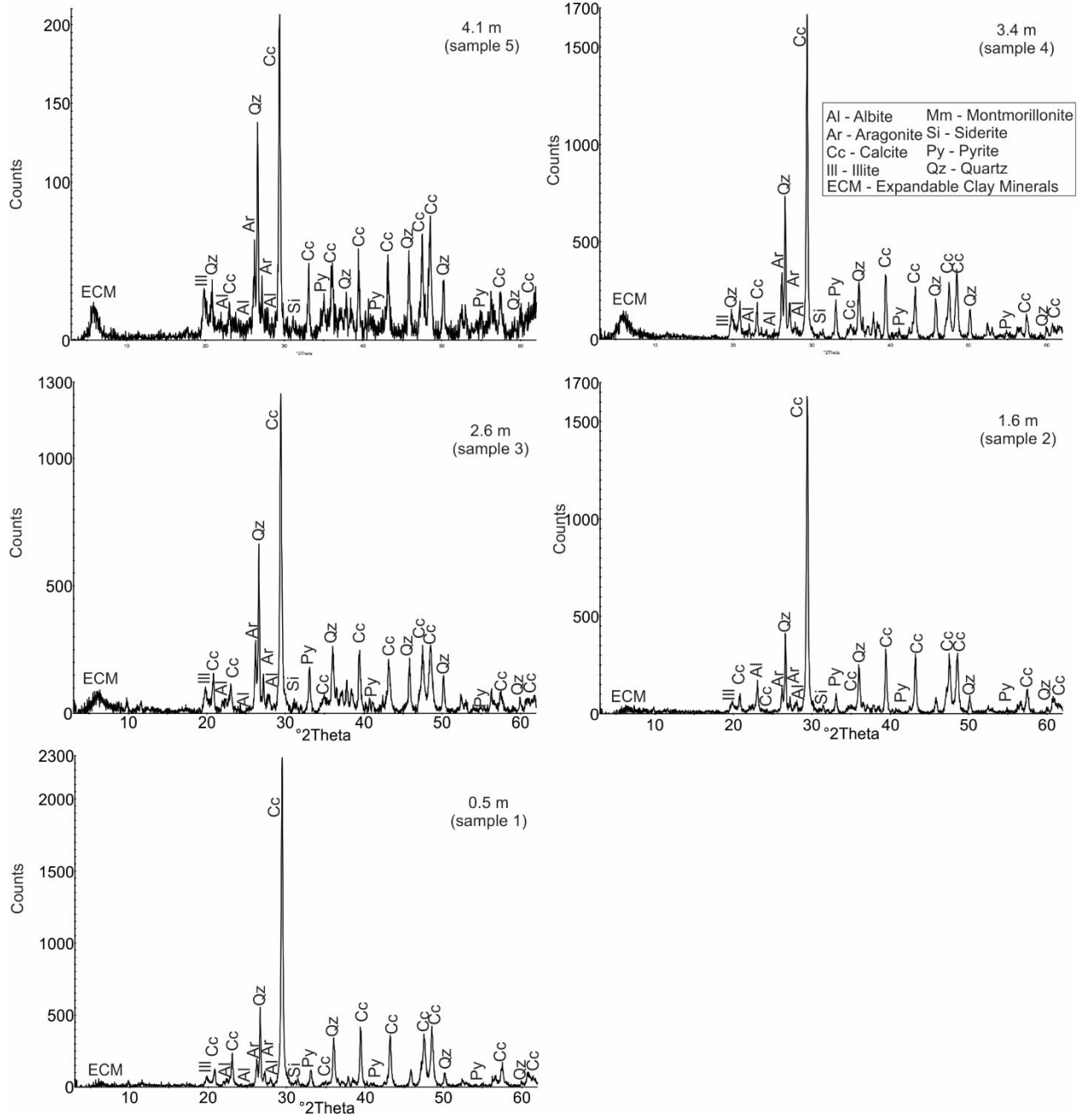
Karaburun, Turkey - Hanging Wall Section



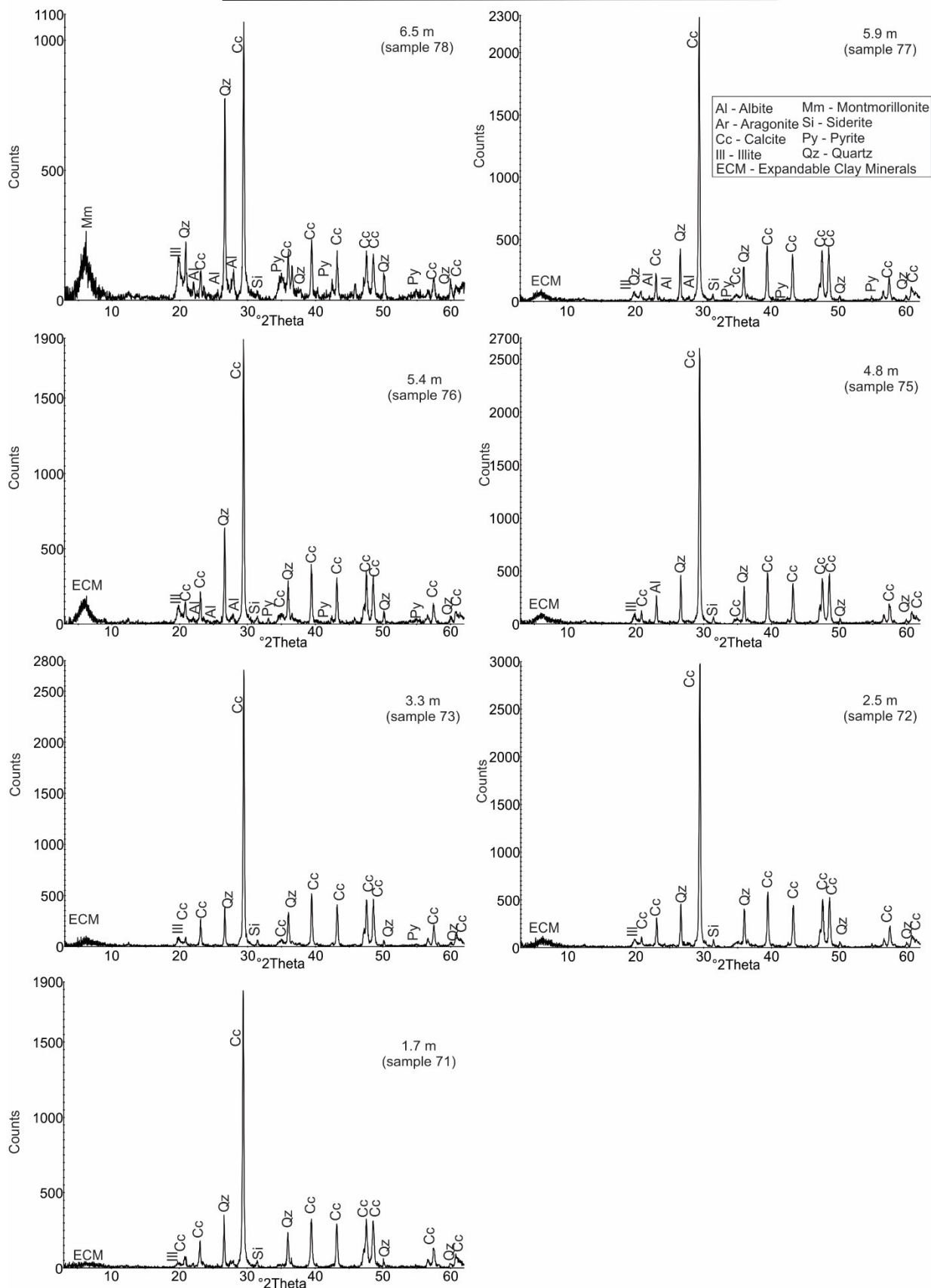
Karaburun, Turkey - Hanging Wall Section



Karaburun, Turkey - Hanging Wall Section

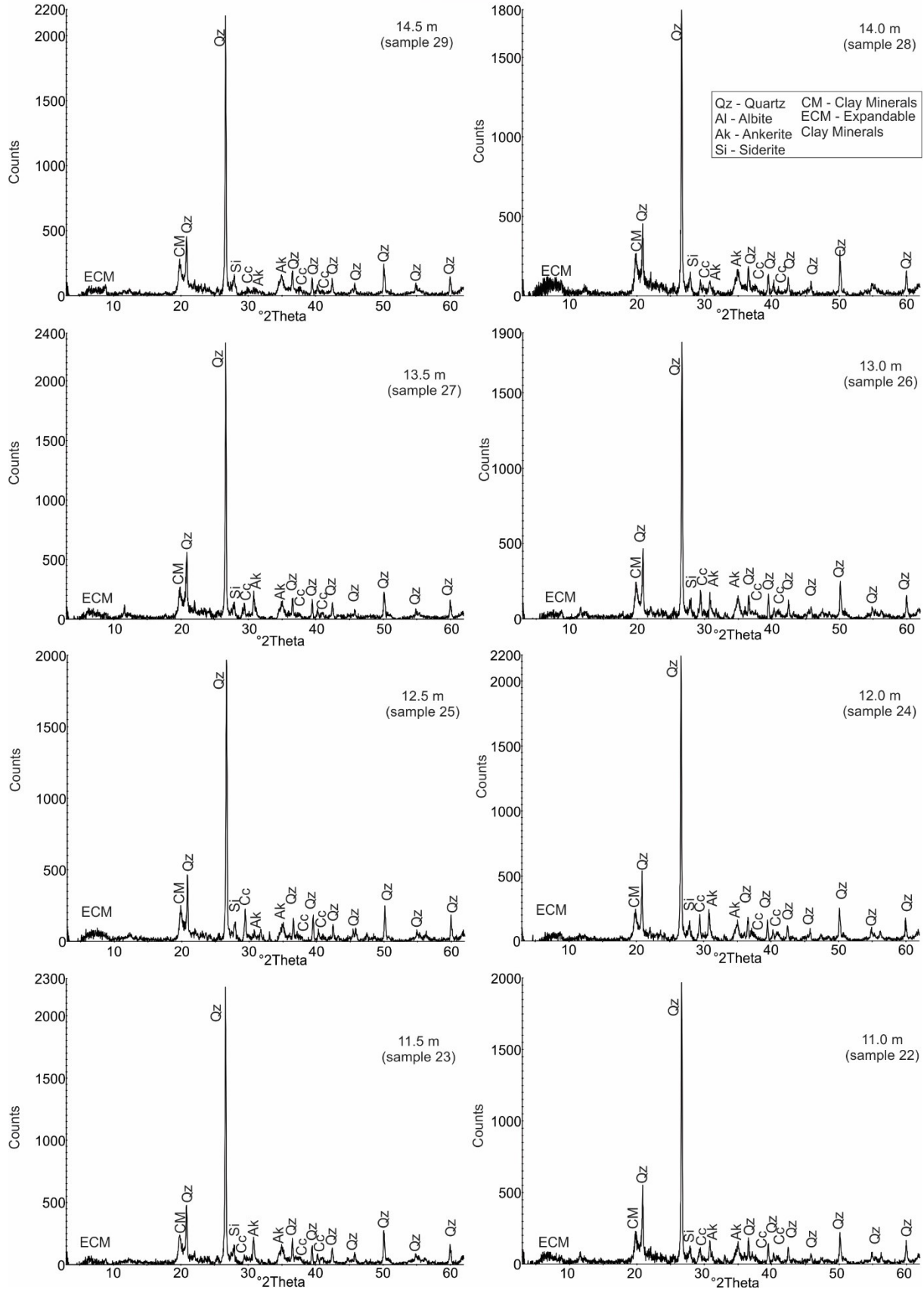


Karaburun, Turkey - Footwall Section

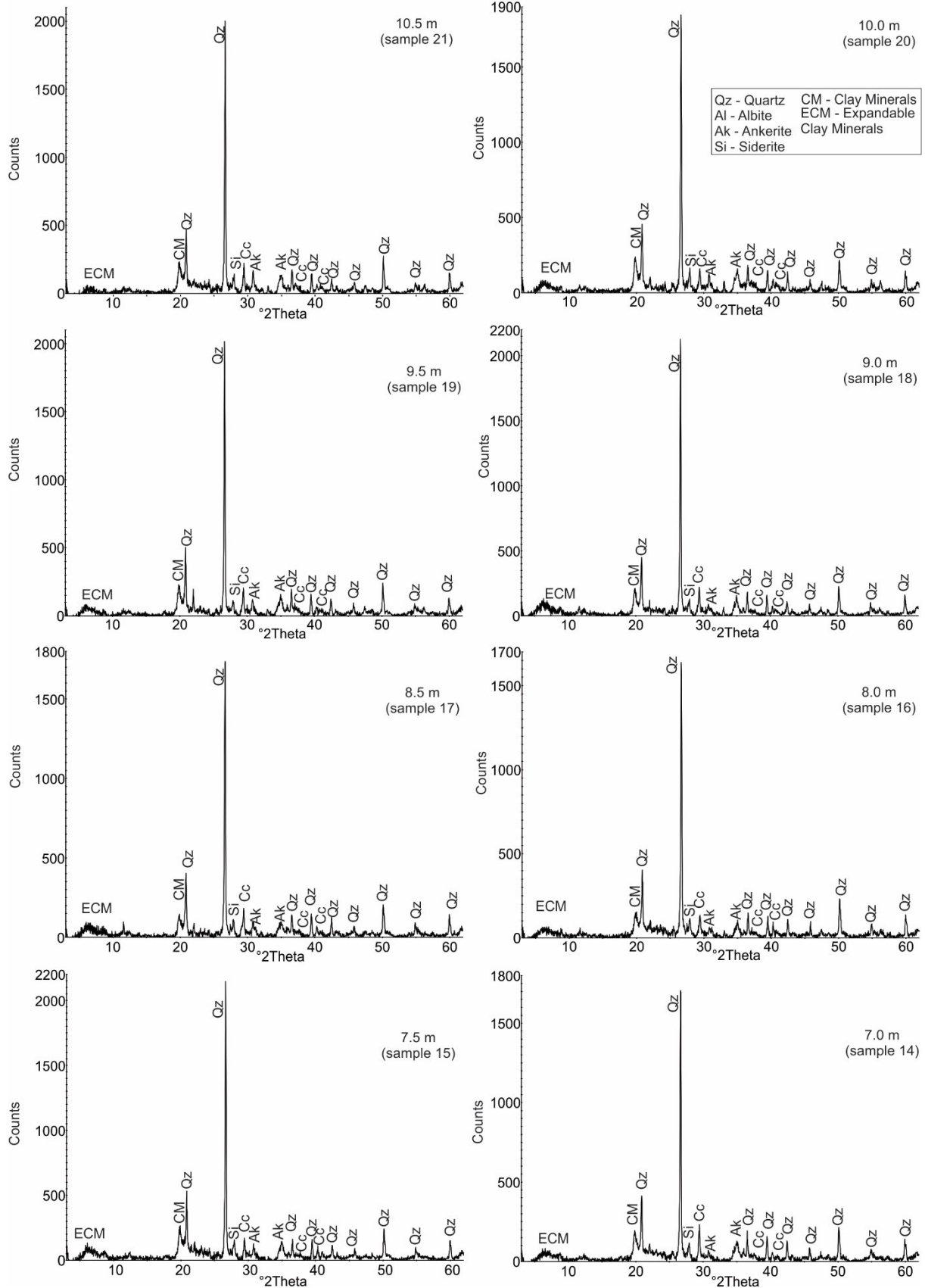




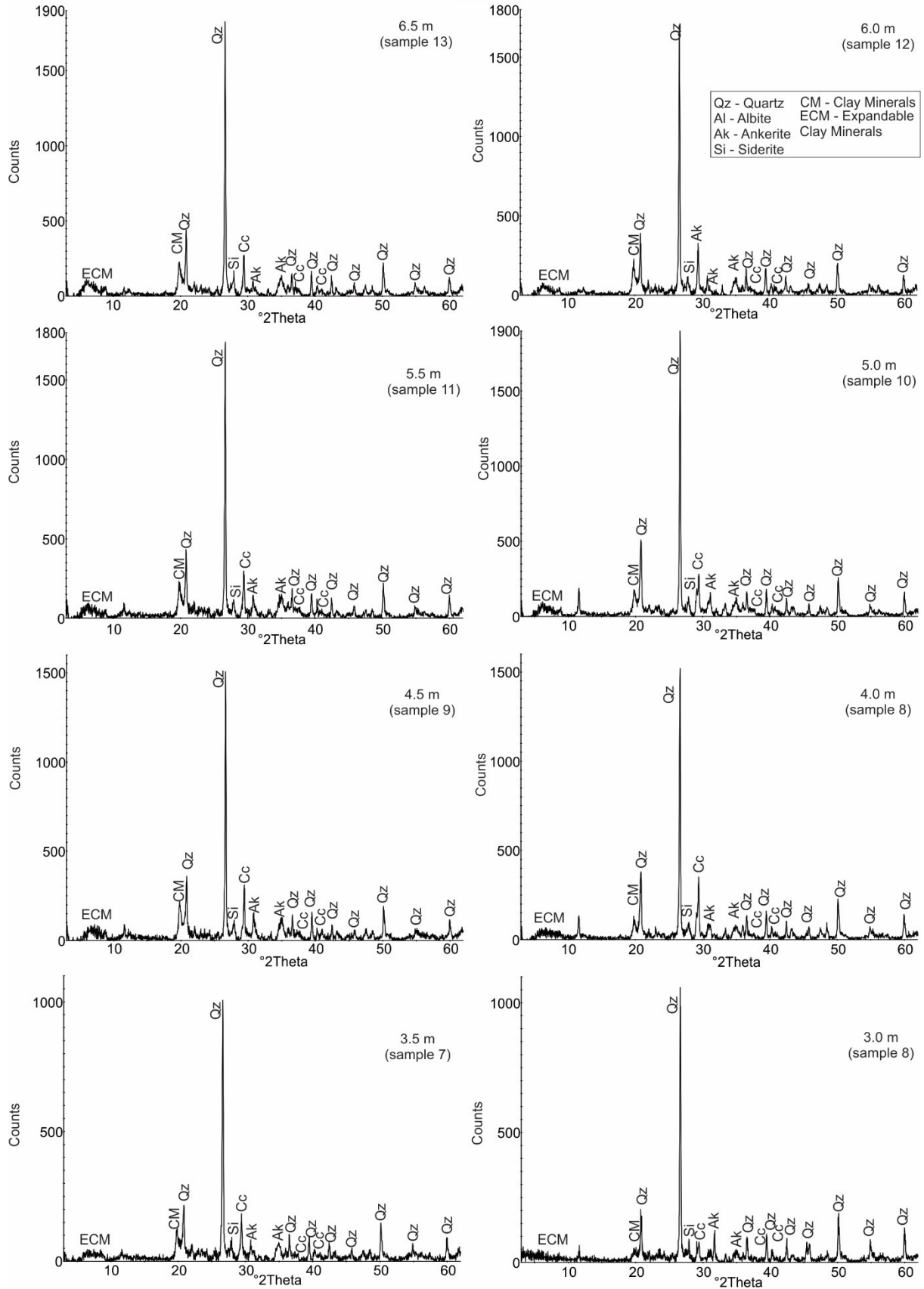
Karadere, Bulgaria - Ruslar Formation



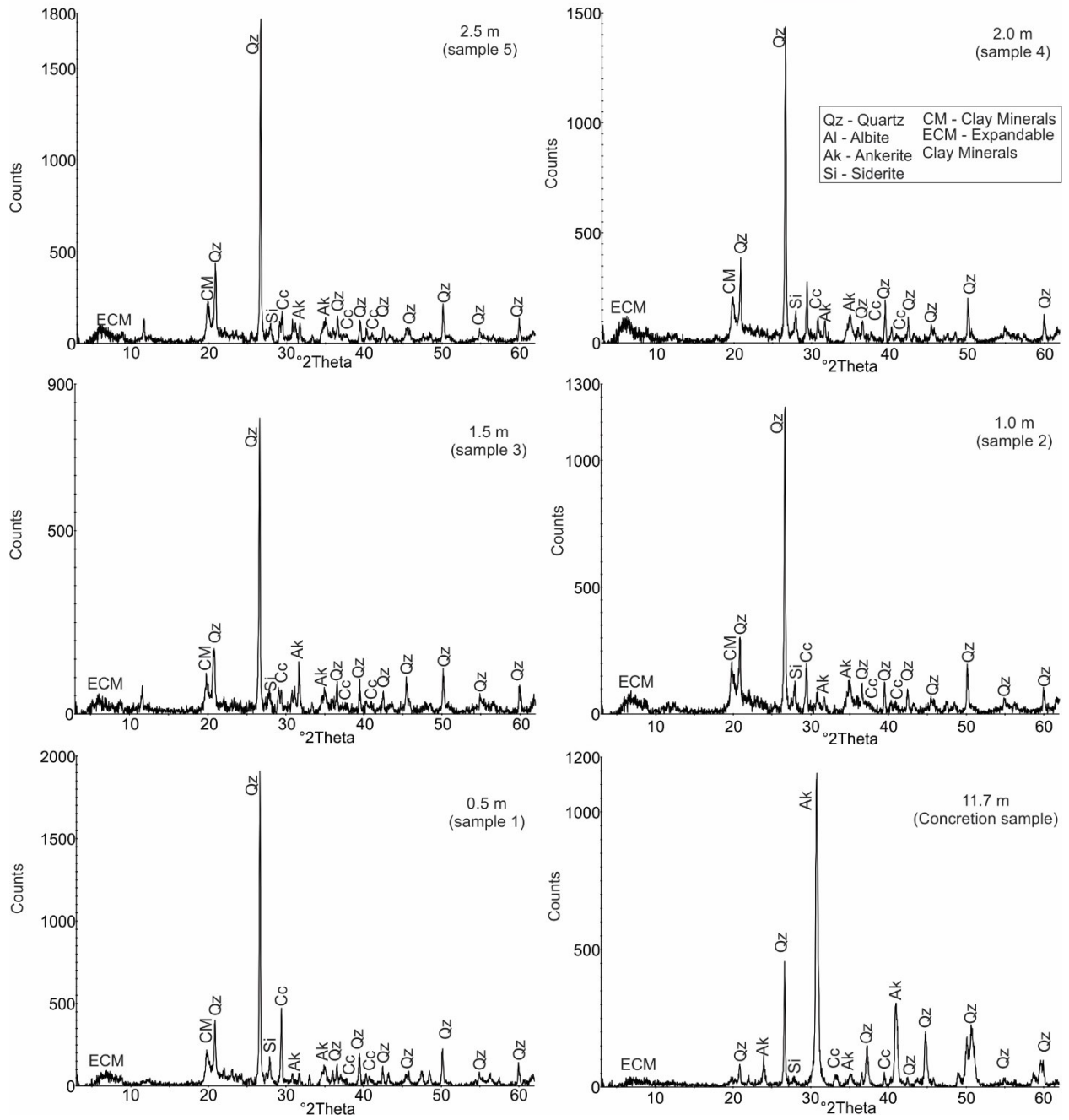
Karadere, Bulgaria - Ruslar Formation



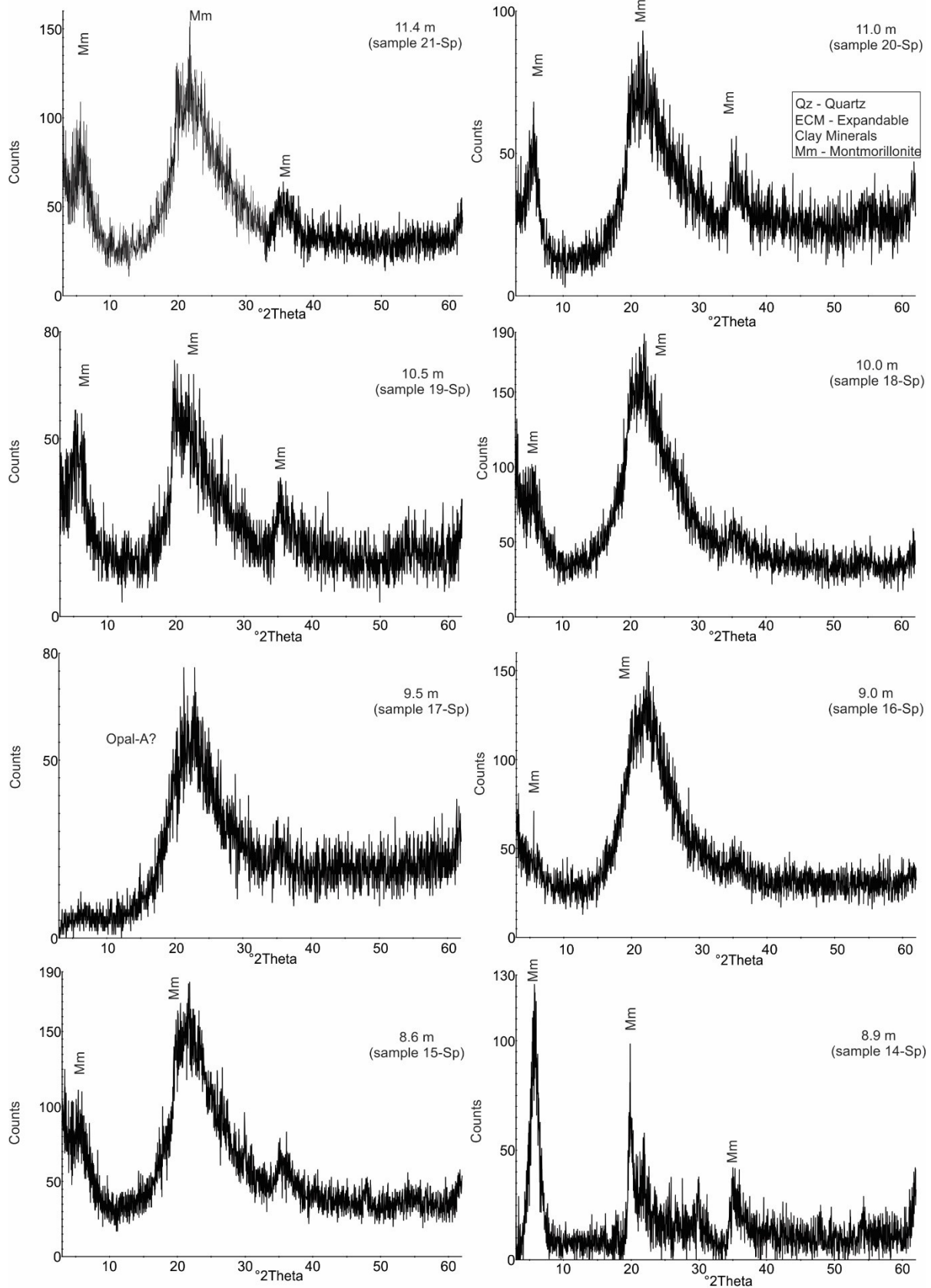
Karadere, Bulgaria - Ruslar Formation



Karadere, Bulgaria - Ruslar Formation

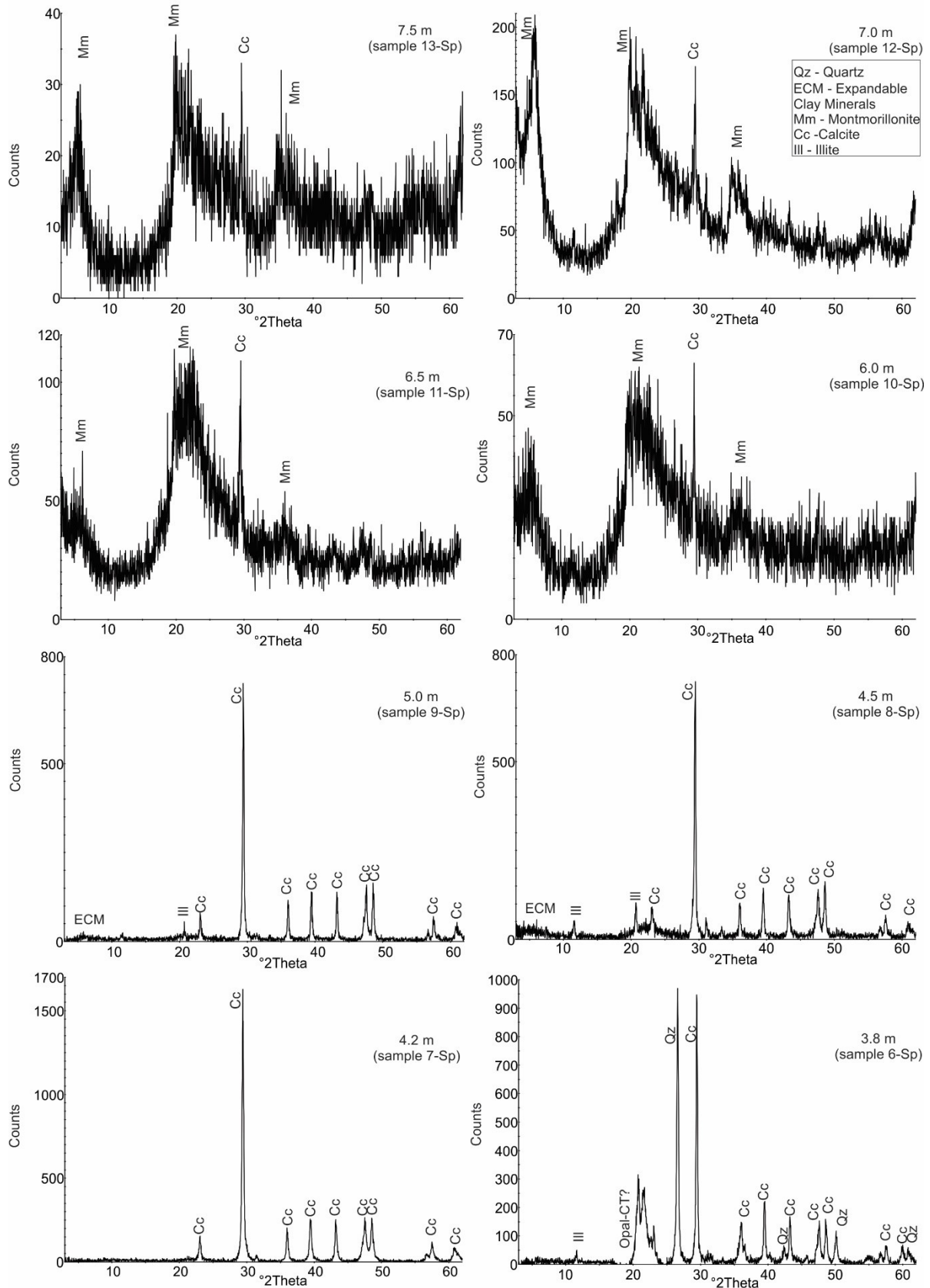


Szurdokpüspöki, Hungary



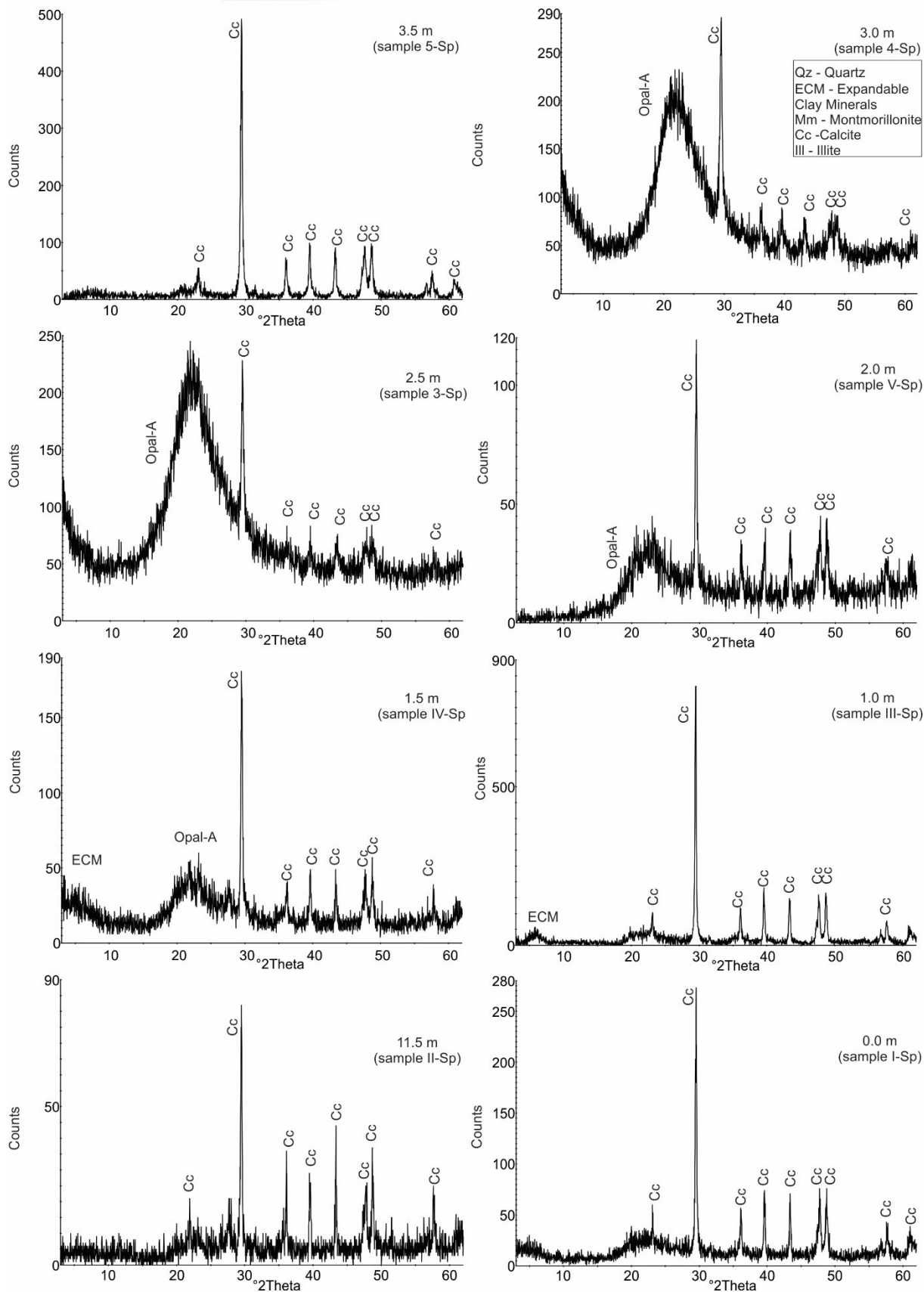
The noise of the samples is not caused by a malfunction during X-ray Diffraction measurements.

Szurdokpüspöki, Hungary

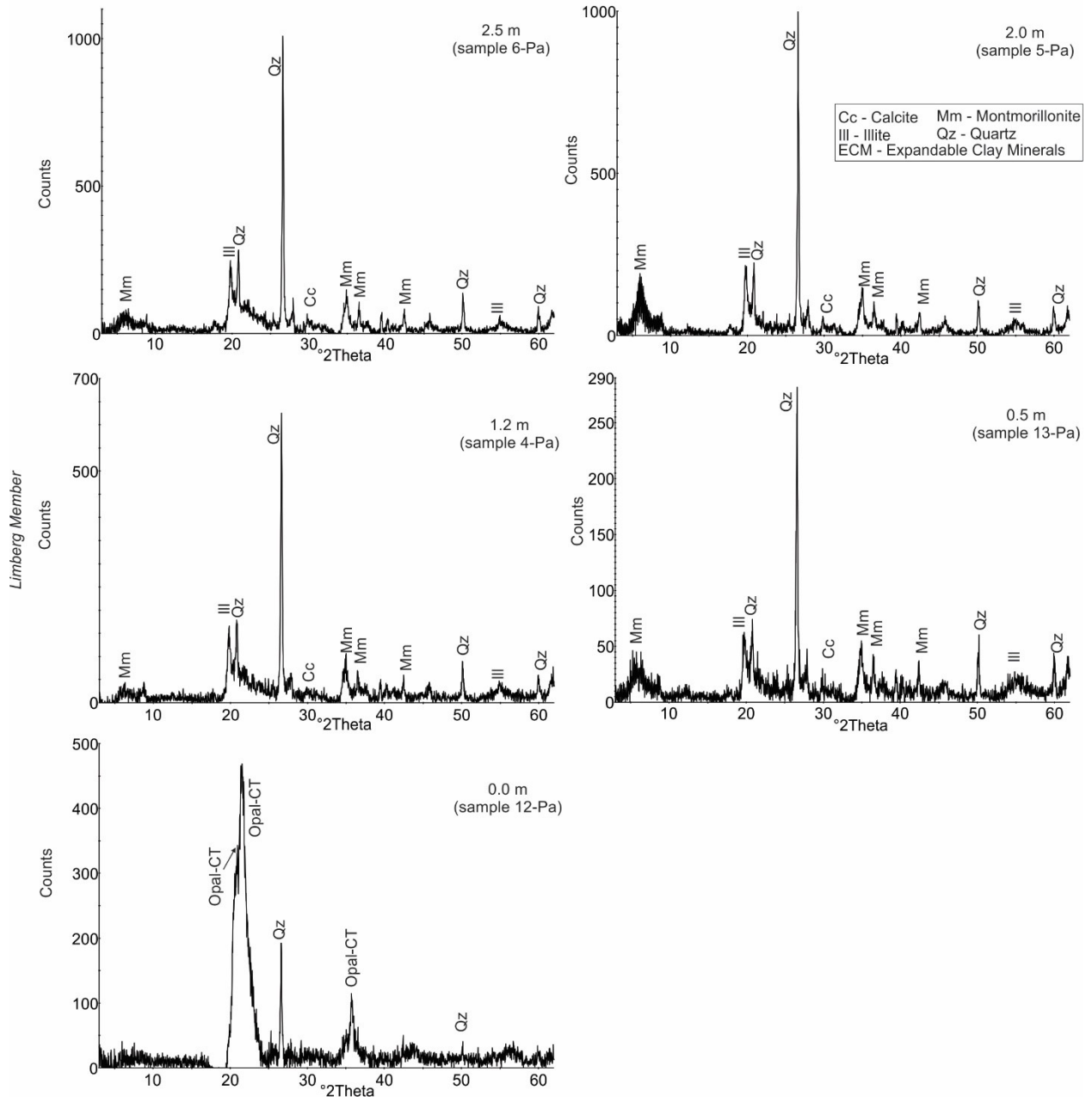


The noise of the samples is not caused by a malfunction during X-ray Diffraction measurements.

Szurdokpüspöki, Hungary

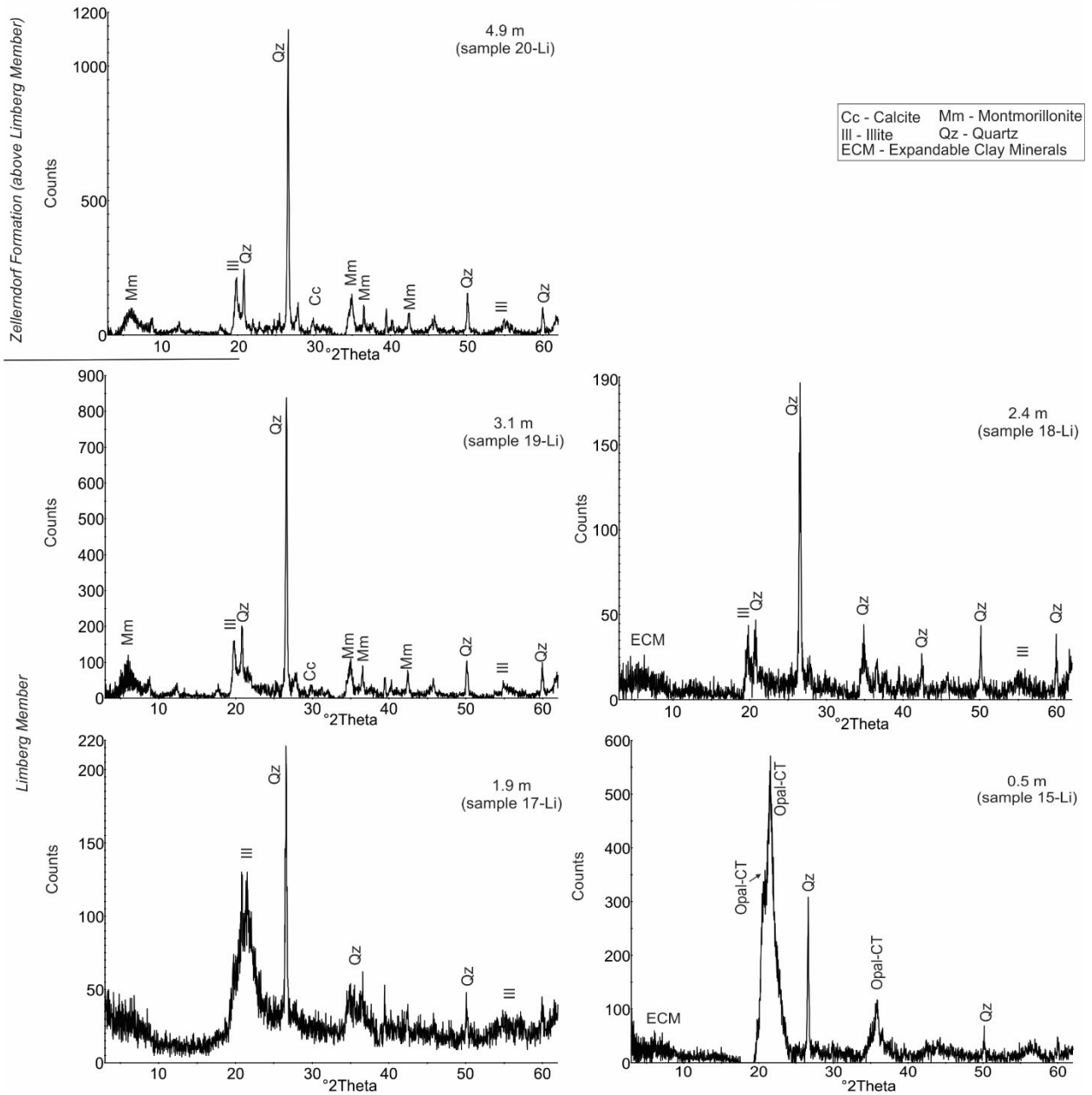


Parisdorf - Austria

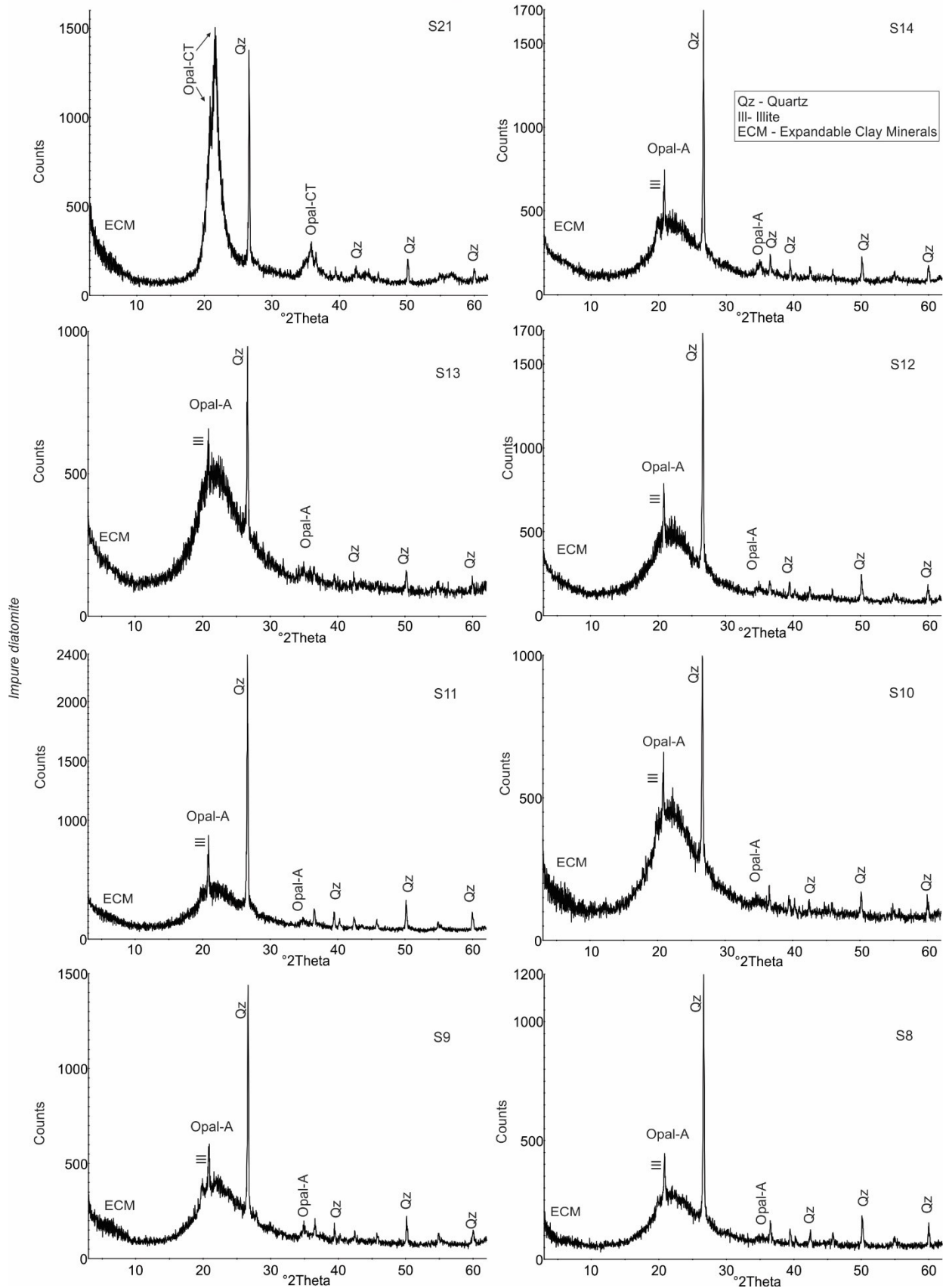




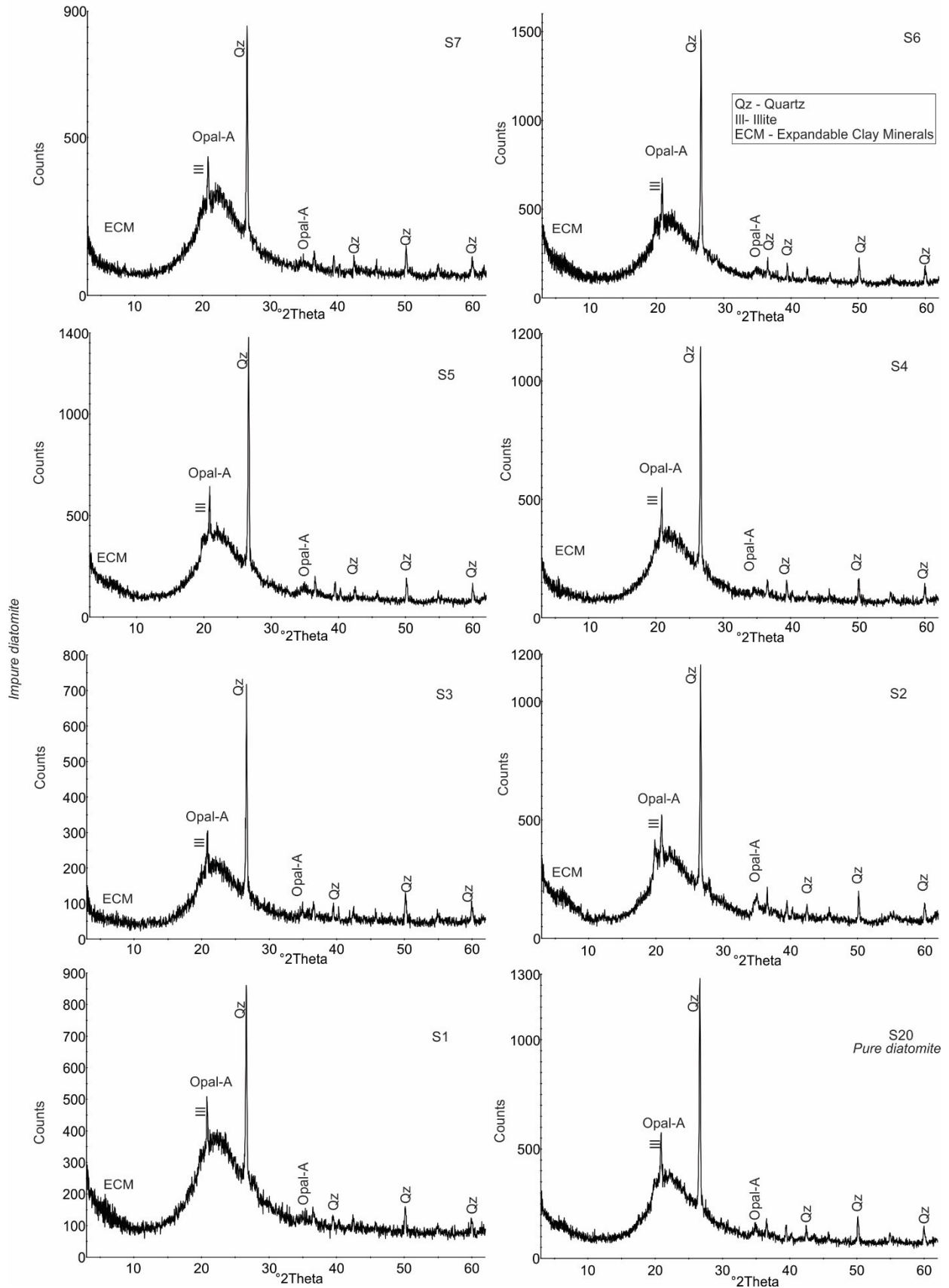
Limberg - Austria



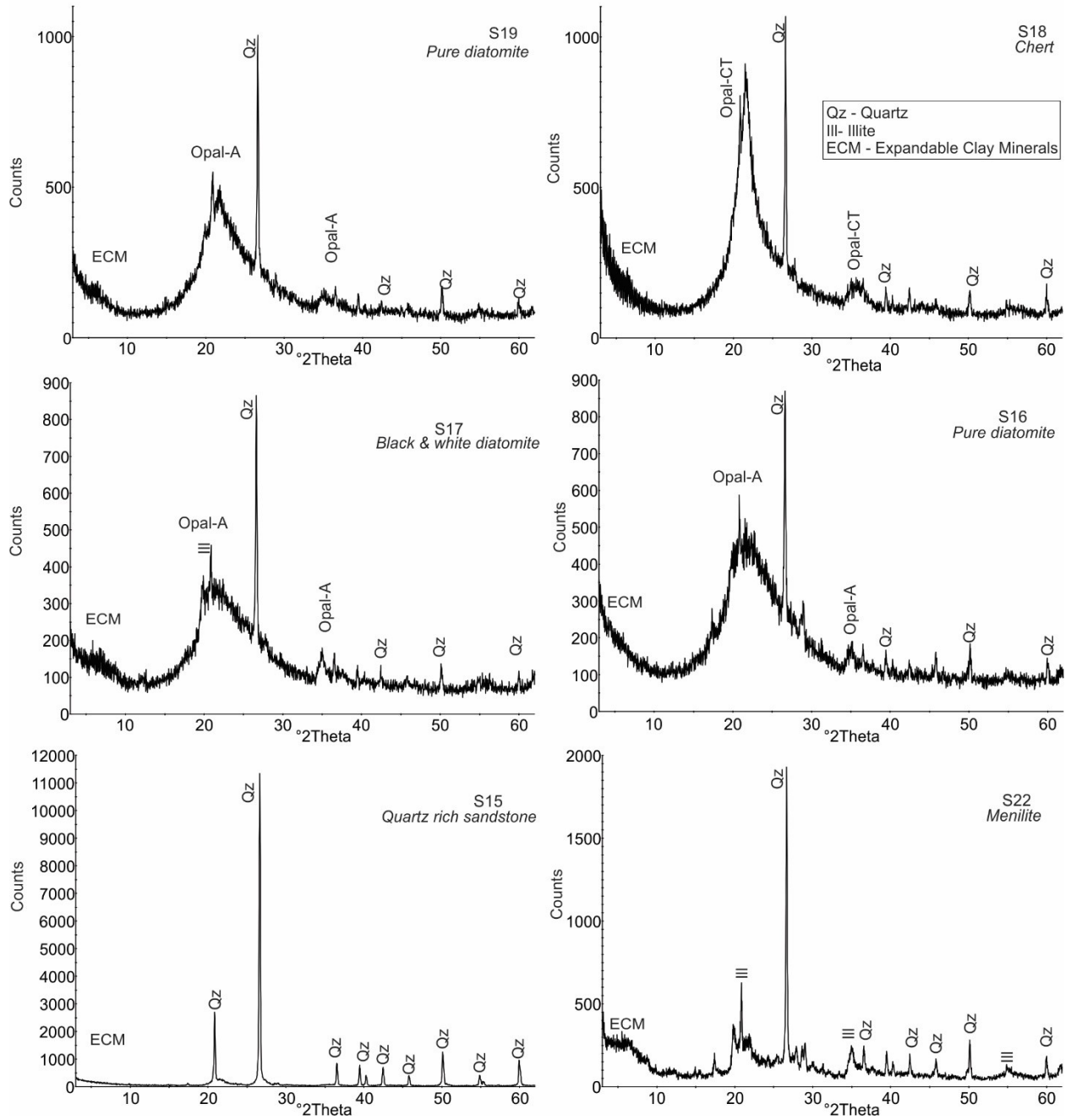
Sibiciu de Sus - Romania



Sibiciu de Sus - Romania



Sibiciu de Sus - Romania



*Appendix 3* - Outcrops pictures, unidentified diatom frustules taken under light microscope and scanning electron microscope pictures are stored in external storage device attached to the printed version.